Exploring quantum many-body systems from an entanglement and nonlocality perspective

PhD candidate

Albert Aloy López

Co-supervisors

Prof. Dr. Maciej Lewenstein
Dr. Jordi Tura i Brugués

Abstract

English

Entanglement and non-local correlations give rise to unprecedented phenomena with no classical analogue. As a result, they have settled themselves as fundamental properties in the study of quantum many-body systems, as well as key resources for emerging quantum technologies. However, the lack for general and efficient criteria to characterize them in many-body systems poses many challenges, often intractable. Consequently, despite the growing interest in their properties, the role of entanglement and non-local correlations in many-body systems remains largely unexplored.

The subject of the present Thesis is to explore quantum many-body systems from an entanglement and non-local correlations perspective, aiming at expanding the interplay between quantum information processing and quantum many-body physics. We examine adequate properties, like symmetries, that allow us to delve into entanglement and non-local correlations in many-body systems of physical relevance. The original results that we present are achieved at the fundamental level, even though many practical methods that can be experimentally implemented stem from them.

First, we explore the complexity to characterize entanglement in simplified cases. In particular, we consider the separability problem for diagonal symmetric states. We establish a connection with the field of quadratic conic optimization that allows us to provide significant sufficient criteria. Furthermore, it allows us to prove that obtaining necessary and sufficient criteria remains an NP-hard problem, even for a case with such a simplified structure.

Second, the elusiveness of the characterization of entanglement motivates certification criteria for its detection, specially in the multipartite scenario. By means of non-local correlations, we provide device-independent certification criteria that characterizes the amount of entanglement present on a quantum many-body system. This type of

certification does not rely on assumptions about the internal workings of the measuring device nor about the system itself. Moreover, by relying solely on non-local correlations, the criteria dismisses all the correlations that have a classical analogue, thus being a natural candidate as a certifier for emerging quantum technologies.

Third, we explore non-local correlations in the vicinity of quantum critical points, which are known to stabilize large-scale entanglement. We show the presence of non-local correlations across the phase diagram via a certain Bell inequality. Furthermore, we show that the Bell inequality is maximally violated at the quantum critical point, hinting at a possible connection between many-body Bell correlators and quantum phase transitions.

Fourth, we present a solution to the quantum marginal problem restricted to symmetric states. This allows to partially circumvent the inefficient representability inherent to the multipartite Hilbert space in cases of interest. In addition, we illustrate some of the applications that our solution brings on central quantum information problems. Namely, (i) as an undemanding and efficient variational method to optimize local Hamiltonians over symmetric states, (ii) to optimize few-body symmetric Bell inequalities over symmetric states and (iii) to explore which symmetric states cannot be self-tested solely from their marginals.

Finally, we conclude by presenting a methodology to derive two-body symmetric Bell inequalities for three-outcomes. These novel Bell inequalities are natural candidates to explore the role of non-local correlations on quantum phenomena tailored to qutrit or spin-1 many-body systems. We select a particular Bell inequality to characterize and show that it reveals non-local correlations in the ground state of many-body Hamiltonians physically relevant to, *e.g.,* nuclear physics.

Español

El entrelazamiento y las correlacions no-locales dan lugar a fenómenos sin precedentes ni analogía clásica. Estos fenómenos les ha llevado a

establecerse como propiedades clave para el estudio de sistemas cuánticos con muchos cuerpos, además de convertirse en recursos primordiales para las tecnologias cuánticas emergentes. Sin embargo, la falta de criterios generales y eficientes para caracterizarlos en sistemas de muchos cuerpos supone muchos retos, a menudo intratables. Por consiguiente, a pesar del creciente interés en sus propiedades, el rol del entrelazamiento y las correlaciones no-locales en sistemas de muchos cuerpos siguen, en gran parte, inexplorados.

El objetivo de esta Tesis es explorar sistemas cuánticos de muchos cuerpos desde la perspectiva del entrelazamiento y las correlaciones no-locales, con la voluntad de ampliar la sinergía entre el campo del procesamiento de información cuántica y la física cuántica de muchos cuerpos. Examinamos propiedades adecuadas, como simetrías, que nos permiten investigar el entrelazamiento y las correlaciones no-locales en sistemas de muchos cuerpos y de interés físico. Los resultados originales que presentamos se obtienen en el ámbito fundamental, al mismo tiempo que se proponen varios métodos prácticos que permiten ser experimentalmente implementados.

En primer lugar, exploramos la complejidad en caracterizar el entrelazamiento en casos simplificados. En particular, consideramos el problema de la separabilidad en estados simétricos diagonales. Establecemos una conexión con el campo de la optimización cónica cuadrática que nos permite demostrar que obtener criterios necesarios y suficientes sigue siendo un problema NP-hard, incluso para un caso con una estructura tan simplificada.

En segundo lugar, la evasividad de la caracterización del entrelazamiento motiva criterios de certificación para su detección, especialmente en el escenario multipartito. Mediante correlaciones no-locales, proporcionamos criterios independientes del dispositivo que certifican la cantidad de entrelazamiento presente en un sistema cuántico de muchos cuerpos. Este tipo de certificación no se basa en suposiciones sobre el funcionamiento intero del dispositivo de medida ni del mismo sistema. Además, al basarse ínicamente en correlaciones no-locales, el criterio descarta todas las correlaciones que tienen un análogo clásico,

siendo así un candidato natural como certificador de tecnologías cuánticas.

En tercer lugar, exploramos correlaciones no-locales alrededor de puntos críticos cuánticos, de los cuáles es sabido que estabilizan el entrelazamiento a gran escala. A través de desigualdades de Bell, mostramos la presencia de correlaciones no-locales a lo largo del diagrama de fase de un modelo de espines. Además, mostramos que la desigualdad de Bell se viola máximamente en el punto crítico, dando indicios de una posible conexión entre la violación de ciertas desigualdades de Bell y transiciones de fase cuánticas.

En cuarto lugar, presentamos una solución para el problema del marginal cuántico restringido a estados simétricos. La solución nos permite eludir parcialmente la ineficiente representabilidad intrínseca del espacio de Hilbert en casos de interés. Además, ilustramos algunas de las aplicaciones que la solución ofrece en problemas centrales de información cuántica. Concretamente, (i) como método variacional poco exigente y eficaz que ofrece optimizar Hamiltonianos locales respecto a estados simétricos, (ii) para optimizar desigualdades de Bell de pocos cuerpos y simétricas respecto estados simétricos y (iii) para explorar qué estados simétricos no se pueden auto-validar sólo a partir de sus marginales.

Finalmente, concluimos presentando una metodología que permite obtener desigualdades de Bell de pocos cuerpos y simétricas con tres posibles resultados de medida. Estas nuevas desigualdades de Bell permiten explorar el rol de las correlaciones no-locales en fenómenos cuánticos específicos para sistemas de muchos cuerpos formados por qutrits o con átomos de espín-1. Seleccionamos una desigualdad de Bell especifica para caracterizar y mostramos que detecta correlaciones no-locales en el estado fundamental de Hamiltonianos físicamente relevante en, e.g., física nuclear.

Català

L'entrellaçament i les correlacions no-locals donen lloc a fenòmens sense precedents ni analogia clàssica. Aquests fenòmens els han portat a establir-se com a propietats primordials per a l'estudi de sistemes quàntics amb molts cossos, així com a recursos primordials per a les tecnologies quàntiques emergents. Tanmateix, la manca de criteris generals i eficients per caracteritzar-los en sistemes de molts cossos suposa molts reptes, sovint intractables. Per consegüent, tot i l'interès creixent en les seves propietats, el rol de l'entrellaçament i les correlacions no-locals en sistemes de molts cossos continuen, en gran part, inexplorats.

L'objectiu d'aquesta Tesi és explorar sistemes quàntics de molts cossos des de la perspectiva de l'entrellaçament i les correlacions no-locals, amb la voluntat d'ampliar la reciprocitat entre els camps del processament d'informació quàntica i la física quàntica de molts cossos. Examinem propietats adequades, com ara simetries, que ens permeten investigar l'entrellaçament i les correlacions no-locals en sistemes de molts cossos i d'interès físic. Els resultats originals que presentem s'obtenen en l'àmbit fonamental, al mateix temps que es proposen un seguit de mètodes pràctics que permeten ser experimentalment implementats.

En primer lloc, explorem la complexitat en caracteritzar l'entrellaçament inclús en casos simplificats. En particular, considerem el problema de la separabilitat en estats simètrics diagonals. Establim una connexió amb el camp d'optimització cònica quadràtica que ens permet proporcionar diversos criteris suficients de separabilitat. A més, ens permet demostrar que criteris necessaris i suficients segueixen sent un problema NP-hard, fins i tot per a un cas amb una estructura tan simplificada.

En segon lloc, l'evasivitat de la caracterització de l'entrellaçament motiva criteris de certificació per a la seva detecció, especialment en l'escenari multipartit. Mitjançant correlacions no-locals, proporcionem criteris independents del dispositiu que caracteritzen la quantitat d'entrellaçament present en un sistema quàntic de molts cossos. Aquest ti-

pus de certificació no es basa en suposicions sobre el funcionament intern del dispositiu de mesura ni del mateix sistema. A més, al basar-se únicament en correlacions no-locals el criteri descarta totes les correlacions que tenen un anàleg clàssic, sent així un candidat natural com a certificador de tecnologies quàntiques.

En tercer lloc, explorem correlacions no-locals en l'entorn de punts crítics quàntics, coneguts per estabilitzar l'entrellaçament a gran escala. A través de desigualtats de Bell, mostrem la presència de correlacions no-locals al llarg del diagrama de fase d'un model d'espins. A més, mostrem que la desigualtat de Bell es viola màximament en el punt crític, donant indicis d'una possible connexió entre la violació de certes desigualtats de Bell i transicions de fase quàntiques.

En quart lloc, presentem una solució pel problema del marginal quàntic restringit a estats simètrics. La solució ens permet eludir parcialment la ineficient representabilitat inherent a l'espai de Hilbert multipartit en casos d'interès. A més, il·lustrem algunes de les aplicacions que la solució ofereix en problemes centrals d'informació quàntica. Concretament, (i) com a mètode variacional poc exigent i eficaç que ofereix optimitzar Hamiltonians locals respecte estats simètrics, (ii) per optimitzar desigualtats de Bell de pocs cossos i simètriques respecte d'estats simètrics i (iii) per explorar quins estats simètrics no es poden auto-validar només a partir dels seus marginals.

Finalment, concloem presentant una metodologia que permet obtenir desigualtats de Bell simètriques de pocs cossos amb tres possibles resultats de mesura. Aquestes noves desigualtats de Bell permeten explorar el rol de les correlacions no-locals en fenòmens quàntics específics per a sistemes de molts cossos formats per qutrits o amb àtoms d'espín-1. Seleccionem una desigualtat de Bell a caracteritzar i mostrem que detecta correlacions no-locals en l'estat fonamental d'Hamiltonians físicament rellevant en, e.g., física nuclear.

List of Publications

Journal Papers

1. J. Tura, A. Aloy, R. Quesada, M. Lewenstein, and A. Sanpera. Separability of diagonal symmetric states: a quadratic conic optimization problem. *Quantum* **2**, 45 (2018).

2. F. Baccari, J. Tura, M. Fadel, A. Aloy, J.-D. Bancal N. Sangouard, M. Lewenstein, A. Acín, and R. Augusiak. Bell correlation depth in many-body systems. *Phys. Rev. A* **100**, 022121 (2019).

3. A. Aloy, J. Tura, F. Baccari, A. Acín, M. Lewenstein, and R. Augusiak. Device-Independent Witnesses of Entanglement Depth from Two-Body Correlators. *Phys. Rev. Lett.* **123**, 100507 (2019).

4. J. Tura, A. Aloy, F. Baccari, A. Acín, M. Lewenstein, and R. Augusiak. Optimization of device-independent witnesses of entanglement depth from two-body correlators. *Phys. Rev. A* **10**, 032307 (2019).

5. A. Piga, A. Aloy, M. Lewenstein, and I. Frérot. Bell Correlations at Ising Quantum Critical Points. *Phys. Rev. Lett.* **123**, 170604 (2019).

Preprints

6. A. Aloy, M. Fadel, and J. Tura. The quantum marginal problem for symmetric states: applications to variational optimization, nonlocality and self-testing. *arXiv* 2001.04440 (2020)

Acknowledgments

I dare say that these past four years have been some of the best in my life. At the very least, the most intellectually stimulating and personally fulfilling ones. That is not to say that there has not been sacrifices and rough periods. The uncertain future and high competitivity conditions intrinsic in nowadays research carry an additional burden of stress that one has to cope with. Luckily for me I got to have Maciek and Jordi as thesis advisors: not ever once I felt unhealthy pressure from their side, while countless times they cared for me. The only pushes from their side were gentle and helped me grow. Maciek and Jordi played a crucial role in me having such enjoyable years, for which I will be forever grateful. Not only they are great scientists, but great human beings.

Thank you Maciek, it has been an honor to get a glimpse at your vast dwell of knowledge and wisdom, and an absolute pleasure to work under your leadership. Apart from an outstanding scientific career you have built an amazing group with amazing and brilliant people, which in part is a reflection of your persona. I will never forget your generosity with all the opportunities you have given me.

Thank you Jordi, most of what I have learnt these past years comes from you. While I had lots of knowledge gaps to be filled, you have always been patient and pedagogical. If today I feel confident with my research skills is thanks to you. And while for the most part of the PhD we were separated by a big distance, you have always been available and willing to help. Your presence can be found throughout all the thesis, which is as much yours as it is mine. It has been an honor to learn from you and to work with you, all while seeing you grow into an even more brilliant scientist with a bright future ahead.

Along the way there have been many co-workers who I have had the honor to meet and work with. To Remigiusz Augusiak and Antonio Acín, you were the first ones that gave me a chance and with whom I got properly introduced to research, for which I will forever be grateful. Both of you have altruistically shared your brilliance with many of your

ideas for scientific projects, which not only have been key for the thesis, but have shed light on a path to follow in times of uncertainty. Thank you Remik and Toni. To Anna Sanpera, it has been a real pleasure to have shared a project with you. Not only for your brilliance, but because you generate an environment of acceptance around you which boosts work flow and enhances the good part of research. Thank you Anna. To Flavio Baccari, Angelo Piga, Irénée Frérot and Matteo Fadel, it has been very inspiring to see you work. You have all been key in distinct periods of the thesis and I have learnt something unique from each one of you. Thank you guys.

Finally, this is my chance to thank the people not directly related to the PhD but that have been patient accompanying me through it. Thank you Diana, for all the support you have given me, for reminding me to enjoy life outside science and for the value you add to my well-being. Gràcies Repu, per estar allà quan necessito algú amb qui parlar i per ser una persona que brilla amb el teu punt de vista únic i constructiu que tants cops m'ha guiat per seguir creixent. A l'Àlex, per ser com ets. Thank you Denis, for all the rewarding discussions when I was down and for your kindness that added stability and comfort at home, once I got to share flat with you my PhD life significantly improved. I finalment vull agraïr a la meva germana Judit per despertar-me l'interès per la física i les matemàtiques que m'ha acabat portant aquí, i als meus pares Pere i Maria pel vostre suport incondicional i per haver-me donat tot el que heu pogut i més.

This thesis would not have been possible without the funding received from the Spanish Ministry MINECO (National Plan 15 Grant: FISICATEAMO No. FIS2016-79508-P), EU FETPRO QUIC, European Social Fund, Fundació Cellex, Generalitat de Catalunya (AGAUR Grant No. 2017 SGR 1341, CERCA/Program), the National Science Centre, Poland-Symfonia Grant No. 2016/20/W/ST4/00314, ERC AdG OSYRIS and NOQIA, EU FEDER and MINECO-EU QUANTERA MAQS.

Table of Contents

Chapter 1

Introduction

Amidst the advent of quantum mechanics in the 20th century, several revolutionary ideas emerged which challenged preconceived notions in classical physics, such as locality or determinism. One of the ideas brought by quantum mechanics, with the most ground-breaking consequences, is the possibility that linear combinations of quantum states are allowed to form another quantum state qualitatively different from the original states. It was soon realized that, when considering quantum composites, such linear combination of quantum states implied non-local features. The non-local features of quantum mechanics sparked a debate that eventually led to the discovery of entanglement.

Entanglement is perhaps the most quintessential phenomena predicted by quantum mechanics [Horodecki *et al.*, 2009], departing entirely from any classical analogy. Roughly speaking, a quantum composite is entangled when the description of its individual components does not suffice to describe the whole composite. While nowadays entanglement is a well-established phenomenon, and routinely verified in laboratories, since the 30s, and during decades, entanglement remained an object of controversy [Einstein *et al.*, 1935; Bohr, 1935]. In particular, the controversial focus was the prediction that entanglement can give rise to some type of instantaneous action on spatially separated objects [Einstein *et al.*, 1935]. Decades later, in the 60s, such

instantaneous action at a distance got formalised as correlations that go beyond the principles of locality and realism [Bell, 1964], referred to as non-local correlations or simply nonlocality [Brunner *et al.*, 2014; Scarani, 2019]. It was not until the 80s that a satisfactory experimental detection of nonlocality would settle the debate in favour for the existence of entanglement [Aspect *et al.*, 1982].

Entanglement supposed many paradigm shifts, not only on scientific aspects but also for technological applications. While the debate about entanglement was going on, by the 50s information theory had been born [Shannon, 1948]. Eventually, the interplay between quantum mechanics and information theory gave rise to Quantum Information Theory (QIT) [Nielsen and Chuang, 2002] from considering the implications of quantum phenomena on the quantification, storage and communication of information. Efforts to build Quantum Information Processing (QIP) tasks increased as the ability to control single or few quantum particles was developed, even considering quantum simulators and quantum computers based on encoding bits of information in quantum particles. By the 80s interest to consider entanglement as a resource for QIP tasks had grown, even though the question of whether the non-local feature of entanglement could be used to signal information faster than light received a negative answer. Since then, entanglement has become one of the main resources for QIP tasks such as quantum teleportation [Bennett *et al.*, 1993], quantum-enhanced metrology [Giovannetti *et al.*, 2011] or quantum key distribution [Ekert, 1991], the latest of which is even commercialized.

The unavoidable imperfections on the implementation of quantum systems or QIP tasks, like the loss of quantum phenomena due to small random perturbations from the environment, has risen the need for certification criteria robust against imperfections. While originally nonlocal correlations were considered as a means to gain fundamental insight from quantum correlations, nonlocality supposed a paradigm shift when it started to be seen as a resource for the Device-Independent (DI) framework and the subsequent Device-Independent Quantum Information Processing (DIQIP). The DI framework takes advantage of

non-local correlations to provide certification criteria that does not require trust on the implementation, and has been successful in providing self-testing protocols [Mayers and Yao, 1998], secure quantum protocols like DI quantum key distribution [Acín *et al.*, 2007; Pironio *et al.*, 2009], certification of genuine randomness [Pironio *et al.*, 2010], or randomness amplification [Colbeck and Renner, 2012]. A feature of DI certification is that it rules out local models. Hence, it guarantees that correlations are generated by intrinsically quantum effects.

As the progress on quantum technological platforms keeps advancing, these start to require the control and manipulation of not only one or few particles, but large systems of quantum particles. Nowadays we are experiencing a new paradigm shift, which arguably started in the 90s with the achievement of the Bose-Einstein condensation (BEC) [Anderson *et al.*, 1995; Bradley *et al.*, 1995; Davis *et al.*, 1995], where it is possible to implement large systems of ultracold atoms to serve as, for instance, quantum simulators [Lewenstein *et al.*, 2007]. Consequently, in the past decades the pursuit for large scale genuinely quantum effects has become a major trend of modern many-body physics. Unfortunately, quantum properties without a classical analogue, like entanglement, are believed to be very fragile against the interaction with other degrees of freedom, bringing the transition from the quantum domain to the classical. Nonetheless, under suitable conditions large scale entanglement becomes relevant for many-body physics [Amico *et al.*, 2008], even playing a crucial role in the understanding of complex many-body phenomena like quantum phase transitions [Osborne and Nielsen, 2002]. Moreover, apart from its fundamental implications, large scale entanglement in many-body systems is a key resource also for quantum simulators [Kim *et al.*, 2010; Simon *et al.*, 2011]. However, whereas entanglement for two quantum particles is well understood, much remains unexplored for large number of quantum particles. Therefore, the certification of genuinely quantum phenomena without a classical analogue in many-body systems is of central importance, both for fundamental science and for validation of quantum technologies. Nonlocality offers the conceptual and technical tool required for

the certification of quantum phenomena without classical analogue. However, nonlocality characterization in many-body systems remains even more unexplored than entanglement, partly due to the increased combinatorial complexity. Remarkably, some recent works have considered desirable properties that allow to explore the role of nonlocality in physically relevant many-body systems [Tura *et al.*, 2014a, 2015], even enabling the experimental implementation to detect nonlocality on many-body systems [Schmied *et al.*, 2016; Engelsen *et al.*, 2017].

1.1 Motivation and main contributions

In this Thesis we aim at expanding the interplay between QIP and many-body physics by exploring quantum many-body systems from an entanglement and nonlocality perspective. Part of our aim is to expand the knowledge on entanglement and nonlocality for large scale systems, which remains quite limited. Due to the lack of general and efficient criteria to address questions regarding entanglement and nonlocality in many-body systems, we shall find adequate situations by examining systems of physical relevance, often considering symmetric properties.

1.1.1 Entanglement in diagonal symmetric states

We start the thesis by exploring the complexity to characterize entanglement. General criteria to determine whether a given quantum state is entangled remains an elusive open problem, usually referred to as *the separability problem*. Consequently, researchers have sought of sufficient, simple and efficient criteria to certify entanglement. An emblematic example is the Positive under Partial Transposition (PPT) criterion [Peres, 1996], which certifies entanglement on those bipartite quantum states that break the PPT criterion. While for some low-dimensional bipartite systems fulfilling the PPT criterion is a necessary and sufficient condition for separability, for higher-dimensional systems the relation between PPT and separability breaks with the existence of entangled states that satisfy the PPT criterion.

However, the Hilbert space accounts for a vast variety of quantum states which are not of particular interest [Goldstein *et al.*, 2006; Popescu *et al.*, 2006]. Instead of considering the separability problem in all its generality, one then may ask whether one can we characterize the separability problem restricted to specific classes of states. This is a recurrent technique that we use throughout the thesis whenever facing a problem of overwhelming complexity. In particular, we shall consider classes of quantum states that inherit some symmetry.

Symmetries play a crucial role in physics to describe nature and its laws. In quantum physics, an important symmetry considered is that of exchange of indistinguishable particles. The so-called *symmetric states* are the class of states that remain invariant under any permutation of its particles [Eckert *et al.*, 2002]. Important subclasses of symmetric states are the GHZ and the Dicke states. Dicke states were firstly characterized in the context of superradiance [Dicke, 1954]. Dicke states are also defined as the simultaneous eigenstates of the total angular momentum and its z-component. They are known to appear as ground states of physical systems described by the Lipkin-Meshkov-Glick (LMG) model, and to be routinely used experimentally [McConnell *et al.*, 2015; Wieczorek *et al.*, 2009; Lu *et al.*, 2007]. Moreover, an appropriate representation of symmetric states uses the basis spanned by Dicke states.

Unfortunately, even in the simpler case of characterizing entanglement restricted to symmetric states, the separability problem remains elusive and open. Therefore, one may consider an even simpler class of states on which to restrict the characterization of entanglement. Recently, there has been a growing interest to consider a specific subclass of the symmetric states called Diagonal Symmetric States (DSS). These are mixtures of Dicke states that are diagonal in the Dicke basis. They form an important subclass of symmetric states which, for instance, appear in dissipative systems such as photonic or plasmonic waveguides [González-Tudela and Porras, 2013]. Their simpler structure, while still being physically relevant, makes DSS states a good candidate to explore the characterization of entanglement in search for

new insights.

Main contributions

In Chapter 3 we explore the characterization of entanglement in bipartite qudit DSS. We show that the separability problem for bipartite symmetric qudits systems can be equivalently posed as a quadratic optimization problem. This novel connection allows us to exchange concepts and ideas between the field of QIT and the field of quadratic conic optimization. For instance, we show that copositive matrices can be understood as indecomposable entanglement witnesses for DSS. Apart from applications, the connection between fields allows us to show that fulfilling the PPT criterion provides necessary and sufficient conditions for separability when the qudits forming the DSS have dimensions $d < 5$. Furthermore, for dimensions $d \geq 5$ we recover the NP-hardness of the separability problem for DSS by leveraging on theory from results from completely positive matrices. We also provide analytical examples of bipartite DSS that fulfill the PPT criterion but are entangled for $d \geq 5$. Finally, we develop new sufficient separability conditions in terms of diagonal dominant approximations to PPTDSS.

The results have been published in [Tura *et al.*, 2018], a joint work with J. Tura, R. Quesada, M. Lewenstein and A. Sanpera.

1.1.2 Device-independent certification of multipartite entanglement in many-body systems

Despite the complexity to characterize entanglement, the need to have more sophisticated criteria that certifies the presence of entanglement keeps growing. This is specially the case for many-body systems, in which case the problem becomes significantly more complex both from computational and experimental points of view.

The simplest and most studied form of entanglement is the bipartite case. On the other hand, a generalization towards larger quantum systems that involve more than two subsystems turns out to be a much

richer and challenging case [Gühne and Tóth, 2009]. As opposed to the bipartite case, multipartite entanglement admits a hierarchy of definitions depending on the strength and type of correlations between the subsystems forming the quantum system. The strongest form of multipartite entanglement, *i.e.* without any type of separability on the system, is often referred to as Genuinely Multipartite Entanglement (GME), which has attracted much attention towards its detection and quantification [Gühne and Seevinck, 2010; Jungnitsch *et al.*, 2011; Huber *et al.*, 2011]. A lot of efforts have also put on the certification of the degree of entanglement present in a given quantum state [Schwemmer *et al.*, 2015; Knips *et al.*, 2016; Tran *et al.*, 2017], often also relying on GME [Bancal *et al.*, 2011a; Zwerger *et al.*, 2019; Barreiro *et al.*, 2013]. However, the techniques involved to detect GME are in general too experimentally demanding, and even too computationally demanding [Navascués *et al.*, 2007, 2008, 2015]. Consequently, researchers have sought for other notions that characterize the entanglement present in the system. For instance, the equivalent notions of *entanglement depth* [Sørensen and Mølmer, 2001] and *k-producibility* [Gühne *et al.*, 2005], which characterize entanglement by considering the maximal amount of GME particles present in the system.

On the other hand, most of the existent entanglement detection techniques for many-body systems face common challenges like (i) the exponential growth of the Hilbert space with the system size; (ii) the requirement of assumptions on precision or idealizations of the system considered, which can lead to wrong conclusions even when the assumptions are slightly off [Bancal *et al.*, 2011b; Liang *et al.*, 2015]; (iii) or technological limitations such as requiring to individually address a large amount of subsystems at once. Not surprisingly, alternative approaches emerged in order to circumvent some of the aforementioned challenges. For example, the Device-Independent framework [Acín *et al.*, 2007; Scarani, 2012a] is designed to avoid assumptions and idealizations by reaching conclusions only through the observed statistics on a Bell-type experiment. Naturally, with the advent of the DI formalism many entanglement witnesses criteria eventually got

upgraded to their DI counterpart [Bancal *et al.*, 2011a; Liang *et al.*, 2015; Moroder *et al.*, 2013; Lin *et al.*, 2019]. However, the upgrade process from entanglement witness to its DI counterpart is far from trivial, since by having less assumptions the requirements of the criteria greatly increases. It might not even be possible to upgrade some of the more sophisticated criteria, while those for which it is possible still remain without upgrade. For instance, to assess the entanglement depth of a many-body system in a DI manner remains broadly unexplored: while remarkable steps towards this direction have been made with the advent of Device-Independent Witnesses of Entanglement Depth (DIWEDs) [Bancal *et al.*, 2011b; Moroder *et al.*, 2013; Liang *et al.*, 2015; Lin *et al.*, 2019], they are far from being implemented in large system sizes.

Therefore, an open problem is the derivation of criteria that certifies the amount of entanglement present in quantum many-body systems without relying on assumptions on the system being probed nor on the internal workings of the measuring device. Namely, the derivation of DIWEDs for quantum many-body systems.

Main contributions

In Chapter 4 we use nonlocality to explore, from a device-independent perspective, the characterization of entanglement depth in quantum many-body systems and provide certification criteria. In particular, we present a general methodology to derive DIWEDs from Bell inequalities, and specifically characterize the case when the Bell inequalities involve few-body symmetric correlators. The methodology is based on two complementary numerical methods: (i) a variational algorithm yielding an upper bound, and (ii) a certificate of optimality via Semidefinite Programming (SDP) yielding a lower bound. Closing the gap between bounds ensures the DIWED criteria.

Based on two-body symmetric Bell inequalities [Tura *et al.*, 2014a, 2015], we derive DIWEDs that involve at most two-body correlators. To reach large system sizes, we consider the derivation of DIWEDs

under different assumptions. From numerical observations, we find a clear pattern on the bounds forming the DIWEDs for large system sizes, which allows us to analytically explore even the thermodynamic limit. Contrary to the state-of-the-art, the DIWEDs we present enjoy many desirable properties that allow them to be effectively measured by accessing only collective measurements and second moments thereof. Indeed, experiments have already been performed for one of the Bell inequalities from which we construct DIWEDs. Here we benchmark our results with an experiment implemented on a quantum many-body system of $5 \cdot 10^2 \sim 5 \cdot 10^5$ atoms on which Bell correlations were detected [Schmied *et al.*, 2016]. Based on the existing experimental data, we probe the performance of the DIWEDs we present and compare them with other entanglement depth criteria.

The results have been published in [Aloy *et al.*, 2019; Tura *et al.*, 2019], a joint work with J. Tura, F. Baccari, A. Acín, M. Lewenstein and R. Augusiak.

1.1.3 Non-local correlations near quantum critical points

Everyday macroscopical physical phenomena differs from the quantum mechanical phenomena observed in small-scale systems. An intense topic of debate in the past decades is the transition from quantum-to-classical that takes place in mesoscopical systems as system sizes increase. Intrinsically quantum properties, *i.e.* without a classical analogue, are believed to be very fragile against thermalization. This is specially the case when interacting with many degrees of freedom, which is considered a main factor leading to the quantum-to-classical transition. On the other hand, the pursuit of large scale genuinely quantum effects in many-body systems often involves large scale entanglement. Hence, to identify suitable conditions under which non-classical features may be probed at increasingly large scales is of fundamental importance to further advance emerging quantum technologies such as quantum simulators.

On one hand, the so-called Quantum Critical Points (QCPs) are known to stabilize quantum correlations at all length scales [Sachdev, 2011], even in a robust way against finite-temperature and experimental imperfections [Hauke *et al.*, 2016; Gabbrielli *et al.*, 2018; Frérot and Roscilde, 2019]. Moreover, the genuine quantum correlation properties of QCPs are a feature of the whole quantum-critical regime and, therefore, span an extended region of the phase diagram around the QCP [Hauke *et al.*, 2016]. On the other hand, Bell inequalities are the conceptual and technical tool to certify genuine quantum correlations and discard correlations with a classical analogue. Therefore, the certification of non-local correlations by means of Bell inequalities provides a complement to QCPs for a fully quantum characterization of the resulting correlations. However, the detection and characterization of non-local correlations for macroscopic systems poses a very complex and challenging task [Brunner *et al.*, 2014].

Consequently, the behaviour of non-local correlations near QCPs remains wildly unexplored. For instance, a first step would be to answer whether QCPs also stabilize non-local correlations among the individual components of the system.

Main contributions

In Chapter 5 we explore non-local correlations in the vicinity of QCPs. In particular, we focus on the Ising model in a transverse-field with tunable range ferromagnetic interactions, and show that the multipartite entanglement stabilized at the QCP is certified via nonlocality detection with the two-body symmetric Bell inequalities. Apart from the QCP, we also observe a regime of nonlocality detection around the QCP. The tunable range of the interactions allows us to explore from the infinite-range to the nearest neighbours case, while quantitatively probing for nonlocality across the phase diagram. We observe the violation by means of finite-size numerical density-matrix renormalization group, which we then extrapolate to the asymptotic limit, as well as by means of analytical spin-wave calculations assuming that in the Bell

test identical measurements are performed on qubits. Furthermore, from the linear spin-wave calculations we show that the origin of the Bell inequality violation is the squeezing of collective-spin fluctuations generated by quantum-critical correlations of the model. Thus, we provide one of the first explorations on non-local correlations in QCPs.

The results have been published in [Piga *et al.*, 2019], a joint work with A. Piga, M. Lewenstein, and I. Frérot.

1.1.4 The quantum marginal problem for symmetric states

Through the thesis, in order to explore non-local correlations in many-body systems we often rely on classes of few-body symmetric Bell inequalities [Tura *et al.*, 2014a]. However, while these classes of Bell inequalities have some desirable properties, the characterization of non-local correlations still remains far from easy. An observed feature of these inequalities is that they are maximally violated by symmetric states [Tura *et al.*, 2014a, 2015]. Consequently, they offer the possibility to be characterized solely from two-body Reduced Density Matrices (RDM), given that the RDMs are compatible with a global symmetric sate. Nonetheless, one would still need to find the compatibility conditions.

The problem of determining whether a given set of RDMs are compatible with a global quantum state is known as the Quantum Marginal Problem (QMP) (see *e.g.* [Schilling, 2015]). In other words, the QMP asks for the compatibility conditions to describe the whole system from its parts. While our original motivation comes from characterizing Bell inequalities, the QMP has a long standing history of appearing in several distinct contexts, not only in physics but also in quantum chemistry, where it is usually referred to as the n-representability problem [Stillinger, 1995; Walter *et al.*, 2013]. The relevance of the QMP comes from being able to compute most physical quantities of interest (*e.g.,* energy, entropy,...) in a many-body system solely from few-body terms, provided the compatibility conditions with a global state are

known.

The QMP dates back to the 60s. In spite of the attention received due to its relevance for the physics and chemistry communities, the advances have been slow and any non-trivial progress has supposed a milestone [Klyachko, 2006]. In fact, it has been shown to be complete for the complexity class Quantum Merlin-Arthur (QMA) [Liu *et al.*, 2007], meaning that it is very hard even for a quantum computer. Nevertheless, over the years important works advancing the QMP field have been obtained, even before the advent of the QIP era [Ruskai, 1969; A. J. Coleman, 2000; Walter *et al.*, 2013].

Most of the advances regarding the QMP have been based on the one-body RDM, *i.e.* to determine whether a given set of one-body RDMs is compatible with a global (pure) state [Klyachko, 2004], resulting many applications for QIP [Walter *et al.*, 2013; Schilling *et al.*, 2017; Huber, 2017]. On the other hand, the few-body QMP remains mostly unexplored, partly because it poses additional challenges. While in the one-body RDM all the supports of different RDMs are disjoint (without overlap), in the few-body case their supports may intersect. Therefore, the few-body QMP contains additional conditions like, for instance, that the RDMs overlapping need to have the same RDMs on the subsystems that coincide in the overlap. In order to account for the bosonic and fermionic formalism, the QMP has also been studied by considering the assumption that the global pure state is fully symmetric or antisymmetric [Klyachko, 2006; Gidofalvi and Mazziotti, 2004; A. J. Coleman, 2000; Beste *et al.*, 2002; Mazziotti, 2012; Christandl *et al.*, 2014]. An important feature is that the resulting RDMs under the symmetric assumption are all equal due to the symmetry of the global state.

Nonetheless, a solution of the QMP for symmetric states still lacks. Such solution would allow, among many other applications, an efficient characterization of non-local correlations in many-body systems.

Main contributions

In Chapter 6 we present a methodology to analytically solve the QMP for systems formed by symmetric qudit states. First we provide analytical compatibility conditions for an m-body RDM to be compatible with an n-qudit density matrix supported on the symmetric space. Then we show how the QMP for symmetric states can be solved via an efficient semidefinite program that uses the compatibility conditions as constraints.

Furthermore, we explore some of the applications our solution to the QMP for symmetric states might bring. In particular we consider three areas of quantum information: (i) variational optimization; (ii) nonlocality detection; and (iii) self-testing. First, we present a variational method, which uses symmetric states as a variational ansatz to optimize local Hamiltonians. We show the performance of the variational method in several exemplary local Hamiltonians, as well as benchmark the performance compared to density-matrix renormalization group computations. Second, we use the QMP for symmetric states method in order to characterize few-body symmetric Bell inequalities in two ways: (i) by finding the symmetric state offering maximal violation of the Bell inequality; and (ii) by using the method to efficiently explore non-local correlations in ground states of local Hamiltonians. From the latter we find non-local correlations on the ground state of an XXZ spin chain with ferromagnetic nearest neighbour interactions under a transverse field. Third, we explore the ability of the QMP for symmetric states method in order to explore under which conditions qubit symmetric states cannot be self-tested from their marginals, and conjecture a relation between the rank of the global symmetric state and the amount of parties in the RDM.

Finally, as a byproduct of benchmarking the variational method, we provide an analytical correspondence to generically express n-qubit symmetric states as translationally invariant diagonal matrix product states of bond dimension n.

The results are part of the preprint [Aloy *et al.*, 2020], a joint work with M. Fadel and J. Tura.

1.1.5 Nonlocality detection in three-level many-body systems

In the quest to explore the role of nonlocality in many-body systems, Bell inequalities involving more than two outcomes remain largely unexplored. Nevertheless, for two parties, the first Bell inequalities for d outcomes [Collins *et al.*, 2002] already presented fundamental implications by showing that entanglement is not equivalent to nonlocality, since maximally entangled states did not maximally violate the Bell inequality. While multipartite Bell inequalities with three outcomes have been obtained [Alsina *et al.*, 2016], the state-of-the-art is far from reaching many-body systems.

For the two outcomes case, the few-body symmetric Bell inequalities [Tura *et al.*, 2014a, 2015] are some of the most successful many-body Bell inequalities, which have even been experimentally implemented [Schmied *et al.*, 2016; Engelsen *et al.*, 2017]. Then, one may consider Bell inequalities for three outcomes that inherit the same desirable properties. However, by increasing the number of outcomes the affine space becomes more complex, which renders inefficient even their representation. On the other hand, the methodology to solve the QMP for symmetric states allows to optimize the Bell inequality solely from the marginals of symmetric quantum states, which synergizes with the evidence that permutationally invariant Bell inequalities are maximally violated by symmetric states [Tura *et al.*, 2014a, 2015]. Therefore, under such consideration the complexity gets greatly reduced, making it possible to consider the derivation and characterization of few-body symmetric Bell inequalities for more than two outcomes.

Three-outcome few-body symmetric Bell inequalities would be natural candidates to explore the non-local correlations in many-body exotic quantum phenomena directly related to the three outcomes case. For instance, one could explore the role of nonlocality in spin-1 models that exhibit exotic phase diagrams [Haldane, 1983], or consider cases in which the correlation length remains finite while the entanglement length diverges [Verstraete *et al.*, 2004; Popp *et al.*, 2005]. As for ex-

perimental implementations, such symmetric Bell inequalities would be particularly fitted for spin-1 BECs, widely explored in the context of ultracold quantum gases [Lewenstein *et al.*, 2007], where it is possible to generate large scale entanglement with symmetric states [Zhang and Duan, 2013; Zou *et al.*, 2018]. Of particular interest is the ferromagnetic spin-1 BEC, routinely implemented in the lab using ^{87}Rb [Barrett *et al.*, 2001; Schmaljohann *et al.*, 2004], due to the spin-squeezing features it presents [Hamley, 2012] as well as the possibility to measure with collective spin observables [Kunkel *et al.*, 2019].

Main contributions

In Chapter 7 we present two methodologies to derive three-outcome few-body symmetric Bell inequalities valid for many-body systems: (i) one based on projecting the set of local correlations to the two-body symmetric affine space for three outcomes; and (ii) a methodology that relaxes the set of local correlations to exploit its algebraic properties and explore all three-outcome two-body symmetric Bell inequalities at once through a feasibility problem. We also present an optimization toolset to characterize any d outcome few-body symmetric Bell inequality based on two steps: (i) a continuous parametrization of unitaries that allows to employ typical optimization techniques with quantum qudit observables; and (ii) an SDP of polynomial size to optimize over qudit symmetric states based on the method to solve the QMP for symmetric states.

We present a selected class of three-outcome two-body symmetric Bell inequality which is useful for many-body systems, and we proceed to characterize it. We illustrate how the methodology presented allows to detect nonlocality with the selected Bell inequality. From it, we discover an analytical class of qutrit symmetric states which violate the Bell inequality and could be used to characterize its asymptotic limit. Finally, we show that the Bell inequality is useful to detect non-local correlations in ground states of relevant three-level physical models, in particular in the three-orbital LMG Hamiltonian [Meredith

et al., 1988; Gnutzmann *et al.*, 2000; Graß *et al.*, 2013].

The results are an unpublished joint work with M. Fadel, M. Lewenstein and J. Tura.

Chapter 2

Preliminaries: key concepts

This chapter is devoted to introduce some of the concepts recurrent throughout the thesis. The aim of the chapter is conciseness and completeness, while setting the notation. The reader may skip ahead and use the chapter as a reference when opportune.

2.1 Symmetric quantum states

Prelude: Quantum states

In quantum physics, the state of a physical system, a *quantum state*, is represented by a normalized element of a Hilbert space $\mathcal{H}$. Hilbert spaces generalize Euclidean spaces by considering complex vector spaces which are complete with the structure of an inner product. Hermitian operators then play the role of observables by acting as linear transformations on quantum states. While quantum mechanics offers an abstract formulation where a particular representation is not required, it is often convenient to represent quantum states as vectors. Originally quantum mechanics considered infinite-dimensional Hilbert spaces, but it was soon formalized for finite-dimensional systems [Weyl, 1931] routinely used in fields like quantum optics or quantum information. For the purposes of the present thesis, we shall consider only

finite-dimensional $\mathcal{H}$ over the field of complex numbers $\mathbb{C}$.

Consider then a d-dimensional complex Hilbert space; *i.e.,* $\mathcal{H} = \mathbb{C}^d$. For instance, the case $d = 2$ corresponds to a system formed by a single *qubit*, $d = 3$ to a *qutrit*, etc. In order to account for quantum statistical mechanics [Von Neumann, 1927], a quantum state can then be represented by a self-adjoint positive semidefinite linear operator ρ of unit trace (which in this context accounts for normalization). The state ρ is then an Hermitian operator $\rho = \rho^\dagger$ acting on $\mathcal{H}$ which, upon the choice of a basis, can be represented as a $d \times d$ matrix with complex entries called the *density matrix*.

Density matrices ρ describing quantum states on $\mathcal{H}$ form a convex set $\mathcal{D}(\mathcal{H}) = \{\rho \,|\, \rho \succeq 0, \mathrm{Tr}(\rho) = 1, \rho = \rho^\dagger\}$. The so-called *pure states* are the extremal points of $\mathcal{D}(\mathcal{H})$ and their interpretation is that one has complete knowledge on the quantum state the system is in. Pure states correspond to density matrices ρ with rank one and, thus, can be described by a single ket vector $|\psi\rangle \in \mathcal{H}$ such that $\rho = |\psi\rangle\langle\psi|$. A convenient orthonormal basis in $\mathcal{H}$ for ket vectors representation is the so-called *computational basis*; *i.e.,* the set of vectors $\{|i\rangle \,|\, i \in \mathbb{Z}, 0 \leq i < d\}$. On the other hand, *mixed states* are non-trivial convex combinations of pure states; *i.e.,* $\rho = \sum_i p_i \, |\psi_i\rangle\langle\psi_i|$ where $p_i \geq 0$ and $\sum_i p_i = 1$ for all i. Thus, mixed states account for statistical ensembles where the pure state $|\psi_i\rangle$ is produced with probability p_i. Notice that the convex set $\mathcal{D}(\mathcal{H})$ is equivalent to the convex hull of its pure states.

To account for composite quantum systems, *i.e.* systems formed by several subsystems, quantum mechanics takes the *tensor product* among the Hilbert spaces of the subsystems. Suppose that we have a composite system formed by n subsystems, then the corresponding n-partite Hilbert space is $\mathcal{H} = \bigotimes_{i=1}^{n} \mathcal{H}_i$, where $\mathcal{H}_i$ is the Hilbert space for the i-th subsystem, and its dimensions are the product of the local Hilbert spaces dimensions; *i.e.,* $\dim(\mathcal{H}) = \prod_{i=1}^{n} \dim(\mathcal{H}_i)$. Given a composite quantum state $\rho \in \mathcal{D}(\mathcal{H})$, it is possible to obtain its subsystems states $\rho^i \in \mathcal{D}(\mathcal{H}_i)$, called *reduced states*, by performing the *partial trace*. For instance, consider a quantum state ρ acting on a bipartite composite quantum system $\mathcal{H} = \mathcal{H}_A \otimes \mathcal{H}_B$, then the reduced state of

ρ on system A, labelled ρ^A, can be obtained by performing the partial trace of ρ with respect to the system B. That is, $\mathrm{Tr}_B(\rho) = \rho^A$.

Permutationally invariant quantum states

A particular feature of quantum mechanics is the existence of the so-called *indistinguishable particles*. Indistinguishable particles refers to the case when two or more particles (*e.g.* electrons, photons, ...) have exactly the same intrinsic properties (*e.g.* spin, electrical charge, mass, ...). In other words, indistinguishable particles have the same defining properties and behave in the same way when probing those properties.

When having a composite quantum system formed by indistinguishable particles, the quantum state describing the composite remains invariant under *any* permutation of its subsystems. This motivates a subclass of quantum states called Permutationally Invariant (PI) states. Formally,

Definition 2.1.1. *Let $\rho \in \mathcal{D}(\mathcal{H})$ be an n-partite quantum state acting on $\mathcal{H} = (\mathbb{C}^d)^{\otimes n}$. Let $\mathcal{S}_n$ be the group of permutations of n elements. Then ρ is said to be* permutationally invariant *if*

$$\rho = V(\pi)\rho V^\dagger(\pi), \qquad \forall \pi \in \mathcal{S}_n(\pi) \tag{2.1}$$

where $V(\pi)$ is the standard representation of the permutation $\pi \in \mathcal{S}_n$ which permutes each component of the computational basis of $\mathcal{H}$.

The symmetry involved in PI quantum states results in redundancies when represented in, for instance, the computational basis. In fact, the redundancies allow for a simpler and more efficient representation. When considering PI quantum states the Hilbert space $\mathcal{H} = (\mathbb{C}^d)^{\otimes n}$, often represented as a $d^n \times d^n$ matrix, can get block-diagonalized by means of the Schur-Weyl duality, a known result from representation theory [Schur, 1901; Weyl, 1946] (see [Fulton *et al.*, 1991] for a more contemporary take on the subject). In particular, the general Hilbert space can get decomposed as:

$$(\mathbb{C}^d)^{\otimes n} \cong \bigoplus_{\lambda \vdash (d,n)} \mathcal{K}_\lambda \otimes \mathcal{H}_\lambda, \tag{2.2}$$

where λ takes all the partitions of n with at most d elements, and $\mathcal{K}_\lambda$ is the multiplicity space. For more details see for instance [Aulbach, 2012; Moroder *et al.*, 2012; Christandl, 2006; Tura, 2017]. Each block will have size $\mathcal{O}\binom{n+d-1}{d-1}$ and will be an invariant subspace corresponding to different spin components. For our purposes, it is sufficient to know that there exists a convenient symmetry-adapted orthonormal basis to represent PI states which block-diagonalizes them. In the present thesis, our interest lies on the particular block of the decomposition corresponding to the largest spin component, which describes the subclass of PI states called *symmetric states*. We present them in what follows.

Symmetric states

A particular subclass of quantum states to be considered throughout the thesis are the so-called called *symmetric states*. These correspond to a subclass of PI quantum states, and are spanned by the *Dicke states*. Dicke states were firstly characterized in the context of superradiance [Dicke, 1954]. Dicke states are used in many distinct contexts, to mention a few: they are defined as the simultaneous eigenstates of the total angular momentum and its z-component (see for instance [Aulbach, 2012]); to appear as ground states of physical systems described by the LMG model (see for instance [Latorre *et al.*, 2005]); to serve for quantum-enhanced metrology [Zhang and Duan, 2014; Apellaniz *et al.*, 2015]; or to be routinely used experimentally [Lu *et al.*, 2007; Wieczorek *et al.*, 2009; McConnell *et al.*, 2015], recently achieving Dicke states with more than 10000 atoms in a ^{87}Rb spin-1 Bose-Einstein condensate [Zou *et al.*, 2018].

Dicke states are often introduced for qubit systems, where they are fully specified by the number of qubits n and the number of excitations k (that is, k of its subsystems are on the excited state $|1\rangle$).

Definition 2.1.2. *An n-qubit Dicke state with k excitations is denoted*

$|D_k^n\rangle$ *and can be expressed as:*

$$|D_k^n\rangle \propto \sum_{\pi\in\mathcal{S}_n} \pi(|0\rangle^{\otimes n-k} |1\rangle^{\otimes k}), \tag{2.3}$$

where $\pi \in \mathcal{S}_n$ *permutes each component of the computational basis of* $\mathcal{H}$*, i.e. one sums over all possible permutations of having* k *excited subsystems, and the Dicke state has* $\binom{n}{k}$ *distinct elements.*

Consider as an example the half-filled Dicke state for $n = 4$ qubits. The state then has $k = 2$ excitations with equal weigh probability to be in each subsystem. That is:

$$|D_2^4\rangle = \frac{1}{\sqrt{6}} \left(|0011\rangle + |0101\rangle + |0110\rangle + |1001\rangle + |1010\rangle + |1100\rangle\right). \tag{2.4}$$

A feature of Dicke states, that we exploit in Chapters 3 and 6, is that they span the symmetric space. That is, if we denote the symmetric space as $\mathrm{Sym}(\mathcal{H})$, then $\mathrm{Sym}(\mathcal{H}) := \mathrm{Span}\{|D_k^n\rangle\}_{k=0,\dots,n}$.

However, through the thesis we do not restrict to multipartite qubit systems but consider also the more general case of multipartite qudit systems acting on the Hilbert space $(\mathbb{C}^d)^{\otimes n}$. For such case, specifying how many $|1\rangle$ excitations there are is not enough, since one also has to specify how many $|2\rangle$ excitations there are, $|3\rangle$ excitations, etc. A natural notation to deal with such scenario is to consider partitions of n into d elements. In particular, let us denote as $\boldsymbol{\lambda} \vdash n$ the partition of n in d elements. Then $\boldsymbol{\lambda}$ is a d-dimensional vector $\boldsymbol{\lambda} = (\lambda_0, \dots, \lambda_{d-1})$, where $\lambda_i \in \mathbb{Z}_{\geq 0}$ counts the number of subsystems in the state $|i\rangle$ and $\sum_{i=0}^{d-1} \lambda_i = n$. Following this notation:

Definition 2.1.3. *An* n*-qudit Dicke state with number of excitations given by* $\boldsymbol{\lambda}$ *is denoted* $|D_{\boldsymbol{\lambda}}\rangle$ *and can be expressed as:*

$$|D_{\boldsymbol{\lambda}}\rangle \propto \sum_{\pi\in\mathcal{S}_n} \pi(|0\rangle^{\otimes\lambda_0} |1\rangle^{\otimes\lambda_1} \cdots |d-1\rangle^{\otimes\lambda_{d-1}}), \tag{2.5}$$

where the Dicke state has $\binom{n}{\boldsymbol{\lambda}}$ *different elements, given by the following multinomial combinatorial quantity:*

$$\binom{n}{\boldsymbol{\lambda}} = \frac{n!}{\lambda_0!\lambda_1!\cdots\lambda_{d-1}!}. \tag{2.6}$$

Because there are as many Dicke states as partitions of n into d subsets (some of which might be empty), a symmetric state can be represented in a subspace of $(\mathbb{C}^d)^{\otimes n}$ with dimensions:

$$\dim\left(\{|D_{\boldsymbol{\lambda}}\rangle \;\middle|\; \boldsymbol{\lambda} \vdash n\}\right) = \begin{pmatrix} n+d-1 \\ d-1 \end{pmatrix}. \tag{2.7}$$

Therefore, instead of representing symmetric states in $(\mathbb{C}^d)^{\otimes n}$ as $d^n \times d^n$ matrices which grow exponentially in n, one can represent symmetric states in the Dicke basis reducing the representation to $\binom{n+d-1}{d-1} \times \binom{n+d-1}{d-1}$ matrices that grow polynomially in n with degree $d-1$. For instance, a qubit symmetric state $\rho \in \mathcal{D}(\mathrm{Sym}(\mathcal{H}))$ has rank at most $n+1$, the number of elements in Eq. (2.3). As we shall see in Chapters 3, 4, 6 and 7, such a drastic reduction of representation complexity will be crucial to obtain many results for the present thesis on situations that would have been otherwise unapproachable.

2.2 Entanglement and separability

Entanglement [Horodecki *et al.*, 2009] is a core property of quantum physics that has revolutionized our perspective on the laws of nature. One of the characteristic features of entanglement is that it can give rise to correlations that go beyond the local-realism principle [Einstein *et al.*, 1935], nowadays referred to as *Bell non-local* correlations or simply as *nonlocality* [Brunner *et al.*, 2014; Scarani, 2019]. Precisely the possibility of having non-local correlations was firstly brought up as an argument on why quantum mechanics *is not* a complete theory [Einstein *et al.*, 1935]. Such argument was the origin many debates, where the counterpart defended that quantum mechanics *is* a complete theory

[Bohr, 1935] that forces us to reconsider the concepts of causality, determinism and locality. However, the exchange of arguments, initiated in the early 30s, remained on a philosophical level for decades without any possible test in sight to prove or disprove the claims. That is until the early 60s, when J. S. Bell presented his seminal work [Bell, 1964], which offers a test in the form of inequalities, called *Bell inequalities*, that set a bound on what statistical correlations can be observed under local-realist theories. Since then, the violation of Bell inequalities have been experimentally observed again and again [Freedman and Clauser, 1972; Aspect *et al.*, 1982; Giustina *et al.*, 2013] until there was no doubt left of the existence of nonlocality [Hensen *et al.*, 2015; Collaboration, 2018]. Thus, confirming the predictions of quantum mechanics on entanglement and its non-classical correlations.

2.2.1 Separability

The property of entanglement manifests in composite quantum systems. In order to understand entanglement, first we need to introduce the notion of *separability*. Roughly speaking, separability refers to the case when a global quantum state $\rho \in \mathcal{D}(\mathcal{H})$ acting on a Hilbert space $\mathcal{H} = \bigotimes_{i=1}^{n} \mathcal{H}_i$, where $\mathcal{H}_i$ denotes the Hilbert space corresponding to the i-th subsystem, can be fully described in terms of the local quantum states $\rho^i \in \mathcal{D}(\mathcal{H}_i)$. However, it is known that in quantum theory this is not always the case, giving rise to entanglement. Formally, for a bipartite composite quantum system:

Definition 2.2.1. *Let ρ be a bipartite quantum state acting a the Hilbert space $\mathcal{H} = \mathcal{H}_A \otimes \mathcal{H}_B$. Then, ρ is said to be* separable *if it admits the following convex decomposition*

$$\rho = \sum_i \lambda_i \rho_i^A \otimes \rho_i^B, \tag{2.8}$$

where ρ_i^A (ρ_i^B) denotes a quantum state acting on $\mathcal{H}_A$ ($\mathcal{H}_B$) and λ_i form a convex combination (i.e., $\lambda_i \geq 0$ and $\sum_i \lambda_i = 1$).

Therefore, one can define entanglement for bipartite systems as:

Definition 2.2.2. *Let ρ be a bipartite quantum state acting on the Hilbert space $\mathcal{H} = \mathcal{H}_A \otimes \mathcal{H}_B$. Then, ρ is said to be* entangled *if it is not separable. That is, if it does not allow a convex decomposition of the form in Eq. (2.8).*

Up until now we have been considering separability in the bipartite case. For the multipartite setting, *i.e.,* composite quantum systems involving more than 2 subsystems, the definition of separability is much richer. It admits many generalizations [Szalay and Kökényesi, 2012; Szalay, 2015, 2019] which give rise to different notions and strengths of entanglement [Gühne and Tóth, 2009].

The most natural and straightforward generalization from the bipartite case is the so-called *K-separability*. Consider a set of n parties indexed by $[n] := \{0, \ldots, n-1\}$. The notion of K-separability takes into account all the possible partitions of $[n]$ into K pairwise disjoint non-empty sets, *i.e.* $\mathcal{A}^1, \ldots, \mathcal{A}^K \subsetneq [n]$ such that $\mathcal{A}^i \neq \emptyset$, $\mathcal{A}^i \cap \mathcal{A}^j = \emptyset$ for $i \neq j$ and $\bigcup_{k=1}^K \mathcal{A}^k = [n]$. Following this notation,

Definition 2.2.3. *Let $\mathcal{P}_K$ be the set formed by all the partitions $\mathcal{P}$ of $[n]$ into K pairwise disjoint non-empty subsets $\mathcal{A}^k \in \mathcal{P}$. Then, a quantum state ρ acting on $\mathcal{H} = \bigotimes_{k=1}^K \mathcal{H}_{\mathcal{A}^k}$ is called K-separable if it can be decomposed as:*

$$\rho = \sum_{\mathcal{P} \in \mathcal{P}_K} \lambda_{\mathcal{P}} \sum_i \lambda_i^{\mathcal{P}} \bigotimes_{k=1}^K \rho_i^{\mathcal{A}^k}, \tag{2.9}$$

where $\lambda_{\mathcal{P}}$ and $\lambda_i^{\mathcal{P}}$ form their respective convex combinations and $\rho_i^{\mathcal{A}^k} \in \mathcal{D}(\mathcal{H}_{\mathcal{A}^k})$.

Therefore, we observe that multipartite entanglement offers many types of partial separability, as opposed to bipartite entanglement where a state is either separable or not. Of particular interest is the case when a quantum state does not admit any type of K-separability, in which case the state is called to be *Genuinely Multipartite Entangled*

(GME). Exemplary quantum states that are GME include the GHZ state [Greenberger *et al.*, 2007; Pan *et al.*, 2000] and all entangled symmetric states [Tura *et al.*, 2012b; Augusiak *et al.*, 2012; Huber *et al.*, 2011]. On the other extreme, an n-partite quantum state is called *fully separable* when it is n-separable. Let us remark that there exist other notions to deal with entanglement in the multipartite case. In fact, in Chapter 4 we will consider the equivalent notions of *entanglement depth* [Sørensen and Mølmer, 2001] and *k-producibility* [Gühne *et al.*, 2005], which instead of considering the partitions of the composite they characterize multipartite entanglement by considering the subsystem within the composite containing the largest amount of GME particles (in Section 4.1 we expand on details).

While the definition of entanglement is clear, to decide whether a given arbitrary quantum state is separable or entangled is in general far from an easy task, referred to as *the separability problem*. The separability problem is formally stated as: given a quantum state $\rho \in \mathcal{D}(\mathcal{H})$, does it admit a decomposition of the form in Eq. (2.8)? Despite its simple formulation, the separability problem is shown to be an NP-hard problem [Gurvits, 2003].

Consequently, researchers have looked for simpler criteria that certifies whether a given ρ is entangled [Horodecki *et al.*, 2009]. While the problem remains open, of special interest are the so-called PPT criterion and the so-called *Entanglement Witnesses*, which provide sufficient conditions to certify the presence of entanglement.

2.2.2 PPT criterion

The *Positive under Partial Transposition* (PPT) criterion [Peres, 1996] provides simple and efficient entanglement detection criteria for bipartite quantum states. The PPT criterion states that if a bipartite $\rho \in \mathcal{D}(\mathcal{H})$ admits the convex decomposition in Eq. (2.8), then ρ must remain positive semi-definite when the transposition T is applied on the local Hilbert space of one of its subsystems; *i.e.*, $(\mathbb{1} \otimes T)[\rho] \succeq 0$.

The operation of transposing one of its subsystems is called *par-*

tial transposition. For instance, applying the partial transposition on Bob's side is denoted as $\rho^{\Gamma_B} := (\mathbb{1} \otimes T)[\rho]$. Let us note that the PPT criterion does not depend on which side of the system the transposition is applied on, since $(\rho^{\Gamma_B})^T = \rho^{\Gamma_A}$. Because $\rho^A \in \mathcal{D}(\mathcal{H}_A)$ and $\rho^B \in \mathcal{D}(\mathcal{H}_B)$ are valid quantum states (*i.e.,* positive semi-definite with unit trace) describing the subsystems, they must remain positive semi-definite after the transposition operation has been applied on them. Hence, the PPT criterion can only be broken when the original state ρ does not admit the decomposition in Eq. (2.8) in the first place. In other words, breaking the PPT criterion certifies the presence of entanglement. However, it only provides necessary and sufficient condition for two qubit [Størmer, 1963] and qubit-qutrit [Woronowicz, 1976] systems. For systems with larger physical dimension there exist counterexamples of states that are PPT but nonetheless entangled [Horodecki, 1997]. Despite not solving the separability problem in the general case, its simple operational character makes of the PPT criterion a very convenient sufficient criterion that finds many applications as we shall see in Chapters 3 and 4.

2.2.3 Entanglement Witnesses

The so-called Entanglement Witness (EW) [Horodecki *et al.*, 1996; Terhal, 2000] constitute another fundamental tool for entanglement detection. EWs correspond to operators that allow to detect entangled states. It is worth noting that the concept behind EWs comes from convex geometry, in particular it is based on the Hahn-Banach theorem,a known result from functional analysis, which allows to characterize convex sets by means of separating hyperplanes (see [Horodecki *et al.*, 1996] for more details). Formally,

Definition 2.2.4. *Let W be an Hermitian operator acting on $\mathcal{H}$ and let $\mathcal{D}_{Sep}(\mathcal{H})$ denote the set of all separable quantum states acting on $\mathcal{H}$. Then W is said to be an* Entanglement Witness *if it satisfies the following conditions:*

(i) $\mathrm{Tr}\,(W\tilde{\rho}) \geq 0$, $\forall \tilde{\rho} \in \mathcal{D}_{Sep}(\mathcal{H})$,

(ii) $\exists\, \rho \in \mathcal{D}(\mathcal{H})$ *s.t.* $\mathrm{Tr}\,(W\rho) < 0$,

where $\mathrm{Tr}\,(W\rho)$ corresponds to the expectation value by taking the usual Hilbert-Schmidt scalar product $\langle W, \rho\rangle = \mathrm{Tr}\left(W^\dagger \rho\right)$. Therefore, the observable W is an EW if it has nonnegative expectation value for all possible separable quantum states, and it has at least one negative eigenvalue; *i.e.*, $W \not\succeq 0$.

In the bipartite setting, a notable classification of EWs is to distinguish between the so-called *decomposable* EWs and *non-decomposable* EWs.

Definition 2.2.5. *An entanglement witness* W^{dec} *is said to be* decomposable *if there exist operators* $P \succeq 0$ *and* $Q \succeq 0$ *such that*

$$W = P + Q^{\Gamma_B}, \tag{2.10}$$

where the partial transposition can be indistinctly taken on any subsystem. If W *cannot be expressed as in Eq. (2.10), then* W *is said to be a non-decomposable EW.*

Relating to the PPT criterion previously seen, while decomposable EWs are easier to characterize they do not detect PPT states which are entangled, as can be easily seen:

Lemma 2.2.1. *Decomposable EWs do not detect entanglement on any PPT state.*

Proof. *Consider a decomposable EW denoted* $W = P + Q^{\Gamma_B}$ *and consider an entangled quantum state* ρ *acting on* $\mathcal{H} = \mathcal{H}_A \otimes \mathcal{H}_B$ *which is PPT; i.e.,* $\rho^{\Gamma_B} \succeq 0$. *Then,*

$$\mathrm{Tr}\,(W\rho) = \mathrm{Tr}\,(P\rho) + \mathrm{Tr}\left(Q^{\Gamma_B}\rho\right) = \mathrm{Tr}\,(P\rho) + \mathrm{Tr}\left(Q\rho^{\Gamma_B}\right) \geq 0, \tag{2.11}$$

where the cyclicity of the (partial) trace has been used.

□

An important question regarding EWs is to ask about their optimality [Lewenstein *et al.*, 2000, 2001]. When comparing two entanglement witnesses denoted W_1 and W_2, one says that W_1 is *finer* than W_2 if all the entangled quantum states detected by W_2 are also detected by W_1. Then, an entanglement witness W is called *optimal* if there does not exist any other entanglement witness $\tilde{W}$ finer than W. If one interprets an EW as the hyperplanes bounding from the outside the convex set of separable states, then the EW is said to be optimal when it is tangent to the set of separable states.

2.3 Nonlocality and the multipartite Bell experiment

Bell inequalities suppose a natural tool for entanglement detection. That is, nonlocality [Brunner *et al.*, 2014; Scarani, 2019], as witnessed by the violation of a Bell inequality, certifies the presence of entanglement. From a quantum theory point of view, Bell inequalities can be seen as entanglement witnesses [Terhal, 2000]. However, as briefly mentioned when introducing entanglement, the concept of nonlocality is based on the principles of local-realism[1] [Einstein *et al.*, 1935; Bell, 1964]. Hence, it is worth noting the subtlety that nonlocality is not necessarily linked to quantum mechanics, albeit quantum mechanics exhibits non-local correlations. Nevertheless, nonlocality has settled as one of the building blocks in modern physics where, apart from its role in quantum foundations, have also driven the recent paradigm shift in quantum protocols [Lydersen *et al.*, 2010], often referred to as *Device-Independent Quantum Information Processing* (DIQIP) [Scarani, 2012a].

As we shall see, the characterization of non-local correlations is an

[1]Not to be confused with the *non-local* notion from the condensed matter field. Throughout the thesis, whenever we referred to *nonlocality* or *non-local correlations*, we shall refer *precisely* to the concept derived from the principles of local-realism.

extremely complex problem. The underlying mathematical complexity [Pitowsky, 1989] (NP-complete in the general case [Babai *et al.*, 1991]) has impeded a full characterization beyond the simplest Bell scenarios [Pitowsky and Svozil, 2001; Śliwa, 2003; Pironio, 2014]. As a result, most works present the Bell experiment in the bipartite or tripartite settings. However, in the present thesis we are interested in Bell inequalities for many-body systems. Hence, despite its complexity, in what follows we shall directly introduce the Bell experiment for the multipartite setting, which in Section 2.3.4 shall be simplified by considering symmetries and few-body correlation functions.

2.3.1 Many-body Bell experiment

A convenient way to introduce nonlocality is by considering the so-called *Bell-type experiments*. In a typical multipartite Bell-type experiment, an n-partite resource (*e.g.* a quantum state) is spatially distributed among n space-like separated observers, which we label from $[n] := \{1, 2, \ldots, n\}$. Each observer can then choose a measurement, out of m possible measurements choices, to be performed on their share of the system. We arbitrarily label the measurement choice of the i-th party as $x_i \in [m] := \{0, \ldots, m-1\}$, whereas the actual measurement performed by the i-th party will be labelled as $\mathcal{M}_{x_i}^{(i)}$. Each measurement then yields an outcome out of d different outcomes labelled $a_i \in [d] := \{0, \ldots, d-1\}$. This setup is referred to as an (n, m, d) *Bell scenario*, which is illustrated in Figure 2.1.

The procedure of distributing an n-partite resource, taking the measurement and collecting the outcomes is repeated over several rounds in order to collect statistics. The parties are allowed to communicate prior to the experiment, but once started they cannot know the measurement choices from the rest. The experiment can then be described in terms of conditional probabilities $p(\boldsymbol{a}|\boldsymbol{x})$, where $\boldsymbol{x} := (x_1, x_2, \ldots, x_n)$ gathers the choice of measurements for all n observers and $\boldsymbol{a} := (a_1, a_2, \ldots, a_n)$ gathers their obtained outcomes. Note that in the (n, m, d) Bell scenario the experiment will have $(md)^n$ possible configurations, from

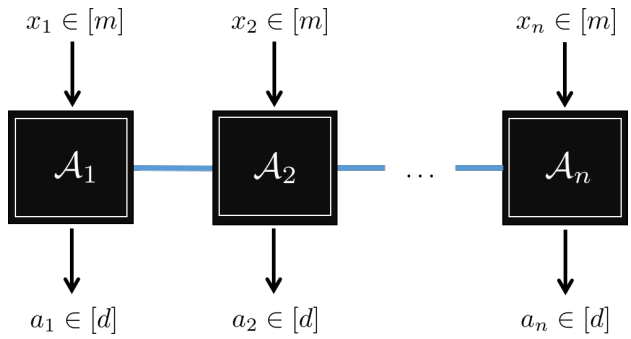

Fig. 2.1 Representation of the multipartite Bell scenario (n, m, d) in a device-independent manner. At each run, an n-partite resource is distributed among n parties which are space-like separated. Each party $\mathcal{A}_i \in \{\mathcal{A}_1, \ldots, \mathcal{A}_n\}$ then sets a measurement choice $x_i \in \{0, \ldots, m-1\}$ and collects the measurement outcome $a_i \in \{0, \ldots, d-1\}$.

which $m^n(d-1)^n$ remain linearly independent when considering that they form a valid probability distribution (*i.e.,* that the probabilities are non-negative and normalized). Consider then a vector $\vec{p} = \{p(\boldsymbol{a}|\boldsymbol{x}), \forall \boldsymbol{a}, \boldsymbol{x}\}$ which encodes all the $m^n(d^n-1)$ possible configurations and thus describes all the possible statistical correlations that can be observed on the experiment.

One can now restrict the probability distributions $\vec{p}$ so that the correlations are compatible with a physical theory. That is, given Bell scenario experimental setup, one has a systematic way to obtain physical insight from the observed statistics by adding constraints on the probability distributions. For instance, based on our classical intuition, one can consider that the conditional probabilities satisfy the principles of locality and realism [Einstein *et al.*, 1935] by taking into account the so-called Local Hidden Variable Model (LHVM) [Bell, 1964]:

$$p(\boldsymbol{a}|\boldsymbol{x}) = \int_{\Lambda} q(\lambda) \prod_{i=0}^{n-1} p(a_i|x_i, \lambda) d\lambda, \tag{2.12}$$

where λ is the so-called *hidden variable*, which is distributed according

to the probability density function $q(\lambda)$ and it is supported on the *hidden variable space* Λ. An operational interpretation often considered is that the parties involved can independently simulate $p(\boldsymbol{a}|\boldsymbol{x})$ without being able to communicate, only by having access to previously shared randomness (*i.e.,* knowing the values of λ for each round of the experiment) [Fine, 1982]. It can be shown that the probability distributions $p(a_i|x_i,\lambda)$ can be thought of as Local Deterministic Strategy (LDS), without loss of generality, by considering them to be deterministic response functions [Fine, 1982]. All the allowed correlations under an LHVM form a polytope[2], whose facets correspond to the so-called *tight Bell inequalities*. Let us denote as $\mathbb{P}_L$ the local polytope fulfilling a LHVM. Then, any correlation embedded in $\mathbb{P}_L$ can be described in a local-realist manner.

The existence of correlations that go beyond $\mathbb{P}_L$ has been observed and, thus, the laws of nature cannot be described in a local-realist manner. Quantum mechanics accounts for non-local correlations by capitalizing on properties that distinguish it from classical physics, like entanglement and non-commuting observables, though their relation to nonlocality is subtle. Consider a quantum state ρ acting on $\mathcal{H} = \bigotimes_{i=1}^{n} \mathcal{H}_i$ and measurements $\{\Pi_{a_i|x_i}\}_{a_i}$ corresponding to the Positive-Operator Valued Measure (POVM) elements of the x_i-th measurement performed at the i-th site. Under the quantum formalism, the probability distributions $p(\boldsymbol{a}|\boldsymbol{x})$ will be given by Born's rule [Born, 1955]:

$$p(\boldsymbol{a}|\boldsymbol{x}) = \mathrm{Tr}\left[\rho \bigotimes_{i=1}^{n} \Pi_{a_i|x_i}\right], \tag{2.13}$$

where one can consider, without loss of generality, that the POVM elements form a projective measurements by considering a purification of ρ, since the dimension of $\mathcal{H}$ has not been specified.

The quantum correlations arising from Eq. (2.13) form a convex set denoted $\mathcal{Q}$. Notice that all the correlations obtained under an LHVM can be recovered in quantum mechanics by considering, for in-

[2] A closed, bounded, compact convex set with finite number of vertices

stance, fully separable states [Werner, 1989]. Therefore, as illustrated in Figure 2.2, the quantum set contains the local polytope as a proper subset; *i.e.*, $\mathbb{P}_L \subset \mathcal{Q}$. Equivalently, quantum correlations offer a way to violate a Bell inequality. The violation of a Bell inequality by some composite quantum state certifies nonlocality and the presence of entanglement. However, although entanglement is a necessary condition to violate a Bell inequality, entanglement does not necessarily lead to non-local correlations [Werner, 1989]. Entangled states exist which can be described under a LHVM [Werner, 1989; Tóth and Acín, 2006; Augusiak *et al.*, 2014; Hirsch *et al.*, 2016, 2017; Augusiak *et al.*, 2015, 2018]. In this sense, nonlocality is a more demanding property than entanglement.

Let us note that there exist other physical models that can go beyond the correlations attainable under quantum mechanics. An operationally relevant one follows the so-called *Non-Signalling* (Non-Signalling (NS)) principle. The NS principle follows the idea that the speed at which information is transmitted is finite, and consequently two space-like separated events cannot influence each other instantaneously. In the context of Bell-type experiments, this implies that the choice of measurements by one of the parties cannot instantaneously influence the rest. Consequently, the parties must observe the same marginal probability distribution. Formally, under the NS principle the conditional probabilities $p(\boldsymbol{a}|\boldsymbol{x})$ fulfill:

$$p(a_1, \ldots, \hat{a}_i, \ldots, a_n|x_1, \ldots, \hat{x}_i, \ldots, x_n) \equiv \sum_{a_i \in [d]} p(a_1, \ldots, a_n|x_1, \ldots, x_n), \tag{2.14}$$

for all $i \in [n], x_i \in [m]$, where $\hat{\cdot}$ denotes the absence of that coordinate and, in this case, the $\equiv$ symbol means that the Left hand side (LHS) of Equation (2.14) is well-defined; *i.e.*, it does not depend on the value of x_i. As illustrated in Figure 2.2, the correlations fulfilling the NS principle form a polytope, denoted $\mathbb{P}_{\text{NS}}$, which contains the quantum correlations set as a proper subset; *i.e.* $\mathcal{Q} \subset \mathbb{P}_{\text{NS}}$ [Popescu and Rohrlich, 1994].

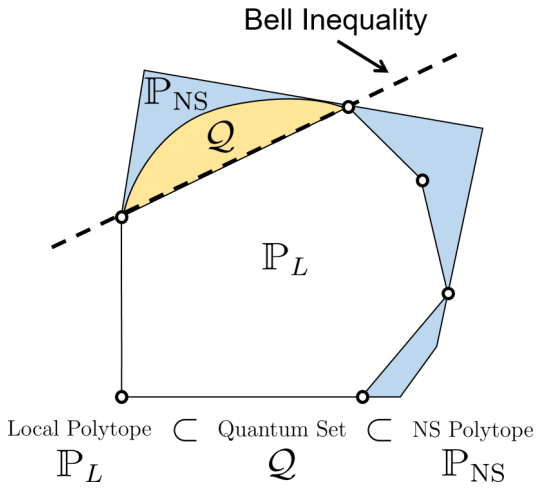

Fig. 2.2 Geometrical interpretation of the correlation sets attainable in a Bell-type experiment. The local polytope $\mathbb{P}_L$ is obtained by those correlations fulfilling Eq. (2.12), the quantum set by the correlations fulfilling Eq. (2.13), and NS polytope by the correlations fulfilling Eq. (2.14). The Bell inequality displayed represents a facet of $\mathbb{P}_L$, in which case is referred to as a *tight* Bell inequality. However, any hyperplane outside $\mathbb{P}_L$ can be considered a Bell inequality too. Hence, any statistical correlation obtained in a Bell-type experiment which violates a Bell inequality will signal non-local correlations, in the sense that the correlation cannot be an element of $\mathbb{P}_L$.

2.3.2 The device-independent framework

Although Bell tests have many applications in probing fundamental aspects of quantum theory, their approach is designed to be quantum theory independent. Consequently, there is an extra layer of significance behind Bell inequalities: a Bell experiment does not rely on assumptions (nor knowledge) on the resource being tested nor on the internal working of the measurement devices.

Notice that, as we have described the Bell experiment in the previous section and is illustrated in Figure 2.1, the parties involved in the Bell test can be seen as a black-box. In particular, the whole Bell-type

experiment is cast in the *Device-Independent* (DI) framework [Scarani, 2012a]. In the DI framework, physical properties are deduced solely from the observed statistics $p(\boldsymbol{a}|\boldsymbol{x})$ that describe the outputs $\boldsymbol{a}$ (the outcomes obtained), given some inputs $\boldsymbol{x}$ (the measurement choices). In other words, only the input-output relations between classical variables are relevant.

Hence, Bell inequalities open the possibility of witnessing entanglement in a DI approach. Because most of the *Quantum Information Processing* (QIP) tasks rely on entanglement, nonlocality supposes a powerful resource for device-independent certification in quantum technologies, opening the doors for the so-called *Device-Independent Quantum Information Processing* (DIQIP) tasks. The DI formalism arguably originated from the context of self-testing [Mayers and Yao, 1998]. Since then, DIQIP tasks have been considered in a variety of contexts like secure quantum key distribution [Acín *et al.*, 2007; Pironio *et al.*, 2009], secure extraction of random bits [Pironio *et al.*, 2010], or randomness amplification [Colbeck and Renner, 2012].

In Chapters 4 to 7 we consider the DI framework in the context of entanglement certification. More precisely, following the criteria established in [Bancal *et al.*, 2011b], we say an entanglement witness follows the DI framework when the test

- does not rely on the type of measurements,
- does not rely on the precision involved,
- does not rely on assumptions about the relevant Hilbert space dimension.

2.3.3 Multipartite Bell inequalities

In this section we take a closer look to the form multipartite Bell inequalities take. Let us start by considering a general (n, m, d) Bell scenario (see Section 2.3.1). Denote the measurement choices as $x_i \in [m]$ and the outcomes as $a_i \in [d]$. Furthermore, let us collect their

measurement choices in $\boldsymbol{x} := (x_1, \ldots, x_n)$ and their obtained outcomes in $\boldsymbol{a} = (a_1, \ldots, a_n)$. Let I be a linear combination of all possible conditional probabilities $p(\boldsymbol{a}|\boldsymbol{x})$:

$$I := \sum_{a_i \in [d]} \sum_{x_j \in [m]} \alpha_{\boldsymbol{a},\boldsymbol{x}} p(\boldsymbol{a}|\boldsymbol{x}), \tag{2.15}$$

where $\alpha_{\boldsymbol{a},\boldsymbol{x}} \in \mathbb{R}$. Then, a generic multipartite Bell inequality can be simply expressed as

$$I - \beta_c \geq 0, \tag{2.16}$$

where β_c is the so-called classical bound defined as $\beta_c = \min_{\text{LHVM}} I$, where the minimum is obtained by considering all the LHVM relations given by Eq. (2.12). Notice that, since any local correlation can be obtained from separable states, then $\beta_c \geq \min_{\mathcal{Q}} I$, where $\mathcal{Q}$ denotes the quantum set (c.f. Section 2.3.1). Hence, the equality case $\beta_c = \min_{\mathcal{Q}} I$ results in Bell inequalities that do not detect non-local correlations.

A particular case of interest is the multipartite Bell scenario with 2 outcomes (*i.e.*, $d = 2$), in which case one can equivalently describe the Bell-type experiment in terms of correlators[3] instead of conditional probabilities. To do so, let us assume without loss of generality that the outcomes a_i take values ± 1. Then, the one-body correlator corresponding to the measurement choice $k \in [m]$ by the party $i \in [n]$ is denoted $\langle \mathcal{M}_k^{(i)} \rangle$ and defined as

$$\langle \mathcal{M}_k^{(i)} \rangle = p_i(1|k) - p_i(-1|k). \tag{2.17}$$

Similarly, the two-body correlator corresponding to the measurement choices $k, l \in [m]$ by the parties $i, j \in [n]$, respectively, is given by the expectation value

$$\langle \mathcal{M}_k^{(i)} \mathcal{M}_l^{(j)} \rangle = p_{ij}(a_i = a_j|kl) - p_{ij}(a_i \neq a_j|kl). \tag{2.18}$$

The p-body correlator then gets similarly defined for any number $p \leq n$ of parties, yielding $\langle \mathcal{M}_{k_1}^{(i_1)} \ldots \mathcal{M}_{k_p}^{(i_p)} \rangle$, where $k_j \in [m]$ and

[3] Also referred to as *correlation functions*.

$i_j \in [n]$.Therefore, in the $(n, m, 2)$ scenario, a generic multipartite Bell inequality gets expressed as in Eq. (2.16), where this time I takes the form

$$I := \sum_{p\in[n]} \sum_{k_1,\ldots,k_p\in[m]} \sum_{1\leq i_1<\ldots<i_p\leq n} \alpha_{(i_1,\ldots,i_p),(k_1,\ldots,k_p)} \langle \mathcal{M}_{k_1}^{(i_1)} \ldots \mathcal{M}_{k_p}^{(i_p)} \rangle \,, \tag{2.19}$$

where $\alpha_{(i_1,\ldots i_p),(k_1,\ldots,k_p)} \in \mathbb{R}$ are the Bell inequality coefficients.

In Section 2.3.1 we have presented the local polytope $\mathbb{P}_L$ in the probability space. The same derivation follows when describing the experiment in terms of collections of correlators, where the vertices of $\mathbb{P}_L$ now correspond to the collection of correlators that factorize as

$$\langle \mathcal{M}_{k_1}^{(i_1)} \ldots \mathcal{M}_{k_p}^{(i_p)} \rangle = \langle \mathcal{M}_{k_1}^{(i_1)} \rangle \cdot \ldots \cdot \langle \mathcal{M}_{k_p}^{(i_p)} \rangle \,, \tag{2.20}$$

where every local expectation value is ± 1, $p \in [n]$, $k_j \in [m]$ and $i_j \in [n]$.

2.3.4 Multipartite symmetric Bell inequalities involving few-body correlators

As mentioned in Section 2.3.1, even in the simplest multipartite Bell scenario $(n, 2, 2)$ the high combinatorial complexity quickly renders the derivation of all Bell inequalities impractical. Furthermore, not only the derivation is highly complex, but also the characterization of such general multipartite Bell inequality. In order to reduce the complexity in the $(n, 2, 2)$ scenario, in [Tura *et al.*, 2014a, 2015] it was proposed to consider families of Bell inequalities inheriting the following properties:

- To describe the Bell experiment probing the system only with one- and two-body correlators.
- To relax the LHVM set to the subset where correlators follow the permutationally invariant symmetry.

These properties allow to derive families multipartite Bell inequalities that inherit desired properties [Tura *et al.*, 2014a, 2015] at the

expense of sacrificing some nonlocality detection ability, since they define an outer approximation to $\mathbb{P}_L$. In what follows we take a closer inspection on their properties.

2-body Bell inequalities

When restricting Bell experiments to involve only one- and two-body correlators (Eqs. (2.17) and (2.18) respectively), while omitting the rest of p-order correlators for $p > 2$ (Eq. (2.20)), one accordingly obtains Bell inequalities that involve at most two-body correlators. We refer to the resulting inequalities simply as *two-body Bell inequalities*, which can be expressed as in Eq. (2.16) where I is now defined as

$$I := \sum_{i\in[n]} \sum_{k\in[2]} \alpha_{i,k} \langle \mathcal{M}_k^{(i)} \rangle + \sum_{\substack{i,j\in[n] \\ i\neq j}} \sum_{k,l\in[2]} \alpha_{(ij),(kl)} \langle \mathcal{M}_k^{(i)} \mathcal{M}_l^{(j)} \rangle \,, \tag{2.21}$$

for some coefficients $\alpha_{i,k}, \alpha_{(ij),(kl)} \in \mathbb{R}$.

2-body permutationally invariant Bell inequalities

The omission of the highest-order correlators reduces some combinatorial complexity, although the problem still remains intractable. A way to further simplify is to relax the LHVM set to the subset where correlators follow the permutationally invariant symmetry. Under the permutationally invariant consideration, the Bell coefficients $\alpha_{i,k}, \alpha_{(i,j),(k,l)}$ in Eq. (2.21) will now not depend on the parties $i, j \in [n]$; *e.g.* $\alpha_{i,k} = \alpha_k$ for all $i \in [n]$. Therefore resulting in two-body Bell inequalities that can be described in terms of the following one- and two-body symmetric correlators:

$$\langle \mathcal{S}_k \rangle := \sum_{i\in[n]} \langle \mathcal{M}_k^{(i)} \rangle \,, \qquad \langle \mathcal{S}_{kl} \rangle := \sum_{i\neq j\in[n]} \langle \mathcal{M}_k^{(i)} \mathcal{M}_l^{(j)} \rangle \,. \tag{2.22}$$

Hence, the two-body Permutationally Invariant Bell Inequalities (PIBIs) are the family of multipartite Bell inequalities that can be

expressed as Eq. (2.16), where I is now defined as

$$I := \sum_{k\in[m]} \alpha_k \mathcal{S}_k + \sum_{k\leq l\in[m]} \alpha_{kl} \mathcal{S}_{kl}, \tag{2.23}$$

for some $\alpha_k, \alpha_{kl} \in \mathbb{R}$.

Recently, the two-body PIBIs have appeared in various contexts [Tura *et al.*, 2014a, 2015; Pelisson *et al.*, 2016a; Wagner *et al.*, 2017; Fadel and Tura, 2017; Deng, 2018; Fadel and Tura, 2018], including experimental implementations [Pelisson *et al.*, 2016b; Schmied *et al.*, 2016; Engelsen *et al.*, 2017]. In the present thesis, the two-body PIBIs are a key ingredient to obtain results in Chapters 4 to 6. Furthermore, in Chapter 7 we present a generalization for the three outcome Bell scenario $(n, 2, 3)$.

Chapter 3

The separability problem for diagonal symmetric states

Alongside the fundamental interest of entanglement, the interest of entanglement as a resource keeps growing. Despite the extra attention, the separability problem (see Section 2.2.1) remains elusive and, in fact, has been shown to be an NP-hard problem in its general case [Gurvits, 2003]. The positive under partial transposition (PPT) criterion (see Section 2.2.2) provides sufficient, simple and efficient criteria to certify entanglement on those quantum states that break the PPT condition. For low-dimensional systems, such as qubit-qubit or qubit-qutrit systems, the PPT criterion has been shown to provide necessary and sufficient conditions, thus fully characterizing separability and entanglement [Horodecki *et al.*, 1996; Størmer, 1963; Woronowicz, 1976]. However, for higher-dimensional systems the correspondence between separability and fulfilling the PPT criterion does not hold: there exist entangled states that fulfill the PPT criterion [Horodecki, 1997].

Several works have considered narrowing down the separability problem for simpler physical systems of interest, like symmetric states. For instance, the PPT criterion has been shown to provide necessary and sufficient conditions for 3-qubit symmetric states [Eckert *et al.*, 2002]. However, adding one more qubit or more already breaks the

necessary property [Tura *et al.*, 2012a; Augusiak *et al.*, 2012]. While several works provide separability criteria for symmetric states (see *e.g.* [Tura, 2017]), the separability problem for symmetric states remains open.

Consequently, the separability problem and entanglement characterization has also been considered for diagonal symmetric states (DSS). These are mixtures of Dicke states that are diagonal in the Dicke basis, thus forming a subclass of symmetric states. In particular, it has been shown that for n-qubit DSS the PPT criterion with respect to every bipartition provides necessary and sufficient conditions for separability [Wolfe and Yelin, 2014; Yu, 2016]. Furthermore, for DSS systems formed by two qudits of dimension $d < 5$, it has been shown that the PPT criterion provide necessary and sufficient conditions [Yu, 2016]. As for the general DSS case, the separability problem has been shown to still remain an NP-hard problem [Yu, 2016], which we independently recover in the results of the present chapter.

In this chapter we are interested in the characterization of entanglement and separability for DSS, the subclass of symmetric states. The chapter is organized as follows: In Section 3.1 we start by recalling the separability problem and pose it for bipartite DSS. In Section 3.2 we introduce some notions from the field of non-convex quadratic optimization. In Section 3.3 we characterize the separability problem for DSS by finding a connection to the field of non-convex quadratic optimization. Finally, in Section 3.4 we present entanglement witnesses and sufficient separability conditions for DSS.

The original results presented in this chapter are based on the publication [Tura *et al.*, 2018], a joint collaboration between J. Tura, R. Quesada, M. Lewenstein and A. Sanpera.

3.1 The separability problem for diagonal symmetric states

When a problem is too hard to tackle in its general form, one may approach a simpler version in search for a new piece of the puzzle. In this chapter, we restrict the entanglement characterization to bipartite diagonal symmetric qudit quantum states, the so-called Diagonal Symmetric States. That is, DSS are bipartite symmetric states which are diagonal in the Dicke basis. Formally:

Definition 3.1.1. *Let ρ be a quantum state acting on $\mathbb{C}^d \otimes \mathbb{C}^d$. The state ρ is said to be Diagonal Symmetric if, and only if, ρ can be written in the form*

$$\rho = \sum_{0 \leq i \leq j < d} p_{ij} \left|D_{ij}\right\rangle\!\left\langle D_{ij}\right|, \tag{3.1}$$

where $p_{ij} \geq 0$, $\sum_{ij} p_{ij} = 1$, $|D_{ii}\rangle := |ii\rangle$ and $|D_{ij}\rangle = (|ij\rangle + |ji\rangle)/\sqrt{2}$.

Let us note that in Section 2.1 we have introduced the Dicke states in its general form for multipartite qudit systems, denoted $|D_{\boldsymbol{\lambda}}\rangle$. In this chapter, however, we consider only *bipartite* qudit symmetric systems. Hence, because the terminology *Dicke states* often refers to the multipartite case, for this chapter it is convenient to introduce the notation $|D_{ij}\rangle$, established in Definition 3.1.1, and henceforth simply refer to them as *symmetric states*.

The separability problem for $\mathbb{C}^d \otimes \mathbb{C}^d$ Diagonal Symmetric (DS) states was independently proven to be an NP-hard problem in [Yu, 2016] before our work. Nonetheless, we independently recover the result by finding a connection to the field of quadratic conic optimization, with said connection having its own interest.

3.2 Overview of quadratic conic optimization and completely positive matrices

Before jumping into the results, let us briefly introduce some concepts behind quadratic conic optimization problems which will facilitate to stablish the equivalence connection among fields later on. For a comprehensive review on quadratic conic optimization and completely positive matrices see, for instance [Berman *et al.*, 2015].

A big part of the quadratic conic optimization fields is interested in the characterization of the so-called Completely Positive (CP)[1] matrices. Formally, CP matrices are defined as follows:

Definition 3.2.1. *Consider a $d \times d$ matrix A. A is said to be* completely positive *if, and only if, it can be decomposed as $A = B \cdot B^T$, where B is a $d \times k$ matrix for some $k \geq 1$ such that $B_{ij} \geq 0$.*

The set of $d \times d$ CP matrices form a proper[2] cone, denoted $\mathcal{CP}_d$. Therefore, addition between two CP matrices result in another CP matrix, as well as multiplying a CP matrix by a non-negative scalar.

Let us note that through this chapter, whenever we refer to the term *completely-positive* we refer to the one defined in Definition 3.2.1. Not to be confused with the concept of completely positive maps common in the context of quantum information.

Part of the interest in CP matrices lies in that non-convex quadratic optimization problems, in general NP-hard, can be reformulated as linear problems in matrix variables over $\mathcal{CP}_d$. Therefore, CP matrices allow to transfer all the complexity of the original problem to the cone constraint. In fact, for every non-convex quadratic optimization

[1] The term *completely positive* to be used throughout this chapter is given in Definition 3.2.1 and it is not to be confused with the concept completely positive map from the quantum information context.

[2] A cone is said to be *proper* if the cone is: convex; closed; with nonempty interior; and pointed

problem there exists an equivalent CP formulation. Formally,

$$\max_{\substack{x_i \geq 0 \\ \langle u|x\rangle = 1}} \langle x|Q|x\rangle = \max_{\substack{X \in \mathcal{CP}_d \\ \langle u|X|u\rangle = 1}} \mathrm{Tr}(XQ), \tag{3.2}$$

where the LHS corresponds to the non-convex quadratic optimization problem, the RHS corresponds to the equivalent CP formulation, $|u\rangle$ is the unnormalized vector of ones and Q can be taken symmetric and positive semi-definite without loss of generality[3].

While checking membership in $\mathcal{CP}_d$ has been shown to be NP-hard [Dickinson and Gijben, 2014], CP matrices add a new perspective and properties that allow to upper bound the optimization in Equation (3.2). For instance, by considering that a CP matrix A is positive semi-definite, which follows directly from its definition since it factorizes as $A = B \cdot B^T$. Another property of CP matrices is that they are entry-wise non-negative (*i.e.*, $A_{ij} \geq 0$), which motivates the following definition:

Definition 3.2.2. *Consider a $d \times d$ matrix denoted A. The matrix A is said to be Doubly Non-Negative (DNN) if, and only if, $A \succeq 0$ and $A_{ij} \geq 0$.*

We are now ready to present our results.

3.3 Characterizing separability in diagonal symmetric states acting on $\mathbb{C}^d \otimes \mathbb{C}^d$

We start by characterizing the bipartite DSS in terms of separability and the PPT properties. In this section we establish an equivalence connection between: (i) separability and the PPT property in DS quantum states; with (ii) quadratic conic optimization problems and their relaxations, respectively.

[3] On one hand one can assume Q to be symmetric since $\langle x|\, Q\, |x\rangle = (\langle x|\, Q\, |x\rangle)^T = \langle x|\, Q^T\, |x\rangle$. On the other, Q can be assumed to be positive semi-definite since adding $\mathbb{1}$ to $(Q + Q^T)/2$ will only bias the maximum but will not vary the optimal $|x\rangle$.

3.3.1 Efficient representation of DSS: the associated M-matrix

To begin with, notice that the representing DS states ρ in the computational basis results in highly sparse $d^2 \times d^2$ matrices. Instead, one can conveniently represent all the relevant information of ρ in an associated $d \times d$ matrix. We call such representation the associated M-matrix of ρ defined as:

Definition 3.3.1. *To every DSS ρ we associate a $d \times d$ matrix $M(\rho)$ of non-negative entries*

$$M(\rho) := \begin{pmatrix} p_{00} & p_{01}/2 & \cdots & p_{0,d-1}/2 \\ p_{01}/2 & p_{11} & \cdots & p_{1,d-1}/2 \\ \vdots & \vdots & \ddots & \vdots \\ p_{0,d-1}/2 & p_{1,d-1}/2 & \cdots & p_{d-1,d-1} \end{pmatrix}. \tag{3.3}$$

Therefore, for each $M(\rho)$ with non-negative entries summing 1, there exists a one-to-one correspondence with a DSS ρ.

To understand from where Eq. (3.3) comes, notice what happens when the partial transposition is applied on a DSS of the form in Eq. (3.1):

- The elements corresponding to the diagonal in the computational basis ($i = j$) remain invariant $p_{ii}(|D_{ii}\rangle\langle D_{ii}|)^{\Gamma_B} = p_{ii}\,|D_{ii}\rangle\langle D_{ii}|$, since $|D_{ii}\rangle = |ii\rangle$.

- The elements corresponding to the off-diagonal ($i \neq j$) suppose a slightly more elaborate situation: one has 4 elements $p_{ij}\,|D_{ij}\rangle\langle D_{ij}| = \frac{p_{ij}}{2}(|ij\rangle\langle ij|+|ij\rangle\langle ji|+|ji\rangle\langle ij|+|ji\rangle\langle ji|)$, of which 2 remain invariant in the diagonal $\frac{p_{ij}}{2}\left((|ij\rangle\langle ij|)^{\Gamma_B} + (|ji\rangle\langle ji|)^{\Gamma_B}\right) = \frac{p_{ij}}{2}\,(|ij\rangle\langle ij| + |ji\rangle\langle ji|)$, while the other 2 vary as $\frac{p_{ij}}{2}\left((|ij\rangle\langle ji|)^{\Gamma_B} + (|ji\rangle\langle ij|)^{\Gamma_B}\right) = \frac{p_{ij}}{2}\,(|ii\rangle\langle jj| + |jj\rangle\langle ii|)$.

Hence, ρ^{Γ_B} is block-diagonal in the Dicke basis where the blocks correspond to the matrix $M(\rho)$ and 1×1 elements corresponding to

p_{ij} with $i < j$. That is,

$$\rho^{\Gamma_B} = M(\rho) \bigoplus_{0 \leq i \neq j < d} \left(\frac{p_{ij}}{2} \right), \tag{3.4}$$

Notice that because $p_{ij} = p_{ji}$, the 1×1 blocks appear with multiplicity 2.

In what follows we characterize the separability properties of ρ in terms of equivalent properties of $M(\rho)$. We will see how this apparently simple associated M-matrix brings forth some of the DSS separability properties, eventually leading us to find a natural connection with the field of quadratic conic optimization.

3.3.2 Separability problem for DSS: a quadratic conic optimization problem

Remarkably, the associated matrix $M(\rho)$ allows us to find a connection between the separability problem for DS states and the field of quadratic conic optimization. In particular,

Theorem 3.3.1. *Let ρ be a DS quantum state acting on $\mathbb{C}^d \otimes \mathbb{C}^d$.*

$$\rho \text{ is separable} \iff M(\rho) \text{ is CP}. \tag{3.5}$$

A proof of Theorem 3.3.1 can be found in Appendix A.1.

The relevance of Theorem 3.3.1 comes clear once we invoke a result from the quadratic conic optimization field: it is NP-Hard to decide whether a matrix admits a CP decomposition [Berman *et al.*, 2015]. Then, by virtue of Theorem 3.3.1, it immediately follows that the separability problem for $\mathbb{C}^d \otimes \mathbb{C}^d$ DS states is NP-Hard.

As previously mentioned, the NP-hardness of the separability problem for DSS was shown before us in [Yu, 2016]. However, the connection we find allows us to further specify that the NP-hardness we

present here holds under polynomial-time Turing reductions[4], instead of poly-time many-one reductions [Gharibian, 2010]. The reason lies in that the NP-hardness of deciding the membership of a matrix in $\mathcal{CP}_d$ follows from polynomial-time Turing reduction. It is worth mentioning that to make the claim completely rigorous from a computer science point of view, one should work out the technicalities to embed the NP-hardness into the formalism of the weak membership problem, similarly as in [Gurvits, 2003; Grötschel *et al.*, 2012]. In practice, among minor details, the main requirement would be to show that the convex set of separable DSS is well-bounded and p-centered (see [Gharibian, 2010] for more details). Alternatively, one can consider the completely positive cone, for which it is known that $\mathcal{CP}_d$ is well-bounded and p-centered and, furthermore, that the weak membership problem in the cone $\mathcal{CP}_d$ is NP-hard [Dickinson *et al.*, 2013]. Then, by the equivalence established between DSS and CP matrices through Definition 3.3.1, the result gets mapped to the DS set.

In what follows we show that the new found connection with quadratic conic optimization problems allows to further characterize DSS separability properties.

3.3.3 Characterizing the extremal elements of DSS

The characterization of extremality in the set of separable DSS facilitates the characterization of the separability properties of DSS. To see why, notice that the separable DSS form a convex set, and thus the set of separable DSS is fully characterized by its extremal elements (*i.e.*, those DS states which cannot be obtained as a convex combination of other DSS. When one considers the general set of all separable quantum states, the extremal ones correspond to rank-1 projectors onto product vectors. But what happens when we restrict to the subset of

[4]Turing reduction is a concept from computability theory which describes how to solve a problem A by reducing it to a problem B whose solution is assumed to be already known. The process may involve running an algorithm for the second problem B multiple times.

the separable states? Then such property gets lost because the set of separable DS states is an intersection with the convex set of separable quantum states (see illustration in Figure 3.1). It follows that the extremal separable DS states do not necessarily correspond to extremal in the general separable set, and thus need not be rank-1 projectors onto product vectors. In fact, only the DS states with the form $|ii\rangle\langle ii|$ are extremal in both sets.

Another consequence of Theorem 3.3.1 is that it allows us to fully characterize extremality in the set of separable DSS in terms of extremal CP matrices by obtaining the following corollary:

Corollary 3.3.1. *The extremal DS separable states correspond to DSS with:*

$$p_{ij} = 2\sqrt{p_{ii}p_{jj}}, \qquad i < j. \tag{3.6}$$

Proof. It was shown in [Berman and Shaked-Monderer, 2003] that the extremal rays of the $\mathcal{C}P_d$ cone are the rank-1 matrices $\vec{b}\,\vec{b}^T$ where $b_i \geq 0$. Then, Eq. (3.6) immediately follows after normalizing and comparing to Eq. (3.3).

□

3.3.4 DS states that are PPT have a doubly non-negative associated M-matrix

Next, we look at what happens when we take a DS state ρ to be PPT. By recalling the definition of DNN matrices (see Definition 3.2.2), we stablish a new connection with the associated matrix $M(\rho)$:

Theorem 3.3.2. *Consider a DS state ρ acting on $\mathbb{C}^d \otimes \mathbb{C}^d$. Then,*

$$\rho \text{ is PPT} \iff M(\rho) \text{ is DNN.} \tag{3.7}$$

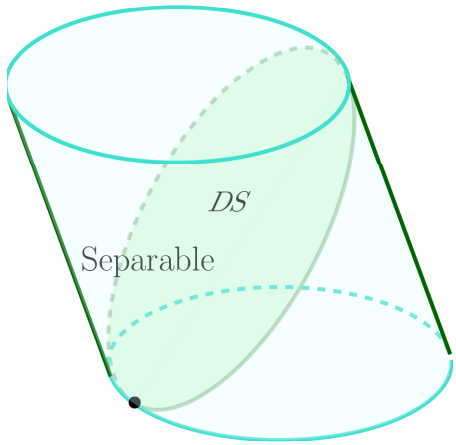

Fig. 3.1 Illustration of the set of SEP states (cylinder) and its intersection with the subspace of diagonal symmetric states DS (ellipse). The separable DS states are those that intersect the subspace of DS states and the set of separable states, represented by the ellipse in the middle, including its interior. Note that, although the extremal separable states are easy to characterize (they correspond to rank-1 projectors onto pure product states, represented in cyan in the figure), when intersecting SEP with the subspace of diagonal symmetric states, the extremal states of the set of separable DS states do not need to be of the same form. In fact, only the states of the form $|ii\rangle\langle ii|$ are extremal in both sets (represented by the black dot in the figure). However, states that were in the boundary of SEP, could now be extremal when viewed in DS (represented by the border of the ellipse in the middle of the figure).

Proof. Assume ρ to be PPT, *i.e.* $\rho^\Gamma \succeq 0$, and express its partial transposition as:

$$\rho^\Gamma = \left(\bigoplus_{0 \leq i < j < d} \left(\frac{p_{ij}}{2} \right) \oplus \left(\frac{p_{ij}}{2} \right) \right) \oplus M(\rho). \tag{3.8}$$

Then Eq. (3.8) implies that $M(\rho) \succeq 0$. Because ρ is a DS state, by definition it follows that $p_{ij} \geq 0$ for all $0 \leq i \leq j < d$. Therefore, all the entries of $M(\rho)$ are also non-negative. Hence, $M(\rho)$ is DNN.

Consider now the converse case: If $M(\rho)$ is DNN, then by definition all its entries are non-negative, *i.e.* $p_{ij} \geq 0$ for $0 \leq i \leq j < d$, which guarantees that $\rho \succeq 0$. Additionally, also by definition $M(\rho) \succeq 0$, which implies that $\rho^\Gamma \succeq 0$. Hence, ρ is PPT.

s □

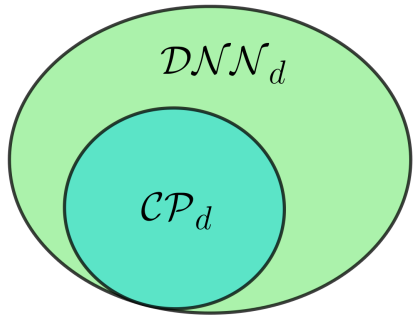

Fig. 3.2 The proper cone of CP matrices is embedded in the proper cone of DNN matrices; *i.e.*, $\mathcal{CP}_d \subseteq \mathcal{DNN}_d$. If the associated M-matrix of a DSS $M(\rho)$ is an element of $\mathcal{CP}_d$, then ρ is separable. If $M(\rho)$ is an element of $\mathcal{DNN}_d$, then ρ is PPT. Finally, if $M(\rho)$ is an element of $\mathcal{DNN}_d$ but not of $\mathcal{CP}_d$, then ρ is PPT but entangled. Because for $d \leq 4$ the cones are equal $\mathcal{CP}_d = \mathcal{DNN}_d$, then for $d \leq 4$ all PPTDS are separable.

Recall that, by definition (cf. Definitions 3.2.1 and 3.2.2), the proper cone of positive matrices is embedded in the proper cone of doubly non-negative matrices $\mathcal{CP}_d \subseteq \mathcal{DNN}_d$ as illustrated in Figure 3.2. However, it is known that for $d \leq 4$ every CP matrix is DNN,

i.e. $\mathcal{CP}_d = \mathcal{DNN}_d$, while for $d \geq 5$ there exist CP matrices which are not DNN, *i.e.* $\mathcal{CP}_d \subsetneq \mathcal{DNN}_d$ [Berman *et al.*, 2015].

Then, by virtue of Theorem 3.3.2 and the results in [Berman *et al.*, 2015], it immediately follows that

Theorem 3.3.3. *Consider a DS state ρ acting on $\mathbb{C}^d \otimes \mathbb{C}^d$, with $d \leq 4$. Then,*

$$\rho \text{ is separable} \iff \rho \text{ is PPT}. \tag{3.9}$$

A constructive proof for the $d = 3$ case is provided in Section A.2.1.

3.3.5 Separability in terms of the ranks of $M(\rho)$

Finally, to conclude the section about separability in DSS, we stablish a sufficient separability criteria for any d in terms of the ranks of $M(\rho)$. In particular,

Theorem 3.3.4. *Consider a PPTDS state ρ acting on $\mathbb{C}^d \otimes \mathbb{C}^d$ with associated $M(\rho)$ of rank at most 2. Then, ρ is separable.*

Proof. If ρ is separable then it is PPT, which in turn requires $M(\rho) \succeq 0$. Because $M(\rho)$ is positive semi-definite, it must admit a factorization $M(\rho) = VV^T$, where V is a $d \times 2$ or a $d \times 1$ matrix. From a geometrical point of view, one can see every row of V as a vector in $\mathbb{R}^2$ if $\text{rank}M(\rho) = 2$ (or a scalar in $\mathbb{R}^1$ if $\text{rank}M(\rho) = 1$). Then, $M(\rho)$ acts as the Gram matrix of those vectors, where each element is their scalar product. Because $M(\rho)$ is DNN, all the corresponding scalar products will be positive. Consequently, the angle between each pair of vectors is smaller or equal than $\pi/2$. Hence, $M(\rho)$ is CP if, and only if, the vectors formed by every row of V can be isometrically embedded into the positive orthant of $\mathbb{R}^k$ for some k. In the case $k = 2$, corresponding to $M(\rho)$ having rank at most 2, said embedding into the positive orthant is always possible to do as illustrated in Figure 3.3.

□

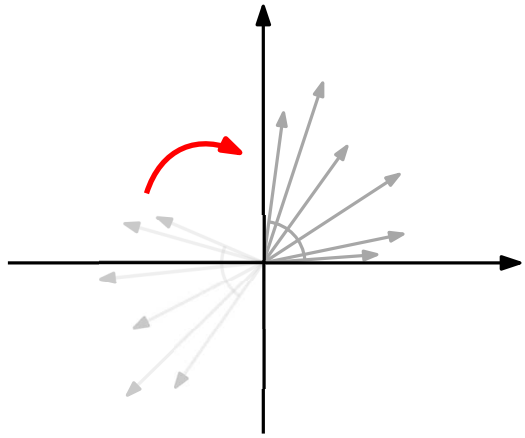

Fig. 3.3 Geometrical interpretation for proof of Theorem 3.3.4 when $rank(M(\rho)) = 2$. Consider the factorization $M(\rho) = VV^T$, where V is a $d \times 2$ whose rows are seen as vectors in $\mathbb{R}^2$. The matrix $M(\rho)$ is a member of $\mathcal{CP}_d$ when the angle between each pair of vectors is smaller or equal than $\pi/2$, meaning that all vectors can be isometrically embedded onto the positive orthant.

3.4 Sufficient criteria for entanglement and separability

With our new gained insight we proceed to further characterize the bipartite DSS. In this section we provide: 1) sufficient criteria to certify entanglement by means of *entanglement witnesses for DSS*; and 2) sufficient separability criteria in terms of $M(\rho)$ by means of the so-called *best diagonal dominant approximation*.

3.4.1 Entanglement Witnesses for DSS

Here we show that the so-called *copositive matrices* serve as entanglement witnesses for DSS and provide some examples. Similarly to CP matrices, copositive matrices have also gained interest in quadratic conic optimization problems. They are defined as follows:

Definition 3.4.1. *A matrix A is said to be* copositive *if, and only if, $\vec{x}^T A\vec{x} \geq 0$ for all $\vec{x}$ with non-negative entries.*

The set of $d \times d$ copositive matrices forms a proper cone, denoted $\mathcal{COP}_d$. In fact, $\mathcal{COP}_d$ is the dual to the proper cone of completely positive matrices $\mathcal{CP}_d$. Another property that will come in handy is that $\mathcal{PSD}_d + \mathcal{N}_d \subseteq \mathcal{COP}_d$, where $\mathcal{PSD}_d$ is the set of positive-semidefinite $d \times d$ matrices, $\mathcal{N}_d$ is the set of symmetric entry-wise non-negative matrix, and the equality holds for $d \leq 4$. In fact, from the inclusion $\mathcal{CP}_d \subseteq \mathcal{DNN}_d$ one observes that $\mathcal{DNN}_d = \mathcal{PSD}_d \cap \mathcal{N}_d$.

The immediate consequence is that one can view copositive matrices as EWs for DS states. Furthermore, the set $\mathcal{PSD}_d + \mathcal{N}_d$ can be thought of as decomposable EWs for DSS, since they serve as EWs but do not detect entangled PPTDSS, while the set of copositive matrices which are not $\mathcal{PSD}_d + \mathcal{N}_d$ can be thought of as non-decomposable EWs for DSS.

A typical example of a copositive matrix which is not in $\mathcal{PSD}_d + \mathcal{N}_d$ is the so-called *Horn matrix* H [Hall and Newman, 1963]:

$$H := \begin{pmatrix} 1 & -1 & 1 & 1 & -1 \\ -1 & 1 & -1 & 1 & 1 \\ 1 & -1 & 1 & -1 & 1 \\ 1 & 1 & -1 & 1 & -1 \\ -1 & 1 & 1 & -1 & 1 \end{pmatrix}. \tag{3.10}$$

Because $H \in \mathcal{COP}_5 \setminus (\mathcal{PSD}_5 + \mathcal{N}_5)$, H witnesses matrices which are DNN but not CP; *i.e.,* H witnesses $M(\rho)$ which correspond to PPTDSS but not separable. We provide some examples of entangled PPTDSS in Section 3.4.1 and Appendix A.4.1, where we also show that H acts as an indecomposable EW by witnessing that their associated $M(\rho)$ is a DNN but not CP matrix.

It is worth mentioning that, while in the general case the boundary of $\mathcal{COP}_d$ remains uncharacterized, $\mathcal{COP}_5$ has been fully characterized in [Dickinson *et al.*, 2013]:

$$\mathcal{COP}_5 = \{DAD : D \text{ is positive diagonal}, A \text{ s. t. } p(A, \vec{x}) \text{ is a sum of squares}\}, \tag{3.11}$$

where $p(A,\vec{x}) := \left(\sum_{i,j} A_{ij}x_i^2x_j^2\right)\left(\sum_k x_k^2\right)$.

Similarly, the characterization of the extremal rays of $\mathcal{COP}_d$ in the general case remains an open problem, while for $d \leq 5$ have been fully characterized and divided into classes [Berman *et al.*, 2015].

In Appendix A.3 we discuss the relation between exposedness properties of the sets of CP and copositive matrices with the separability problem and its geometry.

Example of an entangled $d = 5$ PPTDSS.

Consider the following associated M-matrix of a $d = 5$ bipartite DSS ρ which is PPT and entangled:

$$\tilde{M}(\rho) = \begin{pmatrix} 1 & 1 & 0 & 0 & 1 \\ 1 & 2 & 1 & 0 & 0 \\ 0 & 1 & 2 & 1 & 0 \\ 0 & 0 & 1 & 1 & 1 \\ 1 & 0 & 0 & 1 & 3 \end{pmatrix}. \tag{3.12}$$

In order to check that the state is indeed entangled, one can use the *Range criterion* [Horodecki, 1997] as we show in Appendix A.2.2. By virtue of Theorem 3.3.1, it is equivalent to show [Berman *et al.*, 2015] that $M(\rho) \in \mathcal{DNN}_5 \setminus \mathcal{CP}_5$. Applying the Horn matrix does exactly that since $\mathrm{Tr}(H\tilde{M}(\rho)) = -1 < 0$. Thus the Horn matrix certifies entanglement in the example and illustrates how it can serve as an EW.

3.4.2 Best diagonal dominant approximation: sufficient separability criteria for DSS

Here we present the Best Diagonal Dominant (BDD) approximations, which provide sufficient criteria to certify that a given PPTDSS is separable. Hence, complementing the entanglement certification criteria presented on the preceding section.

The BDD approximations approach follows the idea that, while checking membership in $\mathcal{CP}_d$ is NP-hard, it is actually easy to:

1. Characterize the extremal elements in $\mathcal{CP}_d$ (cf. Corollary 3.3.1)

2. Check for membership in a subset of $\mathcal{DD}_d \subseteq \mathcal{CP}_d$ that is formed by those matrices $A \in \mathcal{N}_d$ that are diagonal dominant. The inclusion $\mathcal{DD}_d \subseteq \mathcal{CP}_d$ was proven in [Kaykobad, 1987]

With these things in mind, we grab inspiration from the so-called Best Separable Approximations (BSA) [Lewenstein and Sanpera, 1998; Quesada and Sanpera, 2014] which allows to express any PPTDSS as a sum of a separable part and an entangled part with maximal weight on the separable part. For our case, we take the associated M-matrix of a DSS ρ and use the BDD approximations to look for an expression of $M(\rho)$ as a sum of an extremal element of $\mathcal{CP}_d$ and an element of $\mathcal{DD}_d$ (see illustration in Figure 3.4). Therefore, if such an expression is found it immediately certifies that $M(\rho) \in \mathcal{CP}_d$, which in turns ensures the separability of ρ.

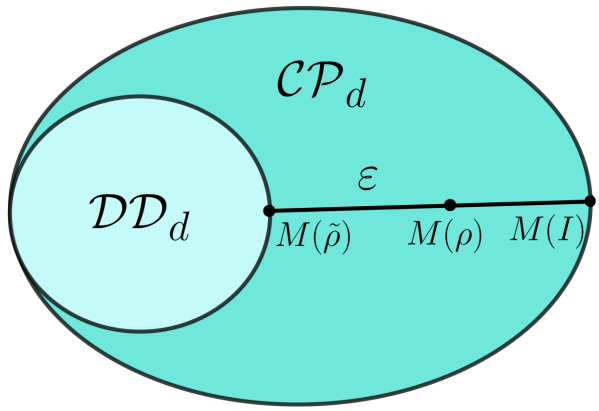

Fig. 3.4 Given a PPTDSS ρ acting on $\mathbb{C}^d \otimes \mathbb{C}^d$, if one can decompose its associated $M(\rho)$ in terms of an extremal element of $\mathcal{CP}_d$ ($M(I)$) and an element of $\mathcal{DD}_d$ ($M(\tilde{\rho})$), then $M(\rho)$ is in $\mathcal{CP}_d$. Therefore, if said decomposition exists then the separability of ρ is certified.

The BDD approximations are presented below in two main theorems. In practice, the idea to derive both theorems is to subtract some separable state from a given DSS ρ while maintaining ρ to be a valid DSS, to be PPT, and to be close enough to the interior of the separable set so that one can obtain the desired expression certifying separability (as illustrated in Figure 3.4). Before we state the main theorems, we need to state an explicit separable decomposition of a quantum state. Let us then start with the following lemma:

Lemma 3.4.1. *Consider the unnormalized quantum state I given by*

$$I = \sum_{i=0}^{d-1} |ii\rangle\langle ii| + \sum_{0\leq i<j<d} 2\,|D_{ij}\rangle\langle D_{ji}|\,, \tag{3.13}$$

where $|D_{ij}\rangle = (|ij\rangle + |ji\rangle)/\sqrt{2}$. For instance, for $d = 3$,

$$I = \left(\begin{array}{ccc|ccc|ccc} 1 & \cdot & \cdot & \cdot & \cdot & \cdot & \cdot & \cdot & \cdot \\ \cdot & 1 & \cdot & 1 & \cdot & \cdot & \cdot & \cdot & \cdot \\ \cdot & \cdot & 1 & \cdot & \cdot & \cdot & 1 & \cdot & \cdot \\ \hline \cdot & 1 & \cdot & 1 & \cdot & \cdot & \cdot & \cdot & \cdot \\ \cdot & \cdot & \cdot & \cdot & 1 & \cdot & \cdot & \cdot & \cdot \\ \cdot & \cdot & \cdot & \cdot & \cdot & 1 & \cdot & 1 & \cdot \\ \hline \cdot & \cdot & 1 & \cdot & \cdot & \cdot & 1 & \cdot & \cdot \\ \cdot & \cdot & \cdot & \cdot & \cdot & 1 & \cdot & 1 & \cdot \\ \cdot & \cdot & \cdot & \cdot & \cdot & \cdot & \cdot & \cdot & 1 \end{array}\right). \tag{3.14}$$

Then, I corresponds to a separable state.

Proof. Let $|e(\vec{\varphi})\rangle = |0\rangle + e^{\mathrm{i}\varphi_1}|1\rangle + \cdots + e^{\mathrm{i}\varphi_{d-1}}|d-1\rangle$. A separable decomposition of I is given by

$$I = \int_{[0,2\pi]^d} \frac{\mathrm{d}\vec{\varphi}}{(2\pi)^d} (|e(\vec{\varphi})\rangle\langle e(\vec{\varphi})|)^{\otimes 2}. \tag{3.15}$$

Indeed,

$$I = \sum_{ijlk} |ij\rangle\langle kl| \int_{[0,2\pi]^d} \frac{\mathrm{d}\vec{\varphi}}{(2\pi)^d} e^{\mathrm{i}(\varphi_i+\varphi_j-\varphi_k-\varphi_l)} = \sum_{ijlk} |ij\rangle\langle kl| \left(\delta_{i,k}\delta_{j,l}+\delta_{i,l}\delta_{j,k}-\delta_{i,j,k,l}\right), \tag{3.16}$$

where δ is the Kronecker delta function.

□

With Lemma 3.4.1 providing a sufficient condition for a state ρ to be separable, we are now ready to present the first main theorem:

Theorem 3.4.1. *Consider a PPTDSS ρ acting on $\mathbb{C}^d \otimes \mathbb{C}^d$ with associated $M(\rho)$. If there exists an $\varepsilon \geq 0$ such that*

1. *$\varepsilon \leq \rho_{ij}$ for all i, j such that $0 \leq i, j < d$.*
2. *$\varepsilon d \leq (\langle u| \frac{1}{M(\rho)} |u\rangle)^{-1}$ and $|u\rangle \in \mathcal{R}(M(\rho))$, $\mathcal{R}(M(\rho))$ is the range of $M(\rho)$ and $\frac{1}{M(\rho)}$ is the pseudo-inverse of $M(\rho)$. Here $|u\rangle$ is a normalized vector of ones.*
3. *for all i such that $0 \leq i < d$, $\rho_{ii} + \varepsilon(d-2) \geq \sum_{j\neq i} \rho_{ji}$.*

Then, ρ is a separable state.

A proof is shown in Appendix A.4.2. The idea behind the theorem is to subtract εI from ρ while the resulting $\tilde{\rho} = \rho - \varepsilon I$ remains a PPTDSS. Then: The first condition in Theorem 3.4.1 forces $\tilde{\rho}$ to remain in the DSS subspace when subtracting I from ρ; The second condition forces $\tilde{\rho}$ to remain PPT subtracting I from ρ. Moreover, the second condition provides the maximal ε that can be subtracted while maintaining $\tilde{\rho}$ to be PPT, since if $|u\rangle \notin \mathcal{R}(M(\rho))$ then $\tilde{\rho}$ would not be PPT for any $\varepsilon \neq 0$; Finally, the third condition guarantees that $\tilde{\rho}$ is separable, which is achieved by considering $M(\tilde{\rho})$ to be diagonal dominant. In practice one might to subtract a minimal amount of I to make $M(\rho)$ diagonal dominant (unless $M(\rho)$ is already diagonal dominant).

An example is presented in Appendix A.4.3 where Theorem 3.4.1 is successfully applied to certify separability. Consequently, it also serves to show that the set $\mathcal{CP}_d \setminus \mathcal{DD}_d$ is not empty.

One can now take Appendix A.4.2 one step further by normalizing and by generalizing I to any other extremal element $I_x \in \mathcal{CP}_d$:

Lemma 3.4.2. *Let $\mathbf{x} \in \mathbb{R}^d$ with $x_i \geq 0$ and $||\mathbf{x}|| > 0$. Consider the quantum state $I_{\mathbf{x}}$ given by*

$$I_{\mathbf{x}} = \frac{1}{||\mathbf{x}||_1^2} \left(\sum_{i=0}^{d-1} x_i^2 \, |ii\rangle\langle ii| + \sum_{0 \leq i < j < d} 2x_i x_j \, |D_{ij}\rangle\langle D_{ij}| \right). \tag{3.17}$$

Then, $I_{\mathbf{x}}$ is a separable state.

A proof is presented in Appendix A.4.4.

Notice that the corresponding $M(I_{\mathbf{x}})$ is given by $|u_{\mathbf{x}}\rangle\langle u_{\mathbf{x}}|$, where $|u_{\mathbf{x}}\rangle = \mathbf{x}/||\mathbf{x}||_1$. Therefore, the sum of the elements of $M(I_{\mathbf{x}})$ is one. That is, $||M(I_{\mathbf{x}})||_1 = 1$.

Then, Lemma 3.4.2 provides a sufficient separability condition. Similar to Theorem 3.4.1, the idea is to decompose a DSS ρ as a convex combination between $I_{\mathbf{x}}$, which is a state extremal in the set of separable DSS, and a state $\tilde{\rho}$ which is deep enough in the interior of the set of separable states, such that we can certify its separability by other means. For instance, by showing that $M(\tilde{\rho})$ is diagonal dominant and doubly non-negative, which in turn implies that it is completely positive [Kaykobad, 1987].

Theorem 3.4.2. *Consider a PPTDSS ρ acting on $\mathbb{C}^d \otimes \mathbb{C}^d$ with associated $M(\rho)$. Let $\mathbf{x} \in \mathbb{R}^d$ with $x_i > 0$. If there exists a $\lambda \in [0, 1)$ such that*

1. *$\lambda \leq (M(\rho))_{ij} ||\mathbf{x}||_1^2 / x_i x_j$ for all i and j,*
2. *$\lambda \leq 1/\langle u_{\mathbf{x}}| \frac{1}{M(\rho)} |u_{\mathbf{x}}\rangle$ and $|u_{\mathbf{x}}\rangle \in \mathcal{R}(M(\rho))$, where $\mathcal{R}(M(\rho))$ is the range of $M(\rho)$ and $\frac{1}{M(\rho)}$ denotes the pseudo-inverse of $M(\rho)$,*
3. *$\lambda x_i (||\mathbf{x}||_1 - 2x_i) \geq ||\mathbf{x}||_1^2 \left[\sum_{j \neq i} (M(\rho))_{ij} - (M(\rho))_{ii} \right]$ for all i,*

then $M(\rho)$ is completely positive and, equivalently, ρ is a separable state.

A proof is presented in Appendix A.4.5. In short, the proof follows a similar reasoning as with Theorem 3.4.1 but this time considering $\rho = (1-\lambda)\tilde{\rho} + \lambda I_{\mathbf{x}}$ and ensuring that the associated $M(\tilde{\rho})$ remains completely positive.

Comparing both theorems, it is clear that Theorem 3.4.2 provides an advantage over Theorem 3.4.1 because the parameters of $I_{\mathbf{x}}$ are not fixed. Hence, Theorem 3.4.2 has more flexibility and considers a bigger family of decompositions $M(\rho) \in \mathcal{CP}_d$ parametrized by $\mathbf{x}$. In what follows we provide an example that illustrates how both theorems can be applied to certify separability. Furthermore, we show said advantage.

Example for Theorems 3.4.1 and 3.4.2

In this example we provide a PPTDSS with associated $M(\rho) \in \mathcal{CP}_d \setminus \mathcal{DD}_d$ and show how to apply Theorem 3.4.2 to certify separability. Furthermore, we then apply Theorem 3.4.1 to illustrate its limitations compared to Theorem 3.4.2.

Let ρ be a DSS acting on $\mathbb{C}^3 \otimes \mathbb{C}^3$ with associated $M(\rho)$ given by:

$$M(\rho) = \begin{pmatrix} \alpha & \beta & \gamma \\ \beta & \delta & \beta \\ \gamma & \beta & \epsilon \end{pmatrix} = \frac{1}{100} \begin{pmatrix} 19 & 8 & 11.5 \\ 8 & 6.4 & 8 \\ 11.5 & 8 & 19.6 \end{pmatrix}, \tag{3.18}$$

where the state ρ has been normalized.

A priori, one does not know whether the state in Eq. (3.18) is separable or not. Our goal is to apply Theorems 3.4.1 and 3.4.2 and check whether separability can be certified. In essence, we want to find an ϵ that satisfies the theorems conditions. Notice that, for both theorems, either condition 1 or condition 2 will provide an upper bound, whereas condition 3 provides a lower bound. The difference between theorems can be appreciated in the lower bound provided by condition 3, since in Theorem 3.4.2 the bound can be varied by fitting $I_{\mathbf{x}}$. The example provides a case where Theorem 3.4.2 certifies separability while Theorem 3.4.1 does not.

Lets start applying Theorem 3.4.2. For the given ρ in Eq. (3.18), we want to find whether it can be convex decomposed as $M(\rho) =$

$(1-\lambda)M(\tilde{\rho})+\lambda M(I_{\mathbf{x}})$ while satisfying the conditions of the theorem. For instance, we fix $\lambda = 0.8$ and by numerical means we find that a possible convex combination takes $M(I_{\mathbf{x}}) = |u_{\mathbf{x}}\rangle\langle u_{\mathbf{x}}|$ where $|u_{\mathbf{x}}\rangle = 1/100(37.46\,|0\rangle + 25.16\,|1\rangle + 37.38\,|2\rangle)$. Let us now show that indeed the given $M(\rho)$ and $M(I_{\mathbf{x}})$ fulfill the conditions in Theorem 3.4.2. For this case, Condition 1 results in the more restrictive upper bound given by

$$\lambda \leq \frac{\gamma||\mathbf{x}||_1^2}{x_1 x_3} = 0.8213, \tag{3.19}$$

while Condition 3 provides the lower bound given by

$$\lambda \geq \frac{||\mathbf{x}||_1^2[2\beta-\delta]}{x_2(||\mathbf{x}||_1-\delta)} = 0.7681. \tag{3.20}$$

Hence, there exists a range of values $\lambda \in [0.7681, 0.8213]$ fulfilling the conditions in Theorem 3.4.2, and the existence of λ certifies that ρ is separable. Let us note that once we found an $M(I_{\mathbf{x}})$ fulfilling the conditions we fixed it for illustrative purposes although more freedom could have been allowed resulting in a bigger range of possible decompositions.

Let us now see what happens with Theorem 3.4.1. For this case, Condition 2 results in the more restrictive upper bound given by

$$\varepsilon \leq \left(\langle u|\,\frac{1}{M(\rho)}\,|u\rangle\right)^{-1} = 0.06, \tag{3.21}$$

while Condition 3 provides the lower bound given by

$$\varepsilon \geq 2\beta - \delta = 0.096. \tag{3.22}$$

Hence, in this case there does not exist an ε fulfilling the conditions for Theorem 3.4.1. Therefore, Theorem 3.4.1 does not certify separability for this case while Theorem 3.4.2 does.

Chapter 4

Device-Independent Witnesses of Entanglement Depth for many-body systems

In the previous chapter we have seen that a general criterion to certify the presence of entanglement on a quantum system remains a very complex problem even for highly symmetric classes of states. Yet, entanglement has become a main feature in quantum mechanics, with vast variety of implications and applications. Hence, despite its complexity, the need to have more sophisticated criteria to certify the presence of entanglement keeps growing. This is specially the case for many-body systems, in which case the problem becomes significantly more complex both from the computational and experimental points of view.

In the previous chapter we have dealt with bipartite entanglement. As opposed to the bipartite case, multipartite entanglement admits a hierarchy of definitions depending on the strength of the correlations between the subsystems (cf. Eqs. (2.8) and (2.9)), the strongest of which is referred to as *Genuinely Multipartite Entanglement* (GME). Alternatively, the equivalent notions of *entanglement depth* [Sørensen and Mølmer, 2001] and *k-producibility* [Gühne *et al.*, 2005] provide an intuitive measure to quantify the degree of entanglement by considering

the subsystem in the quantum composite containing the largest amount of GME particles, which makes it a convenient notion for experiments with many particles [Lücke *et al.*, 2014].

In this chapter we are interested in the certification of the amount of entanglement present in a quantum many-body system. Furthermore, we want the certification criteria to be practical from both computational and experimental points of view, where by practical we mean that the criterion: (i) involves few-body correlators; (ii) avoids idealizations and assumptions; and (iii) can be experimentally implemented within reach of current technological advances. In order to achieve our goals, we develop a methodology that allows to derive *Device-Independent Witnesses of Entanglement Depth* (DIWEDs) based on the so-called two-body *Permutationally Invariant Bell Inequalities* (PIBI), the families of Bell inequalities introduced in [Tura *et al.*, 2014a, 2015].

The chapter is organized as follows: In Section 4.1 we start by introducing the notions of k-producibility and entanglement depth. In Section 4.2 we then introduce the idea of DIWEDs and also narrow them down to involve only symmetric few-body correlators. In Section 4.3 we pose the optimization problem to find the k-producibility bounds that serve to construct DIWEDs based on Bell inequalities, and discuss several scenarios and simplifications. In Section 4.4 we present a methodology to characterize k-producible bounds, which is based on two complementary numerical methods: (i) a variational method; and (ii) a certificate of optimality via semi-definite programming.

In Section 4.5 we consider two case studies, characterize them via the methodology presented, and discuss the obtained numerical results both in the general case and under additional assumptions. In Section 4.6 we perform an asymptotic analysis based on the previous observations, which allows us to characterize k-producible bounds in the many-body regime. In Section 4.7 we unravel the experimental appeal of the DIWEDs we present by showing how they can be effectively evaluated via collective measurements and moments thereof. Finally, in Section 4.8 we rewrite the DIWEDs in terms of spin-squeezing

quantities, which we then use to compare the efficiency of the DIWEDs against actual experimental data and other entanglement depth criteria.

The original results presented in this chapter are based on the publications [Aloy *et al.*, 2019; Tura *et al.*, 2019], a joint collaboration between J. Tura, F. Baccari, M. Lewenstein, A. Acín and R. Augusiak.

4.1 Entanglement depth and k-producibility

In Section 2.2 we have defined the notions of separability and entanglement. Moreover, we have seen that they admit many generalizations to the multipartite setting [Szalay and Kökényesi, 2012; Szalay, 2015, 2019], giving rise to different notions and strength of entanglement [Gühne and Tóth, 2009]. While the natural generalization of bipartite separability (see Definition 2.2.3) is the notion of K-separability (see Definition 2.2.1), from an experimental point of view K-separability is often not the most fitted notion.

For our purposes, the notion of *k-producibility* [Gühne *et al.*, 2005; Gühne and Seevinck, 2010; Wölk and Gühne, 2016] presents to be a better candidate, since it provides an intuitive measure to quantify the amount of entanglement. The idea behind the notion of k-producibility, equivalent to the notion of *entanglement depth* [Sørensen and Mølmer, 2001], is to characterize a quantum system by the largest particle group GME. That is, k-producibility considers largest group of particles within the quantum system whose particles are entangled with each other while not entangled to the rest of particles forming the system.

To be more precise, lets start by considering the formal definition of k-producibility for pure states. Consider n parties, indexed by $[n] := \{1, \ldots, n\}$, sharing a multipartite state. Consider also a partition $\mathcal{P}$ of $[n]$ into m pairwise disjoint, non-empty subsets $\mathcal{A}_i$, each of size at most k; *i.e.*, $\mathcal{P} = \{\mathcal{A}_1, \ldots, \mathcal{A}_m\}$ such that $\bigcup_{i=1}^{m} \mathcal{A}_i = [n]$, $\mathcal{A}_i \cap \mathcal{A}_j = \emptyset$ if $i = j$, $\mathcal{A}_i \neq \emptyset$ and $|\mathcal{A}_i| \leq k$ for all $i \in [n]$. Under this notation,

Definition 4.1.1. *Let $|\Psi\rangle$ be a pure n-partite quantum state. Then, $|\Psi\rangle$ is said to be* k-producible with respect to the partition $\mathcal{P}$ *if, and only if, it admits the following decomposition*

$$|\Psi\rangle = |\phi_1\rangle_{\mathcal{A}_1} \otimes \cdots \otimes |\phi_m\rangle_{\mathcal{A}_m}, \tag{4.1}$$

where each $|\phi_i\rangle_{\mathcal{A}_i}$ is a pure state corresponding to the group $\mathcal{A}_i$.

Notice that in Definition 4.1.1 we are giving the criteria with respect to some fixed partition $\mathcal{P}$. To move to the general case, apart from considering mixed states, one has to consider a set $\mathcal{P}^k_{\text{prod}}$ containing all possible partitions $\mathcal{P}$ of $[n]$ into m pairwise disjoint, non-empty subsets $\mathcal{A}_i$, each of size at most k. Then,

Definition 4.1.2. *Let ρ be a mixed n-partite quantum state. Then, ρ is said to be* k-producible *if, and only if, it admits the following decomposition*

$$\rho = \sum_{\mathcal{P}\in\mathcal{P}^k_{\text{prod}}} \lambda_{\mathcal{P}} \sum_i \lambda_i^{\mathcal{P}} \bigotimes_{\mathcal{A}_j\in\mathcal{P}} \rho_i^{\mathcal{A}_j}, \tag{4.2}$$

where $\lambda_{\mathcal{P}}$ and $\lambda_i^{\mathcal{P}}$ form their respective convex combinations.

The minimal k for which a given multipartite state ρ admits a decomposition Eq. (4.2) is called *entanglement depth*. Conversely, a quantum system that cannot be expressed as in Equation (4.2) is certified to contain at least $k+1$ particles entangled. An operational interpretation for the latter is that in order to reproduce from scratch a state that cannot be expressed as in Equation (4.2), one needs to form groups having more than k parties GME. It is worth noting that when a quantum state is not $(n-1)$-producible, then the state is certified to be GME, exhibiting its strongest form of multipartite entanglement.

The advantage of the k-producibility notion for certification tasks now comes clear. In k-producibility, the k indicates the maximal degree of genuinely multipartite entanglement that the parties forming a quantum composite may be sharing. In Figure 4.1 we schematically illustrate the differences between said separability notions to further clarify.

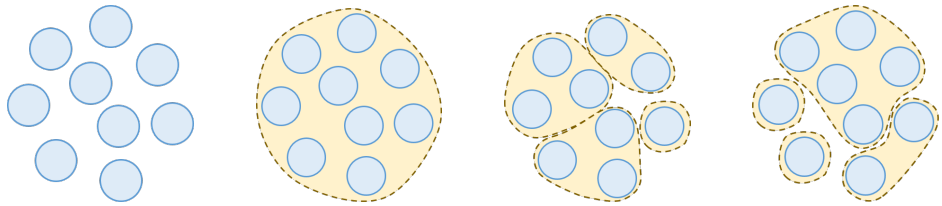

(a) Fully separable, 1-producible

(b) GME, 9-producible

(c) 4-separable, 3-producible

(d) 4-separable, 5-producible

Fig. 4.1 Schematic illustration to compare the notions of l-separability and k-producibility. The operational interpretation is that the parties (represented as blue circles) that form a group (represented as discontinuous lines) can prepare any state they want, whereas among different groups they are allowed only to perform local operations and classical communication. Note that the groupings may change as long as the restrictions imposed by l and k are maintained (cf. Equations (2.9) and (4.2)). In essence, l limits the total number of groups while k limits the maximal number of parties in any group.

4.2 Device-Independent Witnesses of Entanglement Depth

Non-local correlations, as witnessed by a Bell inequality, certify the presence of entanglement on a quantum state (see Section 2.3.1). However, its certification of entanglement does not provide information on the structure of such entanglement. In the present chapter we go significantly beyond by designing Bell-like inequalities capable of revealing entanglement depth in multipartite quantum states. In particular, we present a methodology to derive *Device-Independent Witnesses of Entanglement Depth* (DIWEDs) out of Bell inequalities. In Figure 4.2 we illustrate the difference between a regular entanglement witness and a witness of entanglement depth.

Throughout the present chapter, we are going to consider Bell-type experiments in the simplest multipartite Bell scenario: the $(n, 2, 2)$ Bell

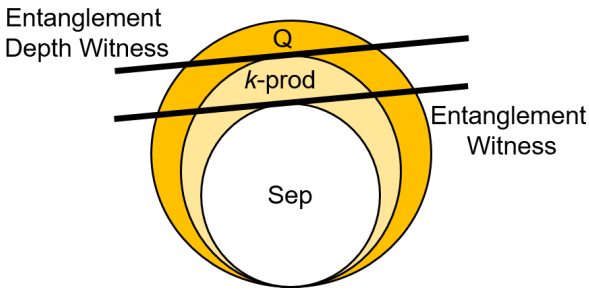

Fig. 4.2 Schematic illustration to distinguish entanglement witnesses (EW) from witnesses of entanglement depth (WED). The set of all separable quantum states (Sep) is embedded in the set of all possible quantum states (Q). From the separable set to the quantum set there is a whole hierarchy of sets formed by all the possible k-producible quantum states, where $1 \leq k \leq n$. The 1-prod set corresponds to the separable set and the n-prod set to the quantum set. An EW can be thought of as an inequality which is necessarily satisfied for all the quantum states in Sep, thus only certifying the presence of entanglement on a quantum composite. On the other hand, WEDs can be thought of as inequalities satisfied for all k-producible states. Because there is a hierarchy of DIWEDs, depending on which ones get violated will provide certification on the presence of entanglement *and* the degree of entanglement present in the quantum composite.

scenario. Let us shortly remind the Bell scenario tailored to the case considered in the present chapter, and refer to Section 2.3.1 for more details. In an $(n, 2, 2)$ Bell scenario, a multipartite resource (*e.g.,* a multipartite entangled state) gets distributed among n parties, indexed by $[n] := \{1, \ldots, n\}$, each of which performs one out of two available dichotomic observables. We denote the observables as $\mathcal{M}_k^{(i)}$, where $k \in [2]$ labels the choice of measurement (input), and we consider the resulting outcomes a_i to take values ± 1 (output). Then, a generic multipartite Bell inequality (see Section 2.3.3 for more details) can be

simply stated as $I - \beta_c \geq 0$, where I takes the form

$$I := \sum_{p\in[n]} \sum_{k_1,\ldots,k_p\in[2]} \sum_{1\leq i_1<\ldots<i_p\leq n} \alpha_{(i_1,\ldots,i_p),(k_1,\ldots,k_p)} \langle \mathcal{M}_{k_1}^{(i_1)} \ldots \mathcal{M}_{k_p}^{(i_p)} \rangle , \tag{4.3}$$

for $\alpha_{(i_1,\ldots i_p),(k_1,\ldots,k_p)} \in \mathbb{R}$, and β_c denotes the classical bound.

Because $I - \beta_c \geq 0$ holds for any local correlation, by measuring I one can obtain information about the non-local correlations in the system. Similarly, in the present chapter we aim at drawing conclusions about the entanglement depth present in the system by measuring I. The difference now is that the inequality does not involve the classical bound β_c, but instead considers a hierarchy of values β_k such that

$$I - \beta_k \geq 0, \tag{4.4}$$

where the inequality is satisfied for all k-producible states and dichotomic measurements of, in principle, any local dimension. Hence, Equation (4.4) constitutes a DIWED.

4.2.1 DIWEDs from symmetric two-body correlators

Unfortunately, in general it is not possible to characterize generic multipartite Bell inequalities due to their high combinatorial complexity. We have seen in Section 2.3.4 that a way to partially circumvent such high complexity is to consider the so-called *two-body Permutationally Invariant Bell Inequalities* (two-body PIBIs) [Tura *et al.*, 2014a, 2015]. These form a family of multipartite Bell inequalities with desirable properties, which reduces the combinatorial complexity even making them appealing for many-body scenarios. These are Bell inequalities that involve at most two-body correlators and furthermore are derived by considering the PI symmetry.

One of the main goals in the present chapter is to derive DIWEDs based on two-body PIBIs. Let us shortly introduce said inequalities while referring to Section 2.3.4 for more details.

The two-body PIBIs involve the following one- and two-body symmetric correlators:

$$\langle \mathcal{S}_k \rangle := \sum_{i\in[n]} \langle \mathcal{M}_k^{(i)} \rangle \,, \qquad \langle \mathcal{S}_{kl} \rangle := \sum_{i\neq j\in[n]} \langle \mathcal{M}_k^{(i)} \mathcal{M}_l^{(j)} \rangle \,. \tag{4.5}$$

Then, two-body PIBIs are inequalities that take the form $I-\beta_c \geq 0$, where β_c is the usual classical bound and I now is defined as

$$I := \sum_{k\in[m]} \alpha_k \mathcal{S}_k + \sum_{k\leq l\in[m]} \alpha_{kl} \mathcal{S}_{kl}, \tag{4.6}$$

where $\alpha_k, \alpha_{kl} \in \mathbb{R}$ are the Bell coefficients of the inequality.

Therefore, PIBIs involving one- and two-body symmetric correlators can be constructed as in Eq. (4.4), but this time considering the I given in Eq. (4.6).

4.3 Attaining the k-producible bounds: an optimization problem

The whole task of constructing PIBIs out of a Bell inequality is reduced to obtain the k-producible bounds, denoted β_k. In this section we present a general method to obtain β_k and, therefore, design PIBIs. In Section 4.3.1 we start by describing the method in its full generality, which applies to any Bell inequality in the $(n, 2, 2)$ scenario. In Section 4.3.2 we then show the significant improvement of considering the cases where Bell inequalities involve few-body correlators. Finally, in Section 4.3.3 we consider the case of few-body correlators and additional symmetries, which will be the object of study for the rest of the chapter.

4.3.1 General case

Let us start by considering a general Bell inequality $I - \beta_c \geq 0$ in the $(n, 2, 2)$ scenario for some I expressed as in Eq. (4.3). Instead

of working with the quantity I, it is convenient to notice there is an operator assigned that to every I, called the *Bell operator* $\mathcal{B}$, which is defined as follows:

$$\mathcal{B} := \sum_{p\in[n]} \sum_{k_j\in[m]} \sum_{1\leq i_1<\ldots<i_p\leq n} \alpha_{(i_1,\ldots,i_p),(k_1,\ldots,k_p)} \mathcal{M}^{(i_1,\ldots,i_p)}_{(k_1,\ldots,k_p)}, \tag{4.7}$$

with $\mathcal{M}^{(i_1,\ldots,i_p)}_{(k_1,\ldots,k_p)} = \bigotimes_{t\in[n]} \mathcal{M}^{(i_t)}_{k_t}$ where $\mathcal{M}^{(i)}_k$ denotes the k-th observable performed by the i-th party, and $\alpha_{(i_1,\ldots,i_p),(k_1,\ldots,k_p)} \in \mathbb{R}$ are the Bell inequality coefficients. Therefore, the expectation value I for some quantum state ρ and local measurements $\mathcal{M}^{(i)}_k$ gets equivalently expressed in terms of its associated Bell operator $\mathcal{B}$ as

$$I = \mathrm{Tr}\left[\mathcal{B}\rho\right]. \tag{4.8}$$

As we have seen in Section 4.2, the obtention of β_k consists in achieving the optimal value of I under all possible k-producible quantum correlations. That is, one needs to optimize Eq. (4.8) over all possible k-producible states and all possible quantum observables. Here we fully appreciate the big challenge we face since, in principle, one should implement the optimization taking into account all the possible dimensions of the local Hilbert spaces $\mathcal{H}_i$ (see e.g. [Pál and Vértesi, 2010]). Moreover, there is no efficient characterization of the set of quantum correlations and there is little prospect to find one (see e.g. [Navascués *et al.*, 2015; Navascués *et al.*, 2007]).

However, because we are restricting to the $(n, 2, 2)$ scenario, there is a couple of significant simplifications without loss of generality that we can benefit from. It was shown in [Toner and Verstraete, 2006] that every Bell operator in the $(n, 2, 2)$ Bell scenario is isometrically equivalent to a Bell operator for qubits. Furthermore, it was also shown in [Toner and Verstraete, 2006] that the local measurements $\mathcal{M}^{(i)}_k$ can be assumed to take place in the x-z plane of the Bloch Sphere without loss of generality due to Jordan's lemma [Jordan, 1875]. This supposes a formidable simplification since not only it suffices to consider n-qubit k-producible states, but one can also simply parametrize every local

measurement as $\mathcal{M}_k^{(i)} = \sin(\theta_{i,k})\sigma_x^{(i)} + \cos(\theta_{i,k})\sigma_z^{(i)}$, where $\sigma_x^{(i)}$ and $\sigma_z^{(i)}$ denote the usual Pauli matrices acting on the i-th party. Therefore, the Bell operator in Eq. (4.7) will depend on the angles $\theta_{i,k}$ of the local measurements. Henceforth, whenever we want to make the dependence explicit, we shall denote the Bell operator $\mathcal{B}$ as $\mathcal{B}(\boldsymbol{\theta})$, where $\boldsymbol{\theta}$ is a vector encoding all the parameters $\theta_{i,k}$.

Therefore, the obtention of β_k gets posed as the following optimization problem:

$$\beta_k = \min_{\rho,\boldsymbol{\theta}} \operatorname{Tr}\left[\mathcal{B}(\boldsymbol{\theta})\rho\right], \tag{4.9}$$

where ρ denotes an n-qubit k-producible quantum state, and $\mathcal{B}(\boldsymbol{\theta})$ denotes the Bell operator with measurement settings $\boldsymbol{\theta}$.

In order to further simplify, another assumption one can consider without loss of generality is that the optimal value of Eq. (4.9) is attained by a pure k-producible state; *i.e.,* by a pure state corresponding to some fixed partition $\mathcal{P} \in \mathcal{P}^k_{\text{prod}}$ (cf. Eq. (4.1)). Notice that said assumption comes without loss of generality by a convex-roof argument. In practice, the simplification implies that

$$\beta_k = \min_{\boldsymbol{\theta},|\Psi_{\mathcal{P}}\rangle} \langle\Psi_{\mathcal{P}}| \mathcal{B}(\boldsymbol{\theta}) |\Psi_{\mathcal{P}}\rangle, \tag{4.10}$$

where $|\Psi_{\mathcal{P}}\rangle = \bigotimes_{\mathcal{A}\in\mathcal{P}} |\psi_{\mathcal{A}}\rangle$.

The optimization problem in Eq. (4.10) can, in principle, be solved exactly without encountering local minima issues. For instance, one could consider Lagrange multipliers by expressing the optimization problem as a polynomial function under polynomial equality constraints given by the normalization of $|\psi_i\rangle$ and $\cos^2\theta_{i,k} + \sin^2\theta_{i,k} = 1$. In practice, however, the degree of the resulting polynomial and the amount of constraints increases with the system size rendering the Lagrange multipliers approach impractical. In Appendix B.1 we expand on the discussion about an exact solution for Eq. (4.10). However, in the following sections we take a more pragmatic path which, as opposed to the general case, can lead to DIWEDs that are within reach of technological advancements to be experimentally evaluated.

4.3.2 Two-body case

In this section, instead of considering general Bell inequalities, we consider Bell inequalities that involve only one- and two-body correlators (recall Section 2.3.4), which we call *two-body Bell inequalities*. This time, the two-body Bell inequalities have an associated *two-body Bell operator* defined as follows:

$$\mathcal{B} = \sum_{k\in[2]} \sum_{i\in[n]} \alpha_{i,k} \mathcal{M}_k^{(i)} + \sum_{k,l\in[2]} \sum_{i\neq j\in[n]} \alpha_{(i,j),(k,l)} \mathcal{M}_k^{(i)} \otimes \mathcal{M}_l^{(j)}, \tag{4.11}$$

for some $\alpha_{i,k}, \alpha_{(i,j),(k,l)} \in \mathbb{R}$.

This time notice that taking the expectation value of Eq. (4.11) over $\Psi_{\mathcal{P}}$, *i.e.* $\langle\Psi_{\mathcal{P}}|\,\mathcal{B}\,|\Psi_{\mathcal{P}}\rangle$, has support onto at most two of the states $|\psi_{\mathcal{A}}\rangle$ that form the k-producible state $|\Psi\rangle_{\mathcal{P}} = \bigotimes_{\mathcal{A}\in\mathcal{P}} |\psi_{\mathcal{A}}\rangle$. Hence, the expansion of Eq. (4.11) yields a polynomial of degree at most 4. The remarkable part is that the degree of the polynomial will remain constant independent of the number of parties n, which supposes a significant reduction on complexity compared to the general case.

Hence, for two-body Bell operators, the expectation value $\langle\Psi_{\mathcal{P}}|\,\mathcal{B}\,|\Psi_{\mathcal{P}}\rangle$ can be efficiently computed for large n with constant k. Let us remark that k does not need to be constant, as long as $k \in \mathcal{O}(\log n)$ the overall evaluation time will still be polynomial in n.

4.3.3 The two-body symmetric case

Finally, we consider Bell inequalities that involve one- and two-body symmetric correlators. That is, in this section we consider the two-body PIBIs presented in Section 4.2.1 (see Section 2.3.4 for more details), which will be the object of study for the rest of the chapter. As we shall see, the one- and two-body correlators restriction together with the symmetry feature allows for an efficient computation of the Bell operator's expectation value.

As usual by now, lets start by considering the *two-body symmetric Bell operator* assigned to a two-body PIBI, which this time takes the

form:

$$\mathcal{B} = \sum_{k\in[2]} \alpha_k \sum_{i\in[n]} \mathcal{M}_k^{(i)} + \sum_{k\leq l\in[2]} \alpha_{kl} \sum_{i\neq j\in[n]} \mathcal{M}_k^{(i)} \otimes \mathcal{M}_l^{(j)}, \tag{4.12}$$

where $\alpha_k, \alpha_{kl} \in \mathbb{R}$ are the usual Bell inequality coefficients.

Then, the expectation value of Eq. (4.12) over $|\Psi_{\mathcal{P}}\rangle$ can be contracted as

$$\begin{aligned}\langle\Psi_{\mathcal{P}}|\,\mathcal{B}\,|\Psi_{\mathcal{P}}\rangle = \sum_{\mathcal{A}\in\mathcal{P}} \Bigg(\sum_{k\in[2]} \alpha_k \underbrace{\langle\psi_{\mathcal{A}}|\mathcal{B}_k^{\mathcal{A}}|\psi_{\mathcal{A}}\rangle}_{\text{one-body terms}} + \sum_{k\leq l\in[2]} \alpha_{kl} \underbrace{\langle\psi_{\mathcal{A}}|\mathcal{B}_{kl}^{\mathcal{A}}|\psi_{\mathcal{A}}\rangle}_{\text{same region terms}} \Bigg) \\ + \sum_{\mathcal{A}\neq\mathcal{A}'\in\mathcal{P}} \Bigg(\sum_{k\leq l\in[2]} \alpha_{kl} \underbrace{\langle\psi_{\mathcal{A}}|\mathcal{B}_k^{\mathcal{A}}|\psi_{\mathcal{A}}\rangle \langle\psi_{\mathcal{A}'}|\mathcal{B}_l^{\mathcal{A}'}|\psi_{\mathcal{A}'}\rangle}_{\text{crossed region terms}} \Bigg),\end{aligned} \tag{4.13}$$

where $|\psi_{\mathcal{A}}\rangle$ has support on the parties forming region $\mathcal{A} \subseteq \mathcal{P}$, and the terms of the Bell operator have been grouped to define

$$\mathcal{B}_k^{\mathcal{A}} := \sum_{i\in\mathcal{A}} \mathcal{M}_k^{(i)}, \quad \mathcal{B}_{kl}^{\mathcal{A}} := \sum_{i\in\mathcal{A}} \sum_{j\in\mathcal{A}\setminus\{i\}} \mathcal{M}_k^{(i)} \otimes \mathcal{M}_l^{(j)}. \tag{4.14}$$

The idea behind carrying out the contraction as shown in Equation (4.13) is to gather the two-body terms in what we call *same region* terms and *crossed region* terms. In Figure 4.3 we graphically represent the terms that appear in Eq. (4.13). As their name suggest, the same region terms correspond to those two-body correlators that involve parties within a shared region $\mathcal{A}$ from the partition $\mathcal{P}$. Whereas the crossed region terms correspond to those two-body correlators that involve parties among different regions $\mathcal{A} \neq \mathcal{A}'$. Albeit simple, this gathering of terms is powerful since it highlights that, for a given k-producible state, the crossed region two-body correlators have to factorize as one-bodies. We will take advantage of this property in Section 4.4.2.

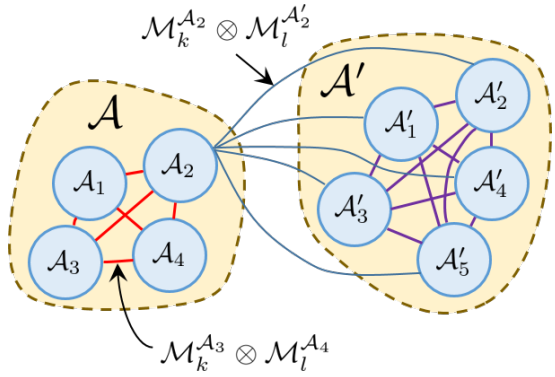

Fig. 4.3 Schematic illustration for the contraction in Eq. (4.13). Two regions $\mathcal{A} \neq \mathcal{A}'$ are represented as blue circles, where the regions form a partition $\mathcal{P} = \{\mathcal{A}, \mathcal{A}'\}$, with $\mathcal{P} \in \mathcal{P}^k_{\text{prod}}$. Each region is formed by several parties (*e.g.*, $\mathcal{A}_1$) represented as blue circles. The one-body terms in Eq. (4.13) are not illustrated, since they correspond to each blue circle (party). The two-body terms can be split in two parts: Those terms involving two parties from the same region (illustrated as red lines for $\mathcal{A}$, and purple lines for $\mathcal{A}'$); and those involving two parties that belong to different regions (of which we have only illustrated the terms connecting $\mathcal{A}_2$ from $\mathcal{A}$ to any party in $\mathcal{A}'$, while omitting the rest for visual clarity).

Optimization over symmetric regions

In this section, motivated by numerical results that we shall see in Section 4.5, in order to compute $\langle \Psi_{\mathcal{P}} | \mathcal{B} | \Psi_{\mathcal{P}} \rangle$ we consider the further assumption that the two-body Bell operator is permutationally invariant on each region $\mathcal{A} \in \mathcal{P}$. In other words, the case in which all parties forming a region $\mathcal{A} \in \mathcal{P}$ perform identical measurement settings.

As mentioned in Section 2.1, by means of the Schur-Weyl duality one can block-diagonalize a permutationally invariant Bell operator into invariant subspaces that correspond to different spin components with their corresponding multiplicities. For a permutationally invariant operator formed by n qudits, the blocks have size $\mathcal{O}\binom{n+d-1}{d-1}$ [Moroder *et al.*, 2012; Tura, 2017; Christandl, 2006].

As an example, consider an operator $\mathcal{B}$ acting on the set of linear

bounded operators for a two qubit space $(\mathbb{C}^2)^{\otimes 2}$, which is permutationally invariant. Then, $\mathcal{B}$ can get block-diagonalized by taking the basis spanned by the Dicke states and the anti-symmetric Bell state: $V^\dagger \mathcal{B} V = \mathcal{B}_{3\times 3} \oplus \mathcal{B}_{1\times 1}$:

$$V^\dagger \mathcal{B} V = \left(\begin{array}{c|c} \mathcal{B}_{3\times 3} & 0 \\ \hline 0 & \mathcal{B}_{1\times 1} \end{array}\right), \; V = \left(\begin{array}{ccc|c} 1 & 0 & 0 & 0 \\ 0 & \frac{1}{\sqrt{2}} & 0 & \frac{1}{\sqrt{2}} \\ 0 & \frac{1}{\sqrt{2}} & 0 & \frac{-1}{\sqrt{2}} \\ 0 & 0 & 1 & 0 \end{array}\right). \tag{4.15}$$

Consider now the Bell operator associated to the expectation value in Eq. (4.13):

$$\mathcal{B} = \sum_{\mathcal{A}\in\mathcal{P}} \left(\sum_{k\in[m]} \alpha_k \mathcal{B}_k^{\mathcal{A}} + \sum_{k\leq l\in[m]} \alpha_{kl} \mathcal{B}_{kl}^{\mathcal{A}} \right) + \sum_{\mathcal{A}\neq\mathcal{A}'\in\mathcal{P}} \sum_{k\leq l\in[m]} \alpha_{kl} \mathcal{B}_k^{\mathcal{A}} \otimes \mathcal{B}_l^{\mathcal{A}'}. \tag{4.16}$$

Furthermore, let $V_{\mathcal{A}}$ be a matrix consisting of the Schur-Weyl basis vectors that block-diagonalize the $\mathcal{A}$-th block arranged in columns. and denote $V = \bigotimes_{\mathcal{A}\in\mathcal{P}} V_{\mathcal{A}}$. Then, one ends up with

$$\begin{aligned} V^\dagger \mathcal{B} V = & \sum_{\mathcal{A}\in\mathcal{P}} \left(\sum_{k\in[m]} \alpha_k V_{\mathcal{A}}^\dagger \mathcal{B}_k^{\mathcal{A}} V_{\mathcal{A}} + \sum_{k\leq l\in[m]} \alpha_{kl} V_{\mathcal{A}}^\dagger \mathcal{B}_{kl}^{\mathcal{A}} V_{\mathcal{A}} \right) \\ & + \sum_{\mathcal{A}\neq\mathcal{A}'\in\mathcal{P}} \sum_{k\leq l\in[m]} \alpha_{kl} \left(V_{\mathcal{A}}^\dagger \mathcal{B}_k^{\mathcal{A}} V_{\mathcal{A}} \right) \otimes \left(V_{\mathcal{A}'}^\dagger \mathcal{B}_l^{\mathcal{A}'} V_{\mathcal{A}'} \right), \end{aligned} \tag{4.17}$$

where we have used that $V_{\mathcal{A}} V_{\mathcal{A}}^\dagger = V_{\mathcal{A}}^\dagger V_{\mathcal{A}} = \mathbb{1}_{\mathcal{H}_{\mathcal{A}}}$. Therefore, any k-producible pure state $|\Psi\rangle$ is expressed as $V^\dagger|\Psi\rangle$ in the tensor product basis of the blocks.

For our purposes, a particular case of interest is when the state $|\psi_A\rangle$ is fully supported on an invariant subspace of $V_{\mathcal{A}}$ (in particular the case when $|\psi_A\rangle$ is a symmetric state). When this is the case, $|\psi_{\mathcal{A}}\rangle$ gets described by, at most, $|\mathcal{A}|$ real parameters. Hence, one obtains an upper bound on the number of local minima given by

$$4^{3|\mathcal{P}|+n/k\cdot k} \leq 4^{n(1+3/k)}. \tag{4.18}$$

For the asymptotic analysis in Section 4.6, we are going to additionally consider that all regions $\mathcal{A}$ have at most k parties (*i.e.* $|\mathcal{A}| < k$, for all $\mathcal{A} \in \mathcal{P}$) and $|\psi_{\mathcal{A}}\rangle = |\psi_{\mathcal{A}'}\rangle$ for every $\mathcal{A}, \mathcal{A}' \in \mathcal{P}$. Under this circumstances, the upper bound in Eq. (4.18) becomes

$$4^{4+k}, \tag{4.19}$$

which is independent of n and supposes a drastic reduction.

4.4 Methodology to attain k-producible bounds

In this section we present the methodology to derive k-producible bounds and construct DIWEDs out of two-body PIBIs. The methodology we propose is based on two numerical methods that complement each other: (i) the method presented in Section 4.4.1 follows a variational approach that upper bounds the k-producible bound, *i.e.* β_k^U to β_k; (ii) the method presented in Section 4.4.2 constructs a certificate that lower bounds the k-producible bound, *i.e.* β_k^L to β_k. Hence, both methods complement each other by approaching β_k from different directions, which results in $\beta_k^L \leq \beta_k \leq \beta_k^U$.

4.4.1 Variational upper bound to β_k

The first method we present builds upon the so-called *see-saw optimization* method [Pál and Vértesi, 2010; Werner and Wolf, 2001] by adapting it to our case. Our method offers a (possibly) local minimum, denoted β_k^U that, by construction, upper bounds β_k, *i.e.* $\beta_k^U \geq \beta_k$. While any expectation value given by any k-producible state and set of measurements leads to an upper bound, our aim here is to describe in detail a methodology that gives a good guess to the optimal solution β_k. we achieve this by proposing an algorithm that constructs a k-producible pure state and finds a suitable set of measurements. The algorithm consists in the following steps:

1. For every partition $\mathcal{P} \in \mathcal{P}^k_{\text{prod}}$,

2. initialize a random k-producible pure state $|\Psi\rangle$ and random measurement settings, parametrized by $\boldsymbol{\theta}$.

3. While keeping $|\Psi\rangle$ fixed, use the see-saw technique (see e.g. [Pál and Vértesi, 2010; Werner and Wolf, 2001]) to decrease β_k^U while varying the measurement settings $\boldsymbol{\theta}$.

   For this case, the see-saw iteration technique consists in optimizing the measurement settings one at a time instead of all of them at once. That is, do a sweep of $[n]$ where at each step the parameter for the j-th party measurement gets optimized while the rest of measurements ($\mathcal{M}_k^{(i)}$ for $i \neq j \in [n]$) remain fixed. Following this scenario, one can write the cost function

$$E_j(\boldsymbol{\theta}_j) = \langle\Psi|\, \mathcal{B}(\boldsymbol{\theta}_j; \boldsymbol{\theta}_0, \ldots, \hat{\boldsymbol{\theta}}_j, \ldots, \boldsymbol{\theta}_{n-1})\, |\Psi\rangle\,, \tag{4.20}$$

   where the only dependence is on the parameter $\boldsymbol{\theta}_j$ since the rest of parameters $\boldsymbol{\theta}_i$, $i \neq j$ are fixed.

   One way to carry out the optimization over $\boldsymbol{\theta}_j$ is by means of stochastic gradient descent methods. Alternatively, notice that Eq. (4.20) is linear in $\mathcal{M}_k^{(j)}$. Then, one can carry out the optimization by means of SDP whose variables are the POVM elements of $\mathcal{M}_k^{(j)}$, with the advantage that the minimum of Eq. (4.20) is guaranteed to be reached in one iteration. Formally, the SDP gets posed as:

$$\begin{aligned} \min_{\Pi_0^k} \quad & \mathrm{Tr}\left[|\psi\rangle\langle\psi|\, \mathcal{B}(\boldsymbol{\theta})\right] \\ \text{s.t.} \quad & 0 \preceq \Pi_0^k \preceq \mathbb{1} \\ & \mathcal{M}_k^{(j)} = \Pi_0^k - \Pi_1^k \\ & \Pi_0^k + \Pi_1^k = \mathbb{1} \end{aligned} \,. \tag{4.21}$$

   Once Eq. (4.20) has been minimized, $\boldsymbol{\theta}_j$ gets updated with the result from Eq. (4.21) and one proceeds to optimize the next j-th party in the sweep. At each step, $\langle\Psi|\, \mathcal{B}(\boldsymbol{\theta})\, |\Psi\rangle$ will either decrease or remain the same, thus converging to a local minimum. Once

the sequence has converged within numerical accuracy, we move to Step 4.

4. In this step we optimize $\langle\Psi|\,\mathcal{B}(\boldsymbol{\theta})\,|\Psi\rangle$ over k-producible pure states while fixing the measurement settings $\boldsymbol{\theta}$. Similar to the previous step, one can consider a see-saw iteration by optimizing the state $|\psi_j\rangle$ corresponding to the j-th region in $\mathcal{P}$, while fixing the rest of states $|\psi_i\rangle$ corresponding to the rest of regions $i \neq j$ in $\mathcal{P}$. It is useful to note that, in this case, out of Eq. (4.16) one can find $|\psi_j\rangle$ as the eigenvector of minimal eigenvalue of

$$\tilde{\mathcal{B}}_j = \sum_k \alpha_k \mathcal{B}_k^{\mathcal{A}_j} + \sum_{k\leq l} \alpha_{kl} \mathcal{B}_{kl}^{\mathcal{A}_j} + \sum_{k\leq l} \alpha_{kl} \sum_{\mathcal{A}_i\neq\mathcal{A}_j\in\mathcal{P}} \langle \mathcal{B}_k^{\mathcal{A}_i}\rangle \mathcal{B}_l^{\mathcal{A}_j} + \mathcal{B}_k^{\mathcal{A}_j} \langle \mathcal{B}_l^{\mathcal{A}_i}\rangle. \tag{4.22}$$

As in Step 3, a sweep is carried over all regions of $\mathcal{P}$, where at each step $|\psi_j\rangle$ gets updated. At each step, the value of $\langle\Psi|\,\mathcal{B}(\boldsymbol{\theta})\,|\Psi\rangle$ will either decrease or remain the same, thus converging to a local minimum. Once the sequence has converged within numerical accuracy, we move to Step 5.

5. Repeat steps 3 and 4 until the value of $\langle\Psi|\,\mathcal{B}(\boldsymbol{\theta})\,|\Psi\rangle$ lies within numerical accuracy. In other words, until the result of changing between Step 3 and Step 4 has converged within numerical accuracy.

6. Define $\beta_k^U(\mathcal{P}) = \langle\Psi|\,\mathcal{B}(\boldsymbol{\theta})\,|\Psi\rangle$. If there are partitions $\mathcal{P} \in \mathcal{P}_{\text{prod}}^k$ left, go to step 1.

   Remarkably, one does not need to consider all $\mathcal{P} \in \mathcal{P}_{\text{prod}}^k$, since one can define a partial order in $\mathcal{P}_{\text{prod}}^k$ induced by inclusion. Formally, for every $\mathcal{P}, \mathcal{Q} \in \mathcal{P}_{\text{prod}}^k$, we say that $\mathcal{P} \preceq \mathcal{Q}$ if, and only if, for every $A \in \mathcal{P}$, there exists a $B \in \mathcal{Q}$ such that $A \subseteq B$. Then it follows that $\beta_k^U(\mathcal{P}) \geq \beta_k^U(\mathcal{Q})$ if $\mathcal{P} \preceq \mathcal{Q}$.

   Therefore, since $\mathcal{P}_{\text{prod}}^k$ is a poset, it is sufficient to pick $\mathcal{P}$ in step 1 from its minimal elements.

7. Output $\beta_k^U = \min_{\mathcal{P}} \beta_k^U(\mathcal{P})$.

Hence, at each iteration the algorithm achieves a lower and lower expectation value $\langle\Psi|\mathcal{B}(\boldsymbol{\theta})|\Psi\rangle$ until a (possibly) local minimum is found. Thus, the end-result of the algorithm provides an upper bound $\beta_k^U \geq \beta_k$.

The method is constructed so that it can be applied to any Bell inequality. However, depending on the form of the Bell inequality, it could be the case that the method leads to poor upper bounds if the problem presents many local minima. As discussed in Section 4.3 and Appendix B.1, the use of Bell inequalities that involve at most two-body correlators has a clear advantage in this respect: the degree of the polynomial resulting from Eq. (4.12) remains constant independently of n. This drastically reduces the amount of local minima in $\langle\Psi|\mathcal{B}(\boldsymbol{\theta})|\Psi\rangle$. In fact, as we shall see, in Section 4.5 we characterize β_k for some two-body PIBIs, in which cases the present method provides a good upper bound that converges within numerical accuracy.

4.4.2 Certificate of lower bound to β_k

The second method provides a certificate of lower bound $\beta_k^L \leq \beta_k$ by means of an SDP which is based on a relaxation of the *quantum marginal problem* (see Chapter 6). By providing a lower bound, the method complements the one presented in Section 4.4.1.

Let us recall that, in principle, one has to consider all the partitions $\mathcal{P} \in \mathcal{P}_{\text{prod}}^k$ in order to attain the optimal value for β_k. On the other hand, following the reasoning in Step 6 of Section 4.4.1, it suffices to run the method for every minimal element of $\mathcal{P}_{\text{prod}}^k$ and keep the best value. Henceforth, we consider that the partition $\mathcal{P}$ is fixed.

The starting point for the method is to consider the expectation value, given by a multipartite quantum state ρ and a Bell operator

$\mathcal{B}(\boldsymbol{\theta})$, expressed as (cf. Equation (4.16)):

$$\begin{aligned}\mathrm{Tr}\left[\mathcal{B}(\boldsymbol{\theta})\rho\right] &= \sum_{\mathcal{A}\in\mathcal{P}}\left(\sum_{k\in[2]}\alpha_k \mathrm{Tr}\left[\mathcal{B}_k^{\mathcal{A}}\rho_{\mathcal{A}}\right] + \sum_{k\leq l\in[2]}\alpha_{kl}\mathrm{Tr}\left[\mathcal{B}_{kl}^{\mathcal{A}}\rho_{\mathcal{A}}\right]\right) \\ &+ \sum_{\mathcal{A}\neq\mathcal{A}'\in\mathcal{P}}\sum_{k\leq l\in[2]}\alpha_{kl}\mathrm{Tr}\left[\mathcal{B}_k^{\mathcal{A}}\otimes\mathcal{B}_l^{\mathcal{A}'}\rho_{\mathcal{A}\cup\mathcal{A}'}\right], \qquad (4.23)\end{aligned}$$

where $\rho_{\mathcal{A}}$ denotes the reduced state of ρ on the parties forming a group $\mathcal{A}\subseteq[n]$, where the rest of parties have been traced out.

By definition, the k-producible state has some degree of separability with respect to the chosen partition $\mathcal{P}$. In fact, a k-producible ρ formed by n parties must be at least $\lceil n/k\rceil$-separable (cf. Definition 4.1.2). Moreover, every cut $\rho_{\mathcal{A}\cup\mathcal{A}'}$ must be separable. Therefore, because we want to lower bound β_k taking into account k-producible quantum states, one has to accommodate said separability features as constraints. Consequently, one ends up with the following optimization problem:

$$\begin{aligned}&\min\ \mathrm{Tr}\left[\mathcal{B}(\boldsymbol{\theta})\rho\right] \qquad (4.24)\\ &\text{s.t. } \rho_{\mathcal{A}}\succeq 0,\ \rho_{\mathcal{A}\cup\mathcal{A}'}\succeq 0\\ &\quad \mathrm{Tr}[\rho_{\mathcal{A}}]=\mathrm{Tr}[\rho_{\mathcal{A}\cup\mathcal{A}'}]=1\\ &\quad \mathrm{Tr}_{\mathcal{A}}[\rho_{\mathcal{A}\cup\mathcal{A}'}]=\rho_{\mathcal{A}}\\ &\quad \rho_{\mathcal{A}\cup\mathcal{A}'}\text{ is separable across }\mathcal{A}|\mathcal{A}'.\end{aligned}$$

If we knew how to pose the condition that $\rho_{\mathcal{A}\cup\mathcal{A}'}$ is separable across the cut $\mathcal{A}|\mathcal{A}'$ as a linear constraint, then the optimization problem in Eq. (4.24) could be posed as an SDP. However, as we have seen in Chapter 3, it is in general NP-hard to determine whether a given quantum state is entangled or separable [Gurvits, 2003].

The methodology we propose is based on Eq. (4.24), but gets posed as an SDP by relaxing the separability constraint across $\mathcal{A}|\mathcal{A}'$ to, instead, satisfy the PPT condition (see Section 2.2.2); *i.e.*, $(\rho_{\mathcal{A}\cup\mathcal{A}'})^{\Gamma}\succeq 0$, where ρ^{Γ} denotes the partial transposition applied to any of the states

subsystems. Notice that the PPT condition conveniently fits as an efficient SDP constraint. Therefore, since there exist entangled quantum states that satisfy the PPT condition, the feasible set results in an outer approximation to that of Eq. (4.24). Formally, the relaxation of Equation (4.24) we propose gets posed as:

$$\begin{aligned} \min\ & \mathrm{Tr}[\mathcal{B}(\boldsymbol{\theta})\rho] \\ \text{s.t. } & \rho_{\mathcal{A}} \succeq 0,\ \ \rho_{\mathcal{A}\cup\mathcal{A}'} \succeq 0 \\ & \mathrm{Tr}[\rho_{\mathcal{A}}] = \mathrm{Tr}[\rho_{\mathcal{A}\cup\mathcal{A}'}] = 1 \\ & \mathrm{Tr}_{\mathcal{A}}[\rho_{\mathcal{A}\cup\mathcal{A}'}] = \rho_{\mathcal{A}} \\ & (\rho_{\mathcal{A}\cup\mathcal{A}'})^{\Gamma} \succeq 0. \end{aligned} \tag{4.25}$$

It is worth mentioning that there exist stronger approximations to the separable set [Harrow *et al.*, 2017; Doherty *et al.*, 2004] which tighten the relaxation in Eq. (4.25). However, they come at the expense to add computational complexity, which makes the method less efficient. For our cases of interest, the two-body PIBIs, we shall see in Section 4.5 that tighter approximations are not necessary since Eq. (4.25) already converges within numerical accuracy.

Before concluding the section, a few comments are in order. Let us start by noting that a state providing the optimal β_k indeed satisfies the SDP conditions in Eq. (4.25), since it has to be of the form of Eq. (4.1) and, therefore, $\rho_{\mathcal{A}\cup\mathcal{A}'} = |\phi_{\mathcal{A}}\rangle\langle\phi_{\mathcal{A}}| \otimes |\phi_{\mathcal{A}'}\rangle\langle\phi_{\mathcal{A}'}|$. Next, let us remark that the method can be applied to any Bell inequality built from marginals. Notice then that, apart from relaxing the separability constraint to a PPT condition, Eq. (4.25) can also be seen as a relaxation of the quantum marginal problem by not accounting for all the compatibility conditions among the resulting reduced states. When relaxing the quantum marginal problem, the feasible set of Eq. (4.25) also contains configurations that do not come from quantum states, which is compatible with providing a certification lower bound. In general, when the SDP in Eq. (4.25) converges it guarantees that the set of marginals used to compute $\mathrm{Tr}\left[\mathcal{B}(\boldsymbol{\theta})\rho\right]$ is actually a minimum. For SDPs, strong duality does not need to hold, albeit the cases where

it does not hold are for the most part pathological [Par, 2013]. In any case, even when strong duality does not hold, weak duality (*i.e.,* a feasible solution to the dual) would still return a lower bound to the minimum. Therefore, for each choice of measurement settings $\boldsymbol{\theta}$ the relation $\beta_k^L(\boldsymbol{\theta}) \leq \beta_k^U(\boldsymbol{\theta})$ holds. Finally, when considering the optimal measurement settings one gets a lower bound $\beta_k^L \leq \beta_k$.

4.5 Numerical characterization

In this section, we illustrate the methodologies above presented in Sections 4.4.1 and 4.4.2 by designing DIWEDs based on two exemplary two-body PIBIs and different number of particles n. In particular, we characterize DIWEDs based on the following two-body PIBIs (cf. Eq. (4.6)) [Tura *et al.*, 2014a, 2015]:

$$-2\langle \mathcal{S}_0 \rangle + \frac{1}{2}\langle \mathcal{S}_{00} \rangle - \langle \mathcal{S}_{01} \rangle + \frac{1}{2}\langle \mathcal{S}_{11} \rangle \geq \beta_k, \tag{4.26}$$

and

$$(n \bmod 2)(n-1)(n\langle \mathcal{S}_0 \rangle + \langle \mathcal{S}_1 \rangle) + \binom{n}{2}\langle \mathcal{S}_{00} \rangle + n\langle \mathcal{S}_{01} \rangle - \langle \mathcal{S}_{11} \rangle \geq \beta_k, \tag{4.27}$$

where the inequalities have already been expressed as DIWEDs, while their original version as Bell inequalities corresponds to the case $\beta_k = \beta_1 = \beta_c$. For Eq. (4.26) the classical bound is known to be $\beta_c = -2n$, whereas for Eq. (4.27) it is known to be $\beta_c = -\binom{n}{2}(n+2+(n \bmod 2))$.

These inequalities have their particular interest. On one hand, the Bell inequality in Eq. (4.26) has already been performed in experiments [Schmied *et al.*, 2016; Engelsen *et al.*, 2017], which provide a scenario in which we can exploit our DIWEDs methodology to extract conclusions about the entanglement depth that was observed in their experiments. On the other hand, the Bell inequality in Eq. (4.27) is tailored to the half-filled Dicke state (recall Section 2.1) [Tura *et al.*, 2015] which makes the inequality appealing for experimental settings in which such

states are prepared (*e.g.* via spin-changing collisions [Lücke *et al.*, 2014]). Moreover, the inequality Eq. (4.27) is a generalization of CHSH [Clauser *et al.*, 1969], probably the most famous Bell inequality, when $n = 2$ is used.

Figure 4.4 presents the k-producible bounds β_k to construct the DIWEDs based on Equation (4.26), while Figures 4.6 and 4.7 presents the β_k's to construct DIWEDs based on Eq. (4.27).

Let us now see how we got there. In Section 4.5.1 we start by discussing the results obtained without any additional hypotheses, in which case the methodologies yield values of $\beta_k^U - \beta_k^L$ within numerical accuracy (thus determining β_k up to numerical accuracy). From the obtained results, we gain insight about some properties that we conjecture are preserved in the many-body regime. In Section 4.5.2 we perform a numerical analysis under these additional assumptions, which allow us to reach much higher values of n.

4.5.1 Unconstrained optimization

For the unconstrained case in its general form, we have obtained an upper bound of β_k with the variational methodology presented in Section 4.4.1, and a lower bound certificate with the SDP methodology presented in Section 4.4.2 with system sizes up to $n = 18$. The maximal amount of parties n that we can reach is limited by the memory requirements to implement the methods (the SDP method being the more demanding one), which varies depending on the k-producibility being considered and its particular partitions. We present the comparison of both unconstrained methods in Figures 4.5 to 4.7.

The goal is to find β_k for Eq. (4.26) and Eq. (4.27). We represent the pure quantum state in the computational basis, and whenever possible we store the whole state vector. For the measurements, recall from Section 4.3.1 that one can parametrize as $\mathcal{M}_k^{(i)} = \cos(\theta_{i,k})\sigma_z^{(i)} + \sin(\theta_{i,k})\sigma_x^{(i)}$, for $k \in [2], i \in [n]$. Because we are optimizing over the states and the measurements, we can, for instance, fix $\mathcal{M}_0^{(i)} = \sigma_z$ for every $i \in [n]$ without loss of generality; *i.e.*, $\theta_{i,0} = 0$ for all $i \in [n]$. Then, the only

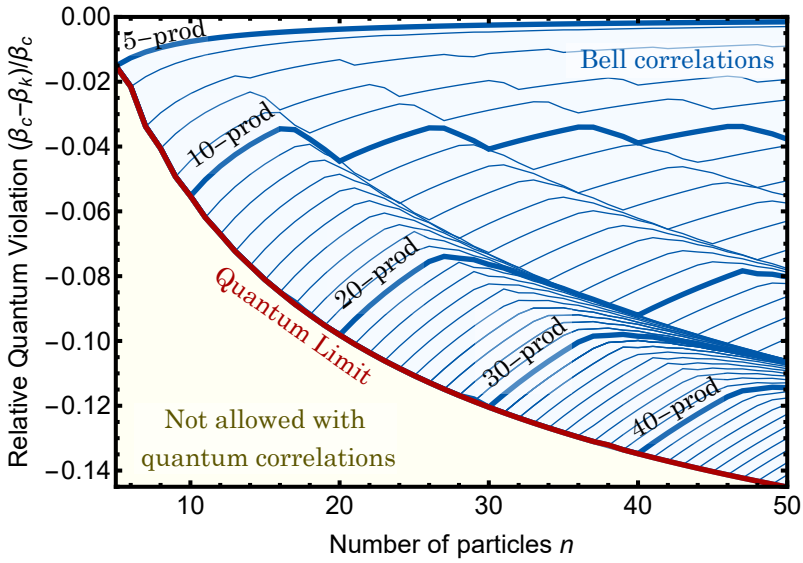

Fig. 4.4 Variational method results up to 50 parties. Each line corresponds to a k-producible bound relative to the classical bound $(\beta_c - \beta_k)/\beta_k$ used to construct the DIWEDs from symmetric two-body correlators in Eq. (4.26). We have been able to obtain unconstrained results without assumptions up to about $n \approx 15$ (depending on the particular complexity of the partition for a pair (n,k)), obtaining a gap $\beta_k^U - \beta_k^L < 10^{-7}$ within the numerical accuracy. In Figure 4.5 we show the result obtained with both methods. For the extrapolation to larger n, in order to reduce the number of parameters involved, we have considered the additional symmetry property within each region $\mathcal{A}_i$ via Eq. (4.28) (see Sections 4.3.3 and 4.5.2). One can observe a wavy-like structure in the β_k's, which can be explained by knowing that the Bell inequality in Eq. (4.26) does not detect nonlocality for systems consisting in less than 5 parties [Tura *et al.*, 2014a]. Therefore, the optimal partition $\mathcal{P}$, for every given pair (n,k), tries to avoid regions $\mathcal{A}$ containing less than 5 parties $|\mathcal{A}| < 5$.

relevant measurement parameters are some $\theta_i := \theta_{i,1}$'s for all $i \in [n]$, which parametrize $\mathcal{M}_1^{(i)} = \cos\theta_i \sigma_z^{(i)} + \sin\theta_i \sigma_x^{(i)}$. The assumption follows without loss of generality since, by means of a local unitary rotation of an angle c_i, the measurements of the i-th party can be simultaneously rotated to any measurements $\tilde{\mathcal{M}}_0^{(i)} = \cos(c_i)\sigma_z^{(i)} + \sin(c_i)\sigma_x^{(i)}$ and $\tilde{\mathcal{M}}_1^{(i)} = \cos(c_i+\theta_i)\sigma_z^{(i)} + \sin(c_i+\theta_i)\sigma_x^{(i)}$. Therefore, for the assumption to hold without loss of generality, one has to compensate by rotating the state with a single-qubit rotation of angle $-c_i$ applied on the i-th site, which does not change the entanglement depth properties of $|\Psi_{\mathcal{P}}\rangle$ [Tura *et al.*, 2015].

We have implemented both methodologies under this setting. For the variational method, we have tried more than 10^4 initial measurement settings, uniformly distributed in the $[0, 2\pi]^n$ hypercube, and k-producible states, where the initial state at each region is chosen uniformly at random according to the Haar measure. We proceed to state our numerical observations.

Given a partition $\mathcal{P}$ which is a maximal element of $\mathcal{P}^k_{\text{prod}}$ with respect to the partial order $\preceq$, *i.e.* the partition $\mathcal{P}$ contains as many regions of k parties as possible, the optimal value of β_k^U can be achieved when all parties within a region $\mathcal{A}$ choose the same measurement settings and the state is a superposition of Dicke states. In other words, the optimal point seems to be reachable when considering the region $\mathcal{A}$ to be permutationally invariant (see Section 4.3.3). However, the measurement settings among different regions are not necessarily the same, although they differ less if the amount of parties forming these regions is similar.

For all cases, the gap between the upper bound given by the variational method and the lower bound given by the SDP certificate is closed within numerical accuracy. That is, we obtain $\beta_k^U - \beta_k^L < 10^{-7}$, where the accuracy limit of 10^{-7} is given by the accuracy of the SDP solver. The SDP solvers we have tried are: SeDuMi [Sturm, 1999], Mosek [Mos, 2009] and SDPT3 [Toh *et al.*, 1998]. The parsers we have tried are: CVX [Grant and Boyd, 2014, 2008] and Yalmip [Lofberg, 2004]. In all cases considered we have obtained similar results.

The observations we extract from the results are similar to the results presented in [Tura *et al.*, 2014a, 2015], where they characterize the two-body PIBI here considered taking into account all possible quantum correlations (*i.e.,* the trivial partition $\mathcal{P} = \{[n]\}$ corresponding to the n-producible case). In their case, the optimal point is also achieved when all parties within the whole system (their single region) choose the same measurement settings. Hence, we recover the same result for the corresponding n-producible case, and conjecture, for lack of a proof, that it extends to the rest of k-producible cases.

An immediate consequence of the conjecture is that one can then use the Schur-Weyl duality result (see [Fulton *et al.*, 1991]) from representation theory to block diagonalize the Hilbert space into invariant subspaces of much smaller dimension. In practice, one would consider the projector

$$\Pi_{\mathbf{J}}^{\mathcal{P}} := \bigotimes_{\mathcal{A}\in\mathcal{P}} \Pi_{j_{\mathcal{A}}}^{\mathcal{A}}, \tag{4.28}$$

where $\Pi_{j_{\mathcal{A}}}^{\mathcal{A}}$ projects the Hilbert space corresponding to the region $\mathcal{A}$ onto the $j_{\mathcal{A}}$-th spin length [Tura i Brugués, 2017; Moroder *et al.*, 2012]. As we have mentioned in Section 2.1, by means of the projector $\Pi_{j_{\mathcal{A}}}^{\mathcal{A}}$ one goes from representing the Hilbert space of region $\mathcal{A}$ in a $2^{|\mathcal{A}|}$-dimensional subspace to represent it on a $(2j_{\mathcal{A}}+1)$-dimensional subspace, with $j_{\mathcal{A}} \leq |\mathcal{A}|/2$. For the DIWEDs in Eqs. (4.26) and (4.27), we observe that the optimal k-producible can be reached for the maximal spin subspace; *i.e.,* when $j_{\mathcal{A}} = |\mathcal{A}|/2$ for all $\mathcal{A} \in \mathcal{P}$.

All these observations brings us to the following section.

4.5.2 Optimization under additional hypotheses

Driven by the numerical results previously observed in Section 4.5.1, in this section we proceed to further characterize the DIWEDs for $n, k \gg 10$, under the following assumptions:

- The optimal measurement settings leading to β_k correspond to the case where, for each region $\mathcal{A} \in \mathcal{P}$, all parties within a region $\mathcal{A}$ perform identical measurement settings.

- The optimal state leading to β_k corresponds to a k-producible pure state $|\Psi_{\mathcal{P}}\rangle = |\psi_{\mathcal{A}_1}\rangle \otimes \cdots \otimes |\psi_{\mathcal{A}_{|\mathcal{P}|}}\rangle$ such that each $|\psi_{\mathcal{A}}\rangle$ is a superposition of symmetric states of the same spin length. For the DIWEDs in Eqs. (4.26) and (4.27), the spin length for each region is maximal $j_{\mathcal{A}} = |\mathcal{A}|/2$. Therefore, the state $|\psi_{\mathcal{A}}\rangle$ can be represented by an $|\mathcal{A}| + 1$ vector, and because superpositions of symmetric states involve only real coefficients, described with $|\mathcal{A}|$ real parameters (where we have considered normalization).

Lets start with the DIWED in Eq. (4.26), for which the numerical results can be seen in Figure 4.4, while a more detailed comparison between both optimization methods can be seen in Figure 4.5. From the numerical results obtained under the assumptions, we observe that the k-producible bounds β_k for large k are well approximated by considering a Gaussian superposition of Dicke states for each $|\psi_{\mathcal{A}}\rangle$, and the corresponding local unitary rotation [Tura *et al.*, 2015], of the form:

$$|\psi_{\mathcal{A}}\rangle \approx \sum_{j=0}^{|\mathcal{A}|} c_j \, |D_j^{|\mathcal{A}|}\rangle \,, \tag{4.29}$$

for $c_j = e^{-(j-\mu_{\mathcal{A}})^2/4\sigma_{\mathcal{A}}} / \sqrt[4]{2\pi\sigma_{\mathcal{A}}}$, where $|D_j^m\rangle$ denotes a qubit Dicke state of m qubits with j excitations (recall Section 2.1).

Albeit this might seem surprising, there are some reasons we believe to be the cause of such behaviour: It is known from [Tura *et al.*, 2014a, 2015] that the Bell inequality corresponding to Eq. (4.26) reaches the maximal violation value β_n for the same type of states. Furthermore, it is also known that the maximal quantum violation β_n, normalized to β_c, monotonically increases with the system size n, tending to a constant value $\beta_n = -1/4$ in the asymptotic limit. Hence, it is not so surprising that, when looking for β_k, the optimization favours this family of states (for each region), specially when the size of the region increases. Another feature of the Bell inequality in Eq. (4.26) is that it does not detect non-local correlations for systems with sizes $n < 5$. This results in a wave-live behaviour, which can be appreciated in Figures 4.4 and 4.5, due to the presence of some regions $\mathcal{A} \in \mathcal{P}$

containing less than 5 parties $|\mathcal{A}| < 5$ which will not add any non-local correlation contribution. Consequently, partitions with larger regions give the optimal β_k, for which we further conjecture that the optimal is achieved in the most balanced partition. In other words, the case where all $\mathcal{A} \in \mathcal{P}$ have k elements, except for when n is not a multiple of k, in which case there will be as many regions with k parties as possible and one region with the residual parties. Later in Section 4.6 we benefit from said observations to carry out an asymptotic analysis under these assumptions.

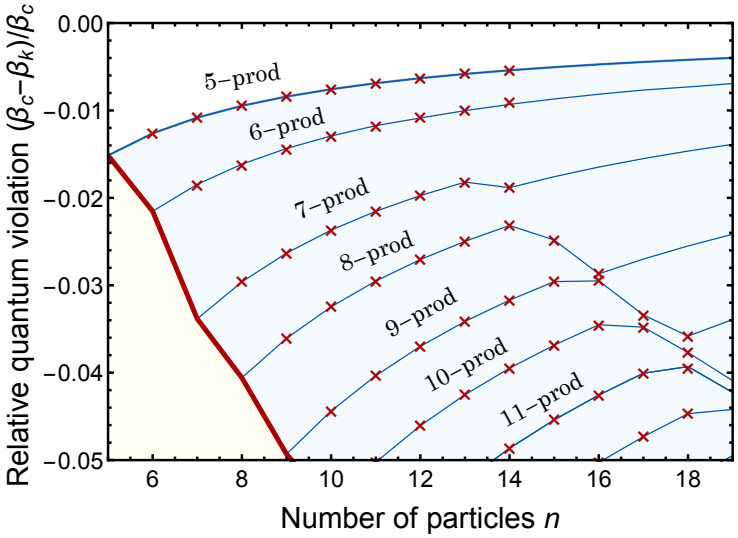

Fig. 4.5 Zoom in of Figure 4.4, corresponding to DIWEDs from symmetric two-body correlators in Eq. (4.26). Each line and cross corresponds to a k-producible bound β_k relative to the classical bound. The lines correspond to the upper bound solution β_k^U given by the variational method (we have connected the results as lines for better visibility), whereas the crosses correspond to the lower bound certificate β_k^L obtained via the SDP method. The SDP method does not follow assumptions and the gap is $\beta_k^U - \beta_k^L < 10^{-7}$, the numerical accuracy of the solver. Therefore, for practical purposes one can consider that β_k has been found.

Lets now move to the DIWED in Eq. (4.27). The numerical results for this DIWED can be seen in Figure 4.6, and normalized to the classical bound in Figure 4.7. We first observe that both numerical methods also provide a gap within numerical accuracy $\beta_k^U - \beta_k^L < 10^{-7}$. For the Bell inequality corresponding to Eq. (4.27), it is known that the optimal state providing maximal quantum violation β_n is the half-filled Dicke state $|D^n_{\lceil n/2 \rfloor}\rangle$ [Tura *et al.*, 2014a, 2015]. However, it can also be appreciated that for this case the optimal partition is more difficult to predict, even with this knowledge. The lack of predictability could be explained by the fact that the quantum violation of Eq. (4.27) relative to the classical bound, decreases as the system size n increases.

4.6 Asymptotic analysis

In this section we carry out an asymptotic analysis for the DIWEDs in Eq. (4.26) for large n, under the following assumptions based on the numerical observations from Section 4.5:

- The optimal partition $\mathcal{P} \in \mathcal{P}^k_{\text{prod}}$ is formed by $\lfloor n/k \rfloor$ regions of k parties each, and if k is not a multiple of n there is an extra region formed by the remaining $n \mod k$ parties.
- The optimal state corresponds to, after suitable local unitary transformations, the family of quantum states given by a product of Gaussian superpositions of Dicke states of the following form:

$$|\Psi\rangle = \bigotimes_{\mathcal{A}\in\mathcal{P}} \left(\sum_{j_{\mathcal{A}}=0}^{|\mathcal{A}|} c_{j_{\mathcal{A}}} |D^{|\mathcal{A}|}_{j_{\mathcal{A}}}\rangle \right), \tag{4.30}$$

  where $c_{j_{\mathcal{A}}} = e^{-(j_{\mathcal{A}}-\mu_{\mathcal{A}})^2/4\sigma_{\mathcal{A}}} / \sqrt[4]{2\pi\sigma_{\mathcal{A}}}$, and $j_{\mathcal{A}}, \mu_{\mathcal{A}}, \sigma_{\mathcal{A}}$ denote the spin length, median and variance for region $\mathcal{A}$ respectively.
- The optimal measurement settings corresponds to the case where all parties forming a region have the same measurement settings (up to local unitaries), for each region forming the system.

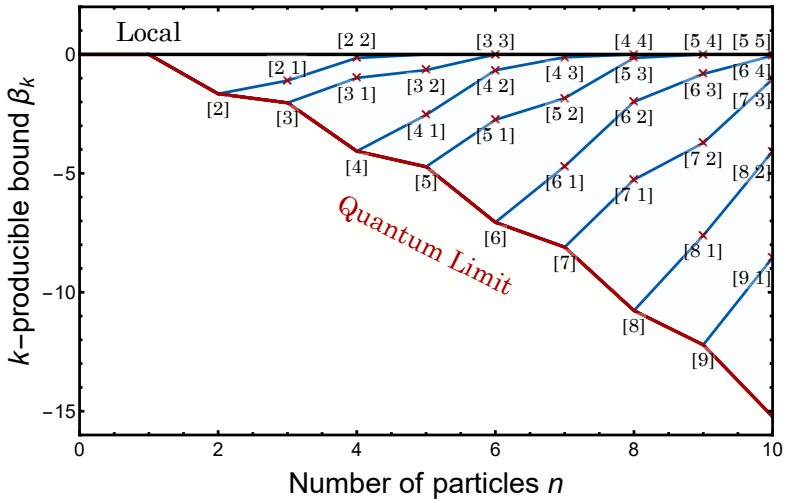

Fig. 4.6 Entanglement depth bounds β_k for the DIWEDs in Eq. (4.27), found via the numerical methods up to 10 particles. Each line represents a k-producible bound found by the variational method, whereas each cross corresponds to the lower bound certificate via the SDP method. The numerical methods provide a gap $\beta_k^U - \beta_k^L < 10^{-7}$, which is within the numerical accuracy of the SDP solver. We also label the partition $\mathcal{P}$ yielding the optimal β_k next to the corresponding point in the plot. For example, for the 6-producible case with $n = 7$, the notation [6 1] means that the partition is formed by two regions which contain by 6 and 1 parties; *i.e.*, $\mathcal{P} = \{\mathcal{A}_1, \mathcal{A}_2\}$, where $|\mathcal{A}_1| = 6$ and $|\mathcal{A}_2| = 1$. For some cases, different partitions yield the same bound, for instance [7 2] and [7 1 1]. We only label one of them for clarity.

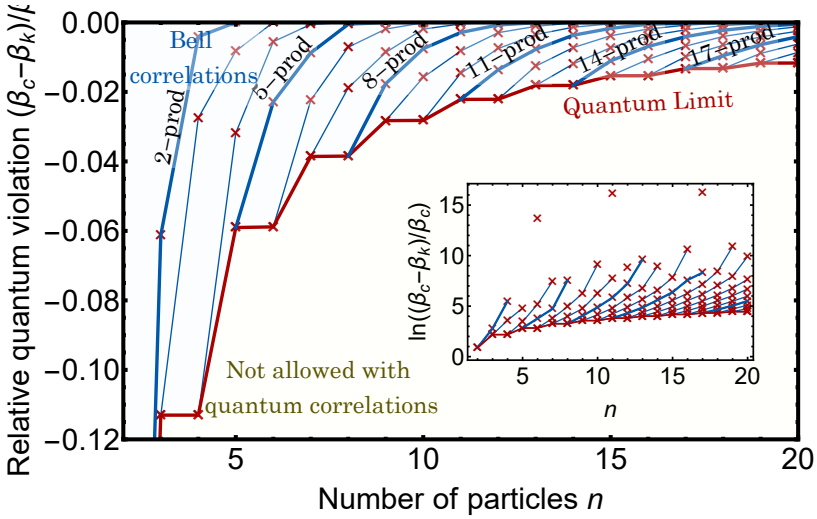

Fig. 4.7 Entanglement depth bounds relative to the classical bound $(\beta_c - \beta_k)/\beta_c$ for the DIWEDs in Eq. (4.27), found via the numerical methods up to 20 particles. One can appreciate that the relative maximal quantum violation, corresponding to $(\beta_c - \beta_n)/\beta_c$, approaches zero as the system size increases. In the inset we take the natural logarithm to illustrate that the precision required to certify entanglement depth increases with the number of particles. The three isolated points in the inset are due to numerical precision, since sometimes the variational method converges towards zero with way more precision than the SDP certificate, which provides a value close to zero with negative sign.

- The measurement settings for distinct regions converge to the same (up to local unitaries) as the size of the system increases.

In what follows, for large values of n, we are going to consider k to be a multiple of n in all cases, thus it will be convenient to define $m = |\mathcal{P}| = n/k$ as the number of regions in the system. We can do this without loss of generality since, for the cases where m does not divide n, the contribution by the small region containing the rest of $n \mod k$ parties will fade away as the system size increases (see e.g. [Fröwis *et al.*, 2017]). Moreover, as previously mentioned, the DIWEDs in Eq. (4.26) do not detect entanglement depths for $k < 5$, due to the nature of the two-body PIBI in which they are based, which does not detect non-local correlations for less than 5 parties.

Under this setting, it is convenient to define $\boldsymbol{\theta} \equiv (\varphi, \theta)$ in order to parametrize the measurements as $\mathcal{M}_0^{(i)} = \cos\varphi\sigma_z^{(i)} + \sin\varphi\sigma_x^{(i)}$ and $\mathcal{M}_1^{(i)} = \cos\theta\sigma_z^{(i)} + \sin\theta\sigma_x^{(i)}$. Then, there is a value $\theta - \varphi$ for which the state Eq. (4.30) can be described with $\sigma_{\mathcal{A}} =: \sigma$ and $\mu_{\mathcal{A}} =: \mu$ for all regions $\mathcal{A} \in \mathcal{P}$. That is, the states describing each region are all the same. Consequently, when doing the expectation value it will suffice to consider the state corresponding to a single region as the one in Eq. (4.29). Now we are ready to start the asymptotic analysis.

The first thing we notice, is that the expectation value for a k-producible state $|\Psi_{\mathcal{P}}\rangle$ and the the two-body Bell operator in Eq. (4.11) can get decomposed as follows:

$$\langle \mathcal{B} \rangle = \sum_{\mathcal{A}\in\mathcal{P}} \langle \mathcal{B}^{\mathcal{A}} \rangle + \sum_{\mathcal{A}\neq\mathcal{A}'\in\mathcal{P}} \frac{\gamma}{2} \langle \mathcal{S}_0^{\mathcal{A}} \rangle \langle \mathcal{S}_0^{\mathcal{A}'} \rangle + \delta \langle \mathcal{S}_0^{\mathcal{A}} \rangle \langle \mathcal{S}_1^{\mathcal{A}'} \rangle + \frac{\varepsilon}{2} \langle \mathcal{S}_1^{\mathcal{A}} \rangle \langle \mathcal{S}_1^{\mathcal{A}'} \rangle , \tag{4.31}$$

where $\mathcal{S}_k^{\mathcal{A}}$ and $\mathcal{B}^{\mathcal{A}}$ are, respectively, $\mathcal{S}_k$ and $\mathcal{B}$ restricted on the region $\mathcal{A}$.

For the particular Bell inequality coefficients that we consider for the DIWED (cf. Eq. (4.26)) we have

$$\langle \mathcal{B} \rangle = \sum_{\mathcal{A}\in\mathcal{P}} \langle \mathcal{B}^{\mathcal{A}} \rangle + \frac{1}{2} \sum_{\mathcal{A}\neq\mathcal{A}'\in\mathcal{P}} \Big(\langle \mathcal{S}_0^{\mathcal{A}} \rangle - \langle \mathcal{S}_1^{\mathcal{A}} \rangle \Big) \Big(\langle \mathcal{S}_0^{\mathcal{A}'} \rangle - \langle \mathcal{S}_1^{\mathcal{A}'} \rangle \Big). \tag{4.32}$$

Arrived at this point we can benefit from two known results in [Tura *et al.*, 2015]:

- The maximal quantum violation β_n of Eq. (4.26) behaves asymptotically as

$$\beta_n = -\frac{5}{2}n + \frac{\sqrt{3}}{2}n^{1/2} - \frac{3}{2} + \mathcal{O}(1). \tag{4.33}$$

  Compared to the approximation in [Tura *et al.*, 2015], here we do a refinement by considering that the parameter σ in Eq. (4.29) can be taken to be $\sigma = \sqrt{n/48}$ for large system sizes n, instead of just $\mathcal{O}(\sqrt{n})$ (see Appendix B.1.1 for more details).

- The one-body reduced density matrix corresponding to the optimal state can be approximated as

$$\rho_1 = \frac{n}{(n-1)}|+\rangle\langle+| + \begin{pmatrix} \frac{-1-2c}{2(n-1)} & 0 \\ 0 & \frac{2c-1}{2(n-1)} \end{pmatrix} + \mathcal{O}(1), \tag{4.34}$$

  where $c = \mu - n/2 = 1/(4\cos\theta)$ and $|+\rangle = (|0\rangle + |1\rangle)/\sqrt{2}$.

Therefore, combining Eqs. (4.33) and (4.34) tailored to our case leads to an approximation of the k-producible bounds for large n and k. Let us mention that, based on [Tura *et al.*, 2015], we will now be using the following measurement parameters optimal in the asymptotic limit: $\varphi = \pi - \theta$, $\theta = 5\pi/6$.

From Eq. (4.33) we observe that the expectation value on a region $\langle \mathcal{B}^A \rangle$ with size k will asymptotically converge to

$$\langle \mathcal{B}^A \rangle = -\frac{5}{2}k + \frac{\sqrt{3}}{2}k^{1/2} - \frac{3}{2} + \mathcal{O}(1). \tag{4.35}$$

Then, from Eq. (4.34) we observe that the expectation values of $\langle \mathcal{S}_0^{\mathcal{A}} \rangle$ and $\langle \mathcal{S}_1^{\mathcal{A}} \rangle$ will asymptotically tend to

$$\langle \mathcal{S}_0^{\mathcal{A}} \rangle = k\left(2c\cos(\theta) + \sin\theta k\right)/(k-1) \tag{4.36}$$

and

$$\langle \mathcal{S}_1^{\mathcal{A}} \rangle = k\left(-2c\cos(\theta) + \sin\theta k\right)/(k-1). \tag{4.37}$$

Which, under the optimal asymptotic value of $\theta = 5\pi/6$, become

$$\langle \mathcal{S}_0^{\mathcal{A}} \rangle - \langle \mathcal{S}_1^{\mathcal{A}} \rangle = \frac{k}{k-1}. \tag{4.38}$$

Therefore, in the asymptotic limit, a partition formed by $m = n/k$ regions leads to the k-producible bound:

$$\beta_k \approx m\left(-\frac{5}{2}k + \frac{\sqrt{3}}{2}k^{1/2} - \frac{3}{2}\right) + \binom{m}{2}\left(\frac{k}{k-1}\right)^2. \tag{4.39}$$

In terms of its relative quantum violation $\tilde{\beta}_k := (\beta_c - \beta_k)/\beta_c$, we have that

$$\tilde{\beta}_k = -\frac{1}{4} + \frac{\sqrt{3m}}{4}n^{-1/2} + \frac{m^2 - 4m}{4}n^{-1} + \mathcal{O}(n^{-3/2}). \tag{4.40}$$

In Figures 4.8 and 4.9 we show different k-producible bounds obtained for large system sizes n. In particular, in Figure 4.8 we consider the bounds corresponding to $k = n/m$ for $m \in [10]$, whereas in Figure 4.9 the bounds correspond to $k = n/m$ with $m = n^{1/x}$ for several integer values of x. As the system size n increases, we observe that the k-producible bounds tend to the relative maximal quantum violation $\beta_n = -1/4$ as $1/\sqrt{n}$, and the approximation holds as long as $m = \mathcal{O}(\sqrt[3]{n})$. Notice that much larger values of m (e.g., $m = \mathcal{O}(n)$) correspond to a small value of k, in which case the approximation in Eq. (4.35) could break down.

4.7 Experimental realizations: Collective measurements

DIWEDs are based on a Bell-type experiment. Thus, ideally the test requires to address the spatially separated parties individually, which

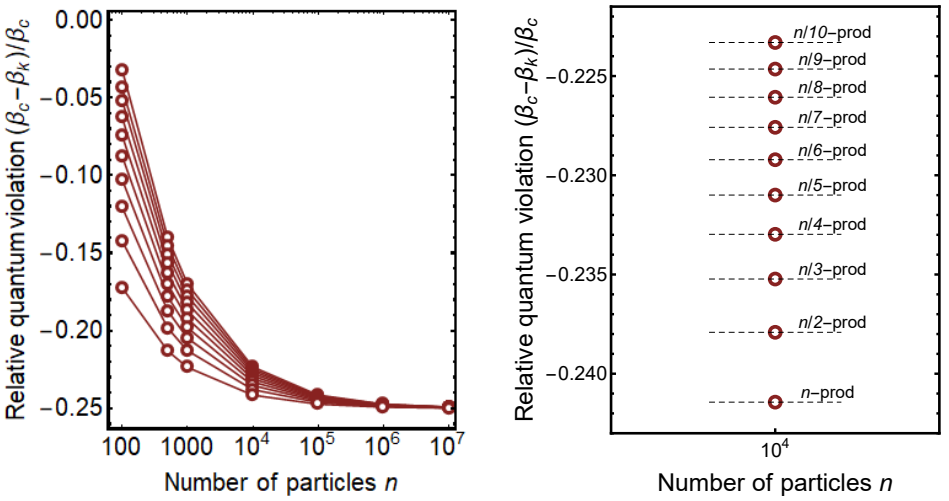

Fig. 4.8 Asymptotic approximation of the k-producible bounds for the DI-WEDs in Eq. (4.26). Left: Each point corresponds to a k-producible bound for $k = n/m$ and $m \in \{1, \ldots, 10\}$, where $m = 1$ corresponds to the lowest line, which coincides with the relative maximal quantum violation of Eq. (4.26). For the cases where $k = n/m$ is not an exact division, as a certificate we choose the value of n closest to a power of 10 and that is a multiple of m. The way we have computed the asymptotic bounds is by taking a state of the form Eq. (4.29) and numerically optimize $\mu_{\mathcal{A}}$ and $\sigma_{\mathcal{A}}$. The optimal value converges to the case where $\mu_{\mathcal{A}}$ and $\sigma_{\mathcal{A}}$ are equal for all regions $\mathcal{A}$, since they all have same cardinality $|\mathcal{A}|$. Let us note that the cases $m = \mathcal{O}(1)$ do not offer an experimentally robust result for large n, consequently we have considered a different scaling in Figure 4.9. Right: We select the particular case $n = 10^4$ to zoom in. The dotted lines are for illustrative purposes.

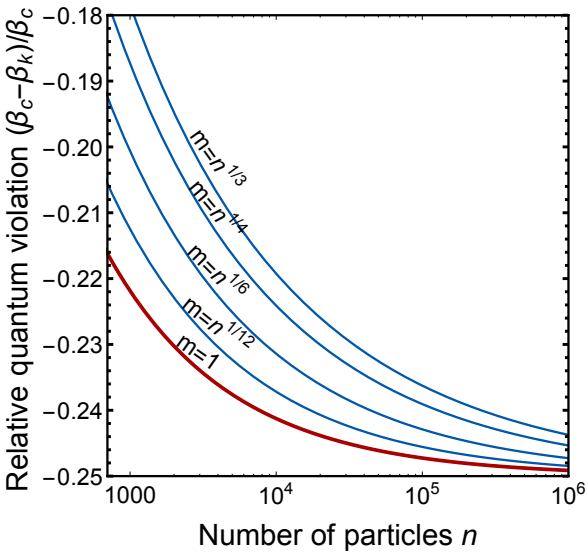

Fig. 4.9 Asymptotic k-producible bounds for the DIWEDs in Eq. (4.26) according to Eq. (4.40). Each line corresponds to a k-producible bound for $k = n/m$. Although in the thermodynamic limit the curves converge to the maximal quantum violation, the curves allow for robust entanglement depth detection in experimentally realistic parameter regimes [Schmied *et al.*, 2016; Engelsen *et al.*, 2017].

it becomes too demanding as the system size increases. Here is where the DIWEDs based on few-body symmetric correlators that we have presented truly shine, since they allow to perform the test by means of *Bell correlation witnesses*, which only require trusted collective measurements [Schmied *et al.*, 2016]. Thus, the DIWEDs in Eq. (4.26) allow to certify the entanglement depth in quantum many-body systems without an explicit characterization of the quantum state describing the system considered. However, it comes at the expense of relaxing the device-independent condition by having to consider assumptions.

In this section we rewrite the DIWEDs in Eq. (4.26) in terms of trusted collective measurements, which have already been implemented in experimental set-ups [Schmied *et al.*, 2016; Engelsen *et al.*, 2017].

In order to measure the DIWEDs in Eq. (4.26) by means of collective measurements, the main problem is the term $\mathcal{S}_{01}$. If we consider that all the parties perform the same measurement settings, $\mathcal{S}_k$ gets directly mapped to a collective spin measurement along the direction of $\mathcal{M}_k$, and its second moments allow to measure the expectation value of $\mathcal{S}_{kk}$ along the direction of $\mathcal{M}_k$ since $\mathcal{S}_{kk} = (\mathcal{S}_k)^2 - n$ [Tura *et al.*, 2015]. But in order to measure the $\mathcal{S}_{01}$ term, there does not seem to be an alternative to individually address the parties in the system. A possibility could be to estimate the second moments of the collective spin component along the directions given by $(\mathcal{M}_0 \pm \mathcal{M}_1)/\sqrt{2}$ [Tura *et al.*, 2015], but then one has to consider two extra directions in the Bell test which renders the approach unsatisfactory.

The Bell correlation witnesses approach was introduced in [Schmied *et al.*, 2016] to effectively measure, in the many-body regime of a BEC, an equivalence class of the Bell inequality associated to the DIWEDs in Eq. (4.26). To derive the Bell correlation witnesses tailored to the DIWEDs involving symmetric few-body correlators, one proceeds in the same way as in [Schmied *et al.*, 2016], except that for the DIWEDs instead of the classical bound β_k one now considers the k-producible bound β_k (and adapt to the Bell inequality coefficients being considered).

The hypotheses to construct Bell correlation witnesses are the following [Schmied *et al.*, 2016]:

- The applicability of quantum mechanical spin algebra.
- The particles in the system do not communicate nor interact through channels unaccounted for.
- The experimental calibration of the measurements is trusted.

Under these hypotheses, it is possible to circumvent the individual addressing of the particles required to measure the $\mathcal{S}_{01}$ term. The steps to derive the Bell correlation witnesses are the following [Schmied *et al.*, 2016]:

- Consider a model of description in which a spin-1/2 particle $\hat{s}^{(i)}$ is associated to each i-th observer, and consider that the measurements are spin projections along a direction $\boldsymbol{d}$ in the Block sphere; *i.e.*, $\mathcal{M}_{\boldsymbol{d}}^{(i)} = 2\hat{s}^{(i)} \cdot \boldsymbol{d} \equiv \boldsymbol{\sigma}^{(i)} \cdot \boldsymbol{d}$, where $\boldsymbol{\sigma}^{(i)} := \{\sigma_x^{(i)}, \sigma_y^{(i)}, \sigma_z^{(i)}\}$. Notice that the spin-1/2 description corresponds to the lowest energy levels of the atoms, while higher energy levels and further degrees of freedom (*e.g.*, atomic motion) are neglected.

- Define the total spin observable along the direction $\boldsymbol{d}$ as $\hat{S}_{\boldsymbol{d}} = \boldsymbol{d} \cdot \sum_i \hat{s}^{(i)}$.

- Consider the two unit vectors $\boldsymbol{a}$ and $\boldsymbol{n}$. Apply a symmetry transformation on $\boldsymbol{n}$ with respect to the symmetry axis defined by $\boldsymbol{a}$ in order to obtain the unit vector $\boldsymbol{m} = 2(\boldsymbol{a} \cdot \boldsymbol{n})\boldsymbol{a} - \boldsymbol{n}$. Notice that if we set the directions $\mathcal{M}_0^{(i)} = \mathcal{M}_{\boldsymbol{n}}^{(i)}$ and $\mathcal{M}_1^{(i)} = \mathcal{M}_{\boldsymbol{m}}^{(i)}$, then $\boldsymbol{a}$ is the bisector of the angle formed between the two directions $\boldsymbol{n}$ and $\boldsymbol{m}$.

- Consider the following identities in terms of the total spin component:

$$\langle \hat{S}_{\boldsymbol{n}} \rangle = \langle \mathcal{S}_0 \rangle / 2, \quad 16(\boldsymbol{a}\cdot\boldsymbol{n})^2 \langle \hat{S}_{\boldsymbol{a}}^2 \rangle = \langle \mathcal{S}_{00} \rangle + 2\langle \mathcal{S}_{01} \rangle + \langle \mathcal{S}_{11} \rangle + 4n(\boldsymbol{a}\cdot\boldsymbol{n})^2. \tag{4.41}$$

- Let $\boldsymbol{d} = -\boldsymbol{n}$, then $\boldsymbol{m} = -2(\boldsymbol{a}\cdot\boldsymbol{d})\boldsymbol{a} + \boldsymbol{d}$ and, therefore, one obtains the identity:

$$16(\boldsymbol{a} \cdot \boldsymbol{d})^2 \langle \hat{S}_{\boldsymbol{a}}^2 \rangle = \langle \mathcal{S}_{00} \rangle - 2\langle \mathcal{S}_{01} \rangle + \langle \mathcal{S}_{11} \rangle + 4n(\boldsymbol{a} \cdot \boldsymbol{d})^2. \tag{4.42}$$

- Finally, normalize to the classical bound in order to obtain:

$$\hat{W}_k = -2\hat{\mathcal{S}}_{\boldsymbol{d}/n} + 4(\boldsymbol{a} \cdot \boldsymbol{d})^2 \hat{S}_{\boldsymbol{a}}^2/n - (\boldsymbol{a} \cdot \boldsymbol{d})^2 - \frac{\beta_k}{2n}\mathbb{1}, \tag{4.43}$$

Concluding, the DIWEDs in Eq. (4.26) have now been turned into the witness in Eq. (4.43) which involves only first and second moments

of trusted collective spin measurements. Therefore, the witness satisfies the inequality $\langle \hat{W}_k \rangle \geq 0$ for all k-producible states. If one obtains an expectation value $\langle \hat{W} \rangle_k < 0$ then it gets certified that the quantum system being probed has an entanglement depth of at least $k+1$ particles. In other words, there are at least $k+1$ particles genuinely multipartite entangled in the system. In the following section we are going to use the witness in Eq. (4.43) to certify entanglement depth with experimental data and do a comparison with other existing entanglement depth criteria.

4.8 Comparison to other entanglement depth criteria and experimental data

In this section we compare the DIWEDs in Eq. (4.26) to other entanglement depth criteria based on spin-squeezing. We have seen in the previous section that the DIWEDs in Eq. (4.26) can be effectively evaluated via Bell correlation witnesses of the form in Eq. (4.43), which only require estimating the first and second moments of the total spin components. Recall for the case $\beta_k = \beta_1$, Eq. (4.43) becomes equivalent to the Bell correlation witness that was derived in [Schmied *et al.*, 2016], and which was experimentally implemented in a BEC formed by 480 ^{87}Rb atoms. Therefore, by rewriting Eq. (4.43) in terms of spin-squeezing quantities, one can use the experimental data presented in [Schmied *et al.*, 2016] as a scenario to compare the performance of the DIWEDs presented in this chapter with other existing witnesses of entanglement depth based on spin-squeezing inequalities, such as the (not DI) Wineland spin-squeezing criterion [Wineland *et al.*, 1994; Sørensen and Mølmer, 2001]. Furthermore, we also compare our DIWEDs with the so-called *Bell correlation depth witnesses* presented in [Baccari *et al.*, 2019; Baccari, 2019].

Let us dedicate some words about Bell correlation depth witnesses, which is another of our work with collaborators that will not be explicitly presented in the present thesis (but is presented in detail in

Baccari's thesis [Baccari *et al.*, 2019]). Bell correlation depth witnesses are based on the same Bell inequality as the DIWEDs in Eq. (4.26), but instead of deriving entanglement depth witnesses, one derives nonlocality depth witnesses by considering hybrid local-nonlocal models. In particular, instead of considering k-producible states and quantum correlations to derive the bounds, in [Baccari *et al.*, 2019] the idea is to obtain bounds by grouping parties in regions of at most k parties and allow them to produce any non-signalling probability distribution within the region. Therefore, one obtains correlations that go beyond the quantum correlations one can obtain with k-producible quantum states (possibly obtaining even supraquantum correlations).

To carry out the comparison benefiting from the experimental data in [Schmied *et al.*, 2016], we first need to rewrite the Bell correlation witnesses in Eq. (4.43) in terms of spin-squeezing quantities. Consider the *scaled collective spin*, also referred to as *spin contrast*, in a direction $\boldsymbol{d}$ defined as

$$C_{\boldsymbol{d}} := \langle 2\hat{S}_{\boldsymbol{d}}/\hat{n}\rangle = \langle 2\hat{S}_{\boldsymbol{d}}\rangle/n, \tag{4.44}$$

where $\hat{n}$ is the particle number operator, and for the last equality we have used the commutation relation $[\hat{S}_{\boldsymbol{d}}, \hat{n}] = 0$.

The experimental implementation now relies on counting the number of particles. Let us note that, because the last equality in Eq. (4.44) holds due to the commutation relations, we do not need to worry about the possible oscillation in number of particles from one test run to another [Schmied *et al.*, 2016].

Consider now the *scaled second moment collective spin* in a direction $\boldsymbol{a}$ defined as

$$\zeta^2_{\boldsymbol{a}} := \langle 4\hat{S}^2_{\boldsymbol{a}}/\hat{n}\rangle = \langle 4\hat{S}^2_{\boldsymbol{a}}\rangle/n, \tag{4.45}$$

where again we have used the commutation relation $[\hat{S}^2_{\boldsymbol{a}}, \hat{n}] = 0$ for the equality.

Then, the Bell correlation witnesses in Eq. (4.43) gets rewritten in terms of spin-squeezing quantities as

$$\langle \hat{W}_k\rangle = -C_{\boldsymbol{d}} + (\boldsymbol{a}\cdot\boldsymbol{d})^2\zeta^2_{\boldsymbol{a}} - (\boldsymbol{a}\cdot\boldsymbol{d})^2 - \frac{\beta_k}{2n}, \tag{4.46}$$

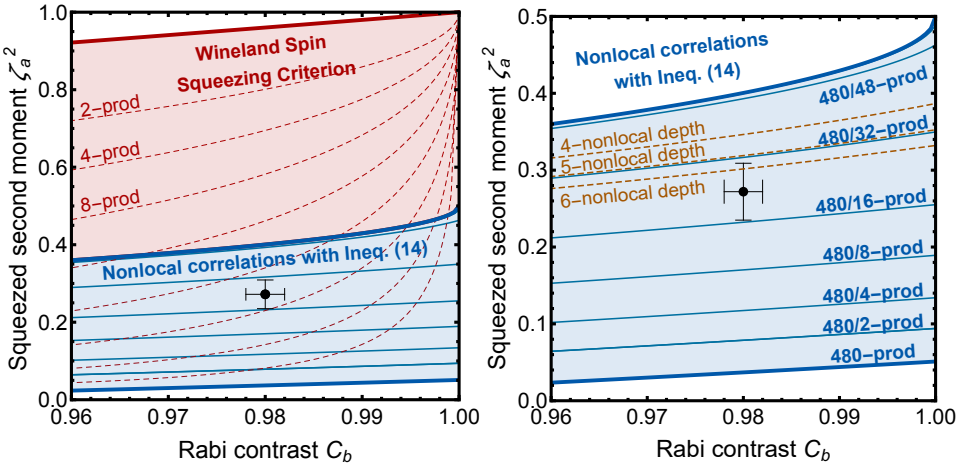

Fig. 4.10 Comparison between witnesses of entanglement depth. The comparison with other known criteria is based on the experimental data presented in [Schmied *et al.*, 2016]. The experimental data is represented as the black dot with 1 standard deviation error bars, which has been obtained on a BEC of $n = 480$ ^{87}Rb atoms. The witnesses are expressed in terms of the Rabi contrast C_b and the squeezed second moment ζ_a^2. The area below a curve denotes violation of the corresponding witness. **Left:** Represented as red dotted lines are the not device-independent witnesses of entanglement depth resulting from the Wineland spin-squeezing criterion [Wineland *et al.*, 1994; Sørensen and Mølmer, 2001]. Represented as the blue thick line is the Bell correlation witness from [Schmied *et al.*, 2016], which is based on an equivalent Bell inequality to the one considered in Eq. (4.26) for the case $\beta_k = \beta_1$. As blue thin lines, the DIWEDs in Eq. (4.26), that we have characterize throughout the chapter, expressed in terms of collective measurements as shown in Eq. (4.47). **Right:** Zoom in to show several k-producible bounds β_k for the DIWEDs in Eqs. (4.26) and (4.47). As yellow discontinuous lines we show the nonlocality depth witnesses derived in [Baccari *et al.*, 2019], also based on the Bell inequality considered in Eq. (4.26). The DIWEDs presented in the present chapter certify an entanglement depth of 15, whereas the criteria [Baccari *et al.*, 2019] certifies a Bell correlations depth of 5 and the Wineland spin-squeezing criteria certifies an entanglement depth of 28.

where the inequality $\langle \hat{W}_k \rangle$ is satisfied for all k-producible states.

Finally, as in [Schmied *et al.*, 2016], let us decompose the direction $\boldsymbol{d}$ into three orthonormal vectors $\boldsymbol{a}, \boldsymbol{b}, \boldsymbol{c}$, such that $\boldsymbol{a}$ is the squeezed axis. Notice that by choosing the direction $\boldsymbol{a}$ to correspond to the squeezed axis, one can assume $C_{\boldsymbol{a}} \approx 0$ and, therefore, it is only required to sweep along the $\boldsymbol{b}$ direction. Under these choice of directions, one can finally rewrite Eq. (4.46) as

$$\zeta_{\boldsymbol{a}}^2 \geq \frac{1}{2}\left(1 + \frac{\beta_k}{2n} - \sqrt{\left(1 - \frac{\beta_k}{2n}\right)^2 - C_{\boldsymbol{b}}^2}\right). \tag{4.47}$$

In Figure 4.10 we present the performance of the DIWEDs and its comparison with other witnesses of entanglement depth. We have used the k-producible bounds β_k of the DIWEDs in Eq. (4.26) to obtain the inequalities in terms of spin-squeezing in Eq. (4.47). We observe that: our DIWEDs certify an entanglement depth of $k \geq 15$; the Wineland spin-squeezing criteria [Wineland *et al.*, 1994] certifies an entanglement depth of $k \geq 28$; and the Bell correlation depth certifies a nonlocality depth of $k \geq 5$. It appears then that the more strict a criteria is, the less depth is certified: on one extreme we have the Bell correlation depth witnesses, which are DI and only based in non-local correlations without quantum mechanics playing a role in the derivation of their bounds; then we have the DIWEDs presented in this chapter, which are DI and the derivation of the bounds uses non-local correlations obtained from quantum correlations; and finally we have the Wineland spin-squeezing criteria which only considers quantum mechanics and has no criteria about non-local correlations.

Chapter 5

Non-local correlations near quantum critical points

In the previous chapter we have seen that non-local correlations serve to characterize multipartite entanglement in the many-body regime. A natural step forward is to consider whether we can use non-local correlations to characterize large-scale quantum phenomena where entanglement plays a role. For instance, *Quantum Critical Points* (QCP) are known to stabilize quantum correlations at all length scales [Sachdev, 2011], but the behaviour of nonlocality near QCPs remains unexplored. However, to consider QCPs we need to characterize nonlocality for large system sizes, which poses a highly complex task [Brunner *et al.*, 2014].

As we have seen in Chapter 4, the two-body permutationally invariant Bell inequalities (PIBI) [Tura *et al.*, 2014a, 2015] offer a way to partially circumvent the complexity by involving only one- and two-body symmetric correlators, which can be effectively measured by first and second moments of collective observables. Furthermore, we have seen in Section 4.7 that two-body PIBIs have been experimentally evaluated via the dynamical generation of spin-squeezed states in BECs [Schmied *et al.*, 2016; Pezzè *et al.*, 2018]. On the other hand, for the Transverse-field Ferromagnetic Ising Model (TFIM) spin-squeezing is

known to arise in the vicinity of its QCP [Frérot and Roscilde, 2018; Gabbrielli *et al.*, 2018]. Therefore, the TFIM supposes a good candidate on which to probe non-local correlations near QCPs via two-body PIBIs. Furthermore, we are also interested in considering a TFIM with tunable range interactions which allow us to explore the Bell inequalities performance near QCPs as the range decreases from infinite-range interactions to nearest neighbours interactions.

In this chapter we investigate non-local correlations at the QCP of the TFIM with tunable range interactions, interpolating between infinite-range and nearest-neighbour interactions. The chapter is organized as follows: In Section 5.1 we start by introducing the two-body PIBI considered and, when all parties perform the same measurement settings on qubits, establish spin-squeezing as a necessary condition for its violation; In Section 5.2 we present the tunable range TFIM and discuss its phase diagram as well as the spin-squeezing properties near the QCPs; then we proceed with a numerical exploration, where in Section 5.3.1 we present the methodology based on Density Matrix Renormalization Group (DMRG) and optimization of the two-body PIBI, and in Section 5.3.2 we display and discuss the results obtained; Finally, in Section 5.4 we present analytical Linear spin wave (LSW) predictions to show that spin-squeezing is a generic feature close to the TFIM QCPs which leads to the maximal violation of the two-body PIBI in the thermodynamic limit.

The original results presented in this chapter are based on the publication [Piga *et al.*, 2019], a joint collaboration between A. Piga, M. Lewenstein, and I. Frérot.

5.1 The 2-body PIBI and spin squeezing

In order to probe non-local correlations near QCPs, we require a Bell inequality which is valid for any number of parties n and offers the possibility to be evaluated for large system sizes. As we have seen in Chapter 4, it is in general not possible to characterize multipartite Bell inequalities due to their high combinatorial complexity, specially

in large system sizes. On the other hand, the two-body PIBIs (cf. Chapter 4 and Section 2.3.4), have desirable properties that reduce a lot their combinatorial complexity. Therefore, in the present chapter we consider again two-body PIBIs. In particular, we are going to use one of the Bell inequalities previously introduced in Chapter 4, which takes the following form:

$$-2\langle \mathcal{S}_0 \rangle + \frac{1}{2}\langle \mathcal{S}_{00} \rangle - \langle \mathcal{S}_{01} \rangle + \frac{1}{2}\langle \mathcal{S}_{11} \rangle - \beta_c \geq 0, \tag{5.1}$$

where the classical bound for this Bell inequality is $\beta_c = 2n$, and $\mathcal{S}_k, \mathcal{S}_{kl}$ denote the one- and two- symmetric correlators respectively (see Equation (4.5)) with $k, l \in \{0, 1\}$. Recall that two-body PIBIs follow an $(n, 2, 2)$ Bell scenario in which an multipartite resource is distributed among n parties, indexed as $[n] := \{1, \ldots, n\}$, who perform one out of two dichotomic measurements.

In terms of collective spin measurements

Because spin-squeezed states are known to stabilize near QCPs [Frérot and Roscilde, 2018; Gabbrielli *et al.*, 2018], we are also going to be willing to sacrifice a fully loophole free Bell test (thus stepping away from the fully DI formalism) in exchange to express the Bell inequality in Eq. (5.1) in terms of collective spin measurements and second moments thereof (as we already did in Section 4.7, where more details are given). In particular, given an n-qubit quantum state, we are going to consider two possible directions $\boldsymbol{n}$ and $\boldsymbol{m}$ as measurement choices on which to project every qubit. Then, the one- and two- symmetric correlators get recast as

$$\mathcal{S}_{\mathbf{u}} = \sum_{i\in[n]} \langle \sigma_{\boldsymbol{u}}^{(i)} \rangle \,, \qquad \mathcal{S}_{\boldsymbol{uv}} = \sum_{i\neq j\in[n]} \langle \sigma_{\boldsymbol{u}}^{(i)} \sigma_{\boldsymbol{v}}^{(j)} \rangle \,, \tag{5.2}$$

where $\sigma_{\boldsymbol{u}}^{(i)} = \boldsymbol{u}\cdot\boldsymbol{\sigma}^{(i)}$ for some directions $\boldsymbol{u}, \boldsymbol{v} \in \{\boldsymbol{n}, \boldsymbol{m}\}$ and $\boldsymbol{\sigma}^{(i)}$ denotes the usual vector of Pauli matrices in the i-th party.

Let us denote as $\boldsymbol{J} = \sum_{i\in[n]} \boldsymbol{\sigma}^{(i)}/2$ and consider a direction $\boldsymbol{a} = (\boldsymbol{n}-\boldsymbol{m})/|\boldsymbol{n}-\boldsymbol{m}|$ which will convenient to find the optimal directions leading to nonlocality detection. Then, by means of common quantum mechanical spin algebra (recall Section 4.7 for details), the Bell inequality in Eq. (5.1) can be rewritten as [Schmied *et al.*, 2016]:

$$\langle W\rangle = 1 - |C_{\boldsymbol{n}}| + (\boldsymbol{a}\cdot\boldsymbol{n})^2(\zeta_{\boldsymbol{a}}^2 - 1) \geq 0, \tag{5.3}$$

where $C_{\boldsymbol{n}} = \langle 2J^{\boldsymbol{n}}\rangle/n \equiv 1 - r < 1$ is the scaled first moment collective spin (also called *spin contrast*) along direction $\boldsymbol{n}$, and $\zeta_{\boldsymbol{a}}^2 = \langle 4(J^{\boldsymbol{a}})^2\rangle/n$ is the scaled second moment collective spin along direction $\boldsymbol{a}$. Let us state clear that, as opposed to the Bell inequality in Eq. (4.26), the Bell correlations witness in Eq. (5.3) relaxes the loophole free and device-independent conditions by requiring the assumptions that the individual subsystems forming the quantum state being probed are qubits and that the measurement axes are well-controlled and trusted. Therefore, given the context of the present chapter the assumptions come naturally. However, strictly speaking a violation of the Bell correlation witness in Eq. (5.3) witnesses the ability by the many-spin quantum state being probed to exhibit non-local correlations if the spins were to be individually measured along directions $\boldsymbol{n}$ and $\boldsymbol{m}$ [Schmied *et al.*, 2016].

The optimization of the directions that maximally violate Eq. (5.3) can now be found analytically. Consider the mean spin direction denoted $\boldsymbol{z}$; *i.e.*, $\langle\boldsymbol{J}\rangle \propto \boldsymbol{z}$. Notice that the cases in which $\mathbf{a}\cdot\mathbf{z} \neq 0$ yield $\zeta_{\mathbf{a}}^2 \propto N$, which contributes to prevent the violation of Eq. (5.3). Therefore, one wants to choose axis $\mathbf{a}$ to be perpendicular to $\mathbf{z}$ in order to observe violation. Under this circumstances, the minimum of Eq. (5.3) is obtained when the direction $\boldsymbol{a}$ corresponds to the direction minimizing the variance of $\boldsymbol{J}$. Notice then that to violate Eq. (5.3) one requires spin-squeezing $\zeta_{\mathbf{a}}^2 < 1$ [Kitagawa and Ueda, 1993; Sørensen and Mølmer, 2001; Pezzè *et al.*, 2018], while maintaining the largest possible spin length; *i.e.*, $r \to 1$. Then, by setting $\boldsymbol{n} = \boldsymbol{z}\cos\theta + \boldsymbol{a}\sin\theta$ one ends up with $\langle W\rangle = -(1-r)\cos\theta + (1-\zeta_{\boldsymbol{a}}^2)\cos^2\theta + \zeta_{\boldsymbol{a}}^2$. The

minimum is then given by $\cos\theta = (1-r)/[2(1-\zeta_{\boldsymbol{a}}^2)]$ which yields:

$$\langle W\rangle_{\min} = \zeta_{\boldsymbol{a}}^2 - \frac{(1-r)^2}{4(1-\zeta_{\boldsymbol{a}}^2)} > -\frac{1}{4}\,. \tag{5.4}$$

The direction for the second moment collective spin measurement is then given by $\boldsymbol{m} = \boldsymbol{z}\cos\theta - \boldsymbol{a}\sin\theta$. Let us note that the minimum found in Eq. (5.4) coincides with the maximal amount of quantum violation that can be achieved with the two-body PIBI in Eq. (5.1) [Tura *et al.*, 2014a, 2015]. Furthermore, notice that said minimum will be achieved for perfect squeezed states (*i.e.*, $\zeta_{\mathbf{a}}^2 \to 0$ and $r \to 0$), which are attainable only in the asymptotic limit $n \to \infty$ [Fadel and Tura, 2018].

5.2 Ferromagnetic Ising model with tunable interactions under a transverse field

In this section we introduce the spin model considered throughout the chapter to carry out our explorations: the Ferromagnetic (FM) Ising model with power-law decaying (as $1/r^{\alpha}$) interactions under a transverse field. The choice of the model is motivated mainly by two reasons: On one hand, spin-squeezed states are known to stabilize near QCPs of the FM Ising Model under transverse field [Frérot and Roscilde, 2018; Gabbrielli *et al.*, 2018]; On the other hand, the two-body PIBI in Eq. (5.1) are known to be violated by symmetric states like, for instance, some ground states of the *Lipkin-Meshkov-Glick* model [Tura *et al.*, 2014a, 2015]. Therefore, by considering the TFIM with tunable interactions we will be able to explore non-local correlations via the two-body PIBIs as the range of interactions in the Ising model decreases from the infinite-range (equivalent to the LMG model, where we know that ground states may have support on the symmetric space) to the nearest neighbours case.

In particular, the model considered gets described by the following

Hamiltonian:

$$\mathcal{H} = -\frac{1}{\gamma_{\mathbf{0}}} \sum_{i \neq j} \gamma_{ij} \mathcal{S}_{\boldsymbol{x}}^{(i)} \mathcal{S}_{\boldsymbol{x}}^{(j)} - h \sum_{i} \mathcal{S}_{\boldsymbol{z}}^{(i)}, \tag{5.5}$$

where i and j run over the sites of a d-dimensional square lattice of size $n = L \times (L/2)^{d-1}$; $\mathcal{S}_{\boldsymbol{a}}^{(i)} = \sigma_{\boldsymbol{a}}^{(i)}/2$ for $\boldsymbol{a} \in \{\boldsymbol{x}, \boldsymbol{y}, \boldsymbol{z}\}$; $\gamma_{ij} = |\boldsymbol{l}_i - \boldsymbol{l}_j|^{-\alpha}$ with $\boldsymbol{l}_i$ denoting the position of the i-th spin and the parameter α tunes the range of interactions; and $\gamma_{\mathbf{0}} = \sum_{i \neq j} \gamma_{ij}/n$ normalizes the interaction term to have a well-defined thermodynamic limit also for $\alpha < d$.

The phase diagram for the tunable range TFIM is well understood. Mean-field theory predicts a QCP at $h = h_c = 1$ between FM phases ($h < h_c$) and Paramagnetic (PM) phases ($h > h_c$). In general the exact QCP can be found at $1/2 \leq h_c \leq 1$. For instance, for a chain configuration ($d = 1$) with nearest neighbours interactions ($\alpha \to \infty$), the exact QCP is at $h_c = 1/2$ [Sachdev, 2011]. In the PM phase, the ground state corresponds to the spins aligning along $\boldsymbol{z}$, whereas in the FM phase the spins spontaneously align along $\tilde{\boldsymbol{z}} = \boldsymbol{z} \cos\theta \pm \boldsymbol{x} \sin\theta$, which for mean-field theory becomes $\cos\theta = h$.

At the vicinity of the QCP, the fluctuations in the magnetization along $\boldsymbol{x}$ diverge as a power-law with the system size; *i.e.*, $\langle (J_{\boldsymbol{x}})^2 \rangle / n \sim n^{\theta(\alpha)}$ for a certain critical exponent $\theta(\alpha)$ that depends on the power-law exponent α. As for the fluctuations in the magnetization along $\boldsymbol{z}$, the presence of the transverse field maintains a finite magnetization $J_{\boldsymbol{z}}$, so that $\langle J_{\boldsymbol{z}} \rangle / n = \mathcal{O}(1)$.

Consequently, Heisenberg's inequality for collective spins opens up the possibility to squeeze the magnetization fluctuations along $\boldsymbol{y}$ as $\zeta_{\boldsymbol{y}} = \langle (J_{\boldsymbol{y}})^2 \rangle / n \geq \mathcal{O}(n^{-\theta(\alpha)})$. However, this is not always the case. While quantum-critical spin squeezing is indeed known to be present in the infinite range interactions limit $\alpha = 0$ [Dusuel and Vidal, 2004; Frérot and Roscilde, 2018], for the cases with nearest neighbours interactions squeezing appears only for lattice dimensions $d \geq 2$, being almost absent for the chain case $d = 1$ [Liu *et al.*, 2013; Frérot and Roscilde, 2018]. On the other hand, FM power-law interactions can be considered to effectively increase the physical dimension of the system,

since they increase the connectivity of the Ising model. Therefore, we can expect a non-trivial behaviour as the power-law exponent α varies at the QCP. In particular, for the chain case $d = 1$ with nearest neighbours interactions $\alpha = 0$ we do not expect spin squeezing to appear and, hence, neither the violation of the inequalities in Eqs. (5.1) and (5.3). However, for small values of α we may expect spin squeezing and violation of the inequalities even in the chain $d = 1$ case.

5.3 Numerical exploration

In this section we numerically explore non-local correlations in a 1-dimensional TFIM with tunable interactions as described in Eq. (5.5) via the Bell inequality in Eq. (5.1). In Section 5.3.1 we present the numerical methods employed, and in Section 5.3.2 we present the numerical results obtained.

5.3.1 Numerical methodology

In order to obtain the numerical results, the whole task boils down to two steps: 1) obtain the ground states; 2) find the optimal measurements that may lead to nonlocality detection.

For the numerics we are going to be considering 1-dimensional lattice systems, in which case it is convenient to utilize the DMRG algorithm [Evenbly, 2019] as a variational method for the ground state. In order to consider power-law and long-range interactions in the DMRG algorithm, we follow the methodology presented in [Crosswhite *et al.*, 2008; Fröwis *et al.*, 2010].

Once we have a ground state, we still need to find the optimal measurement settings in order to observe whether its quantum correlations are sufficient to display violation of the two-body PIBI in Eq. (5.1). In order to tackle the optimization problem we will proceed similar as in Section 4.5. The first thing we notice is that the associated Bell

operator $\mathcal{B}$ of Eq. (5.1) involves at most two-body terms:

$$\mathcal{B} = -2\sum_{i\in[n]} \mathcal{M}_0^{(i)} + \sum_{i\neq j\in[n]} \left(\frac{\mathcal{M}_0^{(i)} \otimes \mathcal{M}_0^{(j)}}{2} - \mathcal{M}_0^{(i)} \otimes \mathcal{M}_1^{(j)} + \frac{\mathcal{M}_1^{(i)} \otimes \mathcal{M}_1^{(j)}}{2} \right), \tag{5.6}$$

where $\mathcal{M}_k^{(i)}$ denotes the measurement to be performed on the i-th party. The immediate implication of Eq. (5.6) is that, from the quantum state given by the DMRG, we do not need to consider the whole state vector contraction, but only the contractions providing the one- and two-body reduced states. In what follows, we denote as σ_i the one-body *Reduced Density Matrix* (RDM) for the i-party and as σ_{ij} the two-body RDM for the i-th and j-th parties. Therefore, the optimization problem to find violation of Eq. (5.1) takes the following form

$$\min_{\boldsymbol{\theta}} \quad \left(-2\sum_{i\in[n]} \mathrm{Tr}\left[\mathcal{M}_0^{(i)}\sigma_i\right] + \sum_{i\neq j\in[n]} \mathrm{Tr}\left[\left(\frac{\mathcal{M}_0^{(i)} \otimes \mathcal{M}_0^{(j)}}{2} - \mathcal{M}_0^{(i)} \otimes \mathcal{M}_1^{(j)} + \frac{\mathcal{M}_1^{(i)} \otimes \mathcal{M}_1^{(j)}}{2} \right) \sigma_{ij} \right] \right), \tag{5.7}$$

where $\boldsymbol{\theta}$ denotes the measurement settings.

As opposed to the case considered in Section 4.5, this time the quantum state is fixed. Hence, in order to optimize the measurements, in this case we consider the measurement parametrization $\mathcal{M}_k^{(i)} = \sin\theta_{i,k}\cos\varphi_{i,k}\sigma_x^{(i)} + \sin\theta_{i,k}\sin\varphi_{i,k}\sigma_y^{(i)} + \cos\theta_{i,k}\sigma_z^{(i)}$ for $k \in [2]$ and $i \in [n]$. Therefore, the Bell operator will now depend on all the parameters $\theta_{i,k}, \varphi_{i,k}$, which we encode on a vector $\boldsymbol{\theta}$.

Finally, to carry out the optimization in Section 5.3.1 we employ the same methodology as in Step 3 from Section 4.4.1. That is, we obtain a variational upper bound via a see-saw technique on the measurements (see e.g. [Werner and Wolf, 2001; Pál and Vértesi, 2010]). In order to reduce the amount of local minima, based on previous numerical evidence presented in Section 4.5.1 and [Tura *et al.*, 2014a, 2015],

as a first quick search one may want to consider the assumption that the measurement settings leading to violation of Eq. (5.1) correspond to the case where all parties in the system perform the same measurement settings; *i.e.*, $\theta_{i,k} = \theta_k$ and $\varphi_{i,k} = \varphi_k$ for all $i \in [n]$ and $k \in [2]$. The assumption can be thought of as a numerical ansatz, which reduces the optimization problem to employ the see-saw technique for only 4 parameters. Then, once the see-saw algorithm has converged within the desired numerical accuracy, one can lift off the assumption and proceed with a general see-saw along all the parameters in $\boldsymbol{\theta}$ and check whether the minimum attained gets reduced. For our numerical results we have considered both approaches: without assumption and starting with the assumption to then lift it off. From the results obtained, we did not find a minimum that was not reachable also under the same measurement settings assumption. Thus providing further numerical evidence that the optimal measurements for the two-body PIBI in Eq. (5.1) correspond to the case when all the parties perform the same measurement settings.

5.3.2 Numerical results

Now we take the model in Eq. (5.5) and, for each range of interactions α and transverse field h, obtain a ground state via DMRG and look for non-local correlations as explained in Section 5.3.1. In Figure 5.1 we show the maximal violation obtained with the two-body PIBI in Eq. (5.1), as well as the half-chain von Neumann Entanglement Entropy (EE). Once observes that for values $\alpha \to 0$ the violation of the two-body PIBI is higher, as expected due to the nature of the two-body PIBI under consideration. Then, as the range of interactions decrease, the violation of Eq. (5.1) also decreases until eventually there is not detection of nonlocality for $\alpha \lesssim 3$, which can be explained by the almost absence of spin squeezing at the nearest neighbour QCP [Liu *et al.*, 2013; Frérot and Roscilde, 2018]. Notice that the detection of non-local correlations appears in the vicinity of the QCP.

Remarkably, in Section 5.3.2 we show that the maximal half-chain

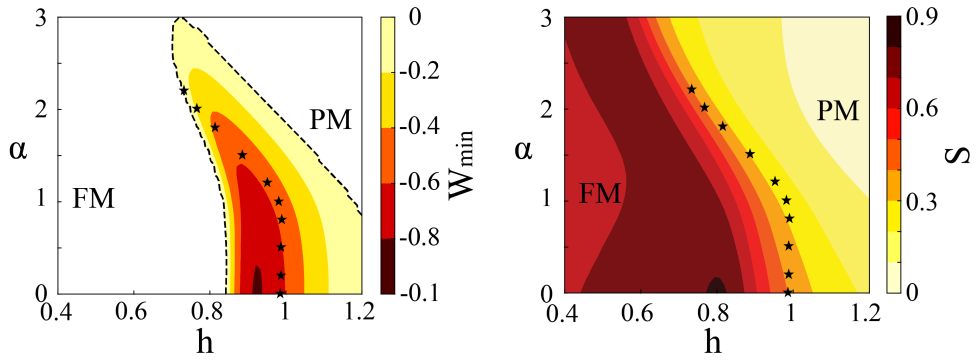

Fig. 5.1 Numerical results through the phase diagram for the tunable range TFIM described in Eq. (5.5) corresponding to an $n = 40$ chain. The stars correspond to extrapolations $n \to \infty$ of the maximal half-system EE, which marks the QCP between the FM phase and the PM phase. **Left:** Maximal violation of the two-body PIBI in Eq. (5.1), denoted as $W_{\min}$, given a ground state. Negative values $W_{\min} < 0$ violate the inequality exhibiting the presence of non-local correlations. **Right:** Half-chains EE of the ground state.

EE and the maximal violation of Eq. (5.1) happen at the same transverse-field value when extrapolating to the thermodynamic limit. Therefore, since in the asymptotic limit the half-chain EE exhibits a maximum at the QCP independently of α, the coincidence of maximums manifests the quantum-critical origin of the violation for Eq. (5.1).

The fits considered in Section 5.3.2 to extrapolate the finite-size computations follow the expression $h_c(N) = h_c(\infty) + aN^{-2/3}$. Finite-size scaling theory predicts $h_c(n) - h_c(\infty) \sim L^{-1/\nu}$, where ν denotes the exponent of the correlation length. For infinite-range interactions, L is replaced by n^{1/d_c} where $d_c = 3$ is the upper critical dimension of the quantum Ising model [Botet *et al.*, 1982]. Hence, with $\nu = 1/2$ (expected for infinite-range interactions), $h_c(n) - h_c(\infty) \sim n^{-2/3}$. Since LSW theory predicts that for $\alpha < 1$ the model is equivalent to the $\alpha = 0$ limit, it is natural to expect that the same scaling law holds up to $\alpha = 1$. On the other hand, for $\alpha > 1$ there is no reason to

expect the same exponent. However, strong finite-size effects do not allow us to observe significant deviations from the mean-field behaviour for $\alpha < 2.2$ (taking into account the system sizes accessible with our DMRG computations). Furthermore, in Section 5.3.2 we also show some k-producible bounds from the DIWEDs previously constructed in Chapter 4 for Eq. (5.1). One we have observed some non-local correlations, the certification of entanglement depth needs no other procedure than to check which k-producible bound is violated. In this way, it can serve as a certification tool to provide insight on how the quantum correlations spread in the vicinity of QCPs, and to certify whether entanglement depth diverges at the critical point.

In Figure 5.3 we show the maximal violation of Eq. (5.1) obtained at the finite-size precursor of the QCPs, as a function of the system size n and the power-law exponent α. We call the value h at which the maximal violation is found the finite-size precursor of the QCP denoted $h_c(n, \alpha)$. With LSW theory applied on the witness in Eq. (5.3), that we shall consider in Section 5.4, we observe that for $\alpha < d$ and $n \to \infty$ (where d is the lattice dimension), the maximal violation tends to $\langle W \rangle_{\min} \to -1/4$. On the other hand, we also observe a quantifiable error on the extrapolation for $n \leq 170$ compared to the prediction, which we attribute it to be due to strong finite-size effects. As one increases α, the violation of Eq. (5.1) weakens up to $\alpha \gtrsim 3$ where the detection of nonlocality with Eq. (5.1) vanishes. To carry out the fit in Figure 5.3 for the extrapolation we have used the analytical results for $\alpha = 0$ in [Dusuel and Vidal, 2004], which predict $\langle J_{\boldsymbol{z}} \rangle \to n/2$ and $\langle (J_{\boldsymbol{y}})^2 \rangle \sim n^{2/3}$ and, therefore, $W_{\min}(n) = W_{\min}(\infty) + an^{-1/3}$ from Eq. (5.4). Since for $\alpha \leq 2.2$ and the system sizes accessible via our DMRG we did not observe deviations from the $\alpha = 0$ behaviour, we used the same fitting function in the $\alpha \leq 2.2$ cases.

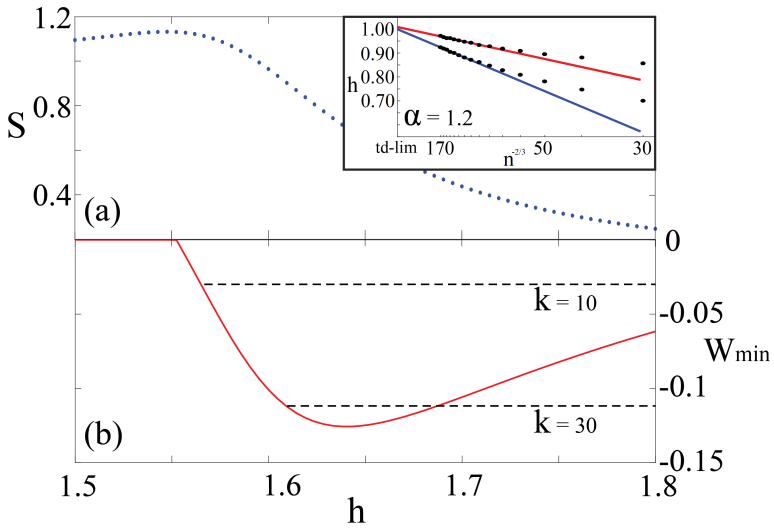

Fig. 5.2 Numerical results for an $n = 170$ chain TFIM described in Eq. (5.5) with $\alpha = 1.2$ and as a function of the transverse field h. In (a) we show the half-chain EE. In (b) we show the maximal violation of Eq. (5.1), where the dashed lines correspond to the k-producible bound for the DIWEDs built upon Eq. (5.1) in Chapter 4. An entanglement depth of $k \geq 30$ is certified at the maximal violation. Finally, the inset in (a) shows the maximum of the half-chain EE and the maximal violation of Eq. (5.1) for several distinct system sizes n, from which the critical point is extrapolated in the thermodynamic limit. The extrapolations follow $h_c(n) = h_c(\infty) + an^{-2/3}$. Remarkably, in the asymptotic limit both the half-chain EE and the maximal violation of Eq. (5.1) occur at the same transverse field h_c.

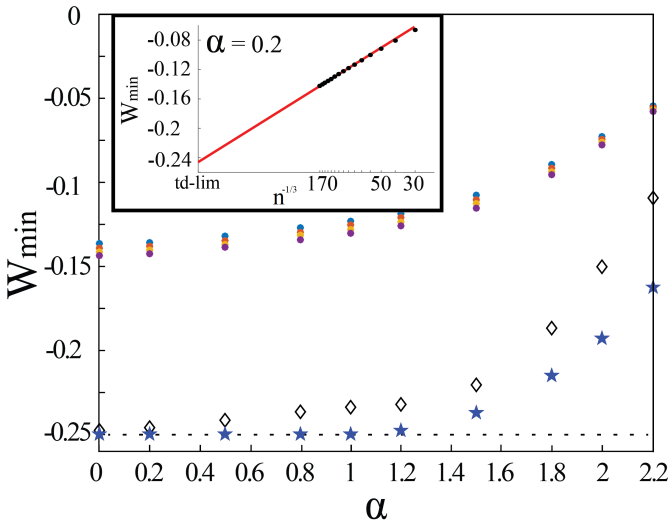

Fig. 5.3 Violation of the two-body PIBI in Eq. (5.1) obtained at the QCP of the 1-dimensional TFIM in Eq. (5.5), as a function of α. The dots correspond to the finite-size DMRG computations (from top to bottom, $n \in \{150, 160, 170\}$ respectively). The diamonds correspond to the extrapolations $n \to \infty$ which have been obtained by using the results for $n \in \{30, 40, \ldots, 170\}$. The stars correspond to the LSW theory results for $n = 10^5$. The inset shows the extrapolation for $\alpha = 0.2$ as an example, where the fit follows $W_{\min}(n) = W_{\min}(\infty) + an^{-1/3}$.

5.4 Analytical exploration: Linear spin-wave theory

In this section we give a physical interpretation on the origin of non-locality detection given by Eq. (5.1). In particular, we take advantage that the two-body PIBI can be rewritten in terms of collective spin moments as in Eq. (5.3), to carry out an exploration of its violation by means of LSW theory.

For the model considered, LSW theory is expected to provide an accurate description since the FM power-law interactions harden the

quantum fluctuations about the mean-field ground state. This is specially the case for small values of the power-law exponent α. In fact, we shall see that for the cases $\alpha < d$, where d denotes the lattice dimension, LSW theory becomes exact in the thermodynamic limit.

In what follows, we choose FM ordering along the direction $+\boldsymbol{x}$. Consider the following Holstein-Primakoff (HP) mapping [Holstein and Primakoff, 1940] from spin operators to bosonic modes:

$$\begin{aligned} \mathcal{S}_{\boldsymbol{z}}^{(j)} &= \cos\theta(1/2 - b_j^\dagger b_j) - \sin\theta(b_j + b_j^\dagger)/2, \\ \mathcal{S}_{\boldsymbol{x}}^{(j)} &= \sin\theta(1/2 - b_j^\dagger b_j) + \cos\theta(b_j + b_j^\dagger)/2, \\ \mathcal{S}_{\boldsymbol{y}}^{(j)} &= (b_j - b_j^\dagger)/2, \end{aligned} \tag{5.8}$$

where all expressions are valid up to order $\mathcal{O}(b_j^3)$, and b_j denote bosonic operators which, in Fourier space, read as $b_{\boldsymbol{k}} = n^{-1/2} \sum_j \exp(-i\boldsymbol{k}\cdot\boldsymbol{r}_j) b_j$. Then, under the HP mapping in Section 5.4, we obtain the following LSW Hamiltonian:

$$\mathcal{H}_{\mathrm{LSW}} = \frac{\max(1,h)}{2} \sum_{\boldsymbol{k}} (\hat{P}_{\boldsymbol{k}} \hat{P}_{-\boldsymbol{k}} + \omega_{\boldsymbol{k}}^2 \hat{X}_{\boldsymbol{k}} \hat{X}_{-\boldsymbol{k}}) \ , \tag{5.9}$$

which is valid up to second order in HP operators. Several quantities have been introduced in Eq. (5.9): we start by introducing $\gamma_{\mathbf{k}} = n^{-1} \sum_{i \neq j} \exp[-\mathbf{k}\cdot(\mathbf{l}_j - \mathbf{l}_i)]\gamma_{ij}$ from which one can obtain the $\gamma_{\boldsymbol{k}} = \gamma_{\mathbf{0}}$, previously used in Section 5.2 to normalize the interaction term to have well-defined thermodynamic limit; then we introduce $\omega_{\boldsymbol{k}} = \sqrt{1 - \gamma_{\boldsymbol{k}}/(h\gamma_{\mathbf{0}})}$ for thePM phase and $\omega_{\boldsymbol{k}} = \sqrt{1 - h^2\gamma_{\boldsymbol{k}}/\gamma_{\mathbf{0}}}$ for the FM phase; and finally $\hat{X}_{\mathbf{k}}$ and $\hat{P}_{\mathbf{k}}$ are defined in terms of HP operators $b_{\mathbf{k}}^\dagger$ for the wave-vector $\boldsymbol{k}$ as

$$\hat{X}_{\mathbf{k}} = \frac{b_{\mathbf{k}} + b_{-\mathbf{k}}^\dagger}{\sqrt{2}}, \qquad \hat{P}_{\mathbf{k}} = \frac{b_{-\mathbf{k}} - b_{\mathbf{k}}^\dagger}{i\sqrt{2}}, \tag{5.10}$$

which satisfy the commutation relations $[\hat{X}_{\mathbf{k}}, \hat{P}_{\mathbf{k}'}] = i\delta_{\mathbf{k},\mathbf{k}'}$, and $[\hat{X}_{\mathbf{k}}, \hat{X}_{\mathbf{k}'}] = [\hat{P}_{\mathbf{k}}, \hat{P}_{\mathbf{k}'}] = 0$.

The LSW Hamiltonian in Eq. (5.9) can then be diagonalized by the Bogoliubov rotation $\beta_{\mathbf{k}} = \hat{X}_{\mathbf{k}}\sqrt{\omega_{\mathbf{k}}/2} + i\hat{P}_{-\mathbf{k}}/\sqrt{2\omega_{\mathbf{k}}}$, such that $\mathcal{H}_{\text{LSW}} = \max(1,h)\sum_{\mathbf{k}}\omega_{\mathbf{k}}(\beta^{\dagger}_{\mathbf{k}}\beta_{\mathbf{k}} + 1/2)$. Notice that, written as in Eq. (5.9), the physical interpretation of the LSW mapping is that the two quadratures $\hat{P}_{\mathbf{k}}$ and $\hat{X}_{\mathbf{k}}$ represent collective spin fluctuations in the two directions transverse to the mean spin orientation; *i.e.,* in the LSW approximation, $\hat{P}_{\mathbf{k}} = J^{\mathbf{y}}_{\mathbf{k}}/\sqrt{n/2}$ and $\hat{X}_{\mathbf{k}} = J^{\tilde{\mathbf{x}}}_{-\mathbf{k}}/\sqrt{n/2}$, with $\tilde{\mathbf{x}} = \mathbf{x}\cos\theta - \mathbf{z}\sin\theta$ and $J^{\mathbf{u}}_{\mathbf{k}} = \sum_{j}\exp(i\mathbf{k}\cdot\mathbf{r}_j)(\mathbf{u}\cdot\mathcal{S}^{(j)})$. Within LSW theory, said fluctuations are harmonic and the sectors corresponding to different wave-vectors $\mathbf{k}$ decouple from each other. Furthermore, one can directly read the eigenfrequencies of the collective spin fluctuations from the LSW Hamiltonian in Eq. (5.9); *i.e.,* $E_{\boldsymbol{k}} = \max(1,h)\omega_{\boldsymbol{k}}$. When approaching the QCP at $h_c = 1$, $\omega_{\boldsymbol{k}=\mathbf{0}}$ becomes gapless, which implies that the fluctuations of the $\hat{X}_{\mathbf{0}}$ quadrature diverge and, hence, the fluctuations of the $\hat{P}_{\mathbf{0}}$ quadrature get squeezed. Indeed, in terms of collective spin degrees of freedom $\vec{J} = \sum_{i}\mathcal{S}^{(i)} \equiv \vec{J}_{\boldsymbol{k}=\mathbf{0}}$, one finds:

$$\langle (J^{\tilde{\boldsymbol{x}}})^2\rangle = \frac{n}{4\omega_{\mathbf{0}}}, \qquad \langle (J^{\mathbf{y}})^2\rangle = \frac{n\omega_{\mathbf{0}}}{4}\ . \tag{5.11}$$

The divergence of the fluctuations of the order parameter (here, $J^{\mathbf{x}} = J^{\tilde{\mathbf{x}}}\cos\theta$) is a generic signature of critical phase transitions (quantum or thermal). On the other hand, the squeezing of fluctuations transverse to the order parameter (here, $J^{\mathbf{y}}$) is a signature of genuine quantum criticality (*i.e.,* criticality that has no classical analogue) [Frérot and Roscilde, 2018]. In the present case, it further signals the presence of GME at the QCP [Pezzé and Smerzi, 2009; Frérot and Roscilde, 2018; Gabbrielli *et al.*, 2018], which in turn provides the maximal violation of the two-body PIBI in Eq. (5.1). At the QCP, LSW theory predicts perfect squeezing of the $J^{\mathbf{y}}$ fluctuations. Therefore, from Eq. (5.4) we observe that the minimal value of $\langle W\rangle$ reduces to

$$\langle W\rangle_{\text{min}} \overset{\text{at QCP}}{=} -\frac{(1-r)^2}{4}\ . \tag{5.12}$$

Therefore, the nonlocality detection at the QCP via the two-body PIBI occurs, under LSW interpretation, due to the reduction of the mean spin length by quantum fluctuations.

The predictions from LSW are reliable as long as the mean spin length,

$$1 - r = 2\langle J^{\tilde{\mathbf{z}}}\rangle/n = 1 - (2/n)\sum_{\mathbf{k}}\langle b^{\dagger}_{\mathbf{k}} b_{\mathbf{k}}\rangle, \tag{5.13}$$

is mildly reduced by the occupation of HP bosonic modes; *i.e.*, $r \ll 1$. We find that $r = (2n)^{-1}\sum_{\mathbf{k}}(1-\omega_{\mathbf{k}})^2/\omega_{\mathbf{k}}$. For the cases $\alpha < d$, the $\gamma_{\mathbf{k}\neq 0}/\gamma_{\mathbf{0}} \to 0$ for $n \to \infty$ [Frérot *et al.*, 2017], so that $\omega_{\mathbf{k}\neq 0} \to 1$, and $r \sim (2n)^{-1}(1-\omega_{\mathbf{0}})^2/\omega_{\mathbf{0}}$. That is, apart from the collective spin fluctuations, the rest of quantum fluctuations frozen out. Notice that for any $h \neq 1$, then $r \to 0$. Therefore, when $\alpha < d$, LSW theory is asymptotically exact at any finite detuning from the QCP. When away from the QCP, $\omega_{\mathbf{k}}$ is gapped resulting in a finite r. Then, the only possible instance of (infrared) divergence for r is at the QCP, where $\omega_{\mathbf{k}} \sim k^z$ with a dynamical exponent $z = \min[1, (\alpha - d)/2]$ [Frérot *et al.*, 2017]. The condition for r to exhibit infrared divergence is equivalent to the divergence of $\int dk k^{d-1}/k^z$ at low k, *i.e.* to the condition $z \geq d$. This condition is only met for $\alpha \geq 3$ ($z = 1$) in $d = 1$, where logarithmic divergence occurs. Otherwise, r converges to a finite value for $n \to \infty$, which must satisfy $r \ll 1$ for LSW theory to be reliable. For example, at the QCP, for $d = 3$ we find $r_{\max} \approx 0.045$ for $\alpha = \infty$; and for $d = 2$, we find $r \lesssim 0.122$. Therefore, LSW is always reliable when $d \in \{2, 3\}$. On the other hand, for $d = 1$ at the QCP we find $r \approx 0.1$ for $\alpha \approx 2$, but already find $r \approx 0.3$ for $\alpha = 2.4$, which indicates a strong effect of quantum fluctuations for larger values of α. Consequently, in $d = 1$ we complement our LSW approach by DMRG computations.

Remarkably, for $\alpha < d$ and in the thermodynamic limit, the two-body PIBI in Eqs. (5.1) and (5.3) attains the maximal amount of quantum violation $\langle W\rangle_{\min} \to -1/4$ [Tura *et al.*, 2014a, 2015]. We show the obtained $\langle W\rangle_{\min}$ across the phase diagram in Figure 5.3 for a 1-dimensional lattice, and in Figure 5.4 for a 2-dimensional lattice. In Figures 5.4 and 5.5 we also present the half-system EE for the 2-

dimensional lattice to compare with the nonlocality detection. Notice in Figure 5.4 that the case with infinite-range interactions $\alpha \to \infty$, which leads to the suppression of quantum fluctuations at $\mathbf{k} \neq 0$ in the ground state, is the one offering maximal violation of Eq. (5.3). On the other hand, for the same case, the half-system EE is suppressed, following at most a $\log(n)$ scaling for $\alpha < d$ [Latorre *et al.*, 2005] instead of a L^{d-1} (area-law) scaling. Such behaviour should be understood as a feature of the two-body PIBI in Eq. (5.1). One explanation may come from the two-body PIBI involving at most two-body correltators, so that in order to detect nonlocality a significant amount of 2-body RDMs from the quantum state must remain entangled when traced out (cf. Section 5.3.1), which directly opposes the notion of maximally bipartite EE (for which all RDMs must be maximally mixed). Nevertheless, in general we always find the maximal violation of the two-body PIBI at criticality where the half-system EE is also maximal (as is the case shown in Figure 5.5), which illustrates the quantum critical nature of the non-local correlations detected by the two-body PIBI. Finally, notice that for lattices of dimensions $d \geq 2$, non-local correlations are detected at the QCP for any value of α (as opposed to the chain $d = 1$), which is consistent with the presence of spin-squeezing for nearest neighbour interactions in $d \geq 2$ [Frérot and Roscilde, 2018].

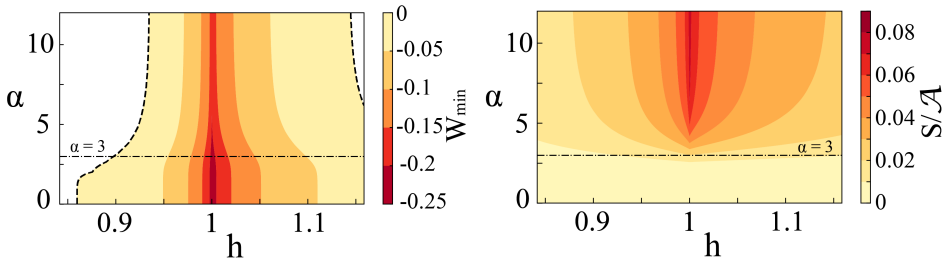

Fig. 5.4 LSW theory results for a 2-dimensional TFIM with tunable interactions described in Eq. (5.5). **Left:** Violation of the Bell correlation witness in Eq. (5.3). **Right:** bipartite EE, computed for half a torus of size $L_x = 200$ times $L_y = 100$, and rescaled to the boundary area ($\mathcal{A} = 2L_y$). A cut across the line $\alpha = 3$ of the phase diagrams can be seen in Figure 5.5.

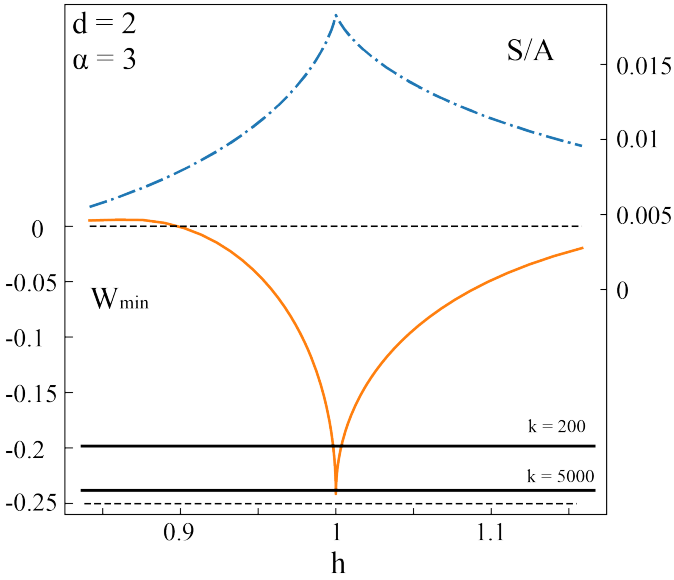

Fig. 5.5 Bipartite EE ($\mathcal{S}$, blue dash dotted curve) and optimal violation ($\langle W \rangle_{\min}$, orange solid curve) of the Bell correlation witness in Eq. (5.3) under LSW for the 2-dimensional TFIM with tunable interactions described in Eq. (5.5). The dashed lines represent the classical ($W_{\min} \geq 0$) and quantum ($W_{\min} \geq -1/4$) bounds of the two-body PIBI. The solid lines display a couple of k-producible bounds (see Chapter 4), which certify an entanglement depth of $k \geq 5000$. The bipartite EE has been computed for half a torus of size $L_x = 200$ times $L_y = 100$, and rescaled to the boundary area ($\mathcal{A} = 2L_y$).

Chapter 6

The quantum marginal problem for symmetric states and applications

In previous chapters, we have used non-local correlations to characterize multipartite entanglement and QCPs in the many-body regime. We have been able to partially circumvent the exponential growth of the Hilbert space by making use of two-body PIBIs. However, we have also perceived that their structure limits the amount of situations one can extract conclusions from. Then, we are interested in generalizing the two-body PIBIs to, for instance, consider arbitrary Hilbert space dimension d or to involve up to m-body correlators. We have observed that when considering the Bell scenario involving identical measurement settings, the characterization of the m-body PIBI inequalities get reduced to consider only m-body RDMs (cf. Sections 4.5.2 and 5.3.1). However, these m-body RDMs must be compatible with a global symmetric quantum state.

The problem we are facing, to find compatibility conditions for a set of m-body RDMs to be compatible with a global state, is referred to as the *Quantum Marginal Problem* (QMP) (see *e.g.* [Schilling, 2015]). However, the interest in the QMP goes past beyond the characteri-

zation of Bell inequalities. Suppose we want to compute the ground state energy of an m-local Hamiltonian; *i.e.*, $\mathcal{H} = \sum_i \mathcal{H}_i$, where each $\mathcal{H}_i$ acts nontrivially on at most m parties. Instead of computing the ground state energy $\langle\psi|\,\mathcal{H}\,|\psi\rangle$ by finding the ground state $|\psi\rangle$, which becomes inefficient as the Hilbert space dimensions grow, one can use the m-locality of the Hamiltonian to compute the ground state energy from its RDMs as $\langle\psi|\,\mathcal{H}\,|\psi\rangle = \sum_i \mathrm{Tr}[\mathcal{H}_i\rho^{(i)}]$, where $\rho^{(i)}$ denotes the reduced state of $|\psi\rangle\langle\psi|$ acting on $\mathcal{H}_i$. However, while the latter approach circumvents the exponential growth of the Hilbert space, we encounter the QMP since one still needs to know the compatibility conditions for the reduced states $\{\rho^{(i)}\}$ to be compatible with the global state $|\psi\rangle\langle\psi|$. Unfortunately, the QMP remains an elusive problem that has been shown to be complete for the complexity class Quantum Merlin-Arthur (QMA) complete [Liu *et al.*, 2007], meaning that it is very hard even for a quantum computer.

In the present chapter we consider the QMP for symmetric states. Namely, we want to characterize the compatibility conditions for a RDM σ of m, *i.e.* acting on $(\mathbb{C}^d)^{\otimes m}$, to be compatible with a global quantum state ρ acting on the symmetric space $\mathrm{Sym}((\mathbb{C}^d)^{\otimes n})$.

The chapter is organized as follows: The core results are presented in Section 6.1, where we provide a method to solve the QMP for symmetric states. To find the solution we (i) use combinatorial algebra to find analytical compatibility conditions for the reduced state σ to be compatible with the global symmetric state ρ, and (ii) we show that these compatibility conditions can be used as constraints on an efficient SDP (polynomially in n, with degree $d-1$) that solves the QMP for symmetric states as a feasibility problem.

In Section 6.2 we proceed to explore some of the implications and applications of our solution in the context of QIP. In Section 6.1.1 we adapt the SDP methodology to construct a computationally undemanding variational approach to the ground state energy of any local Hamiltonian. In Section 6.2.1 we explore the performance of the presented variational ansatz on several exemplary spin models.

In Section 6.2.2 we illustrate how the variational method presented

serves as a natural tool to characterize few-body symmetric Bell inequalities [Tura *et al.*, 2014a; Schmied *et al.*, 2016; Tura *et al.*, 2015].As a byproduct of the benchmarking section, and of individual interest, in Section 6.2.3 we present an analytical correspondence to generically express n-qubit symmetric states as translationally invariant diagonal matrix product states of bond dimension n. Finally, in Section 6.2.4 we use the method presented to explore under which conditions symmetric states cannot be self-tested from their marginals.

The original results presented in this chapter are based on the preprint [Aloy *et al.*, 2020], a joint collaboration between M. Fadel and J. Tura.

6.1 Compatibility conditions with a global symmetric state

Symmetric states

Let us start by briefly recalling symmetric states, for more details on symmetric states see Section 2.1. Due to the PI involved in symmetric states, it is possible to find a representation that partially circumvents the exponential growth of the Hilbert space representability problem. In particular, symmetric states are confined to a subspace of the multipartite Hilbert space whose dimension scales only polynomially with n, with degree $d-1$. Precisely, the symmetric space $\mathrm{Sym}\left((\mathbb{C}^d)^{\otimes n}\right)$ has $\binom{n+d-1}{d-1}$ dimensions.

In particular, the symmetric space is spanned by the Dicke states. Consider the set $[d] := \{0, \ldots, d-1\}$. Then, to describe qudit Dicke states, recall that we denote as $\boldsymbol{\lambda} \vdash n$ the partition of n in d elements, and $\boldsymbol{\lambda}$ consists of a d-dimensional vector $\boldsymbol{\lambda} = (\lambda_0, \ldots, \lambda_{d-1})$, where $\lambda_i \in \mathbb{Z}_{\geq 0}$ counts the number of excitations in state $|i\rangle$, so that $\sum_{i\in[d]} \lambda_i = n$. Then, a qudit Dicke states $|\boldsymbol{\lambda}\rangle$ takes the following form:

$$|\boldsymbol{\lambda}\rangle \propto \sum_{\pi\in\mathcal{S}_n} \pi(|0\rangle^{\otimes\lambda_0} \otimes \cdots \otimes |d-1\rangle^{\otimes\lambda_{d-1}}), \tag{6.1}$$

where $\mathcal{S}_n$ denotes the group of permutations of n elements, π denotes a permutation acting on different Hilbert spaces. The number of different terms in Eq. (6.1) is given by the following multinomial combinatorial expression

$$\binom{n}{\boldsymbol{\lambda}} = \frac{n!}{\lambda_0! \cdots \lambda_{d-1}!}. \tag{6.2}$$

Analytical compatibility conditions

In this section we present the main result for the present chapter. In particular, by means of combinatorial algebra we analytically derive necessary and sufficient conditions for an m-qudit RDM to be compatible with a global n-qudit symmetric density matrix.

The starting point is an n-qudit symmetric quantum system ρ, whose components are denoted $\rho_{\boldsymbol{\mu}}^{\boldsymbol{\lambda}}$, where $\boldsymbol{\lambda}, \boldsymbol{\mu} \vdash n$, so that

$$\rho = \sum_{\boldsymbol{\lambda},\boldsymbol{\mu}\vdash n} \rho_{\boldsymbol{\mu}}^{\boldsymbol{\lambda}} \left|\boldsymbol{\lambda}\right\rangle\!\left\langle\boldsymbol{\mu}\right|. \tag{6.3}$$

Then, our first objective is to find an expression, both in the computational and in the Dicke basis, for the resulting reduced state of ρ after tracing out $n-m$ subsystems. That is, we want to find a general expression for the partial trace of ρ with respect to $n-m$ subsystems. An important feature of symmetric states, that greatly reduces the task at hand, is that it does not matter which $n-m$ we trace out, since all the resulting m-body reduced states have the same form.

In what follows we are going to distinguish matrix elements in the computational basis by labelling them with an overhead arrow (*e.g.* $\vec{i}$), whereas we reserve the boldface notation (*e.g.* $\boldsymbol{\lambda}$) to label matrix elements in the Dicke basis as in Eq. (6.1). Under this notation, the partial trace of ρ is defined as:

Definition 6.1.1. *Let ρ be an n-qudit symmetric state. Let $\vec{i}, \vec{j} \in [d]^m$ and $\boldsymbol{\alpha}, \boldsymbol{\beta} \vdash m$ for some $m \leq n$. Then, the partial trace of ρ with respect to $n-m$ subsystems, denoted $\sigma := \mathrm{Tr}_{n-m}(\rho)$, takes the following form:*

$$\sigma = \sum_{\vec{i},\vec{j}\in[d]^m} \sigma_{\vec{j}}^{\vec{i}} |\vec{i}\rangle\langle\vec{j}| = \sum_{\boldsymbol{\alpha},\boldsymbol{\beta}\vdash m} \sigma_{\boldsymbol{\beta}}^{\boldsymbol{\alpha}} |\boldsymbol{\alpha}\rangle\langle\boldsymbol{\beta}| . \tag{6.4}$$

Then, in Theorem 6.1.1 we present an expression for each component of the resulting reduced state σ after tracing out $n-m$ subsystems:

Theorem 6.1.1. *Let ρ be an n-qudit symmetric state, and consider Theorem 6.1.1 to obtain its reduced state $\sigma = \mathrm{Tr}_{n-m}(\rho)$, for some $m \leq n$. Let also $\vec{i},\vec{j} \in [d]^m$ and $\boldsymbol{\alpha},\boldsymbol{\beta} \vdash m$. Then, the coefficients of σ in the computational basis follow the expression*

$$\sigma_{\vec{j}}^{\vec{i}} = \sum_{\boldsymbol{\lambda},\boldsymbol{\mu}\vdash n} \rho_{\boldsymbol{\mu}}^{\boldsymbol{\lambda}} \sum_{\boldsymbol{\kappa}\vdash n-m} \frac{\binom{n-m}{\boldsymbol{\kappa}}}{\sqrt{\binom{n}{\boldsymbol{\lambda}}\binom{n}{\boldsymbol{\mu}}}} \delta(\boldsymbol{w}(\vec{i}) + \boldsymbol{\kappa} - \boldsymbol{\lambda})\delta(\boldsymbol{w}(\vec{j}) + \boldsymbol{\kappa} - \boldsymbol{\mu}), \tag{6.5}$$

and the coefficients of σ in the Dicke basis follow the expression

$$\sigma_{\boldsymbol{\beta}}^{\boldsymbol{\alpha}} = \sum_{\boldsymbol{\lambda},\boldsymbol{\mu}\vdash n} \rho_{\boldsymbol{\mu}}^{\boldsymbol{\lambda}} \sum_{\boldsymbol{\kappa}\vdash n-m} \binom{n-m}{\boldsymbol{\kappa}} \sqrt{\frac{\binom{m}{\boldsymbol{\alpha}}\binom{m}{\boldsymbol{\beta}}}{\binom{n}{\boldsymbol{\lambda}}\binom{n}{\boldsymbol{\mu}}}} \delta(\boldsymbol{\alpha} + \boldsymbol{\kappa} - \boldsymbol{\lambda})\delta(\boldsymbol{\beta} + \boldsymbol{\kappa} - \boldsymbol{\mu}). \tag{6.6}$$

Proof of Theorem 6.1.1– Notice that, for a given n-qudit density matrix ρ, the partial trace with respect to $n-m$ subsystems can be expressed in the computational basis as

$$\mathrm{Tr}_{n-m}(\rho) = \sum_{\vec{i},\vec{j}\in[d]^m} |\vec{i}\rangle\langle\vec{j}| \sum_{\vec{k}\in[d]^{n-m}} \rho_{\vec{j}|\vec{k}}^{\vec{i}|\vec{k}}, \tag{6.7}$$

where the operator $|$ denotes index concatenation with the indices rearranged so that the $n-m$ traced out parties are the last ones. As an example, consider the case $n=5$, $m=2$ and $d=2$ in which $\vec{i} \in [2]^2$ and $\vec{k} \in [2]^3$; then take, for instance, $\vec{i} = (01)$ and $\vec{k} = (001)$ for which one obtains $\vec{i}|\vec{k} = (01001)$.

The expression in Eq. (6.7) can then be equivalently expressed in the symmetric space. However, notice that in order to apply Eq. (6.7),

we first need to express the symmetric state in the computational basis. To do so, since Dicke states are enumerated by the partitions of m, it is convenient to introduce the following notation:

$$\begin{array}{rccc} w_k: & [d]^n & \longrightarrow & \{0,\dots,n\} \\ & \vec{i} & \mapsto & \#\{i_p \in \vec{i} : i_p = k\} \end{array} \tag{6.8}$$

That is, $w_k(\vec{i})$ counts the amount of coordinates in $\vec{i}$ that are equal to k. Furthermore, we gather the weight counting functions for all the components $k \in [d]$ in a single weight counting function $\boldsymbol{w}(\vec{i}) := (w_0(\vec{i}),\dots,w_{d-1}(\vec{i})))$. Note that, by construction, $\boldsymbol{w}(\vec{i}) \vdash n$ for every $\vec{i} \in [d]^n$, and notice also that $\boldsymbol{w}(\vec{a}|\vec{b}) = \boldsymbol{w}(\vec{a}) + \boldsymbol{w}(\vec{b})$. As an example, consider the case $n = 5$, $d = 4$ and take, for instance, $\vec{i} = (10311)$; then one gets $\boldsymbol{w}(\vec{i}) = (w_0(\vec{i}), w_1(\vec{i}), w_2(\vec{i}), w_3(\vec{i}) = (1,3,0,1)$.

The weight counting function $\boldsymbol{w}$ is then useful to represent the Dicke states $|\boldsymbol{\lambda}\rangle$ in the computational basis, which we denote as $|D_{\boldsymbol{\lambda}}\rangle$ and takes the following expression:

$$|D_{\boldsymbol{\lambda}}\rangle = \binom{n}{\boldsymbol{\lambda}}^{-1/2} \sum_{\vec{i}\in[d]^n} |\vec{i}\rangle\, \delta(\boldsymbol{w}(\vec{i}) - \boldsymbol{\lambda}), \tag{6.9}$$

where δ is the Kronecker Delta function, which is 1 if, and only if, its argument is the zero vector and 0 otherwise. by means of Eq. (6.9) one can now define the operator $\Pi : \mathrm{Sym}\left((\mathbb{C}^d)^{\otimes n}\right) \hookrightarrow (\mathbb{C}^d)^{\otimes n}$ corresponding to an inclusion map onto the symmetric space. That is,

$$\Pi := \sum_{\boldsymbol{\lambda}\vdash n} |D_{\boldsymbol{\lambda}}\rangle\langle\boldsymbol{\lambda}|\,. \tag{6.10}$$

Notice that $\Pi^\dagger : (\mathbb{C}^d)^{\otimes n} \twoheadrightarrow \mathrm{Sym}\left((\mathbb{C}^d)^{\otimes n}\right)$ is the projector onto the symmetric space, with $\Pi^\dagger\Pi = \mathbb{1}_{\mathrm{Sym}\left((\mathbb{C}^d)^{\otimes n}\right)}$.

Therefore, Eq. (6.10) offers a relation between the computational and the Dicke basis. Let ρ be a density matrix acting on $\mathrm{Sym}((\mathbb{C}^d)^{\otimes n})$, and let its components be labelled as $\rho^{\boldsymbol{\lambda}}_{\boldsymbol{\mu}}$ in the Dicke basis, or as $\rho^{\vec{i}}_{\vec{j}}$ in

the computational basis. Then, the components of ρ in both basis are related as

$$\rho_{\vec{j}}^{\vec{i}} = \left(\Pi(\rho_{\boldsymbol{\mu}}^{\boldsymbol{\lambda}})\Pi^{\dagger}\right)_{\vec{j}}^{\vec{i}} = \sum_{\boldsymbol{\lambda},\boldsymbol{\mu}\vdash n} \delta(\boldsymbol{w}(\vec{i}) - \boldsymbol{\lambda})\delta(\boldsymbol{w}(\vec{j}) - \boldsymbol{\mu}) \binom{n}{\boldsymbol{\lambda}}^{-1/2} \binom{n}{\boldsymbol{\mu}}^{-1/2} \rho_{\boldsymbol{\mu}}^{\boldsymbol{\lambda}}. \tag{6.11}$$

Finally, we are now ready to trace out $n-m$ parties from ρ. Since it does not matter which $n-m$ subsystems we trace out, we trace out, for instance, the last $n-m$ parties. Therefore, by means of Eq. (6.7) one obtains $\sigma := \mathrm{Tr}_{n-m}(\rho)$ as:

$$\sigma_{\vec{j}}^{\vec{i}} = \sum_{k\in[d]^{n-m}} \rho_{\vec{j}|\vec{k}}^{\vec{i}|\vec{k}} = \sum_{\boldsymbol{\lambda},\boldsymbol{\mu}\vdash n} \rho_{\boldsymbol{\mu}}^{\boldsymbol{\lambda}} \sqrt{\binom{n}{\boldsymbol{\lambda}}\binom{n}{\boldsymbol{\mu}}} \sum_{\vec{k}\in[d]^{n-m}} \delta(\boldsymbol{w}(\vec{i}) + \boldsymbol{w}(\vec{k}) - \boldsymbol{\lambda})\delta(\boldsymbol{w}(\vec{j}) + \boldsymbol{w}(\vec{k}) - \boldsymbol{\mu}), \tag{6.12}$$

which yields the coefficients of σ in the computational basis shown in Eq. (6.5). Then, to obtain the coefficients in the Dicke basis, we use the transformation $(\sigma_{\boldsymbol{\beta}}^{\boldsymbol{\alpha}}) = \Pi^{\dagger}(\sigma_{\vec{j}}^{\vec{i}})\Pi$ yielding Eq. (6.6).

□

The relevance of Eqs. (6.5) and (6.6), for computational and Dicke basis respectively, is that now one obtains a set of necessary and sufficient conditions for an m-qudit RDM σ to be compatible with an n-qudit global (possibly mixed) symmetric state ρ. Then, one can pose the QMP for symmetric states as a feasibility problem by using the set of compatibility conditions as constraints on a *semidefinite program* (SDP). For instance, in the Dicke basis the SDP is expressed as:

$$\begin{array}{lllll} \min & 0 & & & \\ \text{s.t.} & \rho & \succeq & 0 & \\ & \mathrm{Tr}(\rho) & = & 1 & \\ & \sum_{\boldsymbol{\lambda},\boldsymbol{\mu}\vdash n} \rho_{\boldsymbol{\mu}}^{\boldsymbol{\lambda}} a_{\boldsymbol{\mu},\boldsymbol{\beta}}^{\boldsymbol{\lambda},\boldsymbol{\alpha}} & = & \sigma_{\boldsymbol{\beta}}^{\boldsymbol{\alpha}} \qquad \forall \boldsymbol{\alpha},\boldsymbol{\beta}\vdash m, \end{array} \tag{6.13}$$

where the coefficients $a^{\boldsymbol{\lambda},\boldsymbol{\alpha}}_{\boldsymbol{\mu},\boldsymbol{\beta}}$ are defined from Eq. (6.6); namely,

$$a^{\boldsymbol{\lambda},\boldsymbol{\alpha}}_{\boldsymbol{\mu},\boldsymbol{\beta}} := \sum_{\boldsymbol{\kappa}\vdash n-m} \binom{n-m}{\boldsymbol{\kappa}} \sqrt{\frac{\binom{m}{\boldsymbol{\alpha}}\binom{m}{\boldsymbol{\beta}}}{\binom{n}{\boldsymbol{\lambda}}\binom{n}{\boldsymbol{\mu}}}} \delta(\boldsymbol{\alpha}+\boldsymbol{\kappa}-\boldsymbol{\lambda})\delta(\boldsymbol{\beta}+\boldsymbol{\kappa}-\boldsymbol{\mu}). \quad (6.14)$$

Notice that one can think of the coefficients $a^{\boldsymbol{\lambda},\boldsymbol{\alpha}}_{\boldsymbol{\mu},\boldsymbol{\beta}}$ as the entries of a matrix $A^{\boldsymbol{\alpha}}_{\boldsymbol{\beta}}$ indexed by $\boldsymbol{\lambda}$ and $\boldsymbol{\mu}$, which allows to express the SDP Eq. (6.13) in canonical form as

$$\begin{array}{lllll} \min & \langle 0, \rho\rangle & & & \\ \text{s.t.} & \rho & \succeq & 0 & \\ & \mathrm{Tr}(\rho) & = & 1 & \\ & \langle A^{\boldsymbol{\alpha}}_{\boldsymbol{\beta}}, \rho\rangle & = & \sigma^{\boldsymbol{\alpha}}_{\boldsymbol{\beta}} & \forall \boldsymbol{\alpha},\boldsymbol{\beta}\vdash m, \end{array} \quad (6.15)$$

where $\langle\cdot,\cdot\rangle$ denotes the Hilbert-Schmidt inner product. Notice that the same SDP can be expressed in the computational basis.

Hence, if the SDP in Eq. (6.15) is feasible, then the reduced state σ admits an extension to an n-qudit symmetric state, which corresponds to the solution of the SDP.

If the SDP Equation (6.15) is feasible, then σ admits an extension to a symmetric Dicke state of n qudits ρ which is precisely the solution of that SDP. Later in Section 6.2.4 we shall discuss about the uniqueness of the solution provided by the SDP.

6.1.1 Variational ansatz

An interesting feature of the SDP in Eq. (6.15) is that we can now modify it to optimize any linear functional $\mathcal{H}$ on ρ, while maintaining the compatibility over a given reduced state σ. In particular, one can express the following SDP:

$$\begin{array}{lllll} \min & \langle H, \rho\rangle & & & \\ \text{s.t.} & \rho & \succeq & 0 & \\ & \mathrm{Tr}(\rho) & = & 1 & \\ & \langle A^{\boldsymbol{\alpha}}_{\boldsymbol{\beta}}, \rho\rangle & = & \sigma^{\boldsymbol{\alpha}}_{\boldsymbol{\beta}} & \forall \boldsymbol{\alpha},\boldsymbol{\beta}\vdash m. \end{array} \quad (6.16)$$

A case of significant relevance is when the functional $\mathcal{H}$ can be expressed as a sum of terms with support on, at most, m qudits. Such case has many cases of physical interest, for instance Hamiltonians or Bell operators composed of, at most, m-body interactions/correlators (such as the ones we have seen in Chapters 4 and 5). In particular, let us denote $\mathcal{H} = \sum_i \mathcal{H}_i$. Then, one can express $\langle H, \rho \rangle$ as a linear combination of terms with the form $\langle H_i, \sigma \rangle$. That is,

$$\begin{array}{lccll} \min & \sum_i \langle H_i, \sigma \rangle & & & \\ \text{s.t.} & \rho & \succeq & 0 & \\ & \mathrm{Tr}(\rho) & = & 1 & \\ & \langle A^{\boldsymbol{\alpha}}_{\boldsymbol{\beta}}, \rho \rangle & = & \sigma^{\boldsymbol{\alpha}}_{\boldsymbol{\beta}} & \forall \boldsymbol{\alpha}, \boldsymbol{\beta} \vdash m. \end{array} \tag{6.17}$$

While in Eq. (6.17) both ρ and σ are treated as positive-semidefinite variables, the positive-semidefiniteness of σ is automatically satisfied by that of ρ. In fact, the SDP in Eq. (6.17) can be equivalently expressed with σ embedded into the objective function, although we have chosen to express it as in Eq. (6.17) for clarity of exposition. Hence, the SDP in Equation (6.17) is useful to optimize a functional $\mathcal{H}$ which encodes relevant information in its reduced states, while maintaining compatibility with a global symmetric state. Let us remark that the size of ρ depends polinomially on n, with a degree $d-1$, which makes the procedure efficient even for qudit systems with large system size n and fixed Hilbert space dimensions d.

6.2 Some Applications

In what follows, we illustrate how to implement our method to solve the QMP for symmetric states in several distinct applications. The selected applications are motivated for our purposes, like the optimization of few-body symmetric Bell inequalities.

In Section 6.2.1 we take several paradigmatic Hamiltonians to benchmark the variational ansatz in Eq. (6.17) by obtaining an efficient upper bound to ground state energies and, in some cases, to well approximate

the ground states. In Section 6.2.2 we construct a method to optimize the quantum correlations observed in few-body symmetric Bell inequalities. In Section 6.2.3 we present a methodology to approximate any n-qubit Dicke state with a *Translationally-Invariant* (TI) diagonal Matrix Product States (MPS) of bond dimension n which is necessary for our benchmarking presented in Section 6.2.1. Finally, in Section 6.2.4 we look into the uniqueness of the solution given by our method and discuss which symmetric states cannot be self-tested from few-body marginals.

6.2.1 Variational ansatz exploration

In this section we take several paradigmatic spin models and benchmark the performance of the variational ansatz presented in Section 6.1.1. In Section 6.2.1 we compare the runtime and estimated resources consumed by our methodology with those of the DMRG algorithm.

In particular, for an m-local Hamiltonian, the variational ansatz considers an m-qudit RDM (denoted m-RDM for short hereafter) compatible with a global symmetric state to upper bound the ground state energy and obtained the corresponding approximation of the ground state. Therefore, it is expected that the method provides exact solutions when the ground states of a spin model are symmetric states like, *e.g.,* the LMG model. However, for the rest of the cases the accuracy of the variational method depends on the overlap of the ground state with the symmetric space, yielding the most inaccurate results when the actual ground state is orthogonal to the symmetric space.

Lipkin-Meshkov-Glick model

We start by considering the *Lipkin-Meshkov-Glick* (LMG) model [Lipkin *et al.*, 1965; Meshkov *et al.*, 1965; Glick *et al.*, 1965], which involves long-range interactions that result in PI ground states. The LMG model was originally formulated to describe phase transitions in nuclei. However, since then the model has found several distinct applications

like, for instance, to describe two-mode BECs experiments. Exact solutions for the model are known [Pan and Draayer, 1999; Links *et al.*, 2003; Ribeiro *et al.*, 2008] and its phase transitions are well understood [Latorre *et al.*, 2005]. Due to the symmetry in its ground states, we expect the variational method to exactly reproduce the known solutions. Furthermore, for the isotropic version of the LMG model the ground states correspond to pure Dicke states from which non-local correlations have been observed by means of the two-body PIBIs [Tura *et al.*, 2014a, 2015, 2017].

In particular, the LMG model describes a set of n spin$-1/2$ particles with anisotropic long-range interactions under an external transverse magnetic field h. That is,

$$\mathcal{H} = -\frac{\lambda}{n}\sum_{i<j}\left(\sigma_x^{(i)}\sigma_x^{(j)} + \gamma\sigma_y^{(i)}\sigma_y^{(j)}\right) - h\sum_{i=1}^{n}\sigma_z^{(i)}, \tag{6.18}$$

where $\sigma_k^{(i)}$ denotes the Pauli matrix acting in the i-th party for $k \in \{x, y, z\}$, $\lambda > 0$ ($\lambda < 0$) corresponds to FM (Antiferromagnetic (AFM)) interactions, and γ marks the anisotropy in the coupling terms, with $\gamma = 1$ corresponding to the isotropic case.

Our objective now is to adapt the SDP optimization problem in Eq. (6.17) to approximate its ground state solely from the two-RDM under the compatibility constraints with a global symmetric state. That is, to consider an effective two-body Hamiltonian $\mathcal{H}$ of Eq. (6.18) like:

$$\tilde{\mathcal{H}} := -\binom{n}{2}\frac{\lambda}{n}\left(\sigma_x \otimes \sigma_x + \gamma\sigma_y \otimes \sigma_y\right) - nh\left(\sigma_z \otimes \mathbb{1} + \mathbb{1} \otimes \sigma_z\right)/2, \tag{6.19}$$

so that we can express the following SDP:

$$\begin{array}{lrcll} \min & \mathrm{Tr}\left(\tilde{\mathcal{H}}\sigma\right) & & & \\ \text{s.t.} & \rho & \succeq & 0 & \\ & \mathrm{Tr}(\rho) & = & 1 & \\ & \langle A_{\boldsymbol{\beta}}^{\boldsymbol{\alpha}}, \rho\rangle & = & \sigma_{\boldsymbol{\beta}}^{\boldsymbol{\alpha}} & \forall \boldsymbol{\alpha}, \boldsymbol{\beta} \vdash m. \end{array} \tag{6.20}$$

The obtained results with Eq. (6.20) are shown in Figure 6.1, where one observes that the ground state energy is faithfully recovered by the Variational Method (VM). Recall that the method represents the n-qubit state in the symmetric basis, and therefore the state is efficiently described as a matrix of size $(m+1)\times(m+1)$ instead of the usual $2^n \times 2^n$ matrix sizes in the computational basis. Furthermore, from the given global state by the VM, one can efficiently obtain any associated m-RDM $\forall 1 \leq m \leq n$ by means of Eq. (6.6). Therefore, extensive quantities such as entropy can efficiently be accessed, since it is now easy to obtain the m-block size entanglement entropy $\mathcal{S}_{m,n} = -\sum_{i=0}^{m} p_i \log_2 p_i$ by computing the eigenvalues p_i of the m-RDM [Latorre *et al.*, 2005]. We use such procedure to obtain the half-system EE shown in Figures 6.1 and 6.2, where one observes that the VM reproduces the features of the LMG model phase diagram.

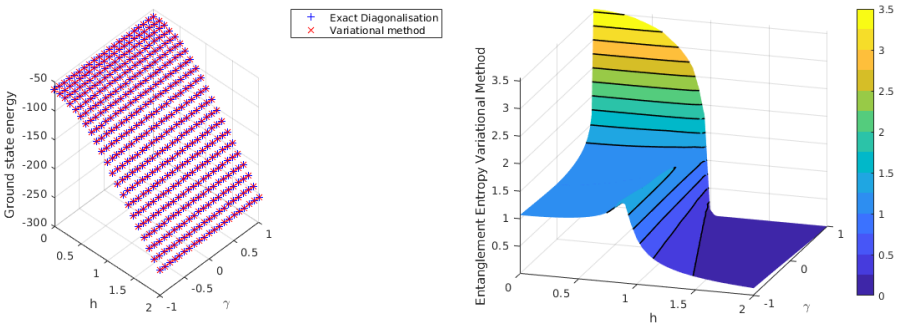

Fig. 6.1 Numerical results obtained by the VM in Eq. (6.20) for the LMG Hamiltonian in Eq. (6.18) taking $\lambda = 1$. **Left:** For $n = 128$, the VM faithfully reproduces the ground state energy within numerical accuracy ($\sim 10^{-14}$ using SeDuMi [Sturm, 1999]). **Right:** For $n = 128$, we compute the $n/2$-RDM in the symmetric basis by means of the RDM compatibility conditions in Eq. (6.6), which allows to efficiently compute the half-system EE and characterize the phase diagram of the LMG model [Latorre *et al.*, 2005].

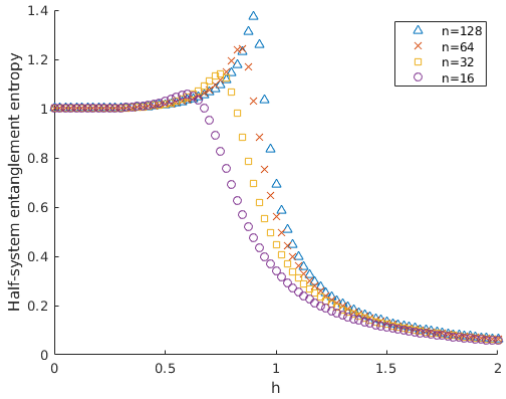

Fig. 6.2 Numerical results obtained by the VM in Eq. (6.20) for the LMG Hamiltonian in Eq. (6.18) taking $\lambda = 1$ and $\gamma = 0$. Half-system EE for different values of n, computed by obtaining the corresponding RDMs in the symmetric basis using the compatibility conditions in the global state given by the VM. One observes an anomaly around $h = 1$ as we increase n, which corresponds to the finite-size precursor of the critical point for $\gamma \neq 1$.

Ising chain with tunable interactions under a transverse field

Next we look at the Ising chain with power-law decaying interactions under a transverse field. In Chapter 5 we have considered the same model only for FM interactions to look at non-local correlations in QCPs. Following the same idea, here we are interested in the tunable range interactions to explore how the VM performs as the range of interactions decreases from infinite-range (equivalent to the LMG model) to the nearest-neighbours case.

This time we consider the following Hamiltonian to describe the model:

$$\mathcal{H} = \sin(\theta) \sum_{i<j} J_{ij} \sigma_z^{(i)} \sigma_z^{(j)} + \cos(\theta) \sum_{i=1}^{n} \sigma_x^{(i)}, \tag{6.21}$$

where $J_{ij} = |i-j|^{-\alpha}$, with the exponent α tuning the range of interactions, and $\theta > 0$ ($\theta < 0$) results in AFM (FM) interactions. In the limit

$\alpha \to 0$ all pairs interact with the equal strength [Fadel and Tura, 2018], while in the limit $\alpha \to \infty$ only the nearest-neighbour interactions contribute. Notice that, compared to the model presented in Chapter 5 this time we do not consider a normalizing factor for the interacting terms, since in the present chapter we remain in finite system sizes. The main reason why this time we describe the model as in Eq. (6.21) is ease the comparison with existing works in which its phase diagram has been characterised [Koffel *et al.*, 2012; Knap *et al.*, 2013; Gabbrielli *et al.*, 2019]. For $\alpha > 0$ the model is known to exhibit three phases: an ordered FM phase for $-\pi/2 \leq \theta < \theta_c^-(\alpha)$; a disordered PM phase for $\theta_c^-(\alpha) < \theta < \theta_c^+(\alpha)$; and an ordered AFM phase for $\theta_c^+(\alpha) < \theta \leq \pi/2$.

This time, to adapt the SDP in Eq. (6.20), the two-body effective Hamiltonian $\tilde{\mathcal{H}}$ associated to Eq. (6.21) takes the following form:

$$\tilde{\mathcal{H}} := J \sin(\theta)\sigma_z \otimes \sigma_z + n \cos(\theta)(\sigma_x \otimes \mathbb{1} + \mathbb{1} \otimes \sigma_x)/2, \tag{6.22}$$

where $J := \sum_{i<j} J_{ij}$.

The obtained results with Eqs. (6.20) and (6.22) are shown in Figure 6.3, where the ground states between the VM and Exact Diagonalization (ED) are compared via the relative energy and fidelity. As a figure of merit to compare the ground state energies we have chosen their ration $E_0^{\mathrm{VM}}/E_0^{\mathrm{ED}}$, since it gives a good visual comparison with the ground states fidelity also shown in Figure 6.3. In all cases considered the energy is sufficiently far from zero to suppose an issue for the ratio. As for the comparison among ground states we employ the fidelity as follows:

$$F(\rho_{\mathrm{ED}}, \rho_{\mathrm{VM}}) := \left(\mathrm{Tr}\sqrt{\sqrt{\rho_{\mathrm{ED}}}\rho_{\mathrm{VM}}\sqrt{\rho_{\mathrm{ED}}}} \right)^2. \tag{6.23}$$

One can observe in Figure 6.3 that the long-range interactions regime is well approximated by the VM, as expected from previous observations. In the transition from $\alpha \gg 1$ to $\alpha \simeq 0$, the accuracy of the VM is *a priori* not so clear. Then, for $\alpha > 0$ fails to capture the AFM phase $\theta_c^+(\alpha) < \theta$, in which eventually the VM yields ground states that are almost orthogonal to the ones obtained via ED. Nevertheless, for

values $\theta < \theta_c^+(\alpha)$ one observes that the VM provides accurate, albeit for large values of α there is a small drop in the accuracy of the VM near the critical point θ_c^-.

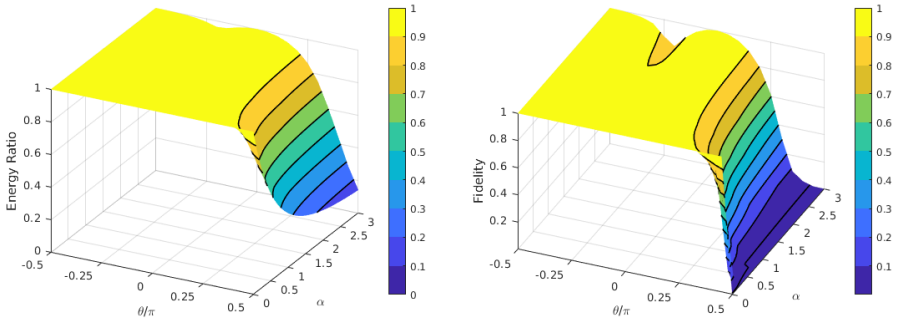

Fig. 6.3 Numerical results obtained by the VM with Eqs. (6.20) and (6.22) for an $n = 10$ Ising chain in Eq. (6.21), compared to ED. **Left:** energy ratio, **Right:** ground state fidelity. The case $\alpha = 0$ is faithfully recovered by the VM. However, as the value of α increases (the range of interaction decreases), one observes that the VM fails to capture the AFM phase, for which the fidelity eventually drops to zero. The ground state energy and fidelity in the FM and PM phases present accurate results, although for large values of α there is some discrepancy near the precursors of critical points $\theta \approx \theta_c^-(\alpha)$.

In Figure 6.4 we compare half-system EE obtained from the VM and ED. One observes a discrepancy in the AFM phase, which is expected due to the little overlap between the ground state and the symmetric space in that region. Interestingly, one also observes that the solution given by the VM might be sufficient to approximate its phase transition (between the PM phase and the FM phase) by considering its scaling with the system size, and extrapolate its asymptotic limit. Such an approximation naturally works better as the range of interactions increases. It might be interesting to further look into this direction, and confirm whether around the critical point the ground state has some overlap with the symmetric space, which is then cap-

tured by the VM. The numerical results presented in Figure 6.4 seem to support this conjecture.

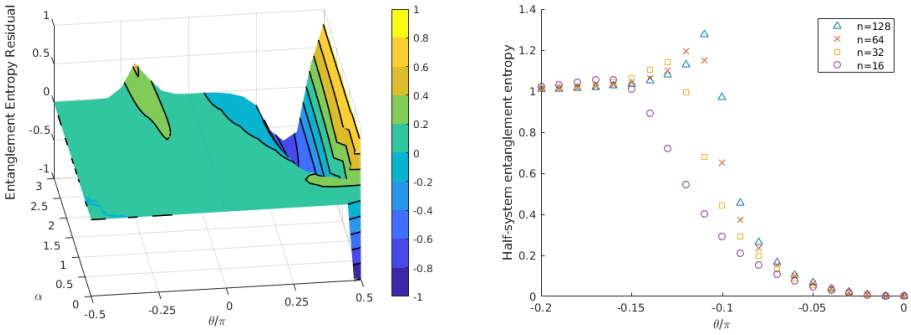

Fig. 6.4 Numerical results obtained by the VM with Eqs. (6.20) and (6.22) for an $n = 10$ Ising chain in Eq. (6.21). **Left:** Half-system EE residual from the comparison between VM and ED (a value of 0 indicates an exact result). While the PM to AFM phase transition seems to not be captured by the VM, the transition from FM to PM seems to be captured despite some discrepancies for values of $\alpha \gtrsim 1.5$. **Right:** Half-system EE for $\alpha = 2$. Note that the transitions from FM to PM manifest in the vicinity of $\theta \simeq -0.1\pi$ for $n = 10$. Based on this observation, we conjecture that the presented VM can be used to extrapolate some critical points where phase transitions occur. Let us remark that the ED has not been used in this case, the observed behaviour arises from the VM alone.

Ising chain for nearest neighbours interactions

In Section 6.2.1 we have considered the limit case of infinite-range interactions (the LMG), while in Section 6.2.1 we have explored how the VM behaves as the range of interactions decreases. For completion, let us now briefly explore what happens in the other limit case: an Ising chain with nearest-neighbour interactions under a transverse field. The

Hamiltonian considered is:

$$\mathcal{H} = -J_z \sum_{i=1}^{n-1} \sigma_z^{(i)} \sigma_z^{(i+1)} - h \sum_{i=1}^{n} \sigma_x^{(i)}, \tag{6.24}$$

where $J_z > 0$ ($J_z < 0$) corresponds to FM (AFM) coupling, and h tunes the transverse field strength. The effective two-body Hamiltonian associated to be used in Eq. (6.20) this time takes the following form:

$$\tilde{\mathcal{H}} := -(n-1) J_z \sigma_z \otimes \sigma_z - nh(\sigma_x \otimes \mathbb{1} + \mathbb{1} \otimes \sigma_x)/2. \tag{6.25}$$

In Figure 6.5 we show the results from the comparison between the VM and ED for low number of particles. As expected, the VM yields almost orthogonal solutions in the AFM interactions region, while it provides fidelities close to unity in the FM interactions region. However, one can observe some discrepancies in the FM case, particularly in the vicinity of on the critical points precursors where the fidelity drops. Nevertheless, despite the drop in fidelity, the VM still provides a good upper bound to the ground state energy (see Figure 6.5). In Figure 6.6 we show the half-system EE obtained from the VM for $J_z = 1/2$, for which one observes an anomaly at $h \approx 1$ signalling the presence of a critical point. Therefore, despite the discrepancy in fidelity, the VM still captures information to extrapolate the presence of a critical point.

XXZ model under a transverse field

The Ising chain with nearest-neighbour previously explored in Section 6.2.1 is exactly solvable by means of the Jordan-Wigner transformation [Jordan and Wigner, 1928], which offers an equivalent description of the system in terms of free fermions (see e.g. [Tura *et al.*, 2017]). Let us now consider the performance of the VM beyond the free fermion scope. In particular, we consider an XXZ spin chain under an homogeneous magnetic field described as:

$$\mathcal{H} = -J \sum_{\langle i,j \rangle} \left(\sigma_x^{(i)} \sigma_x^{(j)} + \sigma_y^{(i)} \sigma_y^{(j)} + \Delta \sigma_z^{(i)} \sigma_z^{(j)} \right) + \sum_i h \sigma_x^{(i)} , \tag{6.26}$$

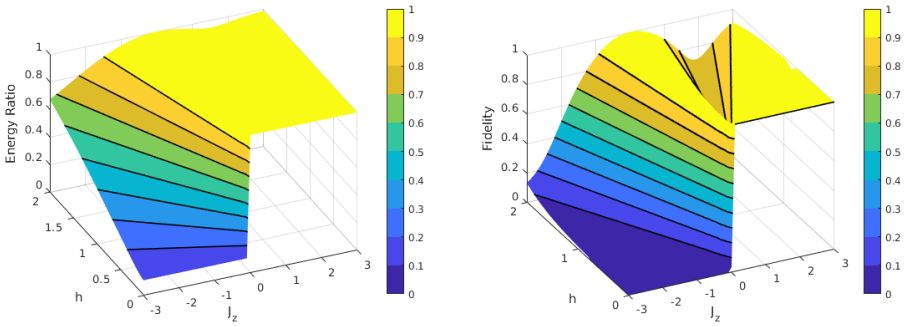

Fig. 6.5 Numerical results obtained by the VM with Eqs. (6.20) and (6.25) for an $n = 10$ Ising chain with nearest-neighbour interactions (see Eq. (6.24)). We compare the ground state energy and fidelity between the VM and ED. One observes that the energies show discrepancies in the AFM interactions regime, possibly due to its inherent asymmetry. The FM interactions case is in general well captured by the VM, albeit there exist some discrepancies near the precursors of the critical points in the asymptotic limit. **Right:** For $J_z = 1/2$ and FM interactions, we use the VM to explore the scaling of the half-system EE, which signals the existence of a critical point when extrapolating to the asymptotic limit.

where we take $J = 1$ ($J = -1$) for the FM (AFM) couplings, Δ marks the anisotropy (where $\Delta = 1$ corresponds to the isotropic case, the XXX model) and h tunes the transverse field strength. This time the two-body effective Hamiltonian to be used in Eq. (6.20) takes the form:

$$\tilde{\mathcal{H}} := J\left((n-1)\left(\sigma_x \otimes \sigma_x + \sigma_y \otimes \sigma_y + \Delta\sigma_z \otimes \sigma_z\right) + nh(\sigma_x \otimes \mathbb{1} + \mathbb{1} \otimes \sigma_x)/2\right). \tag{6.27}$$

As usual by now, in Figure 6.7 we compare the results obtained by the VM and ED, in terms of relative energy and fidelity. In this case one observes that the VM provides accurate results for values $\Delta \gtrsim 1$ ($\Delta \lesssim -1$) when considering FM (AFM) interactions. In particular, in such a regime the VM yields exact results except in the vicinity of the finite-size precursors of critical points [Dmitriev *et al.*, 2002; Alcaraz

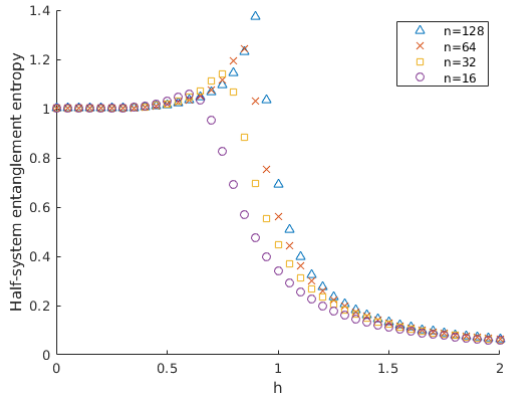

Fig. 6.6 Numerical results obtained by the VM with Eqs. (6.20) and (6.25) for an $n = 10$ Ising chain with nearest-neighbour interactions (see Eq. (6.24)). For $J_z = 1/2$ and FM interactions, we use the VM to explore the scaling of the half-system EE, which signals the existence of a critical point when extrapolating to the asymptotic limit.

and Malvezzi, 1995].

Ferromagnetic XXZ with periodic boundary conditions

Next we consider a particular instance of the XXZ chain: a periodic anisotropic FM spin-1/2 chain, placed in an homogeneous magnetic field. In particular, the model gets described by the following Hamiltonian:

$$\mathcal{H} = -J_x \sum_{i=1}^{n} \left(\sigma_x^{(i)} \otimes \sigma_x^{(i+1)} + \sigma_y^{(i)} \otimes \sigma_y^{(i+1)}\right) - J_z \sum_{i=1}^{n} \sigma_z^{(i)} \otimes \sigma_z^{(i+1)} + b \sum_{i=1}^{n} \sigma_z^{(i)}, \tag{6.28}$$

where $\sigma^{(n+1)} = \sigma^{(1)}$, $J_x, J_z \geq 0$ correspond to the exchange coupling constants, and b tunes the strength of the external magnetic field. In this case, the effective Hamiltonian considered for the VM is the

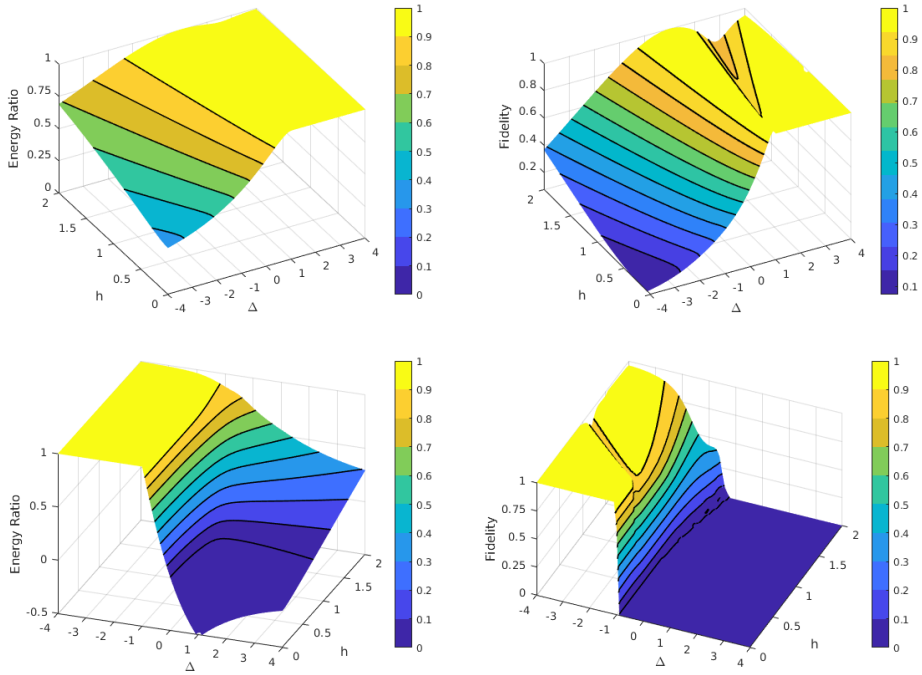

Fig. 6.7 Numerical results obtained by the VM with Eqs. (6.20) and (6.27), compared to ED, for an $n = 10$ XXZ chain described in Eq. (6.26). **First row**: FM interactions ($J = 1$). **Second row**: AFM interactions ($J = -1$). **Left:** Ground energy ratio. **Right:** Ground state fidelity. One observes that the ground state fidelity and energy VM results are accurate for values $\Delta \gtrsim 1$ ($\Delta \lesssim -1$) when considering FM (AFM) interactions. For such range of values, the VM provides close to exact results, except in the vicinity of the critical points precursors which correspond to the phase transitions between regions $2-3$ and $2-4$ of Figure 1 of [Dmitriev *et al.*, 2002].

following:

$$\tilde{\mathcal{H}} := -n\left(J_x\left(\sigma_x \otimes \sigma_x + \sigma_y \otimes \sigma_y\right) + J_z \sigma_z \otimes \sigma_z\right) + n(\sigma_z \otimes \mathbb{1} + \mathbb{1} \otimes \sigma_z)/2. \tag{6.29}$$

The choice of the model is motivated by the work presented in [Zhou *et al.*, 2011], where they investigated the fidelity of preparation of Dicke states as ground states of Eq. (6.28). In Table 6.1 we show the ground state distribution predicted by the perturbative results given in [Zhou *et al.*, 2011]. Notice that the VM is a natural candidate to consider the preparation of Dicke states as ground states. We present the results obtained by the VM in Figure 6.8, where one observes that, up to $n = 10$, the fidelity between the solution of the VM and the ED ground state remains $> 85\%$, which remains consistent with the predictions of [Zhou *et al.*, 2011].

b	Ground state
$b < -\Delta J$	$\lvert D_0^n\rangle$
$-\frac{n-2k+1}{n-1}\Delta J < b < -\frac{n-2k-1}{n-1}\Delta J$	$\lvert D_k^n\rangle$, $0 < k < n$
$\Delta J < b$	$\lvert D_n^n\rangle$

Table 6.1 Ground state distribution for the model in Equation (6.28), as a function of the magnetic field b and the coupling parameter $\Delta J = J_x - J_z$, according to the perturbative results presented in [Zhou *et al.*, 2011]. In Figure 6.8 we recover and strengthen the result.

The perturbative prediction from [Zhou *et al.*, 2011] splits the phase diagram among different regions, each having substantial overlap to a distinct Dicke state. However, in between regions there is a small range of values for which it remains unclear what happens and where the VM displays discrepancy: in Figure 6.8 one observes that for a range of values between each region, the VM provides a better ground state energy by choosing to approximate the first excited state instead of the ground state, since the energy obtained becomes more favourable. The choice of the VM depends on both the overlap with the ground space and the energy gap of the Hamiltonian. In particular, consider

the ground and first excited state energies denoted E_0 and E_1, and let us denote the fidelity between the ground state (first exited state) and the symmetric space as F_0 (F_1). Then, the discontinuities in fidelity may happen when $F_0 E_0 = F_1 E_1$. Indeed, in Figure 6.8 we observe that in between regions the fidelity suddenly drops to zero, whereas the energy ratio is smooth.

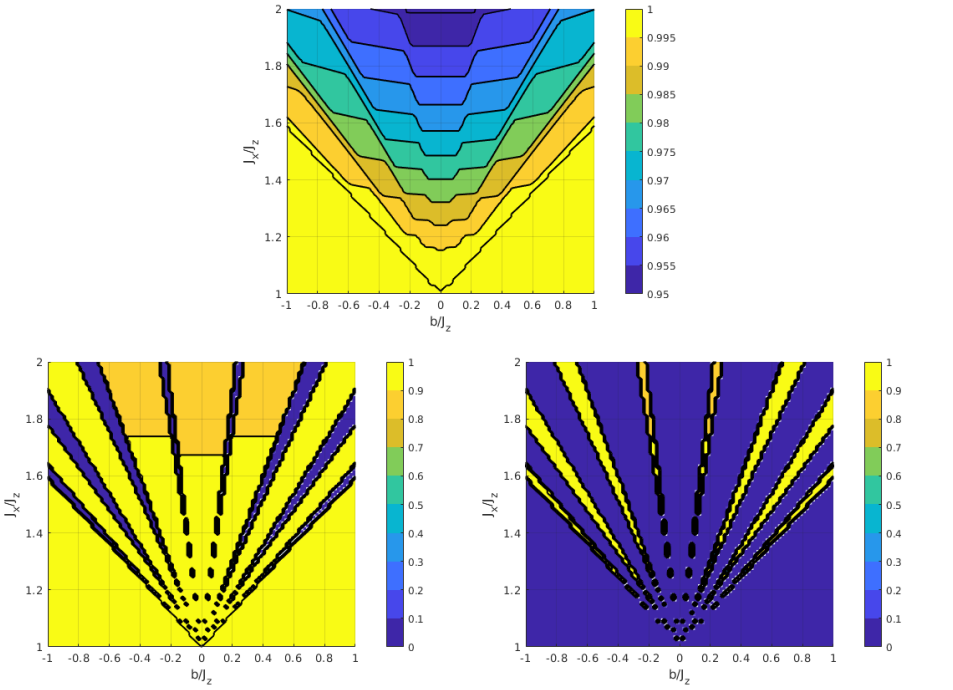

Fig. 6.8 Numerical results obtained by the VM with Eqs. (6.20) and (6.29), compared to ED, for an $n = 10$ XXZ chain as described in Eq. (6.28). **Top:** Energy ratios. **Bottom Left:** Ground state fidelity. **Bottom Right:** First excited state fidelity. Notice that the overlap of the right and center figures recovers the whole phase diagram.

Many-body $SU(3)$ Hamiltonian with collective interactions

Up until now we have been considering only qubit systems, although the VM can easily be applied to systems with local Hilbert space of dimension $d \geq 2$. Let us then consider the three-orbital LMG Hamiltonian [Meredith *et al.*, 1988] (equivalently, the generalisation of the Lipkin Hamiltonian as proposed in [Gnutzmann *et al.*, 2000]). As for the spin$-1/2$ LMG model, the VM is expected to exactly reproduce the ground state properties due to the long-range interactions resulting in symmetric ground states. The model consists of n identical but distinguishable three-level atoms, in particular:

$$\mathcal{H} = a\left(\mathcal{S}_{00} - \mathcal{S}_{22}\right) + b\sum_{i\neq j}\mathcal{S}_{ij}^2, \tag{6.30}$$

where $\mathcal{S}_{ij} = \sum_{l=1}^{n} = \tau_{ij}^{(l)}$ with $\tau_{ij} = |i\rangle\langle j|$ for $i, j = \{0, 1, 2\}$. The associated effective Hamiltonian to be used in the SDP takes the form:

$$\begin{aligned}\tilde{\mathcal{H}} :=& na\left(\mathcal{S}_{00}\otimes\mathbb{1} + \mathbb{1}\otimes\mathcal{S}_{00} - \mathcal{S}_{22}\otimes\mathbb{1} - \mathbb{1}\otimes\mathcal{S}_{22}\right)/2 \\ &+ \binom{n}{2} b\sum_{i\neq j}\left(\mathcal{S}_{ij}\otimes\mathcal{S}_{ij} + (\mathcal{S}_{ij}^2\otimes\mathbb{1} + \mathbb{1}\otimes\mathcal{S}_{ij}^2)/2\right).\end{aligned} \tag{6.31}$$

We present the results in Figures 6.9 and 6.10, where it is observed that the VM attains the exact ground state energy up to the numerical accuracy of the solver. Similarly as in previous cases, we make use of the compatibility conditions in the symmetric basis to efficiently compute the half-system EE, which serves to explore the phase diagram for the model.

Benchmarking performance with existing methods

In this section we benchmark the computational requirements of the presented VM with a DMRG algorithm.

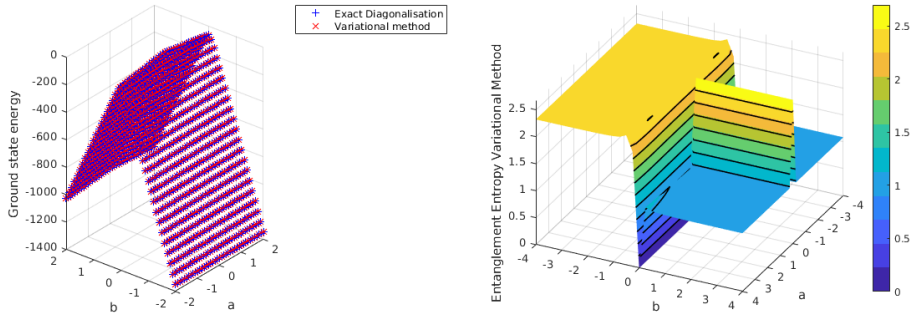

Fig. 6.9 Numerical results obtained by the VM with Eqs. (6.20) and (6.31) for an $n = 32$ three-level generalized Lipkin Hamiltonian in Eq. (7.24). **Left:** The VM provides the exact ground state energy within numerical accuracy of the solver ($\approx 10^{-14}$ using SeDuMi [Sturm, 1999]). **Right:** Half-system EE computed by means of the compatibility conditions in Eq. (6.6), which may serve to explore the phase diagram.

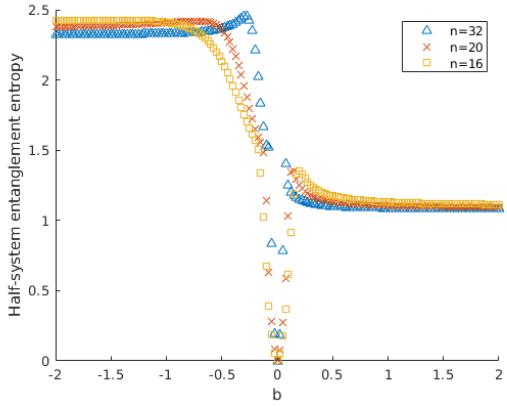

Fig. 6.10 Numerical results obtained by the VM with Eqs. (6.20) and (6.31) for an $n = 32$ three-level generalized Lipkin Hamiltonian in Eq. (7.24) with $a = 3$. Half-system EE computed for different number of particles, which may signal critical points when extrapolating peak anomalies to the asymptotic limit.

We have seen in previous sections that the VM captures relevant information for some quantities of physical interest, although this might be situational. The main advantage of the VM is that it takes place in the symmetric space, and therefore it has the ability to reach large system sizes while remaining modest in time and memory requirements. In particular, the dimension of the states considered by the VM grow only polynomially with the system size: it is linear for qubits, quadratic for qutrits, etc. Hence, the VM supposes a good candidate for a first order exploration before trying more numerically-intensive results.

The runtime of the VM can be split in two steps:

- For a fixed number of parties n, of local Hilbert space dimension d, and with RDMs of size m, compute the A matrices in Eq. (6.15) containing the compatibility conditions.

- Load and solve the SDP.

The most expensive task, both in time and memory, is to compute the compatibility conditions. In order to speed up the process, we recommend to first preallocate and store the compatibility conditions. Then, once the compatibility constraints are preallocated for fixed n, d and m, one can scan the phase diagram of the desired parametrized Hamiltonian model just by loading the compatibility conditions as constraints and solving the corresponding SDP.

In Figure 6.11 we show a representative sample of the computing runtimes we have observed to preallocate the compatibility conditions for the 2-RDMs and half-system $n/2$-RDMs given different number of particles n and different local Hilbert space dimensions d. For comparison, we have considered the 2-RDMs compatibility constraints case both in the computational basis (Eq. (6.5)) and the symmetric basis (Eq. (6.6)). As expected, not only the symmetric basis requires less memory but there is also a significant advantage in runtime. Therefore, it might be desirable to project the effective Hamiltonian onto the symmetric subspace and perform the VM entirely in the symmetric space, specially when the Hamiltonian considered involves high local Hilbert

space dimension or involves high m-body terms. For the $n/2$-RDMs case, used for instance to compute half-system EEs, memory storage quickly becomes a limitation and that is why we have considered only the symmetric representation. Additionally, for a constant value of d, notice that the multinomial coefficients that appear in Eqs. (6.5) and (6.6) can be expressed as closed analytical formulas that do not require full expansion of the factorials (see *e.g.* [Tura *et al.*, 2015]). This has been taken into consideration in our calculations. Moreover, it is desirable to apply such closed expressions, not only for speed, but also for numerical stability (since the quotients of factorials may give problems in floating-point arithmetic if these numbers are of the order of ~ 100).

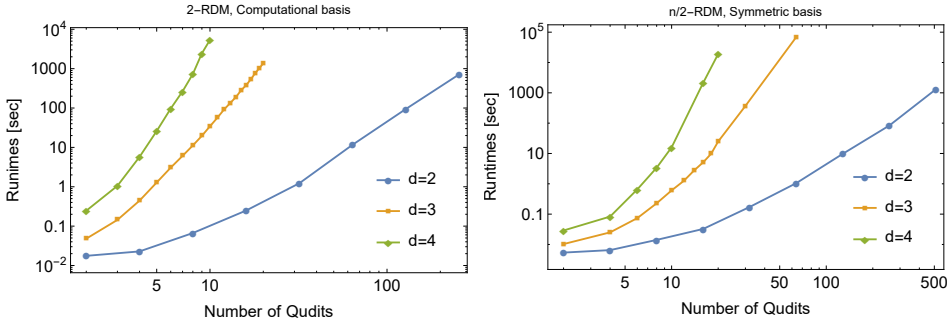

Fig. 6.11 Representative sample of runtimes observed to preallocate the 2-RDMs and $n/2$-RDMs compatibility conditions in the computational and symmetric basis respectively. Apart from the memory storage advantage, the symmetric spaces offers a significant advantage in runtimes. The computations have been carried out on a 64-bit operating system with 32GB ram and a 3.70GHz processor. No parallelization has been used, which can be easily be implemented significantly speeding up the process. The runtimes might slightly vary at each run and are not meant to be taken as exact, but as an illustration of their order.

In Figure 6.12 we show a representative sample of the computing runtimes in order to load the constraints and solve the SDP for the Ising chain with decaying power-law interactions presented in Section 6.2.1.

The constraints and effective Hamiltonian have been computed in the symmetric basis, and to solve the SDP we have set the solver SDPT3 [Toh *et al.*, 1998] to its maximal precision providing a numerical accuracy up to $\mathcal{O}(10^{-14})$ (when the VM can reach the exact solution). In Figure 6.13 we compare the VM with the solution provided by DMRG. In order to find the fidelity between the DMRG solution and the VM solution, we have used the results developed in Section 6.2.3 to represent the VM solution as a translationally invariant diagonal matrix product state.

6.2.2 Bell inequalities and the variational ansatz

In this section we consider the variational ansatz to characterize Bell non-local correlations in many-body systems. In particular, the variational ansatz synergizes with the two-body PIBIs, which have kept appearing throughout the thesis (see Section 2.3.4 for details). In particular, since two-body PIBIs involve at most two-body correlations and some of them are known to be maximally violated for symmetric states [Tura *et al.*, 2015], the variational ansatz is a natural candidate to efficiently find the optimal state leading to maximal violation of such equalities. Furthermore, one can also consider the variational ansatz to explore non-local correlations in ground states of many-body Hamiltonians. Note that in the latter case, the Hamiltonian considered need not correspond to the Bell operator [Tura *et al.*, 2017]. It is worth mentioning that, as we have seen in Chapters 4 and 5, the measurement settings might need to be optimized in order to increase the visibility of the Bell correlations.

Optimizing permutationally invariant two-body Bell inequalities

We consider the same classes of two-body PIBIs previously considered in Chapters 4 and 5, which we recall for clarity (see Sections 2.3.4

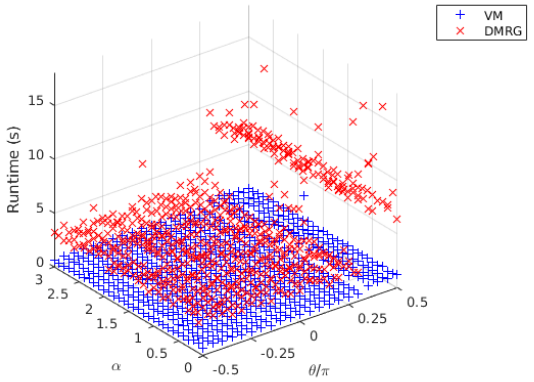

Fig. 6.12 Comparison of the runtimes for the VM and the DMRG methods to reach convergence for an $n = 64$ Ising chain with tunable range interactions as described in Eq. (6.21). The DMRG algorithm is based on [Evenbly, 2019] following the methodology presented in [Crosswhite *et al.*, 2008; Fröwis *et al.*, 2010] to account for power-law and long-range interactions. The bond dimension is increased up to 20. One observes that the VM is significantly faster (at the expense of being less accurate), thus being a suitable candidate for a first rough exploration of large phase diagrams, and to upper bound ground state energies. The runtimes presented are representative and might slightly vary at each run. The total runtimes have been 525.04s (1s preallocation) for the VM and 2854.25s for the DMRG. Let us remark that the DMRG is an extremely optimized and efficient method that has troubles being applied beyond 1 geometric dimension, whereas the application of the VM follows the same principle for any geometric dimension (just by adapting it to the corresponding interactions).

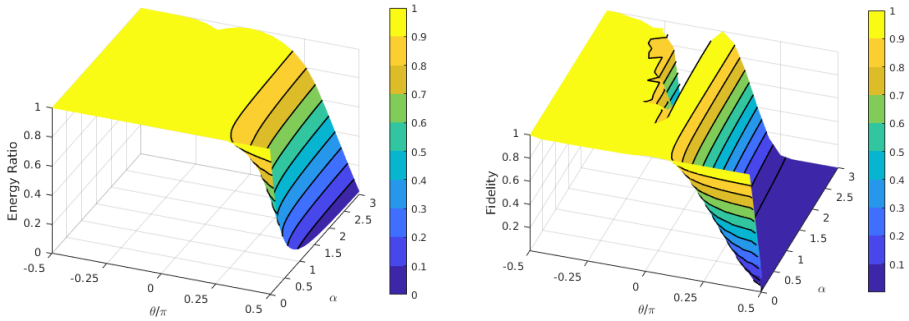

Fig. 6.13 Numerical results comparison between the VM and DMRG solutions for an $n = 64$ Ising chain with tunable range interactions as described in Eq. (6.21). The DMRG algorithm is based on [Evenbly, 2019] following the methodology presented in [Crosswhite *et al.*, 2008; Fröwis *et al.*, 2010] to account for power-law and long-range interactions. The bond dimension is increased up to 20. **Left** and **Right:** Energy ratio and fidelity, respectively, of the VM solution with respect to the DMRG solution. To compute the fidelity, we use the result in Section 6.2.3 to transform the symmetric basis representation of the VM solution into an MPS representation.

and 4.5 for more details):

$$-2\langle \mathcal{S}_0\rangle + \frac{1}{2}\langle \mathcal{S}_{00}\rangle - \langle \mathcal{S}_{01}\rangle + \frac{1}{2}\langle \mathcal{S}_{11}\rangle - \beta_c \geq 0 \tag{6.32}$$

and

$$(n \bmod 2)(n-1)(n\langle \mathcal{S}_0\rangle + \langle \mathcal{S}_1\rangle) + \binom{n}{2}\langle \mathcal{S}_{00}\rangle + n\langle \mathcal{S}_{01}\rangle - \langle \mathcal{S}_{11}\rangle - \beta_c \geq 0, \tag{6.33}$$

where $\beta_c = -2n$, $\beta_c = -\binom{n}{2}(n+2+n \bmod 2)$ are the classical bounds for Eqs. (6.32) and (6.33) respectively, and $\langle \mathcal{S}_k\rangle = \sum_{i=1}^{n}\langle \mathcal{M}_k^{(i)}\rangle$, $\langle \mathcal{S}_{kl}\rangle = \sum_{i\neq j}\langle \mathcal{M}_k^{(i)}\mathcal{M}_l^{(j)}\rangle$ denote the one- and two-body symmetric correlators, and $\mathcal{M}_k^{(i)}$ denotes the i-th party measurement in the direction indexed by $k = \{0,1\}$. The inequality in Eq. (6.32) is particularly fitted to detect non-local correlations in superpositions of Dicke states, whereas

the inequality in Eq. (6.33) is tailored to detect non-local correlations in half-filled pure Dicke states [Tura *et al.*, 2015; Fadel and Tura, 2017].

To find quantum correlations leading to the violation of the Bell inequalities in Eqs. (6.32) and (6.33), we also need to find n appropriate pairs of measurement settings. As we have seen, the procedure to find the optimal measurement settings involves the associated Bell operator, whose expectation value with respect to a quantum state corresponds to the value of the Bell inequality for the chosen measurement settings. In general, to find the optimal measurement settings is a highly complex non-convex optimization problem. However, we have seen in Section 4.5.2 and Chapter 5 that a particular case of interest is when the n parties perform the same measurement settings, which greatly reduces the complexity. Moreover, because under this assumption the Bell operator becomes PI, we can then use the VM in order to find its extremal values within the symmetric space, thus finding the optimal quantum correlations for the Bell inequality considered.

Hence, the VM provides a new approach to characterize two-body PIBIs in which, instead of projecting the PI Bell operator onto the different symmetric blocks by means of the Schur-Weyl duality (see *e.g.* [Tura *et al.*, 2015; Tura, 2017; Tavakoli *et al.*, 2019]), it is now sufficient to consider an effective Hamiltonian. In particular, for the Bell inequality in Eq. (6.32) the effective Hamiltonian takes the following form:

$$\begin{aligned}\tilde{\mathcal{H}} :=& -2n\mathrm{Tr}\Big((\mathcal{M}_0 \otimes \mathbb{1} + \mathbb{1} \otimes \mathcal{M}_0)\, \sigma \Big) \\ &+ \binom{n}{2} \mathrm{Tr}\Big((\mathcal{M}_0 \otimes \mathcal{M}_0 - 2\mathcal{M}_0 \otimes \mathcal{M}_1 + \mathcal{M}_1 \otimes \mathcal{M}_1)\, \sigma \Big),\end{aligned} \tag{6.34}$$

where σ denotes the 2-RDM that can be optimized by means of the variational ansatz. In particular, parametrize the measurements as $\mathcal{M}_k := \sin(\theta_k)\,\sigma_x + \cos(\theta_k)\,\sigma_z$, where $k \in \{0, 1\}$ and σ_x, σ_z are the Pauli matrices, and then employ the VM to obtain the n-qudit symmetric state minimizing the energy of the effective Hamiltonian. Notice that this approach becomes particularly useful when the local Hilbert space dimensions d are large, in which case the number of blocks arising

from the symmetry-adapted basis increases with d quickly rendering other approaches, like the Schur-Weyl duality, unapproachable. On the other hand, since Equations (4.26) and (6.33) are set on an $(n, 2, 2)$ Bell scenario, Jordan's lemma [Jordan, 1875] guarantees that $d = 2$ is sufficient to find find its maximal violation, as shown in [Toner and Verstraete, 2006].

Looking for non-local correlations in Hamiltonian spin systems

Here we propose a two-step process to find non-local correlations in the ground state of Hamiltonians of physical interest. First, we use the VM as an effective quick scan over the parameter space of a given Hamiltonian family, in order to find potential candidates whose ground state might violate a given two-body PIBI. For instance, we have explored non-local correlations in the XXZ chain described in Eq. (6.26), with the results shown in Figure 6.14. However, notice that, provided that one has found violation of the two-body PIBI with the state solution by the VM, one does not have guarantee that the actual ground state would violate the Bell inequality. Nevertheless, we have narrowed down the search to consider the cases whose VM solution violate the two-body PIBI. Then, one can take a more exhaustive method, such as DMRG, to compute the actual ground state, as we show in Figure 6.14. We present the results in Figure 6.14 where, following this procedure, we have been able to detect non-local correlations in the ground state of the XXZ chain in Eq. (6.26), obtained by violating Bell inequality in Eq. (4.26). Remarkably, it is the first time, to the best of our knowledge, that the ground state of said XXZ chain are shown to exhibit non-local correlations by violating a Bell inequality.

A comment is in order. Since now the ground state is given and is not a symmetric state, one can no longer optimize the measurement settings by considering a single 2-RDM as we posed in Eq. (6.34). Instead, similarly as we did in Section 5.3.1, one now needs to sum over all the distinct 2-RDMs obtained with the DMRG, and denoted

σ_{ij}:

$$\tilde{\mathcal{B}} = -2\sum_{i=1}^{n} \mathrm{Tr}\Big(\left(\mathcal{M}_0^{(\mathrm{i})} \otimes \mathbb{1} + \mathbb{1} \otimes \mathcal{M}_0^{(\mathrm{i})}\right) \sigma_{\mathrm{i}} \Big) + \sum_{i<j} \mathrm{Tr}\Big(\left(\mathcal{M}_0^{(\mathrm{i})} \otimes \mathcal{M}_0^{(\mathrm{j})} - 2\mathcal{M}_0^{(\mathrm{i})} \otimes \mathcal{M}_1^{(\mathrm{j})} + \mathcal{M}_1^{(\mathrm{i})} \otimes \mathcal{M}_1^{(\mathrm{j})}\right) \sigma_{\mathrm{ij}} \Big). \tag{6.35}$$

Moreover, because the RDMs are now fixed (by the exact solution), one needs to parametrize the measurements to account for all the Bloch sphere, and moreover the optimal measurement settings do not need to correspond to a scenario where the measurement settings are identical for all parties. Therefore, for this case we parametrize the measurements as $\mathcal{M}_k^{(i)} = \sin\theta_{i,k}\cos\varphi_{i,k}\sigma_x^{(i)} + \sin\theta_{i,k}\sin\varphi_{i,k}\sigma_y^{(i)} + \cos\theta_{i,k}\sigma_z^{(i)}$, for $k \in [2]$ and $i \in [n]$. To carry out the optimization we proceed similarly as in Step 3 in Section 4.4.1.

Let us now consider the two-body PIBI in Eq. (6.33), which is known to detect non-local correlations in half-filled pure Dicke states. Consequently, a good candidate is the FM XXZ chain with periodic boundary conditions and longitudinal magnetic field b presented in Section 6.2.1, for which we have seen pure Dicke states have fidelity close to unity with its ground state. In particular, the half-filled pure Dicke states approximate the ground state in the range $-\frac{1}{n-1}(J_x - J_z) < b < \frac{1}{n-1}(J_x - J_z)$. Therefore, we expect to witness non-local correlations with Equation (6.33) in said region. Indeed, in Figure 6.15 we show the witnessed nonlocality, where we have used the VM to approximate the ground state and optimize using Eq. (6.34). One observes that the region exhibiting non-local correlations goes beyond the specified region where the half-filled Dicke state approximates the ground state. As previously discussed in Section 6.2.1, such extra range of nonlocality detection seems to arise from the VM approximating the first excited state instead of the ground state.

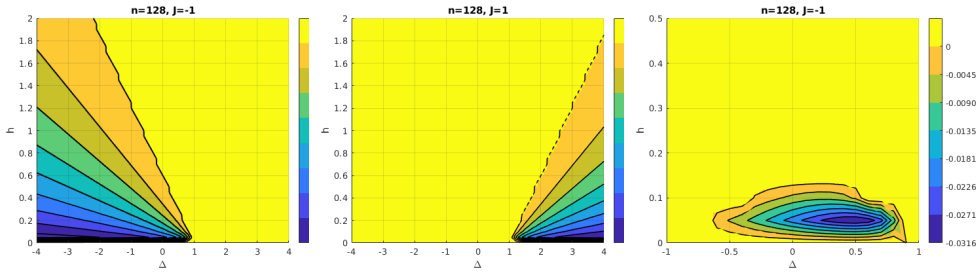

Fig. 6.14 Detection of non-local correlations in an $n = 128$ XXZ chain as described in Equation (6.26), via the two-body PIBI in Eq. (4.26). **Left:** For $J = -1$ FM couplings, we obtain the solution of the VM with Eq. (6.34) and show its corresponding Bell inequality violation (negative values) relative to the classical bound. **Center:** Same for $J = 1$ AFM couplings. **Right:** For FM couplings, we zoom-in on the region with largest relative violation and largest fidelities (according to Figure 6.7), conditioned to the solutions by VM. Then, the shown results correspond to the relative Bell inequality violation obtained with the (non-symmetric) Bell operator in Eq. (6.35), where the ground state has been attained via DMRG. For the DMRG solution we have taken bond dimension of 32.

6.2.3 Generically expressing symmetric states as TI diagonal MPS

In this section we present an analytical method to generically represent any n-qubit symmetric state with a Translationally-Invariant (TI) MPS. For this section we restrict to qubits and denote an n-qubit Dicke states as $|D_k^n\rangle$, where $0 \leq k \leq n$ denotes the number of parties in the state $|1\rangle$ (see Section 2.1 for details).

The goal of this section is then the following: given a superposition of Dicke states

$$|\psi\rangle = \sum_{k=0}^{n} d_k \, |D_k^n\rangle \,, \qquad d_k \in \mathbb{C}, \tag{6.36}$$

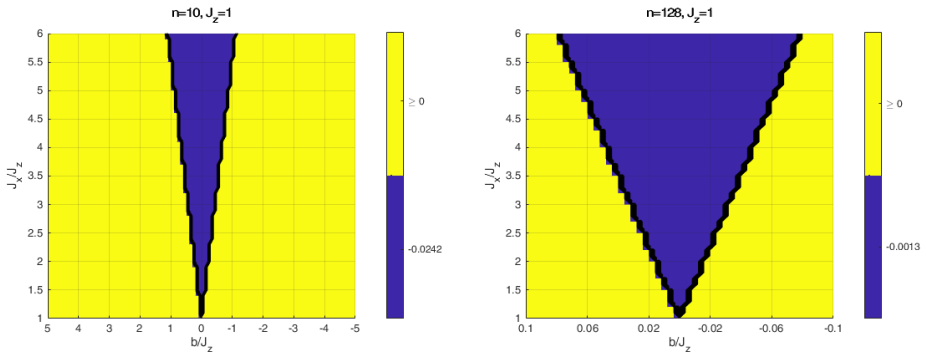

Fig. 6.15 Detection of non-local correlations (negative values) in an $n = 10$ and $n = 128$ FM XXZ chain with periodic boundary conditions and under a longitudinal magnetic field b as described in Eq. (6.28). Its ground state solution is given by the VM, and the two-body PIBI consider is the one in Eq. (6.33). One observes non-local correlations not only in the region where the VM approximates the ground state with pure half-filled Dicke states, but also where the VM approximates the first excited state.

find two matrices $A_0, A_1 \in \mathcal{M}_{D\times D}(\mathbb{C})$ such that

$$\begin{aligned} |\psi\rangle &= \sum_{(i_1,\ldots,i_n)\in\{0,1\}^n} \psi_{(i_1,\ldots,i_n)} |i_1,\ldots,i_n\rangle \\ &= \sum_{(i_1,\ldots,i_n)\in\{0,1\}^n} \mathrm{Tr}[A_{i_1}\cdots A_{i_n}] |i_1,\ldots,i_n\rangle . \end{aligned} \tag{6.37}$$

Representations as TI MPS are known for some symmetric states of interest like the GHZ state or the W state. For example, the GHZ state (up to normalization) can be generated with $D = 2$ [Orús, 2014] using the following TI MPS:

$$A_0 = \begin{pmatrix} 1 & 0 \\ 0 & 0 \end{pmatrix}, \qquad A_1 = \begin{pmatrix} 0 & 0 \\ 0 & 1 \end{pmatrix}. \tag{6.38}$$

As for the $|W\rangle$ state, while there does not exist a TI representation with bond dimension 2, it can be generated (up to normalization) with

the following non-TI representation [Perez-Garcia *et al.*, 2007]:

$$\begin{cases} \{A_0^{[i]}, A_1^{[i]}\} &= \{\sigma^+, \mathbb{1}\} \quad \text{if} \quad i < n \\ \{A_0^{[i]}, A_1^{[i]}\} &= \{\sigma^+\sigma_x, \sigma_x\} \quad \text{if} \quad i = n. \end{cases} \tag{6.39}$$

On the other hand, notice that all the coefficients of the MPS in Eq. (6.39) are either 1 or 0. In fact, some MPS can represent Boolean formula solutions [Biamonte and Bergholm, 2017]. In general, the representability of quantum states as MPS of a particular form is deeply connected with modern algebraic geometry [Sanz *et al.*, 2009, 2016, 2017]. This brings us, for instance, to observe that the $|W\rangle$ state can be arbitrarily well-approximated with a diagonal TI MPS of bond dimension $D = 2$:

Lemma 6.2.1. *Let $\varepsilon > 0$, and the following diagonal TI MPS:*

$$A_0 = \begin{pmatrix} x_0 & 0 \\ 0 & x_1 \end{pmatrix}, \qquad A_1 = \begin{pmatrix} y_0 & 0 \\ 0 & y_1 \end{pmatrix}, \tag{6.40}$$

where

$$\begin{cases} x_0 &= 2^{-1/n}\varepsilon^{-1/[n(n-1)]} \\ x_1 &= e^{\mathrm{i}\pi/n}x_0 \\ y_0 &= 2^{-1/n}\varepsilon^{1/n} \\ y_1 &= -e^{\mathrm{i}\pi/n}y_0. \end{cases} . \tag{6.41}$$

Then, the n-qubit $|W\rangle$ state can be generated with the TI MPS given in Eq. (6.40) in the limit $\varepsilon \to 0$.

Proof: Because the MPS is diagonal, the elements corresponding to the physical index $(i_1, \ldots, i_n)$ with $k := \sum_j i_j$ is given by

$$\psi_{(i_1,\ldots,i_n)} = x_0^{n-k}y_0^k + x_1^{n-k}y_1^k, \tag{6.42}$$

which for $k \equiv 0 \mod 2$ amounts to 0, while for $k \equiv 1 \mod 2$ amounts to $\varepsilon^{(k-1)/(n-1)}$. Then, notice that

$$\lim_{\varepsilon\to 0} \varepsilon^{\frac{k-1}{n-1}} = \begin{cases} 1 & \text{if} \quad k = 1 \\ 0 & \text{if} \quad k > 1 \end{cases} \tag{6.43}$$

which, therefore, yields Lemma 6.2.1.

□

Following the same reasoning as in Lemma 6.2.1, we now generalise to generically approximate any superposition of Dicke states of the form Eq. (6.36) with a diagonal TI MPS of bond dimension n.

Consider the following parametrization for A_0 and A_1:

$$A_0 \propto \mathbb{1}_D; \qquad A_1 = \mathrm{diag}(x_1, \ldots, x_D). \tag{6.44}$$

For simplicity it is convenient to denote $A_0 = y\mathbb{1}$ and $k = \sum_j i_j$. Under this notation and taking into account Eq. (6.37), one obtains the following system of equations:

$$\sum_{a=1}^{D} y^{n-k} x_a^k = \psi_{(i_1,\ldots,i_n)}, \qquad \{i_1, \ldots, i_n\} \in \{0,1\}^n. \tag{6.45}$$

Notice that, since we deal with qubit Dicke states of the form in Eq. (6.36), only $n+1$ equations are required. Consequently, a natural choice is $D = n$. This motivates the following lemmas:

Lemma 6.2.2. *Consider the following system of equations:*

$$\begin{cases} x_1 + \cdots + x_n &= z_1 \\ x_1^2 + \cdots + x_n^2 &= z_2 \\ \qquad \cdots & \\ x_1^n + \cdots + x_n^n &= z_n \end{cases}, \tag{6.46}$$

where $z_1, \ldots, z_n \in \mathbb{C}$. The solutions of Eq. (6.46) correspond to the roots of the polynomial $P(X)$ defined in Eq. (C.10).

Lemma 6.2.3. *The coefficients y and $x_1 \ldots x_n$ of the diagonal tensors A_0 and A_1, used to represent the linear combination of Dicke states*

Eq. (6.36)*, are determined by the following system of equations:*

$$\begin{cases} y & = & \sqrt[n]{d_0/n} \\ x_1 + \cdots + x_n & = & \frac{d_1}{y^{n-1}\sqrt{n}} \\ x_1^2 + \cdots + x_n^2 & = & \frac{d_2}{y^{n-2}\sqrt{\binom{n}{2}}} \\ \cdots & & \\ x_1^k + \cdots + x_n^k & = & \frac{d_k}{y^{n-k}\sqrt{\binom{n}{k}}} \\ \cdots & & \\ x_1^n + \cdots + x_n^n & = & d_n \end{cases} . \tag{6.47}$$

The value of y gets determined from the first equation, whereas to determine the values of the x's one uses the remaining set of equations to construct a polynomial $P(X)$ via Lemma 6.2.2 and then finds its roots.

Therefore, generically, one has n complex solutions up to $n!$ permutations. However, there is the possibility of pathological cases in which the solutions lie at infinity. On the other hand, these pathological cases form a zero-measure set which in practice can be avoided by adding an ε-perturbation to d_k, in the same spirit as in Eq. (6.41).

Arrived to this point, if we find a way to solve the system of equations in Eq. (6.46) from Lemma 6.2.2, we are done. We propose two approaches to solve Eq. (6.46): First, presented in what follows, an adaptation of the Faddeev-Leverrier algorithm (see *e.g.,* [Householder, 2013]) to solve Newton's identities in order to find the roots power-sum symmetric polynomials; Second, presented in Appendix C.1, we propose a step-by-step computation of the solutions via Gröbner basis which could also provide solutions for more general systems of equations.

Let us make a couple of observations which will aid us in solving Eq. (6.46) by adapting the Faddeev-Lverrier algorithm:

- Let A be a matrix with eigenvalues $\{x_1, \ldots, x_n\}$, then Eq. (6.46) can be thought of as

$$\mathrm{Tr}[A^k] = z_k, \qquad 1 \leq k \leq n. \tag{6.48}$$

- One can express the characteristic polynomial of a matrix A in terms of $\mathrm{Tr}[A^k]$. Namely, if $P(X) = \det(X\mathbb{1} - A) = (X - x_1)\cdots(X - x_n) = \sum_{k=0}^{n} c_k X^k$ is the characteristic polynomial of A, then $P(A) = 0$, and taking the trace in both sides yields such an equation.

Then, the Faddeev-Leverrier algorithm provides an expression for coefficients c_k which is easy to compute. In particular, the coefficients c_k are given by:

$$
\begin{aligned}
c_{n-m} &= \frac{(-1)^m}{m!}
\begin{vmatrix}
\mathrm{Tr}[A] & m-1 & 0 & \cdots & 0 \\
\mathrm{Tr}[A^2] & \mathrm{Tr}[A] & m-2 & \cdots & \\
\vdots & \vdots & & & \vdots \\
\mathrm{Tr}[A^{m-1}] & \mathrm{Tr}[A^{m-2}] & \cdots & \mathrm{Tr[A]} & 1 \\
\mathrm{Tr}[A^m] & \mathrm{Tr}[A^{m-1}] & \cdots & \cdots & \mathrm{Tr[A]}
\end{vmatrix} \\
&= \frac{(-1)^m}{m!}
\begin{vmatrix}
z_1 & m-1 & 0 & \cdots & 0 \\
z_2 & z_1 & m-2 & \cdots & \\
\vdots & \vdots & & & \vdots \\
z_{m-1} & z_{m-2} & \cdots & z_1 & 1 \\
z_m & z_{m-1} & \cdots & \cdots & z_1
\end{vmatrix},
\end{aligned}
\tag{6.49}
$$

where the values of x are found by obtaining all the roots of the polynomial $P(X) = \sum_{k=0}^{n} c_k X^k$ with $c_n = 1$. In Appendix C.1 we present an alternative approach to solve the system of equations in Eq. (6.46) from a more algebraic perspective that provides more insight about the combinatorial structure underlying Eq. (6.46).

To conclude, we have obtained an analytical methodology to generically represent any superposition of Dicke states of the form in Eq. (6.36) as a TI MPS. Therefore, since we have an efficient way to represent states of the form in Eq. (6.36) in the symmetric basis, now we can, *e.g.,* efficiently compute their fidelity with DMRG solutions (which are already given in the MPS formalism) for large n, thus being able to benchmark our method as has been done in Section 6.2.1.

6.2.4 Determining which symmetric states cannot be self-tested from their marginals

In this section we explore the uniqueness of the QMP solution for symmetric states in order to extract conclusions about under which conditions symmetric states cannot be self-tested from its marginals.

Self-testing is one of the most prominent DIQIP protocols and, in fact, the DI formalism originated in the context of self-testing. Self-testing protocols are based on the fact that some states and measurements are uniquely determined, up to a local isometries, by the quantum correlations they exhibit on a Bell-type experiment. In other words, self-testing protocols certify states and measurements solely from the statistics observed on a Bell-type experiment [Mayers and Yao, 2004; Šupić and Bowles, 2019; Yang and Navascués, 2013].

There has been a lot of self-testing work around the bipartite case [Bamps and Pironio, 2015; Kaniewski, 2016], in part because it allows for simpler physical implementations [Wang *et al.*, 2018; Zhang *et al.*, 2019], and theoretical analysis Salavrakos *et al.* [2017]; Kaniewski *et al.* [2019]; Šupić *et al.* [2016]. In the multipartite case, symmetric states constitute a natural candidate to begin their study: for instance, the robust self-testing of the W state ($|D_1\rangle$) [Wu *et al.*, 2014] inspired schemes to self-test Dicke states of the form $|D_k\rangle$ [Fadel, 2017; Wu, 2016; Šupić *et al.*, 2018]. Nevertheless, these schemes use full-body correlators and require individual addressing, thus being less appealing from an experimental point of view. Therefore, some studies have been carried to find out whether self-testing is possible using only marginal information [Li *et al.*, 2018] (see also [Baccari *et al.*, 2020; Augusiak *et al.*, 2019]): In [Li *et al.*, 2018], some efforts showed that the three-qubit states maximally violating some of the translationally invariant, two-body Bell inequalities from [Tura *et al.*, 2014b] could be self-tested using two-body correlators, thus giving a positive answer to this question.

One remaining open question is how much information from the statistics is needed (*i.e.*, how many parties can one trace out) in order

to self-test a quantum state. In this section, we show how, depending on the uniqueness of the solution to Eq. (6.15), our solution to the QMP for symmetric states can be used to guarantee a negative answer to the previous question. Furthermore, we also carry out a numerical exploration to provide evidence towards a positive answer as well.

Our goal in what follows, then, is to employ Eq. (6.15) to determine which symmetric states can potentially be self-tested from its marginals, and which symmetric states definitely can not due to its marginals not having a unique (up to local unitaries) extension in the symmetric space.

Let $\rho_{n,k}$ denote an n-qubit density matrix which projects onto an n-qubit Dicke state $|D_k^n\rangle$ (recall Eq. (2.3)). Let $\sigma = \mathrm{Tr}_1(\rho)$ denote the reduced state after having traced out a single particle. In virtue of Equation (6.5), we have

$$\sigma = \binom{n}{k}^{-1} \left(\binom{n-1}{k-1} \rho_{n-1,k-1} + \binom{n-1}{k} \rho_{n-1,k} \right) . \tag{6.50}$$

The first thing we consider, is to explore under which conditions it is possible to show that the purification of σ is unique. Inspired by Lemma 5.2 of [Scarani, 2012b], we first consider a purification with an auxiliary system of the form

$$|\Phi\rangle = |D_{k-1}^{n-1}\rangle\,|P_1\rangle + |D_k^{n-1}\rangle\,|P_2\rangle\,, \tag{6.51}$$

where

$$|P_1\rangle = \alpha_0|0\rangle|x_{10}\rangle + \alpha_1|1\rangle|x_{11}\rangle \tag{6.52}$$
$$|P_2\rangle = \beta_0|0\rangle|x_{20}\rangle + \beta_1|1\rangle|x_{21}\rangle\,. \tag{6.53}$$

Then, with some algebra, one sees that the $(n-1)$-body RDM of $|\Phi\rangle\langle\Phi|$ is equal to σ if, and only if,

$$\alpha_0 = 0, \quad \alpha_1 = \sqrt{\frac{k}{n}}, \quad \beta_0 = \sqrt{\frac{n-k}{n}}, \quad \beta_1 = 0\,. \tag{6.54}$$

Therefore, one concludes that for this case: there exists a purification; it is unique; and it must be of the form

$$|\Phi\rangle = |D_k^n\rangle|x_{11}\rangle \ . \tag{6.55}$$

Corollary 6.2.1. *The $(n-1)-$partite reduced state of $|D_k\rangle$ uniquely determines $|D_k\rangle$ in the symmetric space.*

A generalization of the above example to the case where any number of parties have been traced out is shown in Appendix C.2. Furthermore, it is observed that the uniqueness of the extension is in one-to-one correspondence to the uniqueness of a linear program (see Eq. (C.21)). After some numeric exploration, we have observed that said solution is unique when tracing out up to $n-2$ parties for a basis Dicke state. Having said this, a more in depth analysis is required to know how generic the above property is. In what follows we shall carry out a more in-depth study, which suggests that generically the uniqueness property depends on both the rank of the global density matrix and the number of parties that have been traced out.

In Figure 6.16 we show numerical evidence that, generically, the uniqueness of the symmetric extension depends on the number of parties n in the global density matrix ρ, the number of parties in the RDMs m and the rank of the global density matrix $\text{rank}(\rho)$. The procedure we have followed is outlined below:

1. Generate a random symmetric state such that its density matrix has a given rank

2. Use the compatibility conditions in Eq. (6.6) to obtain its m-RDM

3. Obtain a new global symmetric state $\tilde{\rho}$ by means of the m-RDM and the SDP in Eq. (6.15) and check its fidelity with the original global state, $F(\rho, \tilde{\rho})$ Eq. (6.23). In order to force the SDP to explore the feasible set in different directions, we construct a random Hermitian matrix A which marks the direction by setting the SDP's objective function as $\min(-\langle A, \rho\rangle)$.

4. Repeat step 3) a sufficient number of times in search for distinct solutions (in our case, 100 times).

Therefore, if after following the steps above the fidelity has remained always one up to numerical accuracy error, it shows strong numerical evidence that the global state is unique. Whereas if the fidelity drops below one for some case, it shows that the the number of parties remaining in the RDM m and the rank(ρ) are not sufficient to self-test the original state, since it does not have a unique global extension of size n.

The fact that for some rank configurations and sizes of the RDM the extension to the symmetric state seems to be unique, opens the door to a weaker form of self-testing from its marginals under the assumption that the global state is symmetric (even though mixed states in their generality cannot be self-tested).

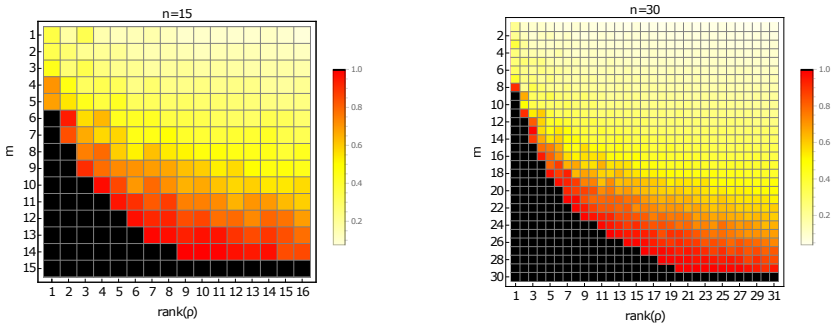

Fig. 6.16 Numerical results illustrating the dependence between n, m and $\text{rank}(\rho)$ for an m-RDM to have a unique symmetric extension ρ of $\text{rank}(\rho)$ and $n = 15$, $n = 30$ qubits respectively. For each case $n, m, \text{rank}(\rho)$ we have carried out 100 trials, forcing the SDP to explore the feasible set in a new random distinct direction A at each trial. The black squares correspond to cases for which the recovered global symmetric state $\tilde{\rho}$ has fidelity $F(\rho, \tilde{\rho}) > 0.9999$ with the original global state in 100% of the trials. Thus, the black squares provide evidence of cases $n, m, \text{rank}(\rho)$ with unique symmetric extension. The numerical tolerance has been arbitrarily set to take into account the imprecision of the SDP solver. The non-black squares correspond to cases in which, from the 100 trials, some of the runs have exhibited a fidelity $F(\rho, \tilde{\rho}) < 0.9999$. When this happens, we show the minimal fidelity obtained out of all the 100 trials, as a way to illustrate the tolerance. One clearly observes a certain correlation between the size of the RDM m and $\text{rank}(\rho)$. In general, the cases for low $\text{rank}(\rho)$ and high m (few particles traced out) show more predilection to have a unique extension.

Chapter 7

Non-local correlations in three-level quantum many-body systems

In Chapters 4 and 5 we got a glimpse at the potential of non-local correlations to characterize many-body systems, even in the thermodynamic limit. The key feature has been to consider few-body symmetric Bell inequalities, which have allowed us to tackle otherwise unapproachable problems. Moreover, an advantage of few-body symmetric Bell inequalities is the possibility to be effectively measured in terms of collective spin observables, allowing its experimental implementation on large-system sizes [Schmied *et al.*, 2016; Engelsen *et al.*, 2017].

One step further is to consider two-body symmetric Bell inequalities for three outcomes. For instance, these would allow to explore the role of non-local correlations in exotic quantum phenomena that appears in spin-1 systems (*e.g.,* [Haldane, 1983; Verstraete *et al.*, 2004]). Furthermore, such inequalities would suppose a good candidate to experimentally probe nonlocality on, for instance, spin-1 BECs made of ^{87}Rb [Barrett *et al.*, 2001; Schmaljohann *et al.*, 2004], which already allows to generate large scale entanglement with symmetric states [Zhang and Duan, 2013; Zou *et al.*, 2018], presents interesting spin-squeezing

features [Hamley, 2012], and also allows for spin collective measurements [Kunkel *et al.*, 2019]. However, 3-outcome 2-body symmetric Bell inequalities remain unexplored, partly due to the increase complexity of having a larger affine space due to the increased number of outcomes, which poses extra challenges both in the derivation of Bell inequalities and in their characterization.

In this chapter we are interested in the derivation and characterization of permutationally invariant Bell inequalities for three outcomes and that involve at most two-body correlators. In Section 7.1 we start with preliminaries by introducing the multipartite Bell scenario for three outcomes and setting the notation. In Section 7.2 we present two distinct methodologies to derive 3-outcome 2-body symmetric Bell inequalities.In Section 7.3 we provide an optimization tool set to characterize the nonlocality detection of few-body symmetric Bell inequalities for any d outcomes. In Section 7.4 we characterize a class of 3-outcome 2-body symmetric Bell inequality which is valid for any system size and show that the inequality detects non-local correlations in the ground state of the three-orbital LMG [Meredith *et al.*, 1988; Gnutzmann *et al.*, 2000; Graß *et al.*, 2013].

The original results presented in this chapter are based on preliminary unpublished results, which are part of a joint collaboration with M. Fadel, M. Lewenstein, and J. Tura.

7.1 Preliminaries: the $(n, 2, 3)$ Bell scenario

The Bell inequalities presented in this chapter take part in an $(n, 2, 3)$ Bell scenario. Recall from Section 2.3.1 that an $(n, 2, 3)$ Bell scenario refers to: an n-partite resource (*e.g.* a quantum state) spatially distributed among n observers indexed by $[n] := \{1, 2, \ldots, n\}$; Each party i chooses to perform a measurement denoted $\mathcal{M}_k^{(i)}$, where $k \in \{0, 1\}$ labels the measurement choice; and this time each measurement yields 3 different outcomes, labelled $a_i \in \{0, 1, 2\}$.

The experiment takes place in several rounds. During each round, a

new n-partite resource is distributed among the observers, who choose their measurement uncorrelated from the state [Brunner *et al.*, 2014; Collaboration, 2018] and collect the resulting outcomes. Afterwards, they communicate their results and they can estimate the conditional probabilities $p(\boldsymbol{a}|\boldsymbol{x})$, where $\boldsymbol{x} := (x_1, x_2, \ldots, x_n)$ labels the choice of measurements and $\boldsymbol{a} := (a_1, a_2, \ldots, a_n)$ labels the obtained outcomes. Note that the experiment has a total of $(2 \cdot 3)^n$ possible conditional probabilities configurations describing the correlations, from which only $2^n(3^n - 1)$ remain linearly independent when considering that probabilities are normalized. All the possible configurations $\{p(\boldsymbol{a}|\boldsymbol{x}), \forall \boldsymbol{a}, \boldsymbol{x}\}$ define a region that accounts for all possible statistical correlations.

7.2 Symmetric, few-body, Bell inequalities for three outcomes

As we have seen through the present thesis, the combinatorial complexity underlying the characterization of multipartite Bell correlations renders them unapproachable in the general case. To partially circumvent it, we have seen that one can trade-off some nonlocality detection ability in exchange for the following desirable properties [Tura *et al.*, 2014a]:

1. To probe the system by looking only at one- and two-body correlations.

2. To relax the LHVM set to be that confined only by permutationally invariant Bell inequalities.

Our objective now is to detect nonlocality in three-level many-body systems, therefore we consider a more complex scenario by having 3 outcomes. Nevertheless, by the use of symmetries and restricting to one- and two- body correlations we are able to present novel three-outcome Bell inequalities useful to characterize many-body systems and set the ground to generalize for any qudit dimension $d \geq 2$. We

call these novel inequalities the 3-outcome 2-body Permutationally Invariant Bell Inequalities (3-outcome 2-body PIBIs for short).

In this section we present 2 independent methodologies to derive 3-outcome 2-body PIBIs: First, by means of a local deterministic model which allows to construct the local polytope; Second, by checking the membership of a given statistical point in a projected spectrahedron containing the local polytope through an SDP.

7.2.1 Local Deterministic Strategy: derivation of the Local Polytope

The most typical way to derive Bell inequalities is by obtaining the facets of the local polytope (recall Section 2.3.1). In order to obtain the local polytope, one first needs to accommodate the LHVM in the conditional probabilities, commonly done through a so-called *Local Deterministic Strategy* (LDS), *i.e.*, a set of response functions $\{p_i(a_i|x_i,\lambda)\}_{i\in[n]}$ each of which is deterministic. LDS play a key role in defining the classical bound of a Bell inequality, as Fine's theorem proves that LDS maximize Bell inequalities under LHVMs [Fine, 1982]. Notice that in an (n,m,d) Bell scenario there are d^{mn} different LDS, and the exponential growth with the number of parties n makes our considered scenario $(n,2,3)$ intractable in the general case.

In this section we devise an LDS for the $(n,2,3)$ Bell scenario under the symmetry and few-body simplifications previously stated. Such simplifications play a crucial role in order to decrease the computational cost. In particular, it reduces the number of LDS from d^{mn} to $\binom{n+d-1}{d-1}$, which allows us to obtain the projected symmetric local polytopes.

The first simplification we consider is to restrict to one- and two-body correlations. Then, the Bell experiment is solely described by conditional probabilities of the form $p(a_i|x_i)$ and $p(a_ia_j|x_ix_j)$, involving parties $i\neq j\in[n]$.

The second simplification is to consider the permutationally invariant symmetry. Under the permutation invariance restriction, many

Bell inequality coefficients take the same values at many LDS. Hence, instead of considering all the d^{mn} possibilities to develop an LDS in the general case, a much more efficient parametrization is the following. Let $c_{a,b}$ be the total number of parties that have obtained the pair of outcomes $a, b \in [d]$ for the measurements $\mathcal{M}_0$ and $\mathcal{M}_1$ respectively. Then, it follows by definition that $c_{a,b} \geq 0$ and $\sum_{a,b} c_{a,b} = n$. Hence, the value of the symmetric one-body conditional probabilities at a given LDS are:

$$\mathcal{P}_{a,k} := \begin{cases} c_{a,0} + c_{a,1} + c_{a,2} & \text{if } k = 0 \\ c_{0,a} + c_{1,a} + c_{2,a} & \text{if } k = 1 \end{cases}, \tag{7.1}$$

$$\mathcal{P}_{a|x} := \sum_{i=0}^{n-1} p_i(a|x) = \mathcal{P}_{a,k}. \tag{7.2}$$

As for the symmetric two-body conditional probabilities, under a given LDS they factorize as:

$$\begin{aligned} \mathcal{P}_{ab|xy} &:= \sum_{i \neq j} p_{ij}(ab|xy) \overset{\text{LDS}}{=} \sum_{i \neq j} p_i(a|x) p_j(b|y) \\ &= \underbrace{\sum_{i \neq j} p_i(a|x) p_j(b|y) + \sum_i p_i(a|x) p_i(b|y)}_{\mathcal{P}_{a|x} \cdot \mathcal{P}_{b|y}} - \underbrace{\sum_i p_i(a|x) p_i(b|y)}_{:= \mathcal{Q}_{ab|xy}}, \end{aligned} \tag{7.3}$$

where

$$\mathcal{Q}_{ab,xy} := \begin{cases} \mathcal{P}_{a|x} & \text{if } a = b, x = l \\ 0 & \text{if } a \neq b, x = y \\ c_{a,b} & \text{if } x = 0, y = 1 \\ c_{b,a} & \text{if } x = 1, y = 0 \end{cases}. \tag{7.4}$$

Let us note that the NS principle (cf. Eq. (2.14)) allows to neglect the outcomes $a_i = 2$, therefore considering Eqs. (7.3) and (7.4) only for $a, b \in \{0, 1\}$ without loss of generality.

Table 7.1 Factorization of the one- and two-body conditional probabilities under a given LDS.

$\mathcal{P}_{0\|0} = c_{0,0} + c_{0,1} + c_{0,2}$	$\mathcal{P}_{00\|00} = \mathcal{P}^2_{0\|0} - \mathcal{P}_{0\|0}$	$\mathcal{P}_{00\|01} = \mathcal{P}_{0\|0}\mathcal{P}_{0\|1} - c_{0,0}$
$\mathcal{P}_{1\|0} = c_{1,0} + c_{1,1} + c_{1,2}$	$\mathcal{P}_{01\|00} = \mathcal{P}_{0\|0}\mathcal{P}_{1\|0}$	$\mathcal{P}_{01\|01} = \mathcal{P}_{0\|0}\mathcal{P}_{1\|1} - c_{0,1}$
$\mathcal{P}_{0\|1} = c_{0,0} + c_{1,0} + c_{2,0}$	$\mathcal{P}_{10\|00} = \mathcal{P}_{01\|00}$	$\mathcal{P}_{10\|01} = \mathcal{P}_{1\|0}\mathcal{P}_{0\|1} - c_{1,0}$
$\mathcal{P}_{1\|1} = c_{0,1} + c_{1,1} + c_{2,1}$	$\mathcal{P}_{11\|00} = \mathcal{P}^2_{1\|0} - \mathcal{P}_{1\|0}$	$\mathcal{P}_{11\|01} = \mathcal{P}_{1\|0}\mathcal{P}_{1\|1} - c_{1,1}$

$\mathcal{P}_{00\|10} = \mathcal{P}_{00\|01}$	$\mathcal{P}_{00\|11} = \mathcal{P}^2_{0\|1} - \mathcal{P}_{0\|1}$
$\mathcal{P}_{01\|10} = \mathcal{P}_{10\|01}$	$\mathcal{P}_{01\|11} = \mathcal{P}_{0\|1}\mathcal{P}_{1\|1}$
$\mathcal{P}_{10\|10} = \mathcal{P}_{01\|01}$	$\mathcal{P}_{10\|11} = \mathcal{P}_{01\|11}$
$\mathcal{P}_{11\|10} = \mathcal{P}_{11\|01}$	$\mathcal{P}_{11\|11} = \mathcal{P}^2_{1\|1} - \mathcal{P}_{1\|1}$

Finally, in Table 7.1 we describe the one-body and the LDS factorization of the two-body conditional probabilities in terms of the quantities $c_{a,b}$.

Therefore, all the correlations that are classical in a Bell test (local-realist correlations) are those that can be simulated following the relations in Table 7.1 and shared randomness. The convex hull of all possible configurations satisfying the relations in Table 7.1 constructs the local polytope for the multipartite Bell experiment that we consider.

7.2.2 Derivation of Bell inequalities via Convex Hull

By means of the LDS presented in Section 7.2.1, we are ready to construct the local polytope and obtain all Bell inequalities from its facets. To construct the local polytope one lists all the LDS as a cloud of points in the polytope coordinates and determines their convex hull. This approach returns a minimal set of tight inequalities, such that any other Bell inequality will be a convex combination of the ones returned by the convex hull algorithm. In our case, we proceed to construct the projected symmetric local polytope.

By construction, the Bell inequalities we find take the following

form:

$$I := \sum_{\substack{a\in[d-1]\\ x\in[m]}} \alpha_{a,x}\mathcal{P}_{a|x} + \sum_{\substack{a,b\in[d-1]\\ x,y\in[m]}} \alpha_{ab,xy}\mathcal{P}_{ab|xy} - \beta_c \geq 0, \tag{7.5}$$

where the $\alpha_{\boldsymbol{a},\boldsymbol{x}} \in \mathbb{R}$ are the corresponding Bell inequality coefficients and $\beta_c \in \mathbb{R}$ denotes the classical bound (cf. Section 2.3.1).

As previously mentioned, the facets of the local polytope correspond to tight Bell inequalities. A computer assisted algorithm [Fukuda, 1997] allows us to obtain the convex hull from all the possible configurations of the LDS given in Table 7.1. The resulting affine space of the 2-body symmetric local polytope for the $(n, 2, 3)$ scenario, and therefore of the inequalities in Eq. (7.5), has 14 dimensions (or, equivalently, a 15-dimensional vector space). These dimensions correspond to:

$$\begin{cases} 1, \mathcal{P}_{0|0}, \mathcal{P}_{0|1}, \mathcal{P}_{1|0}, \mathcal{P}_{1|1}, \\ \mathcal{P}_{00|00}, \mathcal{P}_{10|00}, \mathcal{P}_{11|00}, \\ \mathcal{P}_{01|01}, \mathcal{P}_{10|01}, \\ \mathcal{P}_{00|10}, \mathcal{P}_{11|10}, \\ \mathcal{P}_{00|11}, \mathcal{P}_{10|11}, \mathcal{P}_{11|11}. \end{cases} \tag{7.6}$$

Let us note that in Eq. (7.6) terms such as $\mathcal{P}_{00|01}$ or $\mathcal{P}_{01|11}$ have been omitted, since they are already taken into account due to the permutation invariance as shown in Table 7.1. In general, we will take as a canonical notation for $\mathcal{P}_{ab|xy}$ $x \leq y$ and, when $x = y$, we will choose $a \leq b$.

Solving the convex hull for $n = \{2, 3\}$ we have been able to obtain 165 and 146994 inequalities respectively. Solving the convex hull already becomes computationally too expensive for $n > 3$. Nevertheless, by means of the optimization toolset presented in Section 7.3, we have observed that plenty of these inequalities can detect non-local correlations. However, working with such a high number of inequalities makes it hard to identify families of Bell inequalities that detect nonlocality and are valid for arbitrary n.

This motivates the further symmetrization of the local polytope in order to decrease the dimensions of the affine space of the Bell

inequalities. In particular, we have further symmetrized the inputs and the outputs in order to reduce the affine space dimensions of the Bell inequalities to the following 6-dimensional vector space:

$$\begin{cases} 1, \\ \mathcal{P}_{0|0} + \mathcal{P}_{0|1} + \mathcal{P}_{1|0} + \mathcal{P}_{1|1}, \\ \mathcal{P}_{00|00} + \mathcal{P}_{00|11} + \mathcal{P}_{11|00} + \mathcal{P}_{11|11}, \\ \mathcal{P}_{00|01} + \mathcal{P}_{11|01}, \\ \mathcal{P}_{01|00} + \mathcal{P}_{01|11}, \\ \mathcal{P}_{01|01} + \mathcal{P}_{01|10}. \end{cases} \tag{7.7}$$

Let us remark that, while from the affine vector space in Eq. (7.7) one obtains two-body PIBIs of 5-dimensions, these have been derived from the $(n, 2, 3)$ Bell scenario which makes them structurally and qualitatively different from the 5-dimensional two-body PIBIs presented in [Tura *et al.*, 2014a, 2015]. Under the 6-dimensional affine vector space in Eq. (7.7), we have been able to solve the convex hull from $n = 2$ up until $n = 17$, which has resulted in 8 and 1415 inequalities respectively. Solving a variety of convex hulls for different number of n has allowed us to identify some families of Bell inequalities that keep reappearing independently of n. In what follows we proceed to characterize one of these families of Bell inequalities and in Appendix D.1 we present other candidates that might be interesting to characterize in future works.

A class of 3-outcome 2-body PIBI for many-body systems

Among others, a particular apparently simple inequality that has proven to be useful is the following:

$$\tilde{\mathcal{P}}_0 + \tilde{\mathcal{P}}_{00} - 2\tilde{\mathcal{P}}_{01} \geq 0, \tag{7.8}$$

where $\tilde{\mathcal{P}}_0 := \mathcal{P}_{0|0} + \mathcal{P}_{0|1} + \mathcal{P}_{1|0} + \mathcal{P}_{1|1}$ corresponds to the symmetrized one-body term and $\tilde{\mathcal{P}}_{00} := \mathcal{P}_{00|00} + \mathcal{P}_{00|11} + \mathcal{P}_{11|00} + \mathcal{P}_{11|11}, \tilde{\mathcal{P}}_{01} := \mathcal{P}_{01|01} + \mathcal{P}_{01|10}$ correspond to the symmetrized two-body terms. Notice that for this inequality the classical bound is $\beta_c = 0$. In Appendix D.2 we prove that the classical bound holds for any number

of parties n considered. In Section 7.4 we shall see that the Bell inequality in Eq. (7.8) detects non-local correlations and, furthermore, in Section 7.4.2 we shall show that its non-local detection is useful for physically relevant spin-1 many-body systems.

7.2.3 Theta-Bodies methodology: Checking all Bell inequalities at once

In the previous section we have obtained a family of Bell inequalities by solving the convex hull to obtain the facets of the local polytope. This is a typical approach used to find full lists of Bell inequalities [Śliwa, 2003; Pironio, 2014; Bancal *et al.*, 2010]. However, in such approach the inherent algebraic properties of the symmetric correlators are not used: Convex hull algorithms treat their input as a cloud of points without any particular structure. Furthermore, convex hull algorithms suffer from complexity efficiency issues, specially in higher dimensions [Chazelle, 1993], which makes the polytope approach unapproachable beyond the most basic scenarios.

An alternative approach to derive Bell inequalities has been recently presented in [Fadel and Tura, 2017], which is referred to as the *Theta-Bodies* methodology. The idea behind this alternative methodology is to relax the LDS in order to exploit its algebraic properties, properties that allow to efficiently explore all the Bell inequalities at once through a feasibility problem. In particular, the Theta-Bodies methodology is based on an SDP to efficiently certify whether a given statistical point based on correlations observed on a Bell experiment is a member of the local polytope. If the SDP is infeasible, it shows that the statistical point is outside the local polytope and, thus, exhibits non-local correlations. Furthermore, when infeasible, the dual SDP problem provides a Bell inequality which is violated by the given statistical point.

In this chapter, we present an adaptation of the Theta-Bodies methodology to account for qutrits in the $(n, 2, 3)$ Bell scenario. Furthermore, the adaptation is such that sets the ground to generalize the

method for any dimension d of qudits.

In order to exploit the algebraic properties of the LDS, 2 relaxations are considered [Fadel and Tura, 2017]:

1. Consider $\mathbb{R}_{\geq 0}$ instead of $\mathbb{Z}_{\geq 0}$ (finite set of points that form the LDS).

2. Because the membership of the correlation statistical point in the convex hull can be equivalently posed as whether the resulting multivariate polynomial is non-negative, ask instead whether the multivariate polynomial can be expressed as a sum of squares (efficiently solvable with SDP).

Then, the resulting relaxation that will check the membership in the convex hull, can be written as the following SDP:

$$\begin{array}{lrcl} \min & \lambda & & \\ \text{s.t.} & \hat{\Gamma}(\boldsymbol{y}) & \succeq & 0 \\ & y_0 & = & 1 \\ & y_j & = & \lambda p_j, \end{array} \tag{7.9}$$

where $\boldsymbol{p}$ denotes the given statistical point with components p_j, $\tilde{\Gamma}$ denotes the moment matrix and the y_j components associated to the p_j components are fixed while the remaining components of $\boldsymbol{y}$ are left as free variables that can be varied to make $\tilde{\Gamma}$ positive semidefinite. In order to obtain $\tilde{\Gamma}$, one expresses the constraints $c_{a,b} \geq 0$ from the LDS seen in Section 7.2.1 in terms of the one-body conditional probabilities $\mathcal{P}_{a|x}$ as follows:

$$
\begin{cases}
c_{0,0} &= \mathcal{P}_{0|0}\mathcal{P}_{0|1} - \mathcal{P}_{00|01} \geq 0 \\
c_{0,1} &= \mathcal{P}_{0|0}\mathcal{P}_{1|1} - \mathcal{P}_{01|01} \geq 0 \\
c_{0,2} &= \mathcal{P}_{0|0} - c_{0,0} - c_{0,1} \\
&= \mathcal{P}_{0|0} - \mathcal{P}_{0|0}\mathcal{P}_{0|1} + \mathcal{P}_{00|01} - \mathcal{P}_{0|0}\mathcal{P}_{1|1} + \mathcal{P}_{01|01} \geq 0 \\
c_{1,0} &= \mathcal{P}_{1|0}\mathcal{P}_{0|1} - \mathcal{P}_{10|01} \geq 0 \\
c_{1,1} &= \mathcal{P}_{1|0}\mathcal{P}_{1|1} - \mathcal{P}_{11|01} \geq 0 \\
c_{1,2} &= \mathcal{P}_{1,0} - c_{1,0} - c_{1,1} \\
&= \mathcal{P}_{1|0} - \mathcal{P}_{1|0}\mathcal{P}_{0|1} + \mathcal{P}_{10|01} - \mathcal{P}_{1|0}\mathcal{P}_{1|1} + \mathcal{P}_{11|01} \geq 0 \\
c_{2,0} &= \mathcal{P}_{0|1} - c_{0,0} - c_{1,0} \\
&= \mathcal{P}_{0|1} - \mathcal{P}_{0|0}\mathcal{P}_{0|1} + \mathcal{P}_{00|01} - \mathcal{P}_{1|0}\mathcal{P}_{0|1} + \mathcal{P}_{10|01} \geq 0 \\
c_{2,1} &= \mathcal{P}_{1|1} - c_{0,1} - c_{1,1} \\
&= \mathcal{P}_{1|1} - \mathcal{P}_{0|0}\mathcal{P}_{1|1} + \mathcal{P}_{01|01} - \mathcal{P}_{1|0}\mathcal{P}_{1|1} + \mathcal{P}_{11|01} \geq 0 \\
c_{2,2} &= n - \sum_{\forall (a,b)\in\{0,1\}} c_{a,b} \\
&= n - \mathcal{P}_{0|0} - \mathcal{P}_{1|0} - \mathcal{P}_{0|1} - \mathcal{P}_{1|1} + \\
&\quad + \mathcal{P}_{0|0}(\mathcal{P}_{0|1} + \mathcal{P}_{1|1}) - \mathcal{P}_{00|01} - \mathcal{P}_{01|01} + \\
&\quad + \mathcal{P}_{1|0}(\mathcal{P}_{0|1} + \mathcal{P}_{1|1}) - \mathcal{P}_{10|01} - \mathcal{P}_{11|01} \geq 0
\end{cases}
. \quad (7.10)
$$

Slicing Polytopes: Theta-Bodies Accuracy

In this section we explore the accuracy of the Theta-Bodies methodology to approximate 3-outcome 2-body permutationally invariant local polytopes. To do so, we slice the polytope in planes and proceed to characterize the cross section. In particular, on one hand we use the list of LDS points to find the actual boundary of the local polytope via linear programming. On the other hand, in the same plane cross section, we use the Theta-Bodies methodology as presented in Section 7.2.3 to find its approximation.

The procedure to recover the actual values of the local polytope is outlined in what follows:

1. Select two random directions v_1, v_2, in the 14-dimensional affine space corresponding to the $\mathcal{P}$'s in Eq. (7.6), that will define the plane in which the local polytope will be sliced.

2. Center around the maximally mixed point v_{mix} by taking $p(a_i|x_i) = n/3$ and $p(a_i a_j|x_i x_j) = n(n-1)/9$ for all $i \in [n]$.

3. Parametrize $\boldsymbol{p} = \cos(t)v_1 + \sin(t)v_2$.

4. Look for feasibility with the following Linear Programming (LP) problem in order to find the polytope boundary

$$\begin{array}{lrcl} \min & \mathbf{0}^T \boldsymbol{x} & & \\ \text{s.t.} & \left[A,\, (0,\boldsymbol{p})^T\right] \boldsymbol{x} & = & v_{\text{mix}} \\ & \boldsymbol{x} & \geq & 0 \\ & \boldsymbol{x} & \leq & 1, \end{array} \tag{7.11}$$

where $\boldsymbol{x}$ is the LP variable, $\mathbf{0}$ is the zero column vector and $\left[A,\, (0,\boldsymbol{p})^T\right]$ represents a matrix where A is formed by column vectors in the affine space Eq. (7.6) constructed from all the combinations in Table 7.1.

The procedure to obtain the Theta-Bodies approximation follows the same steps, for the same plane spanned by the directions v_1, v_2, but this time we solve step 4) with the following SDP:

$$\begin{array}{lrcl} \min & \lambda & & \\ \text{s.t.} & \hat{\Gamma}(\boldsymbol{y}) & \succeq & 0 \\ & y_0 & = & 1 \\ & y_j & = & \lambda p_j + (v_{\text{mix}})_j \quad \forall j \in \{0, \ldots, \dim(v_{\text{mix}})\}, \end{array} \tag{7.12}$$

where the y_j components associated to p_j and v_{mix} are fixed while the remaining components of $\boldsymbol{y}$ are left as free variables that can be varied to make the moment matrix $\tilde{\Gamma}$ positive semidefinite.

In Figures 7.1 and 7.2 we present 2 different plane slices randomly chosen and the corresponding cross sections. It can be appreciated that the Theta-Bodies methodology quickly tightens the approximation as the number of parties n is increased.

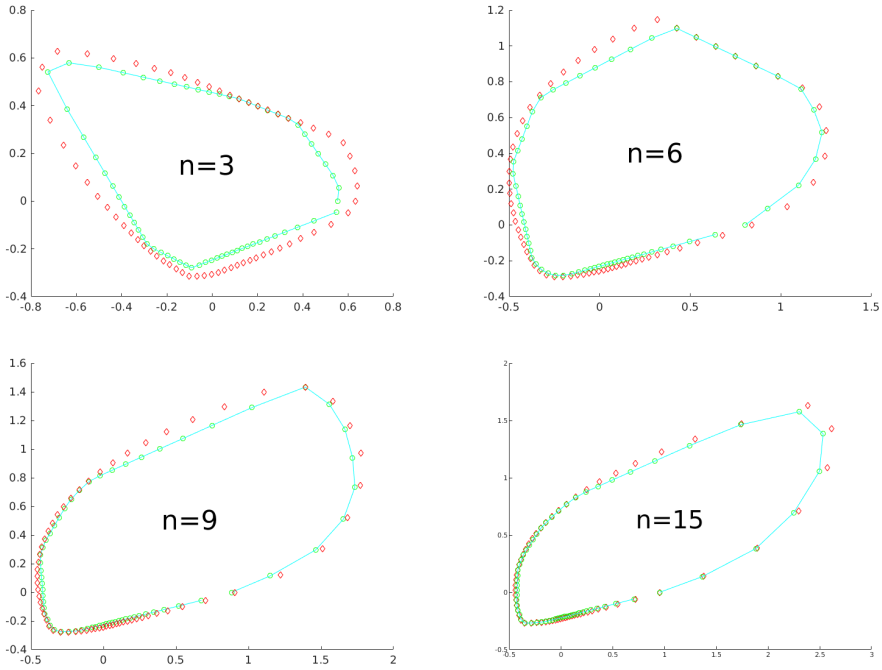

Fig. 7.1 Cross sections, for a plane spanned by some random directions v_1, v_2, of the 3-outcome 2-body symmetric local polytope for different system sizes n. The green circles, connected by a tentative line, represent the actual boundary of the local polytope obtained as outlined in Section 7.2.3. The red diamonds correspond to the approximation given by the Theta-Bodies methodology approximation. One observes how the Theta-Bodies approximation quickly tightens as the system size increases.

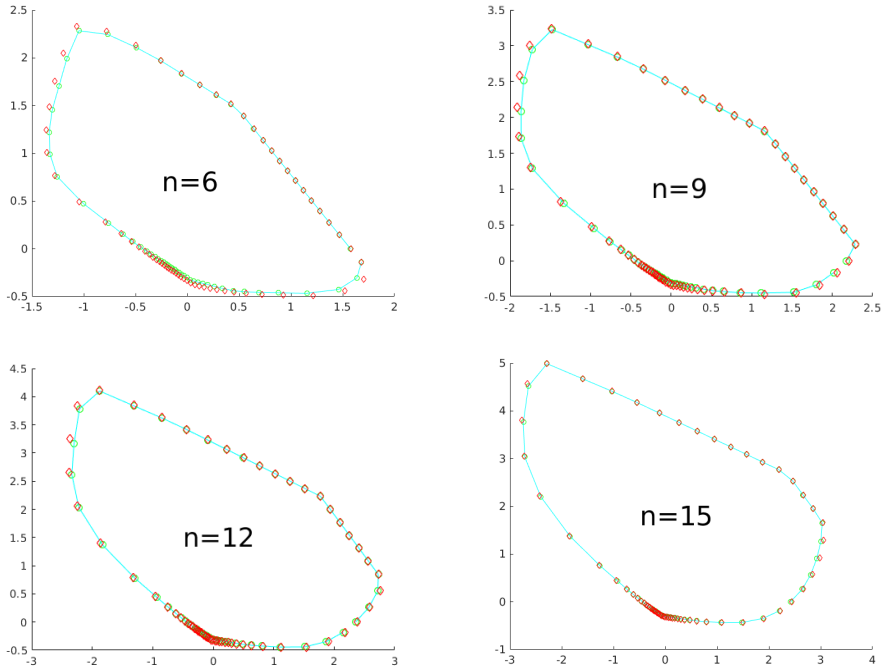

Fig. 7.2 Same as Figure 7.1, but for different random directions v_1, v_2. Cross sections of the 3-outcome 2-body symmetric local polytope for different system sizes n. The green circles, connected by a tentative line, represent the actual boundary of the local polytope obtained as outlined in Section 7.2.3. The red diamonds correspond to the approximation given by the Theta-Bodies methodology approximation. One observes how the Theta-Bodies approximation quickly tightens as the system size increases.

7.3 Optimization toolset for few-body symmetric Bell inequalities with d outcomes

As discussed in Chapter 4, to know whether a given Bell inequality is able to detect nonlocality is, in general, a highly complex task. Let $\mathcal{B}(\boldsymbol{\theta})$ denote the associated Bell operator of a given Bell inequality, where $\boldsymbol{\theta}$ labels the measurement choices. Then, its contraction with a quantum state determines whether the Bell inequality has been violated or not. Therefore, to know whether a Bell inequality can detect non-local correlations amounts to find a quantum state together with particular set of measurements such that their quantum correlations violate a Bell inequality. That is,

$$\mathrm{Tr}\left[\mathcal{B}(\boldsymbol{\theta})\rho\right] \ngeq \beta_{\mathrm{c}}. \tag{7.13}$$

However, how does one find such set of measurements and quantum state that violate a Bell inequality? Similarly as in the optimization problem to find the k-producible bounds in Chapter 4, one typically faces the following optimization problem:

$$\min_{\boldsymbol{\theta},\rho} \mathrm{Tr}[\mathcal{B}(\boldsymbol{\theta})\rho], \tag{7.14}$$

where ρ is an n-partite density matrix of d-dimensional systems. The optimization presents many challenges. In general, it is highly nonlinear and, depending on the physical dimension of the Hilbert space considered, it can be also very inefficient to even represent. Not surprisingly, the optimization in Eq. (7.14) rarely admits an analytically closed form. We have seen in Section 4.4.1 that, by means of the see-saw method [Pál and Vértesi, 2010; Werner and Wolf, 2001], instead of considering the simultaneous multilateral optimization of $\boldsymbol{\theta}$ and ρ one can split it into simpler unilateral optimizations; *i.e.,* to fix $\boldsymbol{\theta}$ and optimize ρ for that choice of $\boldsymbol{\theta}$, and vice-versa, until convergence on a local minimum is achieved within numerical accuracy. Therefore, the optimization problem in Eq. (7.14) can be split into two steps: two optimize over quantum states and to optimize over set of measurements.

For the optimization over the set of measurements, in Section 7.3.1 we develop a methodology to obtain a continuous parametrization of qudit observables, given a set of unitaries $\{U_0, \ldots, U_m\}$ whose spectrum is $\{1, \omega, \ldots, \omega^{d-1}\}$.

As for the optimization over quantum states, in Section 7.3.2 we take advantage of the methodology developed in Chapter 6 to efficiently optimize the few-body symmetric Bell inequalities by means of an SDP of polynomial size.

7.3.1 Optimization over quantum observables: Unitary parametrization

In this section we propose a continuous parametrization of projective, unitary qudit operators such that one can use it to employ typical optimization methods (*e.g.,* conjugate gradient descend). The final purpose is to carry out the optimization problem in Eq. (7.14) over a set of quantum measurements.

In the present thesis, so far we have considered qubit cases in Chapters 4 to 6, where we have been parametrizing the measurements as a combination of Pauli matrices, *e.g.*, $\mathcal{M} = \boldsymbol{n} \cdot \boldsymbol{\sigma} = n_x\sigma_x + n_y\sigma_y + n_z\sigma_z$, which remains unitary for any $\boldsymbol{n}$ unit vector. Furthermore, spherical coordinates can parametrize a Bell experiment, overall allowing the use of unconstrained continuous optimization methods as well as non-convex optimization methods (*e.g.,* gradient descend). However, for qutrits such property gets lost. Consider for instance X, Z as the generalization of σ_x, σ_z, in the sense that X acts by shifting $|0\rangle \to |1\rangle \to |2\rangle$ and Z applies a third root of unity phase shift $|i\rangle \to \omega^i |2\rangle$, where $\omega = \exp(2\pi i/3)$. Then, notice that a unit vector $\boldsymbol{u} = (u_x, u_z)$ does not preserve the unitarity of $u_x X + u_z Z$.

Instead of considering Hermitian operators, we consider unitary setting operators. The convenient representation for unitary operators are the generalized Pauli matrices which form the Weyl-Heisenberg

group. In the case of qutrits, the generators of the group are

$$X = \begin{pmatrix} 0 & 0 & 1 \\ 1 & 0 & 0 \\ 0 & 1 & 0 \end{pmatrix} \qquad Z = \begin{pmatrix} 1 & 0 & 0 \\ 0 & \omega & 0 \\ 0 & 0 & \omega^2 \end{pmatrix}, \tag{7.15}$$

where $\omega = e^{\frac{2\pi i}{3}}$ are the roots of unity. An orthonormal basis is given by the nine elements $X^k Z^j = \sum_{m=0}^{2} |m+k\rangle\, \omega^{jm}\, \langle m|$ which are proportional to the elements of the Weyl-Heisenberg group.

In what follows we propose a method to obtain a continuous parametrization of qutrit observables, given a set of unitaries $\{U_0, \ldots, U_m\}$ whose spectrum is $\{1, \omega, \ldots, \omega^{d-1}\}$. Let us note that each unitary has the same spectrum ordered by complex phase argument $\sigma(U_i) = \{1, \omega, \ldots, \omega^{d-1}\}$.

Let g_k be an Hermitian matrix such that $V_k = \exp(ig_k)$, where V_k is a matrix whose columns are the orthonormal states of U_k.

Theorem 7.3.1. *Let $\{U_i\}_{i=0}^{M}$ be a set of $d \times d$ unitaries, each having the same spectrum, ordered by complex phase argument, which we denote $\sigma(U_i)$. Let V_k be a matrix whose columns are the orthonormal eigenstates of U_k, given in the same order as $\sigma(U_i)$. Consider $\boldsymbol{\theta} \in \mathbb{R}^M$ and define*

$$g(\boldsymbol{\theta}) := g_0 + \sum_{i=1}^{M} \theta_i (g_i - g_0), \tag{7.16}$$

where g_k is a Hermitian matrix such that $V_k = \exp(\mathrm{i}g_k)$. Then the following is a unitary matrix with the same spectrum as U_k for all $\boldsymbol{\theta} \in \mathbb{R}^M$:

$$U(\boldsymbol{\theta}) := e^{\mathrm{i}g(\boldsymbol{\theta})} \mathrm{Diag}(\sigma(U_0)) e^{-\mathrm{i}g(\boldsymbol{\theta})}. \tag{7.17}$$

Note that, in particular, $U(\mathbf{0}) = U_0$ and $U(\boldsymbol{\theta_i}) = U_i$ where $\boldsymbol{\theta_i}$ is the i-th vertex of the unit simplex; i.e., $\boldsymbol{\theta_i} := (0, \overset{(i-3)}{\ldots}), 0, 1, 0, \ldots, 0)$.

Corollary 7.3.1. *If $\sigma(U_i) = \{1, \omega, \ldots, \omega^{d-1}\}$, then $U(\boldsymbol{\theta})$ corresponds to a projective quantum measurement with outcomes ω^k.*

The proof can be found in Appendix D.3, as well as further theorems, details and examples.

For our exploration of non-local correlations we have selected, for instance, the following set of unitaries $\{X, Z, X^2, XZ, ZX, XZ^2, X^2Z, Z^2X, X^2Z^2\}$. Then, since in the scenario we consider each observer can choose among two measurements, we choose two distinct parameters $\boldsymbol{\theta}_0, \boldsymbol{\theta}_1$ that form two unitaries $U_0 = U(\boldsymbol{\theta}_0), U_1 = U(\boldsymbol{\theta}_1)$. From them we can construct the projective measurements that are used to obtain the conditional probabilities as:

$$\begin{aligned} \mathbb{P}_{0,k} &= \left(U_k^3 + U_k^2 + U_k\right)/3 \\ \mathbb{P}_{1,k} &= \left(U_k^3 + \omega U_k^2 + \omega^2 U_k\right)/3 \\ \mathbb{P}_{2,k} &= \left(U_k^3 + \omega^2 U_k^2 + \omega U_k\right)/3, \end{aligned} \tag{7.18}$$

for $k \in \{0, 1\}$.

7.3.2 Optimization over quantum states: a feasibility problem

In Chapters 4 and 6 we have encountered several times that a particular case of interest for symmetric Bell inequalities is when the quantum state offering violation is a symmetric state, which can even give the maximal amount of violation for some two-body PIBIs.

Based on such observations, we consider the *Variational Method* (VM) presented in Chapter 6, which allows to efficiently optimize over symmetric states in search for nonlocality detection in few-body Bell inequalities for any d outcome. Recall that the VM consists of an efficient SDP of polynomial size that optimizes the quantum states solely from their marginals, while maintaining compatibility with a global symmetric quantum state.

Let $\boldsymbol{\alpha}$ be the Bell inequality coefficients and $\boldsymbol{p}(\sigma)$ the probability distribution given some projectors and dependent on the two-body

reduced density matrix σ. Then, the VM can be adapted as:

$$\begin{aligned} \text{minimize:} \quad & \boldsymbol{\alpha} \cdot \boldsymbol{p}(\sigma)^T \\ \text{s.t.} \quad & \sigma = \textstyle\sum_{i,j} A_{i,j} \rho_{i,j} \\ & \rho \succeq 0 \\ & \mathrm{Tr}(\rho) = 1, \end{aligned}$$

where ρ is the global symmetric quantum state of size n and $A_{i,j}$ is the matrix containing the compatibility conditions from Eqs. (6.5) and (6.6). Therefore, the SDP in Eq. (7.19) explores all the feasible regime and returns the symmetric state that minimizes the Bell inequality for the given measurement settings $\boldsymbol{\theta}$.

7.3.3 See-saw optimization for 3-outcome 2-body PIBIs

By combining Sections 7.3.1 and 7.3.2, one can tackle the optimization problem in Eq. (7.14) for 3-outcome 2-body PIBIs. In particular, we propose a see-saw optimization which alternates between optimizing over symmetric quantum states while fixing the set of measurements and vice-versa.

Since we are optimizing over symmetric states, the probability distribution $\boldsymbol{p}(\sigma, \boldsymbol{\theta})$ for two-body symmetric Bell operators are simplified to consider only the following terms:

$$\begin{aligned} \mathcal{P}_{ak} &= n\mathrm{Tr}\left[\sigma\, \mathbb{P}_{\mathrm{a,k}}(\boldsymbol{\theta}) \otimes \mathbb{1}\right], \\ \mathcal{P}_{aa'kk'} &= n(n-1)\mathrm{Tr}\left[\sigma\, \mathbb{P}_{\mathrm{a,k}}(\boldsymbol{\theta}) \otimes \mathbb{P}_{\mathrm{a',k'}}(\boldsymbol{\theta})\right], \end{aligned} \tag{7.19}$$

where $a \in \{0, 1\}$ denotes the outcome (recall that we can neglect $a = 2$ due to the NS constraints), $k \in \{0, 1\}$ denotes the measurement choice and σ denotes the two-body RDM.

Then, given a Bell inequality with coefficients $\boldsymbol{\alpha}$ we search for non-locality detection as follows:

1. Initialize with some random parameters $\boldsymbol{\theta}$ (or initial guess) to construct the projectors in Eq. (7.18) via Theorem 7.3.1.

2. Employ the SDP in Eq. (7.19) to optimize over symmetric states, then fix the quantum state to its solution.

3. Employ the stochastic conjugate gradient descend method to optimize the measurement settings. In particular, minimize $\boldsymbol{\alpha} \cdot \boldsymbol{p}(\boldsymbol{\theta})^T$ by varying $\boldsymbol{\theta}$, and thus obtaining a new set of measurements.

4. Repeat steps 2 and 3 until convergence to a local minima has been reached within numerical accuracy.

Similar as in Section 4.4.1, we recommend to add an extra layer of see-saw optimization in step 3, this time optimizing each of the parameters that form $\boldsymbol{\theta}$ individually, while fixing the remaining parameters.

7.4 A case of study: nonlocality detection with the Bell inequality in Eq. (7.8)

In this section we characterize the the class of 3-outcome 2-body PIBI in Eq. (7.8), and show that it detects nonlocality. In particular, we search for nonlocality detection via the see-saw optimization method and techniques presented in Section 7.3. The method offers an upper bound to the optimal quantum violation of the inequality, sufficient to observe nonlocality and characterize the Bell inequality.

In Figure 7.3 we show the maximal Bell inequality violation that we have observed for different system sizes n, and visualize the 15-qutrit symmetric quantum state that has achieved. The numerical exploration suggests a linear growth of the quantum violation as the system size n increases.

Once we have obtained the quantum correlations maximally violating the Bell inequality, in order to gain insight about what analytical class of states can violate the Bell inequality one can apply local unitaries on the quantum state without loss of generality. In particular, we consider the relation $\mathrm{Tr}\left[\mathcal{B}\rho\right] = \mathrm{Tr}\left[\mathcal{B}U(\boldsymbol{t})^{\otimes n}\rho(U(\boldsymbol{t})^{\otimes n})^{\dagger}\right]$ and vary $\boldsymbol{t}$

to explore equivalent quantum states, where $\boldsymbol{t}$ parametrizes the unitaries $U(\boldsymbol{t})$ as seen in Section 7.3.1. To make the exploration more efficient, one can again take advantage of the results in Chapter 6. In particular, instead of applying the unitaries on the global symmetric state we apply them on its two-body RDM σ; *i.e.*, $\mathrm{Tr}\left[\mathcal{B}\rho\right] = \mathrm{Tr}\left[\tilde{\mathcal{B}}U(\boldsymbol{t})^{\otimes 2}\sigma(U(\boldsymbol{t})^{\otimes 2})^{\dagger}\right]$, where $\tilde{\mathcal{B}}$ corresponds to the symmetric two-body Bell operator constructed by taking the measurements similarly as in Eq. (7.19). Then, we use the VM from Chapter 6 to recover its global symmetric extension. Finally, we visualize its absolute value in the symmetric space as shown in Figure 7.3.

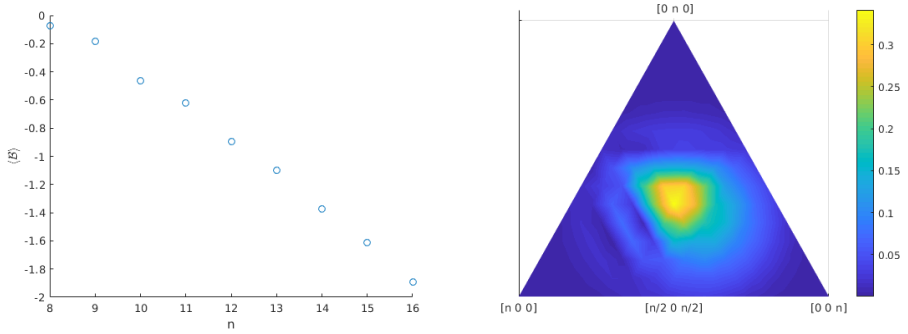

Fig. 7.3 Nonlocality detection with the three-outcome two-body PIBI in Eq. (7.8). Negative values of $\langle\mathcal{B}\rangle$ violate the Bell inequality. **Left:** Maximal violation observed with the methodology in Section 7.3.3 (upper bound) for distinct system sizes n. Numerics suggest a linear growth of the maximal quantum violation as the system size n increases. **Right:** Visualization for $n = 15$ of the qutrit symmetric state providing the maximal quantum violation observed, after adequate local unitaries applied as explained in Section 7.4. One observes that it might be possible to analytically approximate the symmetric state similarly as was done in [Tura *et al.*, 2015] for qubits, which brings us to the analytical class of states in Section 7.4.1.

Following this procedure, we have reached to the form presented in Figure 7.3.

7.4.1 Analytical class of states: Gaussian superposition of qutrit Dicke states

From Figure 7.3, one observes that a Gaussian superpositions of qutrit Dicke states, centered around having balanced number of excitations, are good candidates as an analytical class of states violate the 3-outcome 2-body PIBI in Eq. (7.8).

In particular, the Gaussian superpositions of qutrit Dicke states that we refer to take the form

$$|\psi_n\rangle = \sum_{\boldsymbol{\lambda}\vdash n} c_{\boldsymbol{\lambda}} |\boldsymbol{\lambda}\rangle , \tag{7.20}$$

where $|\boldsymbol{\lambda}\rangle$ denotes the qutrit Dicke state for $\boldsymbol{\lambda} = (\lambda_0, \lambda_1, \lambda_2)$ (recall Section 2.1), and the coefficients $c_{\boldsymbol{\lambda}}$ are defined as

$$c_{\boldsymbol{\lambda}} := \frac{e^{-\frac{1}{2}(\tilde{\boldsymbol{\lambda}}-\tilde{\boldsymbol{\mu}})\Sigma^{-1}(\tilde{\boldsymbol{\lambda}}'-\tilde{\boldsymbol{\mu}}')}}{\sqrt{(2\pi)^2 \det(\Sigma)}}, \tag{7.21}$$

where $\tilde{\boldsymbol{\lambda}}$ represents only 2 components of $\boldsymbol{\lambda}$, $\tilde{\boldsymbol{\mu}} = (n/3, n/3)$ is the 2-component mean chosen to correspond to the case where each level has the same number of excitations, and Σ is the 2×2 covariance matrix $\Sigma = \sigma \begin{pmatrix} 1 & 1/2 \\ 1/2 & 1 \end{pmatrix}^{-1}$ with σ being a parameter to be found. An example of the class of quantum states in Eq. (7.20) is visualized in Figure 7.4.

We are now interested in finding an analytical expression of the two-body RDM of Eq. (7.20). Then, one would be able to efficiently optimize the set of measurements by means of Eq. (7.19) with the corresponding 3-outcome 2-body PIBI in Eq. (7.8). Consider the density matrix as $\rho = |\psi_n\rangle\langle\psi_n'| = \sum_{\boldsymbol{\lambda},\boldsymbol{\nu}\vdash n} c_{\boldsymbol{\lambda}} c_{\boldsymbol{\nu}}^* |\boldsymbol{\lambda}\rangle\langle\boldsymbol{\nu}|$, and let $\vec{i}, \vec{j} \in [d]^m$ such that its m-body RDM takes the form $\sigma = \sum_{\vec{i},\vec{j}\in[d]^m} \sigma_{\vec{j}}^{\vec{i}} |\vec{i}\rangle\langle\vec{j}|$. As in Chapter 6, we use the vector notation $\vec{\cdot}$ specifically for the computational basis. Then, through combinatorial algebraic arguments, one

finds that the quantum state in Eq. (7.20) has a two-body RDM with the following components in the computational basis:

$$\sigma^{\vec{i}}_{\vec{j}} = \sum_{\boldsymbol{\lambda},\boldsymbol{\nu}\vdash n} c_{\boldsymbol{\lambda}} c^*_{\boldsymbol{\nu}} \sum_{\vec{k}\vdash n-2} \frac{\binom{n-2}{\vec{k}}}{\sqrt{\binom{n}{\boldsymbol{\lambda}}\binom{n}{\boldsymbol{\nu}}}} \delta(w(\vec{i}) + \vec{k} - \boldsymbol{\lambda}))\delta(w(\vec{j}) + \vec{k} - \boldsymbol{\nu})) =$$
$$= \sum_{\vec{k}\vdash n-2} c_{\vec{k}+w(\vec{i})} c^*_{\vec{k}+w(\vec{j})} \frac{\binom{n-2}{\vec{k}}}{\sqrt{\binom{n}{\vec{k}+w(\vec{i})}\binom{n}{\vec{k}+w(\vec{j})}}}, \tag{7.22}$$

where $w(\vec{i}) := (w_0(\vec{i}), w_1(\vec{i}), w_2(\vec{i}))$ is the weigh counting function defined in Eq. (6.8), $\vec{k} \vdash n-2$ labels the reduced states which have been traced out, and for the last step we have taken advantage of the Kronecker deltas δ. Furthermore, one can find analytical closed formulas for the different multinomials that appear in Eq. (7.22), which can be found in Appendix D.4.

In Figure 7.4 we show the quantum violation of the 3-outcome 2-body PIBI in Eq. (7.8), achieved with the Gaussian superposition of qutrit Dicke states in Eq. (7.20). For the measurement settings optimization we have used the two-body RDM expression in Eq. (7.22) together with Eq. (7.19). Having to optimize only a pair of measurements, and not the state, makes the process extremely efficient and allows to easily reach values $n \sim 100$ and above. We observe that for this class of states the upper bound to the quantum violation obtained also hints at a linear growth with the number of particles.

To conclude, notice that this Gaussian superposition of Dicke states, generalizes to qutrits the case observed in Section 4.5.2.

7.4.2 Nonlocality detection in quantum many-body systems

In the previous section we have seen that the 3-outcome 2-body PIBI in Eq. (7.8) is able to detect non-local correlations in multipartite states. In this section we take it one step further by showing that it can detect

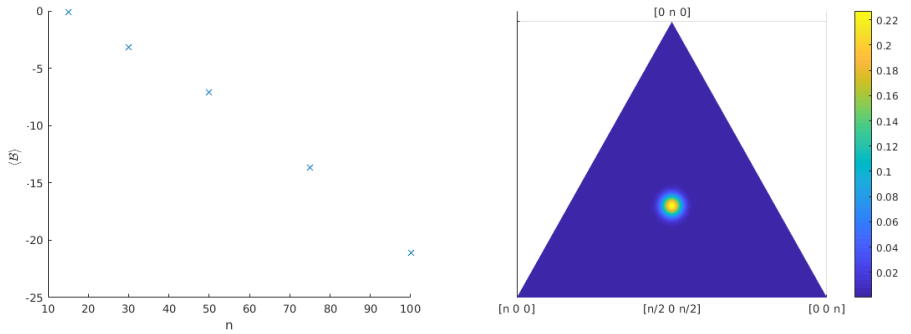

Fig. 7.4 Nonlocality detection with the three-outcome two-body PIBI in Eq. (7.8) and the analytical class of symmetric states in Eq. (7.20). **Left:** Maximal violation observed (upper bound) for distinct system sizes n, where we have used Eqs. (7.19) and (7.22) and Theorem 7.3.1 to optimize the measurements. Numerics suggest a linear growth of the maximal quantum violation as the system size n increases. **Right:** Visualization of the Gaussian superposition of qutrit Dicke states for $n = 100$ and $\sigma = 2, 5$.

non-local correlations in ground states of relevant spin-1 physical models. In particular, we consider the effective SU_3 shell model presented in [Graß *et al.*, 2013]. The Hamiltonian considered is equivalent to the three-level LMG Hamiltonian which has applications in nuclear physics and presents a not fully integrable spin model, making it appealing in the context of quantum chaos [Gnutzmann *et al.*, 2000; Meredith *et al.*, 1988].

The spin Hamiltonian involves the following spin-flip operators:

$$S_{\sigma\sigma'} = \sum_{i\in[n]} |\sigma\rangle\langle\sigma'|^{(i)}\,, \tag{7.23}$$

for $\sigma, \sigma' \in \{0, 1, 2\}$, where $|\sigma\rangle\langle\sigma'|^{(i)}$ acts on the i-th party. We consider the spin-flip to act equally on all spins with coupling constant J and that the particles can occupy three different shells with single-particle

energies $\{-B, 0, B\}$. Then the spin Hamiltonian takes the form:

$$\mathcal{H} = \frac{B}{\sqrt{2}}(\tilde{S}_{00} - \tilde{S}_{22}) + J \sum_{\sigma<\sigma'} \tilde{S}_{\sigma\sigma'}\tilde{S}_{\sigma\sigma'}, \tag{7.24}$$

where the symmetrized spin operators have been defined as $\tilde{S}_{\sigma\sigma'} := (S_{\sigma\sigma'} + S_{\sigma'\sigma})/\sqrt{2}$.

In order to obtain the ground state of the Hamiltonian Equation (7.24) we take advantage of its block-diagonal structure with respect to different representations of SU_3, in order to reduce the Hilbert space dimension of the Hamiltonian from 3^n to $(n+2)(n+1)/2$ as shown in Appendix D.5. Then, we use the compatibility conditions methodology from Chapter 6 to recover its two-body RDM.

Once we have the ground state and its two-body RDM, we build the expectation value based on Eq. (7.19) and optimizing its measurements using the parametrization from Theorem 7.3.1. In Figure 7.5 we show the detection of non-local correlations in the ground state of the model in Eq. (7.24), for a wide range of parameters B. One observes that increasing the number of particles widens the range of parameters B where the ground state exhibits non-local correlations, and that the amount of inequality violation also increases. It remains to further characterize its asymptotic limit in future works.

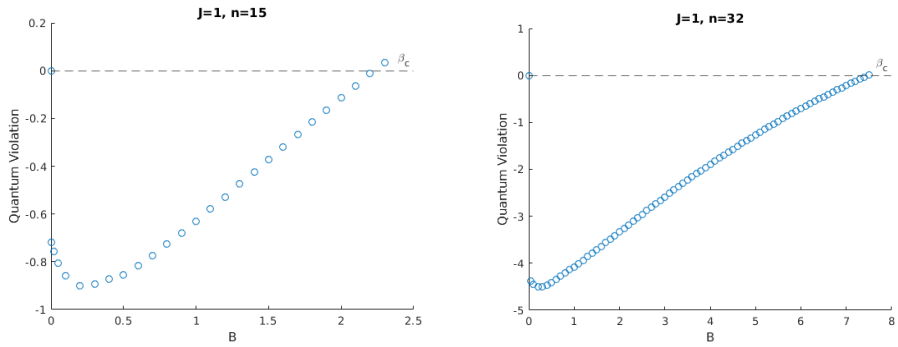

Fig. 7.5 Detection of non-local correlations in the ground state of the three-level LMG model (described in Eq. (7.24)) via the three-outcome two-body PIBI in Eq. (7.8).

Chapter 8

Conclusions and outlook

Large-scale entanglement and nonlocality are of fundamental importance for quantum many-body systems and represent a key resource for emerging quantum technologies.

In this thesis, we have started in Chapter 3 by exploring the complexity to characterize entanglement in simple cases. In particular, we have considered the separability problem for diagonal symmetric states, for which we have provided sufficient criteria, albeit necessary and sufficient criteria remains an NP-hard problem.

The underlying complexity to characterize entanglement motivates certification criteria, specially for the multipartite scenario. Based on non-local correlations, in Chapter 4 we have provided device-independent certification criteria that characterizes the amount of entanglement present on a quantum many-body system. Because the certification is DI, it does not rely on assumptions on the internal workings of the measuring device nor on the system itself. Moreover, by relying solely on nonlocality the criteria dismisses all the correlations that have a classical analogue, therefore supposing a natural candidate to explore quantum technologies based on correlations without classical analogue.

A typical context where large-scale entanglement stabilizes are quantum critical points. In Chapter 5 we have shown that Bell inequalities serve to detect non-local correlations in QCPs, and presented a spin

model whose resulting correlations in the QCP maximally violate a Bell inequality.

In order to explore non-local correlations in more exotic quantum systems, we have required novel techniques to circumvent the inefficient representability of the Hilbert space. Consequently, in Chapter 6 we have provided a solution for the quantum marginal problem restricted to symmetric states, which has allowed to present several applications for QIP beyond the characterization of Bell inequalities.

Finally, based on all the previous observations, in Chapter 7 we have presented a methodology to derive novel few-body symmetric Bell inequalities for three outcomes. These novel Bell inequalities open the door to explore nonlocality in exotic quantum phenomena in three-level many-body systems, as well as device-independent entanglement certification that can be effectively implemented in, for instance, spin-1 BECs.

In what follows we discuss in detail the conclusions for each chapter and discuss further research lines.

8.1 The separability problem for diagonal symmetric states

We have studied the separability problem for bipartite diagonal symmetric states. We have established an equivalence between the separability problem for DSS and quadratic conic optimization problems. This equivalence opens the door to exchange results from the field of quantum information to the field of quadratic conic optimization and vice-versa. For instance, we establish that the separability problem for DSS is equivalent to deciding whether a given matrix is completely positive, which is known to be an NP-hard problem. Hence, by importing a result from the quadratic conic optimization field, we rediscover that the separability problem for DSS is NP-hard for this highly symmetric case. Moreover, we have shown that for DSS of physical dimension smaller than 5, the PPT criterion provides necessary and sufficient

conditions. For higher physical dimension, there exist PPTDSS entangled states and copositive matrices can serve as indecomposable entanglement witnesses, for which we have provided several analytical examples. Finally, we have developed novel separability conditions for DSS via diagonal dominant approximations. Namely, obtaining a decomposition of DSS in terms of an extremal separable DSS and a diagonal dominant DSS (easy to characterize and known to be separable).

Outlook

In our work we have only been importing results from quadratic conic optimization to quantum information, even though the established connection allows to also export results. From the point of view of general quadratic conic optimization, the problems and results in quantum information suppose an instance, which nevertheless provides a new perspective to their known open problems. A research direction we leave as open is to identify which insights from the quantum information field might contribute to advance quadratic conic optimization. For instance, it might be interesting to use quantum information techniques to develop indecomposable entanglement witnesses of any physical dimension, which can then be exported as copositive matrices that serve to detect matrices that are doubly non-negative but not completely positive.

8.2 Device-independent certification of multipartite entanglement in many-body systems

By means of non-local correlations, we have presented certification criteria to quantify the amount of entanglement present in quantum many-body systems. In particular, we have presented a methodology to derive device-independent witnesses of entanglement depth for

many-body systems. The method uses Bell inequalities to construct the DIWEDs by finding the maximal amount of quantum violation achievable by any k-producible quantum state (*i.e.,* to find the k-producible bound). We have presented and discussed in detail the optimization procedure involved in deriving DIWEDs. We particularly focus on two-body permutationally invariant Bell inequalities, which has allowed us to derive DIWEDs that involve at most two-body symmetric correlators. Such DIWEDs have desirable properties, both from computational and experimental points of view. On the one hand, we have been able to numerically derive the k-producible bounds and even obtain results in the thermodynamic limit under reasonable assumptions. On the other hand, remarkably, the DIWEDs we present can be experimentally tested withing current technology, which supposes a step forward compared to the current state of the art. We have used existing experimental data to compare the performance of the DIWEDs with other existing entanglement depth criteria. As is expected, we observe our DIWEDs to perform better when compared to more demanding criteria, like nonlocality depth, and to perform worse when compared to less demanding non-device-independent criteria.

Outlook

A key ingredient that has allowed us to derive the DIWEDs is the use of Jordan's lemma [Jordan, 1875; Toner and Verstraete, 2006], applicable for Bell-type experiments with two dichotomic measurements. A research line we leave open is to extend the method for more general families of Bell inequalities that consider more than two dichotomic measurements. While for the two-body symmetric DIWEDs that we have derived there has been a clear relation between the amount of entanglement depth and the amount of Bell inequality violation, this does not need be the case for more general Bell inequalities. By considering a similar derivation for distinct more general Bell inequalities one could further explore the relation between non-local correlations and entanglement. A first step could be also consider few-body symmetric

Bell inequalities, but this time with more measurements per party or with more outcomes per measurement. Finally, and perhaps the most straightforward research direction, it remains to identify experimental setups or quantum technologies that benefit from DI certification of entanglement depth and implement the DIWEDs to probe entanglement. For instance, on a recent work the notion of k-producibility has been used to establish a connection between the power of quantum batteries and entanglement [Julià-Farré *et al.*, 2020], for which case one might use the DIWEDs as a certifier or to study the role of nonlocality in quantum batteries.

8.3 Non-local correlations near quantum critical points

We have explored non-local correlations in the vicinity of the quantum critical points. To do so, we have focused on the ferromagnetic transverse field Ising model with power-law decaying interactions, and a two-body permutationally invariant Bell inequality. We have shown that the Bell inequality is violated in the vicinity of the QCPs. To detect nonlocality we have proceeded two ways: (i) by finite-size computations without assumptions on the Bell test, which we then extrapolate to the asymptotic limit; and (ii) directly in the asymptotic limit by assuming that identical measurements are performed on a collection of qubits. We have shown that the origin of the two-body PIBI violation is the spin-squeezing generated in the vicinity of the QCP, and that the violation becomes maximal at the QCP. The results are relevant to various experimental platforms implementing the quantum Ising model with power-law interactions, like trapped ions [Zhang *et al.*, 2017], Rydberg atoms [Bernien *et al.*, 2017] and nano-photonic structures [Chang *et al.*, 2018]. In particular, the Bell inequality violation is expected to be robust against thermal noise [Frérot and Roscilde, 2018; Gabbrielli *et al.*, 2018] and particle losses [Tura *et al.*, 2014a].

Outlook

To the best of our knowledge, our results represent the first exploration of non-local correlations in many-body physics. Consequently, there are many open research lines. For instance: (i) to perform a similar study for the TFIM with antiferromagnetic interactions (or other models), in which case it remains to be seen whether the two-body PIBIs detect nonlocality and, if so, what is the physical mechanism leading to the violation; (ii) to use the DIWEDs previously presented as a certification tool to explore how the quantum correlations spread while approaching the QCP, and to certify entanglement depth divergence at critical points; (iii) to consider Bell inequalities tailored to nearest-neighbour interactions, as opposed to the two-body PIBIs which are tailored to the infinite-range interactions case; (iv) to employ the methodology in [Fadel and Tura, 2017] to probe all the two-body PIBIs at once and find the most fitted two-body PIBI, while exploring nonlocality through the phase diagram; (v) to derive Bell inequalities with three-outcomes and consider three-level many-body spin models with more exotic quantum phenomena; and (vi) to consider many-body Bell inequalities constrained to a symmetry group that provide them a different spatial structure than the permutation invariance. Under such inequalities one could explore nonlocality detection in qualitatively different many-body states.

8.4 The quantum marginal problem for symmetric states and applications

We have presented a solution for the quantum marginal problem restricted to symmetric states. The solution consists of the following:

- We provide analytical expressions of the compatibility conditions for an m-body reduced density matrix to be compatible with an n-qudit symmetric state.

- We show that the compatibility conditions can be used as constraints to pose the QMP as a feasibility problem solvable via an efficient SDP (polynomially in n, with degree $d-1$).

The solution we present has several implications in many distinct contexts, from which we have explored applications in quantum information. Namely in: (i) variational optimization; (ii) Bell inequalities characterization; and (iii) self-testing from marginals.

(i) We present a computationally efficient and low demanding variational method to upper bound the ground state energy of m-local Hamiltonians. The method optimizes using the m-body RDMs while considering a global symmetric state as an ansatz. While this is a very restrictive simplification, by exploring several spin models from infinite-range to short-range interactions, we observe there are many contexts in which the variational method carries useful information, with ferromagnetic couplings and long-range interactions being the most fitted. Remarkably, there are many instances for which the ground state of the finite-size precursor QCP has enough overlap with the symmetric state to approximate phase transitions with the variational method. The main advantage of the variational method is its efficiency and low memory requirements, which renders it a good candidate for a first order exploration order exploration of large sets of parameters characterizing the phase diagram of spin Hamiltonians.

(ii) We have considered the VM to optimize Bell inequalities over symmetric states. In particular, we have explored its synergy with two-body PIBI. By taking advantage of the VM low computational cost, we have carried a first order exploration on a spin-1/2 XXZ chain under a transverse field probing for nonlocality detection. This has narrowed down the number of parameters, which we then have recomputed with a more precise method to find, to the best of our knowledge for the first time, non-local correlations in the ground state of a spin-1/2 XXZ chain under a transverse field with nearest-neighbour interactions. Then

we have considered a spin-1/2 XXZ chain with periodic boundary conditions under a longitudinal magnetic field, for which we have detected non-local correlations on its ground state and first excited state for a specific phase.

(iii) We have used the QMP for symmetric states solution to explore which qubit symmetric states cannot be self-tested solely from their marginals. We show numerical evidence correlating the size of the global qubit symmetric state, its rank, the number of particles in the marginal being observed and the uniqueness of the global symmetric state.

Finally, as a byproduct and of independent interest, we have presented an analytical methodology to generically represent an n-qubit pure symmetric state as a translationally invariant diagonal matrix-product state of bond dimension n. This methodology has allowed us to benchmark the VM with DMRG by allowing us to compute the fidelity of the symmetric states given by the VM with the matrix product states given by the DMRG.

Outlook

An interesting research line is to consider the QMP given that the global state follows another type of symmetry that allows to proceed in a similar way. A way to approach it would be to consider whether there exists an SDP invariant formulation of our problem [Bachoc *et al.*, 2012; Tavakoli *et al.*, 2019] that could allow it to be formulated for other symmetry groups. As for the VM we have considered only qubits, qutrits and chain configurations, although it is straightforward to apply the VM to any qudit and lattices of arbitrary geometry and dimension. Thus, an open research line is to consider the VM as a first order exploration in more complex systems and their possible areas of interest. Regarding the Bell inequality characterization, one can now consider the characterization of few-body permutationally invariant Bell inequalities for d outcomes, given that identical measurements are performed. As for the self-testing, an interesting research

line is to provide a weaker form of self-testing by assuming that the global state is symmetric and self-testing solely from its marginals, or to perform tomography/fidelity estimates. This proposal could be particularly interesting in the context of experiments that involve BECs having access only to partial information [Schmied *et al.*, 2016; Fadel *et al.*, 2018]. Finally, a general research line is to explore more applications and contexts in which the solution of the QMP for symmetric states can provide insight.

8.5 Non-local correlations in three-level quantum many-body systems

We have derived Bell inequalities with three outcomes useful to detect nonlocality in three-level many-body systems. Furthermore, we have provided a Bell inequality that is capable of detecting non-local correlations on the ground state of the three-orbital LMG model [Meredith *et al.*, 1988; Gnutzmann *et al.*, 2000; Graß *et al.*, 2013]. To do so, similarly as the work presented in [Tura *et al.*, 2014a, 2015], we derive Bell inequalities constrained by symmetry and involving at most two-body terms, albeit this time the multipartite scenario has three outcomes. We present two methodologies that derive three-outcome two-body permutationally invariant Bell inequalities: (i) obtaining the two-body symmetric local polytope; and (ii) adapting the methodology presented in [Fadel and Tura, 2017] to the three outcomes scenario, which probes all the three-outcome two-body PIBIs at once via a feasible problem posed as an SDP. We have also presented a methodology to characterize the nonlocality detection of the three-outcome two-body PIBIs based on two steps: (i) a unitary parametrization to optimize over the observables; and (ii) an adaptation of the QMP for symmetric states solution to optimize over symmetric states solely from their marginals.

Outlook

An interesting further research line is to experimentally implement these novel Bell inequalities as Bell correlation witnesses. In particular, it should be possible to rewrite the Bell inequalities in terms of collective spin observables, which would allow for an effective test of nonlocality in, *e.g.,* ^{87}Rb ferromagnetic spin-1 BECs [Barrett *et al.*, 2001; Schmaljohann *et al.*, 2004; Hamley, 2012; Kunkel *et al.*, 2019]. Another research direction is to probe for non-local correlations near QCPs, but this time exploring exotic phase diagrams that arises in three-level quantum many-body systems [Haldane, 1983].

From the work we have presented, it still remains to take advantage of the method to derive three-outcome two-body PIBIs via the feasibility problem solvable by SDP. Because the method relies on a given statistical point obtained from probing quantum correlations, it might be particularly fitted for experimental setups. Finally, we have detected non-local correlations in the three-orbital LMG, which has been considered in several works in the context of quantum chaos [Meredith *et al.*, 1988; Gnutzmann *et al.*, 2000; Graß *et al.*, 2013], therefore it might be interesting and plausible to explore the role of non-local correlations in quantum chaos.

Appendices

Appendix A

This appendix completes Chapter 3 providing proofs, examples and further discussion.

A.1 Proof of Theorem 3.3.1

Proof. Let us first assume that ρ is a separable DS state acting on $\mathbb{C}^d \otimes \mathbb{C}^d$. Then, ρ admits the following convex decomposition into a product of vectors:

$$\rho = \sum_i \lambda_i \left|e_i\right\rangle \left|e_i\right\rangle\!\left\langle e_i\right| \left\langle e_i\right|, \tag{A.1}$$

where λ_i form a convex combination, $\left|e_i\right\rangle := \sum_{j=0}^{d-1} e_{ij} \left|j\right\rangle$, $e_{ij} \in \mathbb{C}$ and we have used that ρ is symmetric. From Eq. (A.1) one obtains the following identity:

$$\rho = \sum_{i,x_1,x_2,y_1,y_2} \lambda_i e_{i,x_1} e_{i,x_2} e^*_{j,y_1} e^*_{j,y_2} \left|x_1\right\rangle \left|x_2\right\rangle\!\left\langle y_1\right| \left\langle y_2\right| = \sum_{0\leq a\leq b<d} p_{ab} \left|D_{ab}\right\rangle\!\left\langle D_{ab}\right|. \tag{A.2}$$

By projecting Eq. (A.2) onto the Dicke basis one obtains several conditions that the coefficients e_{ir} must fulfill; *e.g.*, $\sum_i \lambda_i (e_{ir})^2 (e^*_{is})^2 = 0$.

For our purposes, we are interested in the following two conditions:

$$\begin{aligned} \langle rr| \rho |rr\rangle &= p_{rr} = \sum_i \lambda_i |e_{ir}|^4 \\ \langle D_{rs}| \rho |D_{rs}\rangle &= p_{rs} = \sum_i \lambda_i 2|e_{ir}|^2|e_{is}|^2. \end{aligned} \tag{A.3}$$

We are now ready to construct $M(\rho)$, which takes the following form:

$$M(\rho) = \sum_i \lambda_i \begin{pmatrix} |e_{i0}|^4 & |e_{i0}|^2|e_{i1}|^2 & \cdots & |e_{i,0}|^2|e_{i,d-1}|^2 \\ |e_{i0}|^2|e_{i1}|^2 & |e_{i1}|^4 & \cdots & |e_{i,1}|^2|e_{i,d-1}|^2 \\ \vdots & \vdots & \ddots & \vdots \\ |e_{i0}|^2|e_{i,d-1}|^2 & |e_{i1}|^2|e_{i,d-1}|^2 & \cdots & |e_{i,d-1}|^4 \end{pmatrix}. \tag{A.4}$$

One can easily observe from Eq. (A.4) that $M(\rho)$ is a CP matrix, since it admits a factorization $M(\rho) = \sum_i \vec{b_i} \cdot \vec{b_i}^T$, where $\vec{b_i}$ is a vector with components

$$\vec{b_i} := \lambda_i^{1/2} \begin{pmatrix} |e_{i0}|^2 & |e_{i1}|^2 & \cdots & |e_{i,d-1}|^2 \end{pmatrix}^T. \tag{A.5}$$

Moreover, one observes from Eq. (A.5) that $M(\rho)$ is a convex combination of CP matrices, since $b_{ij} \geq 0$. Therefore, because CP matrices form a convex cone, $M(\rho)$ is CP. Indeed, one can express $M(\rho)$ as $M(\rho) = B \cdot B^T$, where $\vec{b_i}$ are the columns of B.

Conversely, let us now assume that $M(\rho)$ is a CP matrix. Note that, as ρ is a DS state, the associated matrix $M(\rho)$ has a one-to-one correspondence with ρ. Because $M(\rho)$ is CP, one can express it as $M(\rho) = B \cdot B^T$, where B is a $d \times k$ matrix fulfilling $B_{ij} \geq 0$. We are interested in finding a separable convex combination of the form in Eq. (A.1) that produces the DS state ρ to which the given $M(\rho)$ is associated. As we shall see, this separable decomposition is not unique. We begin by expressing $M(\rho)$ as

$$M(\rho) = \sum_{i=1}^{k} \vec{b_i} \cdot \vec{b_i}^T, \tag{A.6}$$

where $\vec{b_i}$ are the columns of B, which implies that all the components of $\vec{b_i}$ are non-negative. Consider a set of complex numbers $\{z_{ij}\}_{ij}$ such that $|z_{ij}|^2 = (\vec{b_i})_j \geq 0$ and let us define

$$|z_i\rangle := \sum_{0\leq j<d} z_{ij} |j\rangle . \tag{A.7}$$

Taking a convex combination Eq. (A.1) with the vectors introduced in Eq. (A.7) results in a state that has $M(\rho)$ as the associated matrix as desired. However, in general the resulting state will not be DS. In order to ensure that the constructed ρ is a DS state, we have to build it such that all the unwanted coherences are eliminated. To this end, consider the following more general family of vectors:

$$|\zeta_{i,j,\mathbf{k}}\rangle := \sum_{0\leq l<d} (-1)^{k_l} \omega^{jl} z_{il} |l\rangle , \qquad 0 \leq j < d, \quad 0 \leq \mathbf{k} < 2^d, \tag{A.8}$$

where k_l is the l-th digit of $\mathbf{k}$ in base 2 and ω is a primitive $2d-$th root of the unity (for instance, $\omega = \exp(2\pi\mathbb{i}/2d)$). Then, from Eq. (A.8) one can construct the following (unnormalized) quantum state:

$$\rho_i = \sum_{0\leq j<d} \sum_{0\leq \mathbf{k}<2^d} |\zeta_{i,j,\mathbf{k}}\rangle |\zeta_{i,j,\mathbf{k}}\rangle \langle\zeta_{i,j,\mathbf{k}}| \langle\zeta_{i,j,\mathbf{k}}| , \tag{A.9}$$

Then, expanding Eq. (A.9) leads to

$$\rho_i = \sum_{j,\mathbf{k},l_1,l_2,l_3,l_4} (-1)^{k_{l_1}+k_{l_2}+k_{l_3}+k_{l_4}} \omega^{j(l_1+l_2-l_3-l_4)} z_{i,l_1} z_{i,l_2} z^*_{i,l_3} z^*_{i,l_4} |l_1, l_2\rangle \langle l_3, l_4| , \tag{A.10}$$

which one can rewrite as

$$\begin{aligned} \rho_i = \sum_{0\leq l_1,l_2,l_3,l_4<d} & z_{i,l_1} z_{i,l_2} z^*_{i,l_3} z^*_{i,l_4} |l_1, l_2\rangle \langle l_3, l_4| \cdot \\ & \cdot \left(\sum_{0\leq \mathbf{k}<2^d} (-1)^{k_{l_1}+k_{l_2}+k_{l_3}+k_{l_4}} \right) \left(\sum_{0\leq j<d} \omega^{j(l_1+l_2-l_3-l_4)} \right) . \end{aligned} \tag{A.11}$$

Let us take a closer inspection on Eq. (A.11) to see what are the possible values that the sums in parenthesis may take. Notice that whenever l_1, l_2, l_3, l_4 are all different, the expression involving $\boldsymbol{k}$ will be zero, since half of the sum will have a positive sign while the other half will counter balance with a negative sign. When only two of the l's are equal, the expression involving $\boldsymbol{k}$ will also be zero by the same argument. On the other hand, when two of the indices are equal to the remaining two, the expression involving $\boldsymbol{k}$ takes the value 2^d. Therefore, one has that

$$\sum_{0\leq \mathbf{k}<2^d} (-1)^{k_{l_1}+k_{l_2}+k_{l_3}+k_{l_4}} = \\ 2^d \left(\delta_{l_1-l_2}\delta_{l_3-l_4} + \delta_{l_1-l_3}\delta_{l_2-l_4} + \delta_{l_1-l_4}\delta_{l_2-l_3} - 2\delta_{l_1-l_2}\delta_{l_2-l_3}\delta_{l_3-l_4}\right), \tag{A.12}$$

where δ_x denotes the usual Kronecker Delta function. As for the second parenthesis in Eq. (A.11), one observes that it is a geometrical series which is d if, and only if, $l_1 + l_2 \equiv l_3 + l_4 \mod 2d$ (since ω has been taken to be primitive); otherwise it is 0. Because $0 \leq l_1+l_2, l_3+l_4 < 2d$, this can only happen if $l_1 + l_2 = l_3 + l_4$. Hence,

$$\sum_{0\leq j<d} \omega^{(l_1+l_2-l_3-l_4)j} = d\delta_{l_1+l_2-(l_3+l_4)}. \tag{A.13}$$

By inserting Eqs. (A.12) and (A.13) into Eq. (A.11), one has that the only possible values for (l_1, l_2, l_3, l_4) are (l_1, l_1, l_1, l_1), (l_1, l_2, l_1, l_2) and (l_1, l_2, l_2, l_1) (with $l_1 \neq l_2$). Note that Eq. (A.13) forbids the combination (l_1, l_1, l_2, l_2) if $l_1 \neq l_2$. This leads to

$$\begin{aligned}\rho_i =& d2^d \sum_{0\leq l_1\neq l_2<d} |z_{i,l_1}|^2|z_{i,l_2}|^2(|l_1,l_2\rangle\langle l_1,l_2| + |l_1,l_2\rangle\langle l_2,l_1|) \\ & d2^d + \sum_{0\leq l_1<d} |z_{i,l_1}|^4 \,|l_1,l_1\rangle\langle l_1,l_1|\,.\end{aligned} \tag{A.14}$$

Then, if one expresses Eq. (A.14) in the Dicke basis, one has that ρ_i is

a DS state:

$$\rho_i = d2^d \sum_{0\leq x<y<d} 2|z_{i,x}|^2|z_{i,y}|^2 \, |D_{xy}\rangle\langle D_{xy}| + d2^d \sum_{0\leq x<d} |z_{i,x}|^4 \, |D_{xx}\rangle\langle D_{xx}| \, . \tag{A.15}$$

Finally, from Eq. (A.15) one has that $M(\rho_i)$ is

$$M(\rho_i) = d2^d \vec{b_i} \cdot \vec{b_i}^T . \tag{A.16}$$

Hence, the convex combination that we seek for ρ is the following:

$$\rho = \frac{1}{d2^d ||M(\rho)||_1} \sum_{0\leq j<d} \sum_{0\leq \mathbf{k}<2^d} |\zeta_{i,j,\mathbf{k}}\rangle^{\otimes 2} \langle \zeta_{i,j,\mathbf{k}}|^{\otimes 2} \, , \tag{A.17}$$

where $||.||_1$ is the entry-wise 1-norm (the sum of the absolute values of all the matrix entries). If $M(\rho)$ comes from a quantum state, then $||M(\rho)||_1 = 1$. Therefore, Eq. (A.17) finishes the proof that the state ρ corresponding to $M(\rho)$ is separable.

□

A.2 Examples and counterexamples

A.2.1 Every PPTDSS acting on $\mathbb{C}^3 \otimes \mathbb{C}^3$ is separable

Here we prove that every PPTDSS ρ acting on $\mathbb{C}^3 \otimes \mathbb{C}^3$ is separable. The claim immediately follows from Theorem 3.3.3, which is usually proven [Yu, 2016] using results from quadratic non-convex optimization [Berman *et al.*, 2015]. Nevertheless, our proof presented here uses quantum information tools solely. In particular, the proof consists in building a convex separable decomposition of ρ of the form in Eq. (2.8). We achieve this in two steps: First, we provide a three-parameter class of separable PPTDSS. Second, we see that ρ can be expressed as a convex combination of the mentioned family (for some parameters) by performing a Cholesky decomposition of ρ^Γ. Furthermore, the existence of such Cholesky decomposition is directly related to the PPT conditions.

Recall that ρ can be expressed as

$$\rho = \sum_{0 \leq i \leq j < 3} p_{ij} \left| D_{ij} \right\rangle \left\langle D_{ij} \right|, \tag{A.18}$$

where $|D_{ii}\rangle = |ii\rangle$ and $|D_{ij}\rangle = (|ij\rangle + |ji\rangle)/\sqrt{2}$ if $i < j$. It follows from some algebra that ρ and its partial transpose ρ^{Γ} take the following form:

$$\rho = \bigoplus_{0 \leq i \leq j < 3} (p_{ij}), \tag{A.19}$$

and

$$\rho^{\Gamma} = \left(\frac{p_{01}}{2}\right) \oplus \left(\frac{p_{01}}{2}\right) \oplus \left(\frac{p_{02}}{2}\right) \oplus \left(\frac{p_{02}}{2}\right) \oplus \left(\frac{p_{12}}{2}\right) \oplus \left(\frac{p_{12}}{2}\right) \oplus M, \tag{A.20}$$

where

$$M = \begin{pmatrix} p_{00} & p_{01}/2 & p_{02}/2 \\ p_{01}/2 & p_{11} & p_{12}/2 \\ p_{02}/2 & p_{12}/2 & p_{22} \end{pmatrix}. \tag{A.21}$$

Lemma A.2.1. *Let $x, y, z \in \mathbb{C}$. Let ω be a primitive third root of the unity: $\omega^3 = 1$. Let us define $P_{x,y,z} := |\psi_{x,y,z}\rangle\langle\psi_{x,y,z}|$, where $|\psi_{x,y,z}\rangle := x|0\rangle + y|1\rangle + z|2\rangle$ (we do not normalize $|\psi_{x,y,z}\rangle$). Furthermore, let us define*

$$Q_{x,y,z} := P^{\otimes 2}_{x,y,z} + P^{\otimes 2}_{x,\omega y,\omega^2 z} + P^{\otimes 2}_{x,\omega^2 y,\omega z}. \tag{A.22}$$

Then, the unnormalized quantum state

$$\sigma_{x,y,z} := \frac{1}{12}\left(Q_{x,y,z} + Q_{-x,y,z} + Q_{x,-y,z} + Q_{x,y,-z}\right) \tag{A.23}$$

is diagonal symmetric. Because it is separable, it also has to be PPT. Furthermore, it gets expressed as in Eq. (A.18) using the following weights terms:

$$\begin{cases} p_{00} &= |x|^4 \\ p_{01} &= 2|x|^2|y|^2 \\ p_{02} &= 2|x|^2|z|^2 \\ p_{11} &= |y|^4 \\ p_{12} &= 2|y|^2|z|^2 \\ p_{22} &= |z|^4 \end{cases}, \tag{A.24}$$

where $|\cdot|$ *denotes the complex modulus.*

Proof. The proof follows almost immediately from expressing $\sigma_{x,y,z}$ in the computational basis. After some simple algebra rearranging terms, one obtains Eq. (A.18).

□

We now want to find a decomposition of a positive semi-definite matrix A of the form $A = B \cdot B^T$. We do so in the following Lemma by means of the Cholesky's decomposition.

Lemma A.2.2. *Consider a real, symmetric, positive-semidefinite* 3×3 *matrix* A *given by*

$$A = \begin{pmatrix} a & b & c \\ b & d & e \\ c & e & f \end{pmatrix}. \tag{A.25}$$

Then, A*'s Cholesky decomposition can be expressed as*

$$\begin{aligned} A &= \frac{1}{a}(a,b,c)^T(a,b,c) \\ &+ \frac{1}{a\begin{vmatrix} a & b \\ b & d \end{vmatrix}} \left(0, \begin{vmatrix} a & b \\ b & d \end{vmatrix}, \begin{vmatrix} a & c \\ b & e \end{vmatrix}\right)^T \left(0, \begin{vmatrix} a & b \\ b & d \end{vmatrix}, \begin{vmatrix} a & c \\ b & e \end{vmatrix}\right) \\ &+ \frac{1}{\begin{vmatrix} a & b \\ b & d \end{vmatrix} \det A}(0,0,\det A)^T(0,0,\det A). \end{aligned} \tag{A.26}$$

Proof. The idea behind the proof is to start by using the rank-1 matrix $A_1 := (a,b,c)^T(a,b,c)/a$ to fix the elements of A that lie on the first column and first row. Then, we proceed with the second summand which will fix the elements of the second row and second column of A. Finally, the last summand will fix the bottom-right element of A. Therefore, we have

$$A_1 = \begin{pmatrix} a & b & c \\ b & \cdot & \cdot \\ c & \cdot & \cdot \end{pmatrix}, \tag{A.27}$$

where the $\cdot$ are terms that are not yet fixed. When one adds the second term to A_1 one has

$$A_2 = \begin{pmatrix} a & b & c \\ b & d & e \\ c & e & \cdot \end{pmatrix}, \tag{A.28}$$

and by adding the last term to A_2 one recovers A.

□

We are now ready to prove that every DNN 3×3 matrix is CP:

Lemma A.2.3. *If A is a 3×3 positive-semidefinite matrix, and it is entry-wise non-negative, then there exists a Cholesky decomposition of A with non-negative vectors (i.e., the vectors components are non-negative).*

Proof. The only problem in Lemma A.2.2 might come from the term $\begin{vmatrix} a & c \\ b & e \end{vmatrix}$, since all the other terms are either principal minors of A or entries of A and, thus, they are non-negative. Recall that the Cholesky decomposition of A picks an order of rows which is arbitrary and could be done in any order. For illustrative purposes, consider that we re-order the columns and rows of A then all the possibilities are

$$\left\{ \begin{pmatrix} a & b & c \\ b & d & e \\ c & e & f \end{pmatrix}, \begin{pmatrix} a & c & b \\ c & f & e \\ b & e & d \end{pmatrix}, \begin{pmatrix} d & b & e \\ b & a & c \\ e & c & f \end{pmatrix}, \right.$$
$$\left. \begin{pmatrix} d & e & b \\ e & f & c \\ b & c & a \end{pmatrix}, \begin{pmatrix} f & c & e \\ c & a & b \\ e & b & d \end{pmatrix}, \begin{pmatrix} f & e & c \\ e & d & b \\ c & b & a \end{pmatrix} \right\}. \tag{A.29}$$

Therefore, the corresponding minors that could be negative are

$$\left\{ \begin{vmatrix} a & c \\ b & e \end{vmatrix}, \begin{vmatrix} d & e \\ b & c \end{vmatrix}, \begin{vmatrix} f & e \\ c & b \end{vmatrix} \right\}. \tag{A.30}$$

If any of the numbers in Eq. (A.30) is non-negative, then one can pick the Cholesky decomposition for that particular order and obtain

the result. Otherwise, all of them would be strictly negative, which would contradict the fact that $A \succeq 0$ as we shall see now.

Note that if all the numbers in Eq. (A.30) are strictly negative, then it implies that $d > 0$. Otherwise, if $d = 0$, because of $A \succeq 0$, it would imply that $b = e = 0$. Then, the only possibility would be that all the numbers in Eq. (A.30) are zero. Hence, d must be strictly positive. Similarly, b has to be strictly positive. Otherwise, if $b = 0$, then one would have that $cd < 0$ and $ae < 0$, which contradicts the fact that A is entry-wise non-negative. Hence, $b > 0$.

It suffices to find a contradiction with just a subset of the conditions given by Eq. (A.30): Let us assume that $ae < bc$ and $cd < be$. Then, one has that

$$aed < bcd < b^2 e, \tag{A.31}$$

where we used $ae < bc$ and $d > 0$ in the first inequality and $cd < be$ and $b > 0$ in the second. Hence, $aed < b^2 e$. Therefore, e has to be strictly positive since otherwise one would have $0 < 0$. Then, one obtains that $ad < b^2$, but such relation directly contradicts $A \succeq 0$, since the latter implies $ad \geq b^2$.

□

We are finally ready to prove the original claim from the present example.

Let ρ be a PPTDSS. Then, one has that $p_{ij} \geq 0$ and $M \succeq 0$. Our goal is to write ρ as a convex combination of some elements $\sigma_{x,y,z}$ introduced in Lemma A.2.1 by appropriately picking x, y, z as functions of p_{ij}. Note that the entries of $\sigma_{x,y,z}$ will be non-negative for all $x, y, z \in \mathbb{C}$. Moreover, the matrix M associated to $\sigma_{x,y,z}$ is

$$M_\sigma = \begin{pmatrix} |x|^4 & |x|^2|y|^2 & |x|^2|z|^2 \\ |x|^2|y|^2 & |y|^4 & |y|^2|z|^2 \\ |x|^2|z|^2 & |y|^2|z|^2 & |z|^4 \end{pmatrix}, \tag{A.32}$$

which has rank 1 and is generated as $M_\sigma = (|x|^2, |y|^2, |z|^2)^T (|x|^2, |y|^2, |z|^2)$. Therefore, we want to relate M_σ to each element of the Cholesky decomposition in Lemma A.2.2 such that their sum recovers the original

M. By recovering the given M, one automatically recovers ρ and has its separable convex decomposition. This can be done if, and only if, the components of the vectors appearing in Lemma A.2.2 are non-negative, because one can always find numbers $x, y, z \in \mathbb{C}$ realizing them.

Then, lets apply Lemma A.2.2 to M_σ in order to generate $\rho = \lambda_0\sigma_{x_0,y_0,z_0} + \lambda_1\sigma_{x_1,y_1,z_1} + \lambda_2\sigma_{x_2,y_2,z_2}$. We start by picking

$$\lambda_0 = \frac{1}{p_{00}}, \qquad (x_0, y_0, z_0) = (\sqrt{p_{00}}, \sqrt{p_{01}/2}, \sqrt{p_{02}/2}).$$

All the components are non-negative by hypothesis. As for (x_1, y_1, z_1), we now pick

$$\lambda_1 = \frac{1}{p_{00}(p_{00}p_{11} - p_{01}^2/4)},$$
$$(x_1, y_1, z_1) = \left(0, \sqrt{p_{00}p_{11} - p_{01}^2/4}, \sqrt{p_{00}p_{12}/2 - p_{01}p_{02}/4}\right).$$

In this case $p_{00}p_{11} - p_{01}^2/4 \geq 0$ since it is a principal minor of M. Therefore, $\lambda_1 \geq 0$ and $y_1 \geq 0$. However, z_1 might need to take a negative value. We shall deal with such case at the end.

Finally, let us consider (x_2, y_2, z_2), in which case we have

$$\lambda_2 = \frac{1}{(p_{00}p_{11} - p_{01}^2/4)\det M}, \qquad (x_2, y_2, z_2) = \left(0, 0, \sqrt{\det M}\right).$$

One easily observes that $\lambda_2 \geq 0$ and $z_2 \geq 0$.

To finish the proof we have to argue that z_1 can be taken to be a positive number. Indeed, this is guaranteed by Lemma A.2.3, since there always exists a relabelling of the computational basis elements $|0\rangle$, $|1\rangle$ and $|2\rangle$ such that the Cholesky decomposition of M is done with non-negative vectors.

A.2.2 An example of a PPTDS entangled state acting on $\mathbb{C}^6 \otimes \mathbb{C}^6$

Here we present an example for $d = 6$ of an unnormalized PPTDS entangled state. The unnormalized PPTDS entangled state is based on

a counterexample that appeared in the context of financial engineering [Sonneveld *et al.*, 2009].

Let $p_{ii} = 2, p_{i,i+1} = 3, p_{i,i+2} = 1, p_{i,i+3} = 0, p_{i,i+4} = 1, p_{i,i+5} = 3$, in which case the matrix M takes the following form:

$$M = \begin{pmatrix} 2 & 3/2 & 1/2 & 0 & 1/2 & 3/2 \\ 3/2 & 2 & 3/2 & 1/2 & 0 & 1/2 \\ 1/2 & 3/2 & 2 & 3/2 & 1/2 & 0 \\ 0 & 1/2 & 3/2 & 2 & 3/2 & 1/2 \\ 1/2 & 0 & 1/2 & 3/2 & 2 & 3/2 \\ 3/2 & 1/2 & 0 & 1/2 & 3/2 & 2 \end{pmatrix}. \tag{A.33}$$

One observes that M is a circulant matrix. Moreover, for our purposes it is important to know that M factorizes as $M = Z^T \cdot Z$, where

$$Z = \begin{pmatrix} 1 & 1 & 1 & 1 & 1 & 1 \\ 0 & \sqrt{3}/2 & \sqrt{3}/2 & 0 & -\sqrt{3}/2 & -\sqrt{3}/2 \\ 1 & 1/2 & -1/2 & -1 & -1/2 & 1/2 \end{pmatrix}. \tag{A.34}$$

Note that the factorization $M = Z^T \cdot Z$ proves that ρ is PPT. Because the matrix M does not admit a non-negative matrix factorization [Sonneveld *et al.*, 2009], we can't apply the separable decomposition of the $3 \otimes 3$ case previously seen in Section A.2.1.

The matrix M has rank 3 and its kernel is given by the following three vectors orthogonal to Z:

$$\begin{pmatrix} 1 & 0 & 0 & -1 & 2 & -2 \\ 0 & 1 & 0 & -2 & 3 & -2 \\ 0 & 0 & 1 & -2 & 2 & -1 \end{pmatrix}. \tag{A.35}$$

We can now apply the range criterion to ρ. If ρ is separable, there has to exist a $|\psi\rangle = |\zeta\rangle_A |\zeta\rangle_B$ in the range of ρ such that $|\psi^c\rangle = |\zeta\rangle_A |\zeta^*\rangle_B$ is in the range of ρ^Γ (we assume the same vector $|\zeta\rangle$ on A and B, since ρ acts on the symmetric space). A vector belongs to the range if, and only if, it is orthogonal to the kernel. Therefore, the range criterion implies that, if ρ is separable, then the system of equations imposed by $|\psi\rangle \perp \ker \rho$ and $|\psi^c\rangle \perp \ker \rho^\Gamma$ has a non-trivial solution.

Let us parametrize $|\zeta\rangle = \sum_{0\leq i<6} z_i |i\rangle$. Then on has that

$$|\psi\rangle = \sum_{0\leq i,j<6} z_i z_j |ij\rangle \tag{A.36}$$

and

$$|\psi^c\rangle = \sum_{0\leq i,j<6} z_i z_j^* |ij\rangle . \tag{A.37}$$

The kernel of ρ is spanned by $|D_{03}\rangle , |D_{14}\rangle$ and $|D_{25}\rangle$, since $p_{i,i+3} = 0$. Then, the following equations follow:

$$z_0 z_3 = z_1 z_4 = z_2 z_5 = 0. \tag{A.38}$$

The kernel of ρ^Γ is given by the vectors $|i, i+3\rangle$ and $|i+3, 3\rangle$, as well as the vectors in the kernel of M (in the appropriate basis). The first ones introduce redundant equations:

$$z_0 z_3^* = z_1 z_4^* = z_2 z_5^* = 0. \tag{A.39}$$

Thus, all the important information comes from the kernel of M, which means that

$$\begin{aligned} (\langle 00| - \langle 33| + 2\langle 44| - 2\langle 55|) |\psi^c\rangle = 0 \\ (\langle 11| - 2\langle 33| + 3\langle 44| - 2\langle 55|) |\psi^c\rangle = 0 \\ (\langle 22| - 2\langle 33| + 2\langle 44| - \langle 55|) |\psi^c\rangle = 0 \end{aligned} \tag{A.40}$$

It follows that the above system can be compacted as

$$\begin{pmatrix} |z_0|^2 \\ |z_1|^2 \\ |z_2|^2 \end{pmatrix} = \begin{pmatrix} 1 & -2 & 2 \\ 2 & -3 & 2 \\ 2 & -2 & 1 \end{pmatrix} \begin{pmatrix} |z_3|^2 \\ |z_4|^2 \\ |z_5|^2 \end{pmatrix} . \tag{A.41}$$

In order to include the conditions $z_0 z_3 = z_1 z_4 = z_2 z_5 = 0$, one has to consider several cases:

- If $z_3 = z_4 = z_5 = 0$, then the above system implies $z_0 = z_1 = z_2 = 0$.

- Conversely, because the 3×3 matrix in Eq. (A.41) is invertible (in fact, it is its own inverse), then if $z_0 = z_1 = z_2 = 0$ the above system implies that $z_3 = z_4 = z_5 = 0$.

- If two of the numbers in $\{z_3, z_4, z_5\}$ are zero (which implies that one number in $\{z_0, z_1, z_2\}$ is also zero) one has that the system takes the following form (for instance, for the case $z_0 = z_4 = z_5 = 0$):

$$\begin{pmatrix} 0 \\ |z_1|^2 \\ |z_2|^2 \end{pmatrix} = |z_3|^2 \begin{pmatrix} 1 \\ 2 \\ 2 \end{pmatrix}. \tag{A.42}$$

  This in turn implies that $z_3 = 0$, which also implies that $z_1 = z_2 = 0$.

- The remaining case is that the numbers in $\{z_3, z_4, z_5\}$ are zero and two of the numbers of $\{z_0, z_1, z_2\}$ are zero. By inverting Eq. (A.41), one reduces this case to the previous one.

Therefore, the only solution for the above system of equations is that $z_0 = z_1 = z_2 = z_3 = z_4 = z_5 = 0$. However, this does not result in a valid quantum state. Consequently, there does not exist a quantum state ψ with the properties required by the range criterion. Therefore, ρ is entangled.

A.3 Exposedness

A feature of convex sets is that they are completely determined by their extremal elements, where extremal elements are those that cannot be written as a proper convex combination of the other elements in the set. An important concept towards the characterization of the extremal elements of a convex set is that of facial structure.

Definition A.3.1. *Let $\mathcal{K}$ be a convex cone. Then, the* face *of $\mathcal{K}$ is a subset $\mathcal{F} \subseteq \mathcal{K}$ such that every line segment in the cone with an interior point in $\mathcal{F}$ has both endpoints in $\mathcal{F}$.*

Then, by definition, every extreme ray of $\mathcal{K}$ is a one-dimensional face. In order to understand the facial structure of cones, one wants to know whether $\mathcal{K}$ is facially exposed. Facial exposedness is an important property exploited in optimization, where it allows the design of facial reduction algorithms [Pataki, 2013].

Definition A.3.2. *Let $\mathcal{K}$ be a cone in the space of real, symmetric matrices and let $\mathcal{F} \subseteq \mathcal{K}$ be a non-empty face. $\mathcal{F}$ is said to be an* exposed face *of $\mathcal{K}$ if, and only if, there exists a non-zero real symmetric matrix A such that*

$$\mathcal{K} \subseteq \{X \ s.\ t.\ X \in M_{\mathbb{R}}(d,d),\ X = X^T,\ \langle A, X\rangle \geq 0\} \tag{A.43}$$

and

$$\mathcal{F} = \{X \in \mathcal{K} \ s.\ t.\ \langle A, X\rangle = 0\}. \tag{A.44}$$

In other words, a face is said to be exposed if it intersects the cone with a non-trivial supporting hyperplane.

A cone is facially exposed if all of its faces are exposed. While every extreme ray of $\mathcal{CP}_d$ is exposed [Dickinson, 2011], it remains an open question whether $\mathcal{CP}_d$ is facially exposed. In the case of $\mathcal{COP}_d$, the extreme rays corresponding to $|ii\rangle\langle ii|$ are known to not be exposed [Dickinson, 2011], implying that $\mathcal{PSD}_d + \mathcal{N}_d$ (the set of decomposable EWs for PPTDSS) is not facially exposed. However, the set $\mathcal{DNN}_d$ of PPTDSS states is facially exposed, since both $\mathcal{PSD}_d$ and $\mathcal{N}_d$ are facially exposed [Pataki, 2000] and the intersection of facially exposed cones is facially exposed.

A.4 Proofs and examples for Section 3.4

A.4.1 Example of an entangled PPTDSS for $d = 5$.

An example of an entangled PPTDSS for $d = 5$ is the following [Berman and Shaked-Monderer, 2003]:

$$\hat{M}(\rho) = \begin{pmatrix} 1 & 1 & 0 & 0 & 1 \\ 1 & 2 & 1 & 0 & 0 \\ 0 & 1 & 2 & 1 & 0 \\ 0 & 0 & 1 & 2 & 1 \\ 1 & 0 & 0 & 1 & 6 \end{pmatrix}. \tag{A.45}$$

For this case, the kernel of $\hat{M}(\rho)$ is $\ker \hat{M}(\rho) = \{\vec{0}\}$. Therefore, in order to apply the Range criterion one first needs to subtract some rank-1 projectors, which are $3/16\vec{v_1}\vec{v_1}^T + 1/16\vec{v_2}\vec{v_2}^T$, where $\vec{v_1}^T = (1, 0, 0, 0, 1)$ and $\vec{v_2} = (1, 0, 0, 0, 9)$.

Equivalently, we can use the Horn matrix as an EW (cf. Section 3.4.1) to certify that the state is entangled; *i.e.*, $\mathrm{Tr}(H(\hat{M}(\rho) - 3/16\vec{v_1}\vec{v_1}^T - 1/16\vec{v_2}\vec{v_2}^T)) = -1 < 0$.

A.4.2 Proof of Theorem 3.4.1

Proof. Let us start by rewriting $\rho = \tilde{\rho} + \varepsilon I$, where $\tilde{\rho} = \rho - \varepsilon I$. Then, we note the following observations:

1. $\tilde{\rho}$ is a legitimate DS matrix: $\tilde{\rho}_{ij} \geq 0$. This comes from the fact that $\tilde{\rho}_{ij} = \rho_{ij} - \varepsilon$ and the first hypothesis is precisely $\rho_{ij} - \varepsilon \geq 0$.

2. $\tilde{\rho}$ is PPT. Since $\tilde{\rho}_{ij} \geq 0$, the only remaining condition to prove is that $\tilde{M}(\rho) \succeq 0$. Note that $\tilde{M}(\rho) = M(\rho) - d\varepsilon \left|u\right\rangle \left\langle u\right|$. We want to prove that, for any vector $\left|v\right\rangle$, we have that $\left\langle v\right| (M - \varepsilon d \left|u\right\rangle \left\langle u\right|) \left|v\right\rangle \geq 0$. Note that, since $\left|u\right\rangle \in \mathcal{R}(M(\rho))$, there exists $\left|\Psi\right\rangle$ such that $\left|u\right\rangle = M(\rho) \left|\Psi\right\rangle$. Therefore, one can write $\left\langle v\right\rangle u \left\langle u\right\rangle v = |\left\langle v\right| \sqrt{M(\rho)} \frac{1}{\sqrt{M(\rho)}} \left|u\right\rangle|^2$ and, by virtue of the Cauchy-Schwarz inequality, $\left\langle v\right\rangle u \left\langle u\right\rangle v \leq \left\langle v\right| M(\rho) \left|v\right\rangle \left\langle u\right| \frac{1}{M(\rho)} \left|u\right\rangle$. Notice

now that the positive semi-definiteness of $M(\rho)$ allows one to pick a square root such that $\sqrt{M(\rho)} \succeq 0$. Hence, we have that

$$\langle v| M(\rho) |v\rangle \geq \langle v\rangle u \langle u\rangle v(\langle u| \frac{1}{M(\rho)} |u\rangle)^{-1} \geq \langle v\rangle u \langle u\rangle v d\varepsilon, \tag{A.46}$$

which yields $\langle v| \tilde{M}(\rho) |v\rangle \geq 0$ for all $|v\rangle$.

3. A sufficient condition for a real symmetric non-negative matrix to be completely positive is that the matrix is diagonally dominant [Kaykobad, 1987]. Hence, if we prove that $\tilde{M}(\rho)$ is diagonally dominant, then the corresponding $\tilde{\rho}$ will be a DS separable state. This is guaranteed by the third hypothesis:

$$\tilde{\rho}_{ii} = \rho_{ii} - \varepsilon \geq \sum_{j\neq i} \rho_{ji} - (d-1)\varepsilon = \sum_{j\neq i} \tilde{\rho}_{ji}.$$

Therefore, ρ is separable.

□

A.4.3 An example for Theorem 3.4.1

We want to construct an example to show that $\mathcal{CP}_d \setminus \mathcal{DD}_d \neq \emptyset$. Furthermore, we then want to illustrate how to certify separability by means of Theorem 3.4.1.

Consider a DS quantum state ρ that takes the following form:

$$\rho = \sum_{i=0}^{d-1} \alpha |ii\rangle \langle ii| + \sum_{0\leq i<j<d} 2\beta |D_{ij}\rangle \langle D_{ij}|, \tag{A.47}$$

where $\alpha, \beta \in \mathbb{R}_{\geq 0}$. Normalization imposes the constraint $d\alpha + d(d-1)\beta = 1$.
Let us choose α and β such that $M(\rho)$ lies in the line segment between $M(I)$ and $M(\tilde{\rho})$; *i.e.*, it is a convex combination of the following form:

$$M(\rho) = \lambda M(\tilde{\rho}) + (1-\lambda)M(I) \text{ for } 0 \leq \lambda \leq 1, \tag{A.48}$$

where $M(I)$ is an extremal of $\mathcal{CP}_d$, with the rank-1 state I defined as in Lemma 3.4.1, and $M(\tilde{\rho})$ has the same form as $M(\rho)$ but with coefficients $\tilde{\alpha}, \tilde{\beta}$ chosen as $\tilde{\alpha} = (d-1)\tilde{\beta}$ which corresponds to the limit where $M(\rho)$ becomes $\mathcal{DD}_d$. Together with the normalization constraint, one obtains $\tilde{\alpha} = (2d)^{-1}$ and $\tilde{\beta} = (2d(d-1))^{-1}$.

Therefore, any choice of $\lambda \in [0, 1)$ yields a state with associated $M(\rho)$ being $\mathcal{CP}_d \setminus \mathcal{DD}_d$.

Let us now proceed to illustrate how to certify separability of ρ by virtue of Theorem 3.4.1, given a two qudit PPTDSS ρ. For instance, consider Eq. (A.48) with $\lambda = 1/2$ which results in $M(\rho) = 1/2(M(\tilde{\rho}) + M(I))$ (which is in $\mathcal{CP}_d \setminus \mathcal{DD}_d$ by construction). To certify separability by means of Theorem 3.4.1, we want to find a decomposition $\rho = \tilde{\rho} + \epsilon I$ to show that there exists an ε fulfilling the conditions of the Theorem. In what follows we assume $d \geq 5$.

Condition 1 gives an upper bound given by $\varepsilon \leq \min\{\alpha, \beta\} = \alpha = \frac{d+2}{4d^2}$. Condition 2 gives an even more restrictive upper bound given by:

$$\varepsilon \leq \frac{1}{d}(\langle u| \frac{1}{M(\rho)} |u\rangle)^{-1} = \frac{\alpha + (d-1)\beta}{d} = 1/d^2, \tag{A.49}$$

where the pseudoinverse can be found via the Sherman-Morrison formula (due to the particular form of Equation (A.47)). Finally condition 3 gives the following lower bound:

$$\varepsilon \geq \frac{\beta(d-1) - \alpha}{(d-2)} = \frac{d-1}{4d^2(d-2)}. \tag{A.50}$$

Hence, the separability of ρ gets certified since it is possible to decompose ρ as $\rho = \tilde{\rho} + \epsilon I$ for all $\varepsilon \in [\frac{d-1}{4d^2(d-2)}, \frac{1}{d^2}]$.

A.4.4 Proof of Lemma 3.4.2

Proof. Let $|e(\vec{\varphi})\rangle = \sum_{i=0}^{d-1} \sqrt{x_i/||\mathbf{x}||_1} e^{\mathrm{i}\varphi_i} |i\rangle$. A separable decomposition of $I_{\mathbf{x}}$ is given by

$$I_{\mathbf{x}} = \int_{[0,2\pi]^d} \frac{\mathrm{d}\vec{\varphi}}{(2\pi)^d} (|e(\vec{\varphi})\rangle \langle e(\vec{\varphi})|)^{\otimes 2}. \tag{A.51}$$

Indeed, note that

$$\begin{aligned} I_{\mathbf{x}} &= \sum_{ijkl} |ij\rangle\langle kl| \int_{[0,2\pi]^d} \frac{\mathrm{d}\vec{\varphi}}{(2\pi)^d} \frac{\sqrt{x_i x_j x_k x_l}}{||\mathbf{x}||_1^2} e^{\mathbb{i}(\varphi_i+\varphi_j-\varphi_k-\varphi_l)} \\ &= \sum_{ijkl} |ij\rangle\langle kl| \frac{\sqrt{x_i x_j x_k x_l}}{||\mathbf{x}||_1^2} (\delta_{i,k}\delta_{j,l} + \delta_{i,l}\delta_{j,k} - \delta_{i,j,k,l}), \quad \text{(A.52)} \end{aligned}$$

where δ is the Kronecker delta function. □

A.4.5 Proof of Theorem 3.4.2

Proof. Let us start by expressing ρ as $\rho = (1-\lambda)\tilde{\rho}+\lambda I_{\mathbf{x}}$. Consequently, one has

$$M(\tilde{\rho}) = \frac{1}{1-\lambda}(M(\rho) - \lambda M(I_{\mathbf{x}})). \quad \text{(A.53)}$$

Our goal is to prove that $M(\tilde{\rho})$ is CP. By proving that $M(\tilde{\rho})$ is CP, then we also show that $M(\rho)$ is CP and that ρ is separable.

1. First we show that $M(\tilde{\rho})$ is non-negative component-wise. Indeed, one has

$$\begin{aligned} (M(\tilde{\rho}))_{ij} &= \frac{1}{1-\lambda}((M(\rho))_{ij} - \lambda(M(I_{\mathbf{x}}))_{ij}) \\ &\geq \frac{1}{1-\lambda}((M(\rho))_{ij} - \frac{(M(\rho))_{ij}||\mathbf{x}||_1^2}{x_i x_j}(M(I_{\mathbf{x}}))_{ij}) = 0, \end{aligned}$$

   because $(M(I_{\mathbf{x}}))_{ij} = \frac{x_i x_j}{||\mathbf{x}||_1^2}$.

2. Next, we show that $M(\tilde{\rho})$ is positive semi-definite. In such case one has that $\langle v| M(\tilde{\rho}) |v\rangle \geq 0$ for every $|v\rangle$. Since we assume that $1-\lambda > 0$, it is sufficient to check that $\langle v| (M(\rho) - \lambda M(I_{\mathbf{x}})) |v\rangle \geq 0$ holds. Recall that $\langle v| M(I_{\mathbf{x}}) |v\rangle = |\langle v| u_{\mathbf{x}}\rangle|^2$. Since $|u_{\mathbf{x}}\rangle \in \mathcal{R}(M(\rho))$, it means that $\langle u_{\mathbf{x}}| M(\rho) |u_{\mathbf{x}}\rangle > 0$ and, therefore, $\langle u_{\mathbf{x}}| \frac{1}{M(\rho)} |u_{\mathbf{x}}\rangle >$

0. Hence, we can apply the Cauchy-Schwarz inequality to $\langle v| M(I_{\mathbf{x}}) |v\rangle$ to obtain

$$\begin{aligned} \langle v\rangle u_{\mathbf{x}} \langle u_{\mathbf{x}}\rangle v &= |\langle v| \sqrt{M(\rho)} \frac{1}{\sqrt{M(\rho)}} |u_{\mathbf{x}}\rangle|^2 \\ &\leq \langle v| M(\rho) |v\rangle \langle u_{\mathbf{x}}| \frac{1}{M(\rho)} |u_{\mathbf{x}}\rangle . \end{aligned} \tag{A.54}$$

Note that the positive semi-definiteness of $M(\rho)$ allows to choose a square root branch of $M(\rho)$ such that $\sqrt{M(\rho)} \succeq 0$. Therefore, we have that

$$\begin{aligned} &\langle v| (M(\rho) - \lambda M(I_{\mathbf{x}})) |v\rangle \\ &\quad \geq \langle v| M(\rho) |v\rangle (1 - \lambda \langle u_{\mathbf{x}}| \frac{1}{M(\rho)} |u_{\mathbf{x}}\rangle) \\ &\quad \geq \langle v| M(\rho) |v\rangle (1 - 1) = 0. \end{aligned}$$

3. Up until this point we have proved that conditions 1 and 2 of Theorem 3.4.2 guarantee that $M(\tilde{\rho})$ is doubly non-negative. The third condition guarantees that it is diagonal dominant. In order to prove that

$$(M(\tilde{\rho}))_{ii} - \sum_{j\neq i} (M(\tilde{\rho}))_{ij} \geq 0 \tag{A.55}$$

for all i, we note that it can be rewritten as

$$(M(\rho))_{ii} - \sum_{j\neq i} (M(\rho))_{ij} - \lambda \left(\frac{x_i^2}{||\mathbf{x}||_1^2} - \sum_{j\neq i} \frac{x_i x_j}{||\mathbf{x}||_1^2} \right) \geq 0. \tag{A.56}$$

One can rearrange the condition we want to prove by adding and subtracting x_i^2 to the parenthesis so that

$$(M(\rho))_{ii} - \sum_{j\neq i} (M(\rho))_{ij} - \frac{\lambda x_i}{||\mathbf{x}||_1^2} (2x_i - ||\mathbf{x}||_1) \geq 0. \tag{A.57}$$

From this last expression, the result immediately follows since we assumed that $\lambda x_i(||\mathbf{x}||_1 - 2x_i) \geq ||\mathbf{x}||_1^2 \left[\sum_{j\neq i}(M(\rho))_{ij} - (M(\rho))_{ii}\right]$ for all i.

Hence, the conditions of Theorem 3.4.2 guarantee that $M(\tilde{\rho})$ is doubly non-negative and diagonal dominant. Since every diagonally dominant real symmetric non-negative matrix is CP [Kaykobad, 1987], the associated $\tilde{\rho}$ is a separable DS state. Hence, ρ can be expressed as a convex combination of separable states; showing that ρ is separable.

□

Appendix B

B.1 Discussion on exactly solving the optimization problem in Eq. (4.10)

In what follows, we show that, in principle, it is possible to exactly solve the optimization problem Eq. (4.10). To find exact solutions of Eq. (4.10) finding β_k without encountering local minima issues. For our purposes we shall make use of arguments typically applied on systems of polynomial equations. In particular, note that for every k-partition $\mathcal{P}$, there is a corresponding system of polynomial equations which defines $\beta_k^{\mathcal{P}}$ under polynomial equality constraints.

In order to obtain the system of equations, consider the variables defined as $x_{i,k} \equiv \cos(\theta_{i,k})$ and $y_{i,k} \equiv \sin(\theta_{i,k})$. Then, one immediately has the constraint that $x_{i,k}^2 + y_{i,k}^2 = 1$ for every $i \in [n]$ and $k \in [2]$. On the other hand, one can assume that the quantum state $|\psi_{\mathcal{P}}\rangle$ is real, since $\mathcal{B}$ is a real, symmetric operator. Therefore, it is possible to expand $|\psi_A\rangle = (\psi_0^A, \ldots, \psi_{2^{|A|}-1}^A)^T$ for every $A \in \mathcal{P}$, where $\sum_{i=0}^{2^{|A|}-1} [\psi_i^A]^2 = 1$.

Hence, $\langle \Psi_{\mathcal{P}} | \mathcal{B} | \Psi_{\mathcal{P}} \rangle$ is a polynomial with $4n + \sum_{A \in \mathcal{P}} 2^{|A|}$ variables of degree 2 in the ψ_i^A variables and degree at most n in the $x_{i,k}$ and $y_{i,k}$ variables, subject to $2n + |\mathcal{P}|$ equality constraints. One way to determine the critical points of $\langle \Psi_{\mathcal{P}} | \mathcal{B} | \Psi_{\mathcal{P}} \rangle$ subject to the above constraints is by means of Lagrange multipliers. If we define $g_{i,k} = x_{i,k}^2 + y_{i,k}^2 - 1$

and $h_A = \sum_{i=0}^{2^{|A|}-1} [\psi_i^A]^2 - 1$ and associate the dual variables $\lambda_{i,k}$, μ_A to each of them, one can build the following Lagrangian function:

$$\mathcal{L}(\boldsymbol{x}, \boldsymbol{y}, \boldsymbol{\psi}, \boldsymbol{\lambda}, \boldsymbol{\mu}) = \langle \Psi_{\mathcal{P}} | \, \mathcal{B} \, | \Psi_{\mathcal{P}} \rangle + \sum_{i,k} \lambda_{i,k} g_{i,k} + \sum_A \mu_A h_A. \tag{B.1}$$

In practice, it is convenient to fix one of the measurements, *e.g.* $\mathcal{M}_0^i = \sigma_x$ (or, equivalently, $x_i, 0 = 1$ for all $i \in [n]$), since one can then apply a local rotation on the measurements and the inverse rotation on the quantum state without varying the value of $\langle \Psi_{\mathcal{P}} | \, \mathcal{B} \, | \Psi_{\mathcal{P}} \rangle$ [Tura *et al.*, 2015], which reduces the number of variables in the optimization.

From Eq. (B.1) one obtains a system of polynomial equations, such that one of their solutions (the minimal among the real ones) corresponds to $\beta_k^{\mathcal{P}}$. By means of Bézout's Theorem one can then upper bound the number of solutions in the generic case [Harris, 1992]. Let us recall that two algebraic curves of degrees m and n intersect at mn points (which may be real, complex, or at infinity) and, thus, cannot meet at more than mn points (given that they do not have a common component, which is generically the case).

To find the solutions of a system of polynomials involving p equations and p unknowns is a long-studied problem [Noether and van der Waerden, 1928], yet it still remains an area of intense research [Sturmfels, 2002]. In our case we have $p > 2$ equations, and therefore we are interested in generalizations of Bézout's theorem. For instance, generalizations based on the homotopy method (see e.g. [Wright, 1985; Garcia and Li, 1980; Kojima and Mizuno, 1983]) imply that, generically, the number of solutions is given by the product of the degrees of the p polynomials.

Therefore, we can upper bound the number of solutions from counting how many curves of which degree we have. To begin with, note that there is an equation for each variable involved in $\mathcal{L}$, which is $n + n + \sum_{A \in \mathcal{P}} 2^{|A|} + n + |\mathcal{P}| \leq 3n + (n/k)2^k + n/k \leq n(2^k/k + 4)$. Then, note that the degree of every polynomial is upper-bounded by the degree of $\mathcal{L}$, which is at most $n + 2$. Therefore, the upper bound

to the number of solutions is:

$$(n+2)^{n(2^k/k+4)}. \tag{B.2}$$

In order to find the solutions, one proceeds by calculating a Gröbner basis [Sturmfels, 2005, 2002] such that it solves the system of polynomials arising from Eq. (B.1). In the worst case, The computation of a Gröbner basis grows exponentially in complexity with the number of variables, which can even be doubly-exponential in very pathological cases [Faugère, 1999]. In practice, however, most current computer algebra routines find Gröbner basis in times nowhere near these complexity bounds [Faugère, 1999, 2002].

To conclude the discussion, let us briefly comment on the non-generic case. For instance, consider the most extreme case where all the polynomias have degree 1; *i.e.,* a system of linear equations, the most well-known cases. While systems of linear equations with non-trivial kernel arise in a variety of contexts, a random ε-perturbation on the system brings it to the generic case. Thus, the underlying structure of polynomial systems is extremely rigid, which gives rise to the above mentioned bounds in the worst-case. However, for the purposes of the present work, if necessary one can always take an ε-perturbation of the coefficients $\alpha^{i_1,\ldots,i_p}_{k_1,\ldots,k_p}$ of the DIWED. Therefore, we have seen that it is, in principle, possible to find exactly the k-producible bound of a DIWED of the form of in Equation (4.7).

B.1.1 Asymptotic analysis details

In this appendix we argue the approximation choice of $\sigma = \sqrt{n/48}$ employed in Section 4.6. As mentioned in the main text, an asymptotic analysis for the $k = n$-producible bound (*i.e.,* the maximal quantum violation) of the Bell inequality in Eq. (4.26) was performed in [Tura *et al.*, 2015]. However, for their case considered only the scaling was relevant. In our case we also need to determine the coefficient of the second order term, which we find exactly in what follows.

Let us start by recalling that the expectation value of the optimal state (cf. Eq. (4.29)) violating Eq. (4.26) can be expressed as [Tura *et al.*, 2015]:

$$\langle \mathcal{B} \rangle = \left(\frac{\beta_c}{n} - \frac{B}{2} + e^{-1/8\sigma} A' \right) n + (2B\sigma - A^2/2B + e^{-1/8\sigma} A') + O(\sigma/n), \tag{B.3}$$

where $A = 2\cos\theta$, $B = 4\cos^2\theta$ and $A' = -2\sin\theta$, with $\theta = 5\pi/6$ are the optimal asymptotic values. We use these values in order to determine the width σ of the Gaussian superposition of Dicke states, and we find that σ must fulfill

$$e^{-1/8\sigma}(n+1) = 48\sigma^2, \tag{B.4}$$

which is a transcendental equation. However, since in the first order the scaling of σ is $\sqrt{n}$, for large values of n we can ignore the $e^{-1/8\sigma}$ term. Hence, one can approximate σ as $\sigma = \sqrt{(n+1)/48} \approx \sqrt{n/48}$.

Appendix C

C.1 Alternative solution to the system of equations in Lemma 6.2.2

The idea is to turn Eq. (6.46) into an equivalent system which is much easier to solve. These mentioned equivalent system will form a reduced Groebner basis; *i.e.,* its first equation is a polynomial in a single variable, the second is a polynomial in the previous variable and a new one, etc. Therefore, one can then find all the solutions by solving only univariate polynomials and using the found roots to solve the subsequent equations by substitution. Let us start with a sequence of examples to illustrate the form of the polynomials $P(X)$.

- $n = 2$. Solving the system of equations

$$\begin{cases} x_1 + x_2 - z_1 &= 0 \\ x_1^2 + x_2^2 - z_2 &= 0 \end{cases} \tag{C.1}$$

  is equivalent to solving

$$\begin{cases} 2x_2^2 - 2z_1 x_2 + (z_1^2 - z_2) &= 0 \\ x_1 + x_2 - z_1 &= 0 \end{cases} \tag{C.2}$$

- $n = 3$. Solving the system of equations

$$\begin{cases} x_1 + x_2 + x_3 - z_1 &= 0 \\ x_1^2 + x_2^2 + x_3^2 - z_2 &= 0 \\ x_1^3 + x_2^3 + x_3^3 - z_3 &= 0 \end{cases} \tag{C.3}$$

is equivalent to solving

$$\begin{cases} 6x_3^3 - 6z_1x_3^2 + 3(z_1^2 - z_2)x_3 + (-z_1^3 + 3z_1z_2 - 2z_3) &= 0 \\ 2x_3^2 - 2(z_1 - x_2)x_3 + [(z_1 - x_2)^2 - (z_2 - x_2^2)] &= 0 \\ x_2 + x_3 - (z_1 - x_1) &= 0 \end{cases} \tag{C.4}$$

- $n = 4$. Solving the system of equations

$$\begin{cases} x_1 + x_2 + x_3 + x_4 - z_1 &= 0 \\ x_1^2 + x_2^2 + x_3^2 + x_4^2 - z_2 &= 0 \\ x_1^3 + x_2^3 + x_3^3 + x_4^3 - z_3 &= 0 \\ x_1^4 + x_2^4 + x_3^4 + x_4^4 - z_4 &= 0 \end{cases} \tag{C.5}$$

is equivalent to solving

$$\begin{cases} 24x_4^4 - 24z_1x_4^3 + 6(z_1^2 - z_2)x_4^2 \\ \quad -2(z_1^3 - 3z_1z_2 + 2z_3)x_4 + (z_1^4 - 6z_1^2z_2 + 3z_2^2 + 8z_1z_3 - 6z_4) = 0 \\ 6x_4^3 - 6(z_1 - x_3)x_4^2 + 3([z_1 - x_3]^2 - [z_2 - x_3^2])x_4 \\ \quad -([z_1 - x_3]^3 - 3[z_1 - x_3][z_2 - x_3^2] + 2[z_3 - x_3^3]) = 0 \\ 2x_4^2 - 2(z_1 - x_2 - x_3)x_4 + [(z_1 - x_2 - x_3)^2 - (z_2 - x_2^2 - x_3^2)] = 0 \\ x_2 + x_3 + x_4 - (z_1 - x_1) = 0 \end{cases} \tag{C.6}$$

From these examples one observes a clear recursion. Note that in the rewritten systems in Eq. (C.2), Eq. (C.4) and Equation (C.6) the first equation is a univariate polynomial in x_n. Then, note that the remaining equations correspond to systems of equations for $n-1$ with a slight transformation, where the index of x_i decreases in steps of 1; *i.e.*, $x_i \mapsto x_{i-1}$ with the substitution $z_i \mapsto z_i - x_{n-1}^i$ in the first equation, then $z_i \mapsto z_i - x_{n-2}^i$ in the second equation and so on until we substitute $z_1 \mapsto z_1 - x_1$ in the last equation. Let us note that, since the first equation is a polynomial in x_n, the second equation will be a polynomial in x_n, x_{n-1}, the third equation a polynomial in x_n, x_{n-1}, x_{n-2} and so on. Therefore, the transformed systems form a reduced Groebner basis, which makes it easily solvable.

Before considering the Groebner basis in its full generality, let us make the following observation:

Corollary C.1.1. *Let $P(X)$ be the first element of the Groebner basis for Eq. (6.46). Since the system of equations Eq. (6.46) is permutationally invariant, one has*

$$P(X) = (X - x_1) \cdots (X - x_n), \tag{C.7}$$

In other words, the roots of P correspond to the values of x_i up to a permutation.

Hence, by finding the general form of $P(X)$ we are done. Since the coefficients of $P(X)$ are closely related to the partitions of n, it is convenient to introduce the following definition:

Definition C.1.1. *Let $\boldsymbol{\lambda} \vdash m$ denote a partition of m; i.e., $\boldsymbol{\lambda} = (\lambda_1^{\mu_1}, \ldots \lambda_k^{\mu_k})$ where $\sum_{i=1}^{k} \mu_i \lambda_i = m$ and $\lambda_i > \lambda_{i+1}$ with $\lambda_i, \mu_i \in \mathbb{N}$. We define the polynomial*

$$Q_m(\boldsymbol{z}) := \sum_{\boldsymbol{\lambda} \vdash m} \xi_{\boldsymbol{\lambda}} \prod_{i=1}^{k} z_{\lambda_i}^{\mu_i}, \tag{C.8}$$

where

$$\xi_{\boldsymbol{\lambda}} = m! \prod_{i=1}^{k} \frac{(-1)^{\mu_i}}{\mu_i! \lambda_i^{\mu_k}}. \tag{C.9}$$

We define by convention $Q_0 := 1$.

It follows by definition that $\sum_{\boldsymbol{\lambda} \vdash m} |\xi_{\boldsymbol{\lambda}}| = m!$, since $\xi_{\boldsymbol{\lambda}}$ counts (with sign) the number of permutations of m elements of cycle type $\boldsymbol{\lambda}$. Moreover, note that the number of partitions $p(m)$ of a given integer m scales as $\log p(m) \sim C\sqrt{m}$, where C is a universal constant. Thus, already for modestly large values of m it is not possible to evaluate the sum Equation (6.6). Nevertheless, as we have shown in Section 6.2.3, it is possible to efficiently compute $Q_m(\boldsymbol{z})$ without splitting it into its different summands.

Definition C.1.2. *Let $P(X)$ be*

$$P(X) := \sum_{m=0}^{n} \frac{n!}{m!} Q_m(\boldsymbol{z}) X^{n-m}. \tag{C.10}$$

Therefore, we now know how to obtain the $\boldsymbol{x}$ that satisfy $\boldsymbol{z}$ in Eq. (6.46). Our next step is to consider the system of equations that arises from Eq. (6.37). Since Equation (6.46) does not take into consideration the z_0 term, we incorporate the condition that $A_0 \propto \mathbb{1}$. Then, the system of equations we are interested in becomes Eq. (6.47).

The system of equations Eq. (6.46) is also known as the power sum ideal, and its reduced Groebner Basis can be found as the elimination ideal of the power sums.

Corollary C.1.2. *The elimination ideal of the power sums provides the compatibility conditions on the weights d_k of Eq. (6.36) for the state to be representable with a diagonal TI MPS of bond dimension $D < n$.*

For instance, let us consider the case $n = 4$ and $D = 3$. Then, the elimination ideal of the power sums of three variables and degree four is

$$\begin{aligned}&\langle x_1 + x_2 + x_3 - z_1, x_1^2 + x_2^2 + x_3^2 - z_2, \\ &\qquad x_1^3 + x_2^3 + x_3^3 - z_3, x_1^4 + x_2^4 + x_3^4 - z_4\rangle \cap \mathbb{K}[z_1, z_2, z_3, z_4] \\ &= \langle q(z_1, z_2, z_3, z_4)\rangle,\end{aligned} \tag{C.11}$$

where

$$q(z_1, z_2, z_3, z_4) = z_1^4 - 6z_1^2 z_2 + 3z_2^2 + 8z_1 z_3 - 6z_4 \tag{C.12}$$

Note that the compatibility polynomial in Eq. (C.12) is precisely the same polynomial $Q_4(\boldsymbol{z})$ that appears in the constant term of the univariate polynomial in Eq. (C.6). Therefore, the symmetric Dicke states that can be represented as a diagonal TI MPS of the form $A_0 \propto \mathbb{1}$ and $A_1 = \mathrm{diag}(\boldsymbol{x})$ are those for which their corresponding $\boldsymbol{z}$ belongs to the elimination ideal of the power sums of D variables with degree n.

C.2 Linear programming approach for diagonal Dicke states

In this section we want to apply Eq. (6.13) in a more systematic way in order to determine that the states of the Dicke basis are the only

possible ones in which Corollary 6.2.1 applies.

Let ρ be a rank-1 projector onto a quantum state of the form in Eq. (6.36). By virtue of Eq. (6.6), we have

$$\sigma_\beta^\alpha = \sum_{p=0}^{n-m} \sqrt{\frac{\binom{m}{\alpha}\binom{m}{\beta}}{\binom{n}{\alpha+p}\binom{n}{\beta+p}}} \binom{n-m}{p} d^*_{\alpha+p} d_{\beta+p}, \tag{C.13}$$

where we write α instead of $\boldsymbol{\alpha}$ since for qubits the partition of n is identified by a single number.

- If we set $d_\alpha = \delta(\alpha - k)$ then we have

$$\sigma_\beta^\alpha = \delta(\alpha-\beta)\binom{n}{k}^{-1}\binom{m}{\alpha}\binom{n-m}{k-\alpha} I_{[0,n-m]}(k-\alpha), \tag{C.14}$$

  where $I_S(x)$ is the indicator function, which evaluates to 1 if $x \in S$ and 0 otherwise. This allows us to write the set of equations for any basis Dicke state:

$$\begin{aligned} &\sum_{p=0}^{n-m} \rho^{\alpha+p}_{\beta+p} \sqrt{\frac{\binom{m}{\alpha}\binom{m}{\beta}}{\binom{n}{\alpha+p}\binom{n}{\beta+p}}} \binom{n-m}{p} \\ &\quad = \delta(\alpha-\beta)\binom{n}{k}^{-1}\binom{m}{\alpha}\binom{n-m}{k-\alpha} I_{[0,n-m]}(k-\alpha). \end{aligned} \tag{C.15}$$

  – If we take $m = n-1$, we recover the result of Corollary 6.2.1 in the following way: Since we have that

$$\sigma = \binom{n}{k}^{-1} \sum_{\alpha=k-1}^{k} \binom{n-1}{\alpha} |\alpha\rangle \langle\alpha|, \tag{C.16}$$

  the conditions of the SdP Equation (6.13) can be now rewritten as

$$\sum_{p=0}^{1} \rho^{\alpha+p}_{\beta+p} \sqrt{\frac{\binom{n-1}{\alpha}\binom{n-1}{\beta}}{\binom{n}{\alpha+p}\binom{n}{\beta+p}}} \binom{1}{p} = \delta(\alpha-\beta)\binom{n-1}{\alpha}\binom{n}{k}^{-1} I_{[0,1]}(k-\alpha). \tag{C.17}$$

Note that the right hand side of Equation (C.17) is zero if $\alpha > k$ or $\alpha < k-1$. In these cases, in the diagonal ($\alpha = \beta$) we have the following condition:

$$\rho_{\alpha}^{\alpha}\xi_{\alpha} + \rho_{\alpha+1}^{\alpha+1}\xi_{\alpha+1} = 0, \tag{C.18}$$

for some $\xi_{\alpha} > 0$. Next, note that the semidefinite positivity condition on ρ from the SdP Eq. (6.13) implies that the diagonal elements must be non-negative; *i.e.,* $\rho_{\alpha}^{\alpha} \geq 0$. Hence, for all $\alpha \geq k+1$ and $\alpha \leq k-2$ we must have that $\rho_{\alpha}^{\alpha} = \rho_{\alpha+1}^{\alpha+1} = 0$. Moreover, the condition $\rho \succeq 0$ further implies that all the elements in the respective rows and columns must be zero. Thus, the only non-zero element ρ_{α}^{α} left is ρ_{k}^{k}, which must be 1 by virtue of Eq. (C.17).

– If we trace out two parties (*i.e.,* $m = n-2$), we proceed similarly. In particular, note that for $\alpha > k$ or $\alpha < k-2$ we have a condition in the diagonal similar to the form of Eq. (C.18)

$$\rho_{\alpha}^{\alpha}\xi_{\alpha} + \rho_{\alpha+1}^{\alpha+1}\xi_{\alpha+1} + \rho_{\alpha+2}^{\alpha+2}\xi_{\alpha+2} = 0. \tag{C.19}$$

Again, in Eq. (C.19) we have a linear combination of $\rho_{\alpha+p}^{\alpha+p} \geq 0$ (since $\rho \succeq 0$) with strictly positive weights $\xi_{\alpha+p}^{\alpha+p} > 0$. Thus, we have that $\rho_{\alpha}^{\alpha} = 0$ for $\alpha \neq k$, and a similar argument follows. However, one has to be wary about counting the number of zero and non-zero equations, since one needs $n > 4$ for Eq. (C.19) to exist. To this end, lets look at the general case:

– If we trace out $n-m$ parties, then we generalize the last two points: For $\alpha > k$ or $\alpha < k-(n-m)$ the condition on the diagonal is

$$\sum_{p=0}^{n-m} \rho_{\alpha+p}^{\alpha+p}\xi_{\alpha+p} = 0, \tag{C.20}$$

which implies $\rho_{k+1+p}^{k+1+p} = \rho_{k-1-p}^{k-1-p} = 0$ for $p \geq 0$. This condition is non-trivial as long as the number of equations $(m-1)$ is

greater than the number of non-zero left hand sides $(n - m + 1)$; *i.e.,* whenever $m > n/2$. Thus, the condition $\rho \succeq 0$ implies that all the off-diagonal elements must be zero and, therefore, $\rho_k^k = 1$.

– Suppose we trace out $n - m$ parties, which results in the following system of equations:

$$\begin{pmatrix} \binom{n-m}{0} & \binom{n-m}{1} & \cdots & \binom{n-m}{n-m} & \cdots & 0 \\ 0 & \binom{n-m}{0} & \cdots & \binom{n-m}{n-m-1} & \cdots & 0 \\ \vdots & \vdots & \ddots & \vdots & \ddots & \vdots \\ 0 & 0 & \cdots & \binom{n-m}{n-2m} & \cdots & \binom{n-m}{n-m} \end{pmatrix} \begin{pmatrix} x_0 \\ x_1 \\ \vdots \\ x_{n-m} \\ \vdots \\ x_n \end{pmatrix}$$

$$= \begin{pmatrix} \binom{n-m}{k} I_{[0,n-m]}(k) \\ \binom{n-m}{k-1} I_{[0,n-m]}(k-1) \\ \vdots \\ \binom{n-m}{k-m} I_{[0,n-m]}(k-m) \end{pmatrix}, \tag{C.21}$$

where we have defined $x_p := \rho_p^p \binom{n}{k} / \binom{n}{p}$. If $m > n/2$, then there must necessarily be zeroes in the right hand side of Eq. (C.21).

To conclude, let us comment that characterizing the uniqueness of solutions of linear programs [Mangasarian, 1984] and semidefinite programs [Zhu *et al.*, 2010; Alfakih, 2007] remains an intensive field of research, with high interest due to its connection to rigidity theory. For instance, the general solution to the uniqueness of Eq. (6.15) can be expressed via the following theorem:

Theorem C.2.1. *[Zhu et al., 2010] If ρ is a max-rank solution of Eq. (6.15), and we write $\rho = L^\dagger L$, where $L \in \mathbb{C}^{r \times n}$, then ρ is the unique solution of Eq. (6.15) if, and only if, the kernel of the linear space spanned by $L^\dagger A_\beta^\alpha L$ is trivial.*

Corollary C.2.1. *[Zhu et al., 2010] If all the solutions to Equation (6.15) share the same rank, then the solution must be unique.*

Appendix D

D.1 5-dimensional three-outcome two-body symmetric Bell inequalities

Some families of 3-level 2-body PIBI in 5-dimensions (6-dimensional affine vector space) shown in Eq. (7.7).

5-dim case						
Family	β_c	α_1	α_2	α_3	α_4	α_5
1	0	1	1	-2	2	-2
2	4	-2	1	2	0	2
3	0	1	1	0	0	-2
4	12	-6	1	4	2	4
5	24	-6	1	4	0	0

D.2 Classical bound for inequality Equation (7.8)

The inequality [0 1 1 0 0 -2] corresponds to the 5-dimensional (6-dimensional affine vector space) case after having symmetrized the

inputs and outputs. It looks as follows:

$$\begin{aligned} I =& 0 + 1(\mathcal{P}_{0|0} + \mathcal{P}_{0|1} + \mathcal{P}_{1|0} + \mathcal{P}_{1|1}) + 1(\mathcal{P}_{00|00} + \mathcal{P}_{00|11} + \mathcal{P}_{11|00} + \mathcal{P}_{11|11}) + \\ &+ 0(\mathcal{P}_{00|01} + \mathcal{P}_{11|01}) + 0(\mathcal{P}_{01|00} + \mathcal{P}_{01|11}) - 2(\mathcal{P}_{01|01} + \mathcal{P}_{01|10}) \\ =& (\mathcal{P}_{0|0} + \mathcal{P}_{0|1} + \mathcal{P}_{1|0} + \mathcal{P}_{1|1}) + (\mathcal{P}_{00|00} + \mathcal{P}_{00|11} + \mathcal{P}_{11|00} + \mathcal{P}_{11|11}) \\ &- 2(\mathcal{P}_{01|01} + \mathcal{P}_{01|10}). \end{aligned} \tag{D.1}$$

We want to prove that the classical bound is zero, *i.e.* $\beta_c = 0$. First we apply the inequality coefficients and the local deterministic strategy (see Section 7.2.1). After rearranging the terms one ends up with the following polynomial:

$$\begin{aligned} I =& (c_{00} + c_{02})^2 + (c_{00} + c_{20})^2 + (c_{11} + c_{12})^2 + (c_{11} + c_{21})^2 \\ &+ (c_{00} - c_{12})^2 + (c_{00} - c_{21})^2 + (c_{11} - c_{02})^2 + (c_{11} - c_{20})^2 \\ &+ 2(c_{10} + c_{01}) - 2(c_{00} + c_{11})^2 - (c_{12} + c_{20})^2 - (c_{02} + c_{21})^2, \end{aligned} \tag{D.2}$$

where $c_{i,j} \geq 0$ for all $i, j \in \{0, 1, 2\}$ and they fulfill the constraint $\sum_{0 \leq i,j < 3} c_{ij} = n$ with n the total number of parties. Notice that the term c_{22} does not appear in the expression, thus we can set any $0 \leq c_{22} \leq n$ without contributing in the classical bound. Thus it is trivial to see that there exists at least one strategy leading to $I = 0$, *i.e.* setting $c_{22} = n$. Therefore if we can proof that I cannot take negative values, then we are done.

Proof that $I \geq 0$. We are interested in the minimal value that (D.2) can achieve. Since the terms $2(c_{10} + c_{01})$ will always add a positive or zero contribution, we can set them to $c_{10} = c_{01} = 0$ without loss of generality to find the minimal value of I. Therefore we simplify the problem to look at the minimal value of:

$$\begin{aligned} \tilde{I} \;=\; & (c_{00} + c_{02})^2 + (c_{00} + c_{20})^2 + (c_{11} + c_{12})^2 + (c_{11} + c_{21})^2 \\ & + (c_{00} - c_{12})^2 + (c_{00} - c_{21})^2 + (c_{11} - c_{02})^2 + (c_{11} - c_{20})^2 \\ & - 2(c_{00} + c_{11})^2 - (c_{12} + c_{20})^2 - (c_{02} + c_{21})^2. \end{aligned} \tag{D.3}$$

After expanding and rearranging the terms we reach the following equivalent polynomial:

$$\begin{aligned}\tilde{I} \;=\; & 2\Bigg[c_{00}^2 + c_{11}^2 + \frac{c_{02}^2 + c_{20}^2}{2} + \frac{c_{12}^2 + c_{21}^2}{2} \\ & + c_{00}(c_{02} + c_{20}) - c_{11}(c_{02} + c_{20}) + c_{11}(c_{12} + c_{21}) - c_{00}(c_{12} + c_{21}) \\ & - c_{02}c_{21} - c_{12}c_{20} - 2c_{00}c_{11}\Bigg]. \end{aligned} \tag{D.4}$$

Then, the condition for (D.4) to take negative values is the following:

$$\begin{gathered} c_{11}(c_{02} + c_{20}) + c_{00}(c_{12} + c_{21}) + c_{02}c_{21} + c_{12}c_{20} + 2c_{00}c_{11} \\ > \\ c_{00}^2 + c_{11}^2 + \tfrac{c_{02}^2 + c_{20}^2}{2} + \tfrac{c_{12}^2 + c_{21}^2}{2} + c_{00}(c_{02} + c_{20}) + c_{11}(c_{12} + c_{21}) \quad , \end{gathered} \tag{D.5}$$

which can be rearranged as:

$$(c_{00} - c_{11})(c_{12} + c_{21} - c_{02} - c_{20}) > (c_{00} - c_{11})^2 + \frac{(c_{02} - c_{21})^2}{2} + \frac{(c_{12} - c_{20})^2}{2}. \tag{D.6}$$

Our goal is to find that such condition leads to a contradiction for all cases, which would show that I cannot take a negative value.

First, it is convenient to define the variables $x := c_{00} - c_{11}, y := c_{12} - c_{20}, z := c_{02} - c_{21}$, so that the condition gets expressed as:

$$x(y - z) - \left(x^2 + \frac{y^2}{2} + \frac{z^2}{2}\right) > 0. \tag{D.7}$$

Take now $f(x, y, z) = x(y - z) - x^2 + \frac{y^2}{2} + \frac{z^2}{2}$ in order to find its critical points $\nabla f(x, y, z) = (2x - y + z, y - x, z + x)$, $\nabla f(x^*, y^*, z^*) = 0 \Rightarrow x^* = y^*, z^* = -x^*$. Next, by looking at its Hessian matrix $\boldsymbol{H}\left(f(x, y, z)\right)$, where $\left(\boldsymbol{H}\left(f(x, y, z)\right)\right)_{ij} = \frac{\partial^2 f}{\partial x_i \partial x_j}$, one sees that the resulting Hessian matrix has eigenvalues $\{-3, -1, 0\}$ and therefore it is negative semidefinite. Thus, the critical point corresponds to the maximum.

We conclude that (D.7) leads to a contradiction for all values of c_{ij} and, consequently, I cannot take negative values. Finally, since the argument is independent of n and we have seen that $I = 0$ is a valid local deterministic strategy, it follows that the classical bound is $\beta_c = 0$ for all n.

□

D.3 Details, theorem proof and examples for Section 7.3.1

Proof for Theorem 7.3.1. Let us start by noting that if V_k contains the orthonormal eigenstates of U_k as its columns, then $U_k = V_k D_k V_k^\dagger$, where D_k is a diagonal matrix containing its eigenvalues. Since all U_k have the same spectrum and the V_k are written in the order defined above, it follows that all D_k are equal. Therefore, we can write $D_k = \mathrm{Diag}(\sigma(U_0))$.

Let us now prove that g_k always exists, and how to find it: This follows from the fact that V_k is unitary, therefore it has orthonormal eigenvectors and eigenvalues of the form $e^{\mathbb{i}\psi_{k,i}}$, with $\psi_{k,i} \in [0, 2\pi)$. Hence, it diagonalizes as $V_k = W_k e^{\mathbb{i}\Psi_k} W_k$, where Ψ_k is a diagonal matrix containing the phases $\psi_{k,i}$ in its diagonal. Therefore, using the following property of the matrix exponential: $Ae^B A^{-1} = e^{ABA^{-1}}$, for invertible A, we can write $V_k = W_k e^{\mathbb{i}\Psi_k} W_k^\dagger = e^{\mathbb{i}W_k\Psi_k W_k^\dagger}$. Hence, we find $g_k = W_k \Psi_k W_k^\dagger$ and we see that it is Hermitian.

The idea now is simple: in order to "combine" different unitaries U_k to obtain new ones, it is hard to do so with their unitary form, as this yields very nonlinear equations. However, we can move this combination to the Hermitian g_k we have obtained, as they form a $\mathbb{R}$-vector space. Hence, we consider $g(\boldsymbol{\theta})$ defined as in Equation (7.16), which implements that combination, with the property that $g(\mathbf{0}) = g_0$ and $g(\boldsymbol{\theta_i}) = g_i$.

To conclude, we observe that since $U_k = e^{\mathbb{i}g_k}\mathrm{Diag}(\sigma(U_0))e^{-\mathbb{i}g_k}$, it suffices to change g_k by $g(\boldsymbol{t})$ to obtain the desired interpolating function

$U(\boldsymbol{\theta})$ in Equation (7.17).

Example. Let us take $d = 2$ and take $\sigma(U_0) = \{1, -1\}$. Let us further take $U_0 = \sigma_x$ and $U_1 = \sigma_z$. Then we see that g_1 is the zero-matrix and that $g_0 = \frac{\pi}{4-2\sqrt{2}} \begin{pmatrix} 3-2\sqrt{2} & 1-\sqrt{2} \\ 1-\sqrt{2} & 1 \end{pmatrix}$. A simple calculation shows that $e^{\mathbb{i}g_0} = H$, where H is the Hadamard matrix, so that $X = HZH^\dagger$. Let us consider the uniparametric family of Hermitian matrices $g(\theta) = (1-\theta)g_0$, yielding the family of Unitary matrices $U(\theta) = e^{\mathbb{i}g(\theta)} Z e^{-\mathbb{i}g(\theta)}$. This describes the following family of unitaries:

$$U(t) = \cos(\pi\theta/2)^2\sigma_x - \frac{1}{\sqrt{2}}\sin(\pi\theta)\sigma_y + \sin(\pi\theta/2)^2\sigma_z$$

.

Let us comment about the approximation power of $U(\boldsymbol{\theta})$; i.e., given a unitary matrix U with the same spectrum as each of the U_k, we would like to find out under which conditions there exists a $\boldsymbol{\theta} \in \mathbb{R}^m$ such that $\inf_{\boldsymbol{\theta}\in\mathbb{R}^m} ||U(\boldsymbol{\theta}) - U|| = 0$. This is important for optimization, as we want $U(\boldsymbol{\theta})$ to be able to represent any unitary U with a fixed spectrum.

Theorem D.3.1. *Let U be a unitary $d \times d$ matrix and $\{U_0, \ldots, U_M\}$ a family of unitaries with the same spectrum as U. Let g (g_k) be a $d \times d$ Hermitian matrix such that $U = e^{\mathbb{i}g}\mathrm{Diag}(\sigma(U))e^{-\mathbb{i}g}$ ($U_k = e^{\mathbb{i}g_k}\mathrm{Diag}(\sigma(U))e^{-\mathbb{i}g_k}$). Then $U = U(\boldsymbol{\theta}^*)$ for some $\boldsymbol{\theta}^* \in \mathbb{R}^M$ if g is a $\mathbb{R}$-linear combination of $g_0, \ldots, g_M$.*

Proof. Since g is a linear combination of $g_0, \ldots, g_M$, there exists a $\boldsymbol{\theta}^* \in \mathbb{R}^m$ such that $g(\boldsymbol{\theta}^*) = g$. Hence, $U(\boldsymbol{\theta}) = U$ at $\boldsymbol{\theta} = \boldsymbol{\theta}^*$.

The converse of Theorem D.3.1 holds, but in principle $\boldsymbol{\theta}^*$ does not need to be unique.

Theorem D.3.2. *Let U (U_k), g (g_k) be defined as in Theorem D.3.1. Let us further assume that all the eigenvalues of U are different. Then, if $U = U(\boldsymbol{\theta}^*)$, $e^{\mathbb{i}g(\boldsymbol{\theta}^*)} = e^{\mathbb{i}\Phi}e^{\mathbb{i}g}$, where $e^{\mathbb{i}\Phi}$ is a diagonal matrix that contains arbitrary complex phases.*

D.4 Analytical expressions for the multinomials in Equation (7.22)

Recall that we are dealing with the 2-body RDM of the gaussian superposition of Dicke states presented in Eq. (7.20), whose components follow the expression in Eq. (7.22). First we explicitly do the case for the first component of the 2-body RDM in the computational basis. The first component corresponds to $\vec{i} = \vec{j} = (0,0)$, for which $w(\vec{i}) = (2,0,0)$. Then:

$$\begin{aligned}
\sigma^{(0,0)}_{(0,0)} &= \sum_{\vec{k}\vdash n-2} c_{\vec{k}+(2,0,0)} c^*_{\vec{k}+(2,0,0))} \frac{\binom{n-2}{\vec{k}}}{\sqrt{\binom{n}{\vec{k}+(2,0,0)}\binom{n}{\vec{k}+(2,0,0)}}} = \\
&= \sum_{\vec{k}\vdash n-2} c_{\vec{k}+(2,0,0)} c^*_{\vec{k}+(2,0,0))} \frac{(n-2)!(k_0+2)!k_1!k_2!}{n!k_0!k_1!k_2!} = \\
&= \sum_{\vec{k}\vdash n-2} c_{\vec{k}+(2,0,0)} c^*_{\vec{k}+(2,0,0))} \frac{(k_0+2)(k_0+1)}{n(n-1)}.
\end{aligned} \tag{D.8}$$

Now, instead of listing explicitely all the possible combinations $\vec{i}, \vec{j} \in [3]^2$, let us rearrange the multinomial as

$$\sqrt{\frac{\binom{n-2}{\vec{k}}}{\binom{n}{\vec{k}+w(\vec{i})}}}\sqrt{\frac{\binom{n-2}{\vec{k}}}{\binom{n}{\vec{k}+w(\vec{j})}}} = \frac{\sqrt{f(\vec{i})f(\vec{j})}}{n(n-1)}, \tag{D.9}$$

where the values of $f(\vec{i})$ are easy to find and are listed in Table D.1. Notice that due to the permutationally invariance symmetry there we skip from listing some terms that will have the same result (*e.g.* $f((0,1)) = f((1,0))$).

Table D.1 Values to obtain the multinomial coefficients in Equation (D.9)

$\vec{i}$		$f(\vec{i})$
$(0,0)$	$=$	$(k_0+2)(k_0+1)$
$(0,1)$	$=$	$(k_0+1)(k_1+1)$
$(1,1)$	$=$	$(k_1+2)(k_1+1)$
$(1,2)$	$=$	$(k_1+1)(k_2+1)$
$(0,2)$	$=$	$(k_0+1)(k_2+1)$
$(2,2)$	$=$	$(k_2+2)(k_2+1)$

D.5 Symmetric representation of the spin operators used in hamiltonian Equation (7.24)

Following the notation introduced in Section 2.1, we denote a qudit Dicke state as $|\boldsymbol{\lambda}\rangle$ where $\boldsymbol{\lambda}$ is a partition of n in d elements, *i.e.* a vector of d non-negative integers that sum n. In Chapter 7 we are interested in the qutrits case $d=3$ corresponding to $\boldsymbol{\lambda}=(\lambda_0,\lambda_1,\lambda_2)$.

Then, the spin operators defined in Section 7.4.2 can be projected

onto the symmetric space as follows:

$$\begin{aligned}
\Pi\tilde{\mathcal{S}}_{ii}\Pi^\dagger &= \frac{2}{\sqrt{2}}\sum_{\boldsymbol{\lambda}} |\boldsymbol{\lambda}\rangle\langle\boldsymbol{\lambda}|\,\lambda_i, \quad \text{for } i \in \{0,1,2\} \\
\Pi\tilde{\mathcal{S}}_{01}\Pi^\dagger &= \sum_{\boldsymbol{\lambda},\boldsymbol{\mu}} \frac{\binom{n}{\boldsymbol{\mu}}}{\sqrt{2\binom{n}{\boldsymbol{\lambda}}\binom{n}{\boldsymbol{\mu}}}} \left(\mu_0\delta(\boldsymbol{\lambda},\boldsymbol{\mu}+(-1,1,0)) + (\mu_1\delta(\boldsymbol{\lambda},\boldsymbol{\mu}+(1,-1,0))\right) \\
\Pi\tilde{\mathcal{S}}_{02}\Pi^\dagger &= \sum_{\boldsymbol{\lambda},\boldsymbol{\mu}} \frac{\binom{n}{\boldsymbol{\mu}}}{\sqrt{2\binom{n}{\boldsymbol{\lambda}}\binom{n}{\boldsymbol{\mu}}}} \left(\mu_0\delta(\boldsymbol{\lambda},\boldsymbol{\mu}+(-1,0,1)) + (\mu_2\delta(\boldsymbol{\lambda},\boldsymbol{\mu}+(1,0,-1))\right) \\
\Pi\tilde{\mathcal{S}}_{12}\Pi^\dagger &= \sum_{\boldsymbol{\lambda},\boldsymbol{\mu}} \frac{\binom{n}{\boldsymbol{\mu}}}{\sqrt{2\binom{n}{\boldsymbol{\lambda}}\binom{n}{\boldsymbol{\mu}}}} \left((\mu_1\delta(\boldsymbol{\lambda},\boldsymbol{\mu}+(0,-1,1)) + \mu_2\delta(\boldsymbol{\lambda},\boldsymbol{\mu}+(0,1,-1))\right),
\end{aligned} \tag{D.10}$$

where δ is the Kronecker Delta function and we have used the multinomial combinatorial expression:

$$\binom{n}{\boldsymbol{\lambda}} = \frac{n!}{\lambda_0!\lambda_1!\lambda_2!}. \tag{D.11}$$

The methodology to obtain the spin operators follows the same reasoning as the methodology presented in [Tura *et al.*, 2015].

Acronyms

AFM Antiferromagnetic 131, 133–138, 140, 152

BDD Best Diagonal Dominant 53–55
BEC Bose-Einstein condensation 3, 15, 96, 98, 100, 130, 165, 192, 199, 200
BSA Best Separable Approximations 54

CP Completely Positive 42, 43, 45–47, 49–53

DI Device-Independent 2, 3, 7, 8, 33, 34, 98, 101, 191, 195
DIQIP Device-Independent Quantum Information Processing 2, 28, 34, 158
DIWED Device-Independent Witness of Entanglement Depth 8, 9, 65–67, 70, 75, 81–83, 85–88, 90, 91, 93–101, 112, 113, 194–196
DMRG Density Matrix Renormalization Group 109–112, 114, 115, 118, 130, 143, 146–148, 151, 152, 158, 198
DNN Doubly Non-Negative 43, 47, 49, 50, 52
DS Diagonal Symmetric 41, 43–50, 52

DSS Diagonal Symmetric States 5, 6, 40, 41, 43–47, 49–58, 192, 193

ED Exact Diagonalization 134–138, 141
EE Entanglement Entropy 111–113, 118–120, 132–134, 136–139, 143–145
EW Entanglement Witness 26–28, 52, 53, 66

FM Ferromagnetic 107, 108, 112, 114, 116, 131–140, 152, 153

GME Genuinely Multipartite Entanglement 7, 25, 63, 64, 117

HP Holstein-Primakoff 114, 116

LDS Local Deterministic Strategy 31, 168–171, 173–175
LHS Left hand side 33, 43
LHVM Local Hidden Variable Model 30, 31, 35–37, 167, 168
LMG Lipkin-Meshkov-Glick 5, 15, 20, 107, 130–133, 136, 142, 143, 166, 188, 190, 199, 200
LP Linear Programming 176
LSW Linear spin wave 104, 112, 114–118, 120

MPS Matrix Product States 130, 153–155, 158

NS Non-Signalling 32, 33, 183

PI Permutationally Invariant 19, 20, 130, 150

PIBI Permutationally Invariant Bell Inequality 37, 38, 67, 68, 71, 75, 78, 80, 81, 85, 104, 105, 107, 109, 111, 112, 114, 115, 117–121, 131, 148–153, 168, 172, 182–184, 186–188, 190, 195–197, 199, 200

PM Paramagnetic 108, 112, 116, 134–136

POVM Positive-Operator Valued Measure 31, 76

PPT Positive under Partial Transposition 4, 6, 25–27, 39, 40, 43, 47, 49, 50, 52–58, 79, 80, 192, 193

QCP Quantum Critical Point 10, 11, 104, 105, 107, 108, 111–119, 121, 133, 191, 192, 195–197, 200

QIP Quantum Information Processing 2, 4, 12, 34, 122, 192

QIT Quantum Information Theory 2, 6

QMA Quantum Merlin-Arthur 12

QMP Quantum Marginal Problem 11–15, 121, 122, 127, 129, 158, 159, 196, 198, 199

RDM Reduced Density Matrix 11–13, 110, 118, 121, 122, 124, 127, 130–133, 145, 146, 150, 151, 160–163, 183, 185–187, 189, 197

RHS Right hand side 43

SDP Semidefinite Programming 8, 15, 76, 78–80, 82, 84, 87, 89, 90, 122, 127–129, 131, 134, 143, 145, 146, 161, 163, 168, 173, 174, 176, 180, 182–184, 196, 198–200

TFIM Transverse-field Ferromagnetic Ising Model 107–109, 112, 113, 115, 119, 120, 196

TI Translationally-Invariant 153–155, 158

VM Variational Method 131–148, 150–153, 182, 183, 185, 197, 198

Bibliography

(2009). The MOSEK optimization software.

(2013). *Semidefinite Optimization and Convex Algebraic Geometry*. SOC FOR INDUSTRIAL & APPLIED M.

A. J. Coleman, V.I.Y. (2000). *Reduced Density Matrices*. Springer Berlin Heidelberg.

Acín, A., Brunner, N., Gisin, N., Massar, S., Pironio, S. and Scarani, V. (2007). Device-independent security of quantum cryptography against collective attacks. *Phys. Rev. Lett.*, **98**, 230501.

Alcaraz, F.C. and Malvezzi, A.L. (1995). Critical and off-critical properties of the XXZ chain in external homogeneous and staggered magnetic fields. *Journal of Physics A: Mathematical and General*, **28**, 1521–1534.

Alfakih, A.Y. (2007). On dimensional rigidity of bar-and-joint frameworks. *Discrete applied mathematics*, **155**, 1244–1253.

Aloy, A., Tura, J., Baccari, F., Acín, A., Lewenstein, M. and Augusiak, R. (2019). Device-independent witnesses of entanglement depth from two-body correlators. *Physical Review Letters*, **123**, 100507.

Aloy, A., Fadel, M. and Tura, J. (2020). The quantum marginal problem for symmetric states: applications to variational optimization, nonlocality and self-testing. *arXiv preprint arXiv:2001.04440*.

Alsina, D., Cervera, A., Goyeneche, D., Latorre, J.I. and Życzkowski, K. (2016). Operational approach to bell inequalities: Application to qutrits. *Physical Review A*, **94**, 032102.

Amico, L., Fazio, R., Osterloh, A. and Vedral, V. (2008). Entanglement in many-body systems. *Rev. Mod. Phys.*, **80**, 517–576.

Anderson, M.H., Ensher, J.R., Matthews, M.R., Wieman, C.E. and Cornell, E.A. (1995). Observation of bose-einstein condensation in a dilute atomic vapor. *science*, 198–201.

Apellaniz, I., Lücke, B., Peise, J., Klempt, C. and Tóth, G. (2015). Detecting metrologically useful entanglement in the vicinity of dicke states. *New Journal of Physics*, **17**, 083027.

Aspect, A., Grangier, P. and Roger, G. (1982). Experimental realization of einstein-podolsky-rosen-bohm gedankenexperiment: A new violation of bell's inequalities. *Phys. Rev. Lett.*, **49**, 91–94.

Augusiak, R., Tura, J., Samsonowicz, J. and Lewenstein, M. (2012). Entangled symmetric states of n qubits with all positive partial transpositions. *Physical Review A*, **86**, 042316.

Augusiak, R., Demianowicz, M. and Acín, A. (2014). Local hidden–variable models for entangled quantum states. *Journal of Physics A: Mathematical and Theoretical*, **47**, 424002.

Augusiak, R., Demianowicz, M., Tura, J. and Acín, A. (2015). Entanglement and nonlocality are inequivalent for any number of parties. *Phys. Rev. Lett.*, **115**, 030404.

Augusiak, R., Demianowicz, M. and Tura, J. (2018). Constructions of genuinely entangled multipartite states with applications to local

hidden variables (LHV) and states (LHS) models. *Physical Review A*, **98**.

Augusiak, R., Salavrakos, A., Tura, J. and Acín, A. (2019). Bell inequalities tailored to the greenberger–horne–zeilinger states of arbitrary local dimension. *New Journal of Physics*, **21**, 113001.

Aulbach, M. (2012). Classification of entanglement in symmetric states. *International Journal of Quantum Information*, **10**, 1230004.

Babai, L., Fortnow, L. and Lund, C. (1991). Non-deterministic exponential time has two-prover interactive protocols. *Computational Complexity*, **1**, 3–40.

Baccari, F. (2019). *Certification of many-body systems*. Ph.D. thesis.

Baccari, F., Tura, J., Fadel, M., Aloy, A., Bancal, J.D., Sangouard, N., Lewenstein, M., Acín, A. and Augusiak, R. (2019). Bell correlation depth in many-body systems. *Physical Review A*, **100**, 022121.

Baccari, F., Augusiak, R., Šupić, I., Tura, J. and Acín, A. (2020). Scalable bell inequalities for qubit graph states and robust self-testing. *Physical Review Letters*, **124**, 020402.

Bachoc, C., Gijswijt, D.C., Schrijver, A. and Vallentin, F. (2012). Invariant semidefinite programs. In *Handbook on semidefinite, conic and polynomial optimization*, 219–269, Springer.

Bamps, C. and Pironio, S. (2015). Sum-of-squares decompositions for a family of Clauser-Horne-Shimony-Holt-like inequalities and their application to self-testing. *Physical Review A*, **91**.

Bancal, J.D., Gisin, N. and Pironio, S. (2010). Looking for symmetric bell inequalities. *Journal of Physics A: Mathematical and Theoretical*, **43**, 385303.

Bancal, J.D., Brunner, N., Gisin, N. and Liang, Y.C. (2011a). Detecting genuine multipartite quantum nonlocality: A simple approach and generalization to arbitrary dimensions. *Physical Review Letters*, **106**.

Bancal, J.D., Gisin, N., Liang, Y.C. and Pironio, S. (2011b). Device-independent witnesses of genuine multipartite entanglement. *Phys. Rev. Lett.*, **106**, 250404.

Barreiro, J., Bancal, J.D., Schindler, P., Nigg, D., Hennrich, M., Monz, T., Gisin, N. and Blatt, R. (2013). Demonstration of genuine multipartite entanglement with device-independent witnesses. *Nature Physics*, **9**, 559 EP –, article.

Barrett, M., Sauer, J. and Chapman, M. (2001). All-optical formation of an atomic bose-einstein condensate. *Physical Review Letters*, **87**, 010404.

Bell, J.S. (1964). On the einstein podolsky rosen paradox. *Physics*, **1**, 195–200.

Bennett, C.H., Brassard, G., Crépeau, C., Jozsa, R., Peres, A. and Wootters, W.K. (1993). Teleporting an unknown quantum state via dual classical and Einstein-Podolsky-Rosen channels. *Phys. Rev. Lett.*, **70**, 1895–1899.

Berman, A. and Shaked-Monderer, N. (2003). *Completely positive matrices*. World Scientific.

Berman, A., Dur, M. and Shaked-Monderer, N. (2015). Open problems in the theory of completely positive and copositive matrices. *Electronic Journal of Linear Algebra*, **29**, 46–58.

Bernien, H., Schwartz, S., Keesling, A., Levine, H., Omran, A., Pichler, H., Choi, S., Zibrov, A.S., Endres, M., Greiner, M. *et al.* (2017). Probing many-body dynamics on a 51-atom quantum simulator. *Nature*, **551**, 579–584.

Beste, A., Runge, K. and Bartlett, R. (2002). Ensuring n-representability: Coleman's algorithm. *Chemical Physics Letters*, **355**, 263–269.

Biamonte, J. and Bergholm, V. (2017). Tensor networks in a nutshell.

Bohr, N. (1935). Can quantum-mechanical description of physical reality be considered complete? *Phys. Rev.*, **48**, 696–702.

Born, M. (1955). Statistical interpretation of quantum mechanics. *Science*, **122**, 675–679.

Botet, R., Jullien, R. and Pfeuty, P. (1982). Size scaling for infinitely coordinated systems. *Physical Review Letters*, **49**, 478.

Bradley, C.C., Sackett, C., Tollett, J. and Hulet, R.G. (1995). Evidence of bose-einstein condensation in an atomic gas with attractive interactions. *Physical review letters*, **75**, 1687.

Brunner, N., Cavalcanti, D., Pironio, S., Scarani, V. and Wehner, S. (2014). Bell nonlocality. *Rev. Mod. Phys.*, **86**, 419–478.

Chang, D., Douglas, J., González-Tudela, A., Hung, C.L. and Kimble, H. (2018). Colloquium: Quantum matter built from nanoscopic lattices of atoms and photons. *Reviews of Modern Physics*, **90**, 031002.

Chazelle, B. (1993). An optimal convex hull algorithm in any fixed dimension. *Discrete & Computational Geometry*, **10**, 377–409.

Christandl, M. (2006). *The Structure of Bipartite Quantum States - Insights from Group Theory and Cryptography*. Ph.D. thesis.

Christandl, M., Doran, B., Kousidis, S. and Walter, M. (2014). Eigenvalue distributions of reduced density matrices. *Communications in Mathematical Physics*, **332**, 1–52.

Clauser, J.F., Horne, M.A., Shimony, A. and Holt, R.A. (1969). Proposed experiment to test local hidden-variable theories. *Phys. Rev. Lett.*, **23**, 880–884.

Colbeck, R. and Renner, R. (2012). Free randomness can be amplified. *Nature Physics*, **8**, 450–453.

Collaboration, T.B.B.T. (2018). Challenging local realism with human choices. *Nature*, **557**, 212–216.

Collins, D., Gisin, N., Linden, N., Massar, S. and Popescu, S. (2002). Bell inequalities for arbitrarily high-dimensional systems. *Physical review letters*, **88**, 040404.

Crosswhite, G.M., Doherty, A.C. and Vidal, G. (2008). Applying matrix product operators to model systems with long-range interactions. *Physical Review B*, **78**, 035116.

Davis, K.B., Mewes, M.O., Andrews, M.R., van Druten, N.J., Durfee, D.S., Kurn, D. and Ketterle, W. (1995). Bose-einstein condensation in a gas of sodium atoms. *Physical review letters*, **75**, 3969.

Deng, D.L. (2018). Machine learning detection of bell nonlocality in quantum many-body systems. *Physical Review Letters*, **120**.

Dicke, R.H. (1954). Coherence in spontaneous radiation processes. *Phys. Rev.*, **93**, 99–110.

Dickinson, P.J. (2011). Geometry of the copositive and completely positive cones. *Journal of Mathematical Analysis and Applications*, **380**, 377–395.

Dickinson, P.J. and Gijben, L. (2014). On the computational complexity of membership problems for the completely positive cone and its dual. *Computational optimization and applications*, **57**, 403–415.

Dickinson, P.J., Dür, M., Gijben, L. and Hildebrand, R. (2013). Scaling relationship between the copositive cone and parrilo's first level approximation. *Optimization Letters*, **7**, 1669–1679.

Dmitriev, D.V., Krivnov, V.Y., Ovchinnikov, A.A. and Langari, A. (2002). One-dimensional anisotropic heisenberg model in the transverse magnetic field. *Journal of Experimental and Theoretical Physics*, **95**, 538–549.

Doherty, A.C., Parrilo, P.A. and Spedalieri, F.M. (2004). Complete family of separability criteria. *Physical Review A*, **69**.

Dusuel, S. and Vidal, J. (2004). Finite-size scaling exponents of the lipkin-meshkov-glick model. *Phys. Rev. Lett.*, **93**, 237204.

Eckert, K., Schliemann, J., Bruß, D. and Lewenstein, M. (2002). Quantum correlations in systems of indistinguishable particles. *Annals of Physics*, **299**, 88 – 127.

Einstein, A., Podolsky, B. and Rosen, N. (1935). Can quantum-mechanical description of physical reality be considered complete? *Physical review*, **47**, 777.

Ekert, A.K. (1991). Quantum cryptography based on Bell's theorem. *Phys. Rev. Lett.*, **67**, 661–663.

Engelsen, N.J., Krishnakumar, R., Hosten, O. and Kasevich, M.A. (2017). Bell correlations in spin-squeezed states of 500 000 atoms. *Phys. Rev. Lett.*, **118**, 140401.

Evenbly, G. (2019). Tensors. net.

Fadel, M. (2017). Self-testing dicke states.

Fadel, M. and Tura, J. (2017). Bounding the set of classical correlations of a many-body system. *Phys. Rev. Lett.*, **119**, 230402.

Fadel, M. and Tura, J. (2018). Bell correlations at finite temperature. *Quantum*, **2**, 107.

Fadel, M., Zibold, T., Décamps, B. and Treutlein, P. (2018). Spatial entanglement patterns and einstein-podolsky-rosen steering in bose-einstein condensates. *Science*, **360**, 409–413.

Faugère, J.C. (1999). A new efficient algorithm for computing Gröbner bases (F4). *Journal of Pure and Applied Algebra*, **139**, 61–88.

Faugère, J.C. (2002). A new efficient algorithm for computing gröbner bases without reduction to zero (F5). In *Proceedings of the 2002 international symposium on Symbolic and algebraic computation - ISSAC02*, ACM Press.

Fine, A. (1982). Hidden variables, joint probability, and the Bell inequalities. *Physical Review Letters*, **48**, 291–295.

Freedman, S.J. and Clauser, J.F. (1972). Experimental test of local hidden-variable theories. *Phys. Rev. Lett.*, **28**, 938–941.

Frérot, I. and Roscilde, T. (2018). Quantum Critical Metrology. *Phys. Rev. Lett.*, **121**, 020402.

Frérot, I. and Roscilde, T. (2019). Reconstructing the quantum critical fan of strongly correlated systems using quantum correlations. *Nature Communications*, **10**, 577.

Frérot, I., Naldesi, P. and Roscilde, T. (2017). Entanglement and fluctuations in the XXZ model with power-law interactions. *Phys. Rev. B*, **95**, 245111.

Fröwis, F., Nebendahl, V. and Dür, W. (2010). Tensor operators: Constructions and applications for long-range interaction systems. *Physical Review A*, **81**, 062337.

Fröwis, F., Strassmann, P.C., Tiranov, A., Gut, C., Lavoie, J., Brunner, N., Bussières, F., Afzelius, M. and Gisin, N. (2017). Experimental certification of millions of genuinely entangled atoms in a solid. *Nature Communications*, **8**.

Fukuda, K. (1997). cdd/cdd+ reference manual. *Institute for Operations Research, ETH-Zentrum*, 91–111.

Fulton, W., Harris, W. and Harris, J. (1991). *Representation Theory: A First Course*. Graduate Texts in Mathematics, Springer New York.

Gabbrielli, M., Smerzi, A. and Pezzè, L. (2018). Multipartite entanglement at finite temperature. *Scientific Reports*, **8**, 15663.

Gabbrielli, M., Lepori, L. and Pezzè, L. (2019). Multipartite-entanglement tomography of a quantum simulator. *New Journal of Physics*, **21**, 033039.

Garcia, C.B. and Li, T.Y. (1980). On the number of solutions to polynomial systems of equations. *SIAM Journal on Numerical Analysis*, **17**, 540–546.

Gharibian, S. (2010). Strong NP-hardness of the quantum separability problem. *Quantum Info. Comput.*, **10**, 343–360.

Gidofalvi, G. and Mazziotti, D.A. (2004). Boson correlation energies via variational minimization with the two-particle reduced density matrix: ExactN-representability conditions for harmonic interactions. *Physical Review A*, **69**.

Giovannetti, V., Lloyd, S. and Maccone, L. (2011). Advances in quantum metrology. *Nature Photonics*, **5**, 222 EP –, review Article.

Giustina, M., Mech, A., Ramelow, S., Wittmann, B., Kofler, J., Beyer, J., Lita, A., Calkins, B., Gerrits, T., Nam, S.W., Ursin, R. and Zeilinger, A. (2013). Bell violation using entangled photons without the fair-sampling assumption. *Nature*, **497**, 227 EP –.

Glick, A., Lipkin, H. and Meshkov, N. (1965). Validity of many-body approximation methods for a solvable model. *Nuclear Physics*, **62**, 211–224.

Gnutzmann, S., Haake, F. and Kus, M. (2000). Quantum chaos of SU3 observables. *Journal of Physics A: Mathematical and General*, **33**, 143.

Goldstein, S., Lebowitz, J.L., Tumulka, R. and Zanghì, N. (2006). Canonical typicality. *Physical review letters*, **96**, 050403.

González-Tudela, A. and Porras, D. (2013). Mesoscopic entanglement induced by spontaneous emission in solid-state quantum optics. *Physical review letters*, **110**, 080502.

Grant, M. and Boyd, S. (2008). Graph implementations for nonsmooth convex programs. In V. Blondel, S. Boyd and H. Kimura, eds., *Recent Advances in Learning and Control*, Lecture Notes in Control and Information Sciences, 95–110, Springer-Verlag Limited, http://stanford.edu/~boyd/graph_dcp.html.

Grant, M. and Boyd, S. (2014). CVX: Matlab software for disciplined convex programming, version 2.1. http://cvxr.com/cvx.

Graß, T., Juliá-Díaz, B., Kuś, M. and Lewenstein, M. (2013). Quantum chaos in su (3) models with trapped ions. *Physical review letters*, **111**, 090404.

Greenberger, D.M., Horne, M.A. and Zeilinger, A. (2007). Going beyond Bell's theorem.

Grötschel, M., Lovász, L. and Schrijver, A. (2012). *Geometric algorithms and combinatorial optimization*, vol. 2. Springer Science & Business Media.

Gühne, O. and Seevinck, M. (2010). Separability criteria for genuine multiparticle entanglement. *New Journal of Physics*, **12**, 053002.

Gühne, O. and Tóth, G. (2009). Entanglement detection. *Physics Reports*, **474**, 1 – 75.

Gühne, O., Tóth, G. and Briegel, H.J. (2005). Multipartite entanglement in spin chains. *New Journal of Physics*, **7**, 229.

Gurvits, L. (2003). Classical deterministic complexity of edmonds' problem and quantum entanglement. In *Proceedings of the Thirty-fifth Annual ACM Symposium on Theory of Computing*, STOC '03, 10–19, ACM, New York, NY, USA.

Haldane, F.D.M. (1983). Continuum dynamics of the 1-D Heisenberg antiferromagnet: Identification with the O(3) nonlinear sigma model. *Physics Letters A*, **93**, 464–468.

Hall, M. and Newman, M. (1963). Copositive and completely positive quadratic forms. *Mathematical Proceedings of the Cambridge Philosophical Society*, **59**, 329–339.

Hamley, C.D. (2012). *Spin-nematic squeezing in a spin-1 Bose-Einstein condensate*. Ph.D. thesis, Georgia Institute of Technology.

Harris, J. (1992). *Algebraic Geometry*. Springer New York.

Harrow, A.W., Natarajan, A. and Wu, X. (2017). An improved semidefinite programming hierarchy for testing entanglement. *Communications in Mathematical Physics*, **352**, 881–904.

Hauke, P., Heyl, M., Tagliacozzo, L. and Zoller, P. (2016). Measuring multipartite entanglement through dynamic susceptibilities. *Nature Physics*, **12**, 778–782.

Hensen, B., Bernien, H., Dréau, A.E., Reiserer, A., Kalb, N., Blok, M.S., Ruitenberg, J., Vermeulen, R.F.L., Schouten, R.N., Abellán, C., Amaya, W., Pruneri, V., Mitchell, M.W., Markham, M., Twitchen, D.J., Elkouss, D., Wehner, S., Taminiau, T.H. and Hanson, R. (2015). Loophole-free Bell inequality violation using electron spins separated by 1.3 kilometres. *Nature*, **526**, 682 EP –.

Hirsch, F., Quintino, M.T., Vértesi, T., Pusey, M.F. and Brunner, N. (2016). Algorithmic construction of local hidden variable models for entangled quantum states. *Phys. Rev. Lett.*, **117**, 190402.

Hirsch, F., Quintino, M.T., Vértesi, T., Navascués, M. and Brunner, N. (2017). Better local hidden variable models for two-qubit Werner states and an upper bound on the Grothendieck constant $K_G(3)$. *Quantum*, **1**, 3.

Holstein, T. and Primakoff, H. (1940). Field dependence of the intrinsic domain magnetization of a ferromagnet. *Physical Review*, **58**, 1098.

Horodecki, M., Horodecki, P. and Horodecki, R. (1996). Separability of mixed states: necessary and sufficient conditions. *Physics Letters A*, **223**, 1 – 8.

Horodecki, P. (1997). Separability criterion and inseparable mixed states with positive partial transposition. *Physics Letters A*, **232**, 333 – 339.

Horodecki, R., Horodecki, P., Horodecki, M. and Horodecki, K. (2009). Quantum entanglement. *Rev. Mod. Phys.*, **81**, 865–942.

Householder, A.S. (2013). *The theory of matrices in numerical analysis*. Courier Corporation.

Huber, F. (2017). *Quantum states and their marginals: from multipartite entanglement to quantum error-correcting codes*. Ph.D. thesis, Universität Siegen.

Huber, M., Erker, P., Schimpf, H., Gabriel, A. and Hiesmayr, B. (2011). Experimentally feasible set of criteria detecting genuine multipartite entanglement in n-qubit Dicke states and in higher-dimensional systems. *Phys. Rev. A*, **83**, 040301.

Jordan, C. (1875). Essai sur la géométrie à n dimensions. *Bulletin de la Société Mathématique de France*, **3**, 103–174.

Jordan, P. and Wigner, E. (1928). Über das paulische Äquivalenzverbot. *Zeitschrift für Physik*, **47**, 631–651.

Julià-Farré, S., Salamon, T., Riera, A., Bera, M.N. and Lewenstein, M. (2020). Bounds on the capacity and power of quantum batteries. *Physical Review Research*, **2**, 023113.

Jungnitsch, B., Moroder, T. and Gühne, O. (2011). Taming multiparticle entanglement. *Phys. Rev. Lett.*, **106**, 190502.

Kaniewski, J. (2016). Analytic and nearly optimal self-testing bounds for the Clauser-Horne-Shimony-Holt and mermin inequalities. *Physical Review Letters*, **117**.

Kaniewski, J., Šupić, I., Tura, J., Baccari, F., Salavrakos, A. and Augusiak, R. (2019). Maximal nonlocality from maximal entanglement and mutually unbiased bases, and self-testing of two-qutrit quantum systems. *Quantum*, **3**, 198.

Kaykobad, M. (1987). On nonnegative factorization of matrices. *Linear Algebra and its Applications*, **96**, 27 – 33.

Kim, K., Chang, M.S., Korenblit, S., Islam, R., Edwards, E.E., Freericks, J.K., Lin, G.D., Duan, L.M. and Monroe, C. (2010). Quantum simulation of frustrated ising spins with trapped ions. *Nature*, **465**, 590 EP –.

Kitagawa, M. and Ueda, M. (1993). Squeezed spin states. *Phys. Rev. A*, **47**, 5138–5143.

Klyachko, A. (2004). Quantum marginal problem and representations of the symmetric group.

Klyachko, A.A. (2006). Quantum marginal problem and n-representability. *Journal of Physics: Conference Series*, **36**, 72–86.

Knap, M., Kantian, A., Giamarchi, T., Bloch, I., Lukin, M.D. and Demler, E. (2013). Probing real-space and time-resolved correlation functions with many-body ramsey interferometry. *Physical Review Letters*, **111**.

Knips, L., Schwemmer, C., Klein, N., Wieśniak, M. and Weinfurter, H. (2016). Multipartite entanglement detection with minimal effort. *Physical Review Letters*, **117**.

Koffel, T., Lewenstein, M. and Tagliacozzo, L. (2012). Entanglement entropy for the long-range ising chain in a transverse field. *Physical Review Letters*, **109**.

Kojima, M. and Mizuno, S. (1983). Computation of all solutions to a system of polynomial equations. *Mathematical Programming*, **25**, 131–157.

Kunkel, P., Prüfer, M., Lannig, S., Rosa-Medina, R., Bonnin, A., Gärttner, M., Strobel, H. and Oberthaler, M.K. (2019). Simultaneous readout of noncommuting collective spin observables beyond the standard quantum limit. *Physical review letters*, **123**, 063603.

Latorre, J.I., Orús, R., Rico, E. and Vidal, J. (2005). Entanglement entropy in the lipkin-meshkov-glick model. *Phys. Rev. A*, **71**, 064101.

Lewenstein, M. and Sanpera, A. (1998). Separability and entanglement of composite quantum systems. *Phys. Rev. Lett.*, **80**, 2261–2264.

Lewenstein, M., Kraus, B., Cirac, J.I. and Horodecki, P. (2000). Optimization of entanglement witnesses. *Physical Review A*, **62**, 052310.

Lewenstein, M., Kraus, B., Horodecki, P. and Cirac, J. (2001). Characterization of separable states and entanglement witnesses. *Physical Review A*, **63**, 044304.

Lewenstein, M., Sanpera, A., Ahufinger, V., Damski, B., Sen, A. and Sen, U. (2007). Ultracold atomic gases in optical lattices: mimicking condensed matter physics and beyond. *Advances in Physics*, **56**, 243–379.

Li, X., Cai, Y., Han, Y., Wen, Q. and Scarani, V. (2018). Self-testing using only marginal information. *Physical Review A*, **98**, 052331.

Liang, Y.C., Rosset, D., Bancal, J.D., Pütz, G., Barnea, T.J. and Gisin, N. (2015). Family of Bell-like inequalities as device-independent witnesses for entanglement depth. *Phys. Rev. Lett.*, **114**, 190401.

Lin, P.S., Hung, J.C., Chen, C.H. and Liang, Y.C. (2019). Exploring bell inequalities for the device-independent certification of multipartite entanglement depth. *Physical Review A*, **99**, 062338.

Links, J., Zhou, H.Q., McKenzie, R.H. and Gould, M.D. (2003). Algebraic bethe ansatz method for the exact calculation of energy spectra and form factors: applications to models of bose einstein condensates and metallic nanograins. *Journal of Physics A: Mathematical and General*, **36**, R63–R104.

Lipkin, H., Meshkov, N. and Glick, A. (1965). Validity of many-body approximation methods for a solvable model. *Nuclear Physics*, **62**, 188–198.

Liu, W.F., Ma, J. and Wang, X. (2013). Quantum fisher information and spin squeezing in the ground state of the xy model. *Journal of Physics A: Mathematical and Theoretical*, **46**, 045302.

Liu, Y.K., Christandl, M. and Verstraete, F. (2007). Quantum computational complexity of theN-representability problem: QMA complete. *Physical Review Letters*, **98**.

Lofberg, J. (2004). YALMIP : a toolbox for modeling and optimization in MATLAB. In *2004 IEEE International Conference on Robotics and Automation (IEEE Cat. No.04CH37508)*, IEEE.

Lu, C.Y., Zhou, X.Q., Gühne, O., Gao, W.B., Zhang, J., Yuan, Z.S., Goebel, A., Yang, T. and Pan, J.W. (2007). Experimental entanglement of six photons in graph states. *Nature Physics*, **3**, 91–95.

Lücke, B., Peise, J., Vitagliano, G., Arlt, J., Santos, L., Tóth, G. and Klempt, C. (2014). Detecting multiparticle entanglement of dicke states. *Physical review letters*, **112**, 155304.

Lücke, B., Peise, J., Vitagliano, G., Arlt, J., Santos, L., Tóth, G. and Klempt, C. (2014). Detecting multiparticle entanglement of Dicke states. *Phys. Rev. Lett.*, **112**, 155304.

Lydersen, L., Wiechers, C., Wittmann, C., Elser, D., Skaar, J. and Makarov, V. (2010). Hacking commercial quantum cryptography systems by tailored bright illumination. *Nature Photonics*, **4**, 686 EP –.

Mangasarian, O.L. (1984). Normal solutions of linear programs. In *Mathematical Programming at Oberwolfach II*, 206–216, Springer.

Mayers, D. and Yao, A. (1998). Quantum cryptography with imperfect apparatus. In *Proceedings 39th Annual Symposium on Foundations of Computer Science (Cat. No. 98CB36280)*, 503–509, IEEE.

Mayers, D. and Yao, A. (2004). Self testing quantum apparatus. *Quantum Information & Computation*, **4**, 273–286.

Mazziotti, D.A. (2012). Structure of fermionic density matrices: CompleteN-representability conditions. *Physical Review Letters*, **108**.

McConnell, R., Zhang, H., Hu, J., Ćuk, S. and Vuletić, V. (2015). Entanglement with negative wigner function of almost 3,000 atoms heralded by one photon. *Nature*, **519**, 439–442.

Meredith, D.C., Koonin, S.E. and Zirnbauer, M.R. (1988). Quantum chaos in a schematic shell model. *Physical Review A*, **37**, 3499–3513.

Meshkov, N., Glick, A. and Lipkin, H. (1965). Validity of many-body approximation methods for a solvable model. *Nuclear Physics*, **62**, 199–210.

Moroder, T., Hyllus, P., Tóth, G., Schwemmer, C., Niggebaum, A., Gaile, S., Gühne, O. and Weinfurter, H. (2012). Permutationally invariant state reconstruction. *New Journal of Physics*, **14**, 105001.

Moroder, T., Bancal, J.D., Liang, Y.C., Hofmann, M. and Gühne, O. (2013). Device-independent entanglement quantification and related applications. *Physical Review Letters*, **111**.

Navascués, M., Pironio, S. and Acín, A. (2007). Bounding the set of quantum correlations. *Physical Review Letters*, **98**, 010401.

Navascués, M., Pironio, S. and Acín, A. (2007). Bounding the set of quantum correlations. *Phys. Rev. Lett.*, **98**, 010401.

Navascués, M., Pironio, S. and Acín, A. (2008). A convergent hierarchy of semidefinite programs characterizing the set of quantum correlations. *New Journal of Physics*, **10**, 073013.

Navascués, M., Guryanova, Y., Hoban, M.J. and Acín, A. (2015). Almost quantum correlations. *Nature Communications*, **6**, 6288 EP –, article.

Nielsen, M.A. and Chuang, I. (2002). Quantum computation and quantum information.

Noether, E. and van der Waerden, B.L. (1928). *Die alternative bei nichlinearen Gleichungen*. No. 77-87 in Nachrichten der Gesselschaft der Wissenschaften zu Gottingen, Math. Phys. Klasse.

Orús, R. (2014). A practical introduction to tensor networks: Matrix product states and projected entangled pair states. *Annals of Physics*, **349**, 117–158.

Osborne, T.J. and Nielsen, M.A. (2002). Entanglement in a simple quantum phase transition. *Physical Review A*, **66**, 032110.

Pál, K.F. and Vértesi, T. (2010). Maximal violation of a bipartite three-setting, two-outcome bell inequality using infinite-dimensional quantum systems. *Physical Review A*, **82**.

Pál, K.F. and Vértesi, T. (2010). Maximal violation of a bipartite three-setting, two-outcome Bell inequality using infinite-dimensional quantum systems. *Phys. Rev. A*, **82**, 022116.

Pan, F. and Draayer, J. (1999). Analytical solutions for the LMG model. *Physics Letters B*, **451**, 1–10.

Pan, J.W., Bouwmeester, D., Daniell, M., Weinfurter, H. and Zeilinger, A. (2000). Experimental test of quantum nonlocality in three-photon greenberger–horne–zeilinger entanglement. *Nature*, **403**, 515–519.

Pataki, G. (2000). The geometry of semidefinite programming. *Handbook of semidefinite programming*, 29–65.

Pataki, G. (2013). Strong duality in conic linear programming: facial reduction and extended duals. In *Computational and analytical mathematics*, 613–634, Springer.

Pelisson, S., Pezzè, L. and Smerzi, A. (2016a). Nonlocality with ultracold atoms in a lattice. *Physical Review A*, **93**, 022115.

Pelisson, S., Pezze, L. and Smerzi, A. (2016b). Nonlocality with ultracold atoms in a lattice. *Physical Review A*, **93**, 022115.

Peres, A. (1996). Separability criterion for density matrices. *Phys. Rev. Lett.*, **77**, 1413–1415.

Perez-Garcia, D., Verstraete, F., Wolf, M. and Cirac, J. (2007). Matrix product state representations. *QUANTUM INFORMATION & COMPUTATION*, **7**, 401–430.

Pezzé, L. and Smerzi, A. (2009). Entanglement, Nonlinear Dynamics, and the Heisenberg Limit. *Phys. Rev. Lett.*, **102**, 100401.

Pezzè, L., Smerzi, A., Oberthaler, M.K., Schmied, R. and Treutlein, P. (2018). Quantum metrology with nonclassical states of atomic ensembles. *Rev. Mod. Phys.*, **90**, 035005.

Piga, A., Aloy, A., Lewenstein, M. and Frérot, I. (2019). Bell correlations at ising quantum critical points. *Physical review letters*, **123**, 170604.

Pironio, S. (2014). All clauser–horne–shimony–holt polytopes. *Journal of Physics A: Mathematical and Theoretical*, **47**, 424020.

Pironio, S., Acín, A., Brunner, N., Gisin, N., Massar, S. and Scarani, V. (2009). Device-independent quantum key distribution secure against collective attacks. *New Journal of Physics*, **11**, 045021.

Pironio, S., Acín, A., Massar, S., de la Giroday, A.B., Matsukevich, D.N., Maunz, P., Olmschenk, S., Hayes, D., Luo, L., Manning, T.A. and Monroe, C. (2010). Random numbers certified by bell's theorem. *Nature*, **464**, 1021 EP –.

Pitowsky, I. (1989). *Quantum Probability — Quantum Logic*. Lecture Notes in Physics, Springer-Verlag.

Pitowsky, I. and Svozil, K. (2001). Optimal tests of quantum nonlocality. *Phys. Rev. A*, **64**, 014102.

Popescu, S. and Rohrlich, D. (1994). Quantum nonlocality as an axiom. *Foundations of Physics*, **24**, 379–385.

Popescu, S., Short, A.J. and Winter, A. (2006). Entanglement and the foundations of statistical mechanics. *Nature Physics*, **2**, 754–758.

Popp, M., Verstraete, F., Martín-Delgado, M.A. and Cirac, J.I. (2005). Localizable entanglement. *Physical Review A*, **71**, 042306.

Quesada, R. and Sanpera, A. (2014). Best separable approximation of multipartite diagonal symmetric states. *Physical Review A*, **89**, 052319.

Ribeiro, P., Vidal, J. and Mosseri, R. (2008). Exact spectrum of the lipkin-meshkov-glick model in the thermodynamic limit and finite-size corrections. *Physical Review E*, **78**.

Ruskai, M.B. (1969). N-representability problem: Conditions on geminals. *Physical Review*, **183**, 129–141.

Sachdev, S. (2011). *Quantum Phase Transitions*. Cambridge Univ. Press, Cambridge.

Salavrakos, A., Augusiak, R., Tura, J., Wittek, P., Acín, A. and Pironio, S. (2017). Bell inequalities tailored to maximally entangled states. *Phys. Rev. Lett.*, **119**, 040402.

Sanz, M., Wolf, M.M., Pérez-García, D. and Cirac, J.I. (2009). Matrix product states: Symmetries and two-body hamiltonians. *Physical Review A*, **79**.

Sanz, M., Egusquiza, I.L., Candia, R.D., Saberi, H., Lamata, L. and Solano, E. (2016). Entanglement classification with matrix product states. *Scientific Reports*, **6**.

Sanz, M., Braak, D., Solano, E. and Egusquiza, I.L. (2017). Entanglement classification with algebraic geometry. *Journal of Physics A: Mathematical and Theoretical*, **50**, 195303.

Scarani, V. (2012a). The device-independent outlook on quantum physics. *Acta Physica Slovaca*, **62**, 347–409.

Scarani, V. (2012b). The device-independent outlook on quantum physics. *Acta Physica Slovaca*, **62**, 347–409.

Scarani, V. (2019). *Bell nonlocality*. Oxford University Press.

Schilling, C. (2015). The quantum marginal problem. In *Mathematical Results in Quantum Mechanics: Proceedings of the QMath12 Conference*, 165–176, World Scientific.

Schilling, C., Benavides-Riveros, C.L. and Vrana, P. (2017). Reconstructing quantum states from single-party information. *Physical Review A*, **96**.

Schmaljohann, H., Erhard, M., Kronjäger, J., Kottke, M., Van Staa, S., Cacciapuoti, L., Arlt, J., Bongs, K. and Sengstock, K. (2004). Dynamics of f= 2 spinor bose-einstein condensates. *Physical review letters*, **92**, 040402.

Schmied, R., Bancal, J.D., Allard, B., Fadel, M., Scarani, V., Treutlein, P. and Sangouard, N. (2016). Bell correlations in a bose-einstein condensate. *Science*, **352**, 441–444.

Schur, I. (1901). *Ueber eine klasse von matrizen, die sich einer gegebenen matrix zuordnen lassen....* Friedrich Wilhelms Universität, Berlin.

Schwemmer, C., Knips, L., Tran, M.C., de Rosier, A., Laskowski, W., Paterek, T. and Weinfurter, H. (2015). Genuine multipartite entanglement without multipartite correlations. *Physical Review Letters*, **114**.

Shannon, C.E. (1948). A mathematical theory of communication. *Bell system technical journal*, **27**, 379–423.

Simon, J., Bakr, W.S., Ma, R., Tai, M.E., Preiss, P.M. and Greiner, M. (2011). Quantum simulation of antiferromagnetic spin chains in an optical lattice. *Nature*, **472**, 307 EP –, article.

Śliwa, C. (2003). Symmetries of the bell correlation inequalities. *Physics Letters A*, **317**, 165 – 168.

Sonneveld, P., van Kan, J., Huang, X. and Oosterlee, C. (2009). Non-negative matrix factorization of a correlation matrix. *Linear Algebra and its Applications*, **431**, 334 – 349.

Sørensen, A.S. and Mølmer, K. (2001). Entanglement and extreme spin squeezing. *Physical Review Letters*, **86**, 4431–4434.

Sørensen, A.S. and Mølmer, K. (2001). Entanglement and extreme spin squeezing. *Phys. Rev. Lett.*, **86**, 4431–4434.

Stillinger, F.H. (1995). *Mathematical Challenges from Theoretical/Computational Chemistry*. National Academies Press.

Størmer, E. (1963). Positive linear maps of operator algebras. *Acta Math.*, **110**, 233–278.

Sturm, J.F. (1999). Using sedumi 1.02, a matlab toolbox for optimization over symmetric cones. *Optimization Methods and Software*, **11**, 625–653.

Sturmfels, B. (2002). *Solving Systems of Polynomial Equations (CBMS Regional Conference Series in Mathematics)*. American Mathematical Society.

Sturmfels, B. (2005). What is a Gröbner basis? *Notices of the American Mathematical Society*, **52**, 1199–1200.

Šupić, I., Augusiak, R., Salavrakos, A. and Acín, A. (2016). Self-testing protocols based on the chained bell inequalities. *New Journal of Physics*, **18**, 035013.

Šupić, I., Coladangelo, A., Augusiak, R. and Acín, A. (2018). Self-testing multipartite entangled states through projections onto two systems. *New Journal of Physics*, **20**, 083041.

Szalay, S. (2015). Multipartite entanglement measures. *Physical Review A*, **92**.

Szalay, S. (2019). k-stretchability of entanglement, and the duality of k-separability and k-producibility. *Quantum*, **3**, 204.

Szalay, S. and Kökényesi, Z. (2012). Partial separability revisited: Necessary and sufficient criteria. *Physical Review A*, **86**.

Tavakoli, A., Rosset, D. and Renou, M.O. (2019). Enabling computation of correlation bounds for finite-dimensional quantum systems via symmetrization. *Physical Review Letters*, **122**.

Terhal, B.M. (2000). Bell inequalities and the separability criterion. *Physics Letters A*, **271**, 319–326.

Toh, K.C., Todd, M., Tütüncü, R. and Tutuncu, R.H. (1998). Sdpt3 - a matlab software package for semidefinite programming. *Optimization Methods and Software*, **11**, 545–581.

Toner, B. and Verstraete, F. (2006). Monogamy of bell correlations and tsirelson's bound.

Tóth, G. and Acín, A. (2006). Genuine tripartite entangled states with a local hidden-variable model. *Phys. Rev. A*, **74**, 030306.

Tran, M.C., Zuppardo, M., de Rosier, A., Knips, L., Laskowski, W., Paterek, T. and Weinfurter, H. (2017). Genuine n -partite entanglement without n -partite correlation functions. *Physical Review A*, **95**.

Tura, J. (2017). *Characterizing Entanglement and Quantum Correlations Constrained by Symmetry*. Springer International Publishing.

Tura, J., Augusiak, R., Hyllus, P., Kuś, M., Samsonowicz, J. and Lewenstein, M. (2012a). Four-qubit entangled symmetric states with positive partial transpositions. *Phys. Rev. A*, **85**, 060302.

Tura, J., Augusiak, R., Hyllus, P., Kuś, M., Samsonowicz, J. and Lewenstein, M. (2012b). Four-qubit entangled symmetric states with positive partial transpositions. *Physical Review A*, **85**.

Tura, J., Augusiak, R., Sainz, A.B., Vértesi, T., Lewenstein, M. and Acín, A. (2014a). Detecting nonlocality in many-body quantum states. *Science*, **344**, 1256–1258.

Tura, J., Sainz, A.B., Vértesi, T., Acín, A., Lewenstein, M. and Augusiak, R. (2014b). Translationally invariant multipartite bell inequalities involving only two-body correlators. *Journal of Physics A: Mathematical and Theoretical*, **47**, 424024.

Tura, J., Augusiak, R., Sainz, A., Lücke, B., Klempt, C., Lewenstein, M. and Acín, A. (2015). Nonlocality in many-body quantum systems detected with two-body correlators. *Annals of Physics*, **362**, 370 – 423.

Tura, J., De las Cuevas, G., Augusiak, R., Lewenstein, M., Acín, A. and Cirac, J.I. (2017). Energy as a detector of nonlocality of many-body spin systems. *Phys. Rev. X*, **7**, 021005.

Tura, J., Aloy, A., Quesada, R., Lewenstein, M. and Sanpera, A. (2018). Separability of diagonal symmetric states: a quadratic conic optimization problem. *Quantum*, **2**, 45.

Tura, J., Aloy, A., Baccari, F., Acín, A., Lewenstein, M. and Augusiak, R. (2019). Optimization of device-independent witnesses of entanglement depth from two-body correlators. *Physical Review A*, **100**, 032307.

Tura i Brugués, J. (2017). *Characterizing entanglement and quantum correlations constrained by symmetry*. Springer.

Šupić, I. and Bowles, J. (2019). Self-testing of quantum systems: a review.

Verstraete, F., Martin-Delgado, M.A. and Cirac, J.I. (2004). Diverging entanglement length in gapped quantum spin systems. *Physical review letters*, **92**, 087201.

Von Neumann, J. (1927). Wahrscheinlichkeitstheoretischer aufbau der quantenmechanik. *Nachrichten von der Gesellschaft der Wissenschaften zu Göttingen, Mathematisch-Physikalische Klasse*, **1927**, 245–272.

Wagner, S., Schmied, R., Fadel, M., Treutlein, P., Sangouard, N. and Bancal, J.D. (2017). Bell correlations in a many-body system with finite statistics. *Phys. Rev. Lett.*, **119**, 170403.

Walter, M., Doran, B., Gross, D. and Christandl, M. (2013). Entanglement polytopes: Multiparticle entanglement from single-particle information. *Science*, **340**, 1205–1208.

Wang, J., Paesani, S., Ding, Y., Santagati, R., Skrzypczyk, P., Salavrakos, A., Tura, J., Augusiak, R., Mančinska, L., Bacco, D., Bonneau, D., Silverstone, J.W., Gong, Q., Acín, A., Rottwitt, K., Oxenløwe, L.K., O'Brien, J.L., Laing, A. and Thompson, M.G. (2018). Multidimensional quantum entanglement with large-scale integrated optics. *Science*, **360**, 285–291.

Werner, R.F. (1989). Quantum states with einstein-podolsky-rosen correlations admitting a hidden-variable model. *Phys. Rev. A*, **40**, 4277–4281.

Werner, R.F. and Wolf, M.M. (2001). Bell inequalities and entanglement. *Quantum Info. Comput.*, **1**, 1–25.

Weyl, H. (1931). The theory of groups and quantum mechanics dover publications. *Inc. c*, **1951**.

Weyl, H. (1946). *The classical groups: their invariants and representations*, vol. 45. Princeton university press.

Wieczorek, W., Krischek, R., Kiesel, N., Michelberger, P., Tóth, G. and Weinfurter, H. (2009). Experimental entanglement of a six-photon symmetric dicke state. *Phys. Rev. Lett.*, **103**, 020504.

Wineland, D.J., Bollinger, J.J., Itano, W.M. and Heinzen, D.J. (1994). Squeezed atomic states and projection noise in spectroscopy. *Physical Review A*, **50**, 67–88.

Wolfe, E. and Yelin, S.F. (2014). Certifying separability in symmetric mixed states of n qubits, and superradiance. *Phys. Rev. Lett.*, **112**, 140402.

Wölk, S. and Gühne, O. (2016). Characterizing the width of entanglement. *New Journal of Physics*, **18**, 123024.

Woronowicz, S. (1976). Positive maps of low dimensional matrix algebras. *Reports on Mathematical Physics*, **10**, 165 – 183.

Wright, A.H. (1985). Finding all solutions to a system of polynomial equations. *Mathematics of Computation*, **44**, 125–125.

Wu, X. (2016). *Self-testing: Walking on the boundary of the quantum set*. Ph.D. thesis, National University of Singapore, ph.D. Thesis.

Wu, X., Cai, Y., Yang, T.H., Le, H.N., Bancal, J.D. and Scarani, V. (2014). Robust self-testing of the three-qubitWstate. *Physical Review A*, **90**.

Yang, T.H. and Navascués, M. (2013). Robust self-testing of unknown quantum systems into any entangled two-qubit states. *Physical Review A*, **87**.

Yu, N. (2016). Separability of a mixture of dicke states. *Phys. Rev. A*, **94**, 060101.

Zhang, J., Pagano, G., Hess, P.W., Kyprianidis, A., Becker, P., Kaplan, H., Gorshkov, A.V., Gong, Z.X. and Monroe, C. (2017). Observation of a many-body dynamical phase transition with a 53-qubit quantum simulator. *Nature*, **551**, 601–604.

Zhang, W.H., Chen, G., Yin, P., Peng, X.X., Hu, X.M., Hou, Z.B., Zhou, Z.Y., Yu, S., Ye, X.J., Zhou, Z.Q., Xu, X.Y., Tang, J.S., Xu, J.S., Han, Y.J., Liu, B.H., Li, C.F. and Guo, G.C. (2019). Experimental demonstration of robust self-testing for bipartite entangled states. *npj Quantum Information*, **5**.

Zhang, Z. and Duan, L. (2014). Quantum metrology with dicke squeezed states. *New Journal of Physics*, **16**, 103037.

Zhang, Z. and Duan, L.M. (2013). Generation of massive entanglement through an adiabatic quantum phase transition in a spinor condensate. *Physical review letters*, **111**, 180401.

Zhou, J., Hu, Y., Zou, X.B. and Guo, G.C. (2011). Ground-state preparation of arbitrarily multipartite dicke states in the one-dimensional ferromagnetic spin-12chain. *Physical Review A*, **84**.

Zhu, Z., So, A.M.C. and Ye, Y. (2010). Universal rigidity: Towards accurate and efficient localization of wireless networks. In *2010 Proceedings IEEE INFOCOM*, 1–9, IEEE.

Zou, Y.Q., Wu, L.N., Liu, Q., Luo, X.Y., Guo, S.F., Cao, J.H., Tey, M.K. and You, L. (2018). Beating the classical precision limit with spin-1 dicke states of more than 10,000 atoms. *Proceedings of the National Academy of Sciences*, **115**, 6381–6385.

Zwerger, M., Dür, W., Bancal, J.D. and Sekatski, P. (2019). Device-independent detection of genuine multipartite entanglement for all pure states. *Physical review letters*, **122**, 060502.